Identification of differential nutrient starvation responses.

Thesis submitted in accordance with the requirements of the University of Liverpool for the degree of Doctor in Philosophy

By

Ioannis Poursaitidis

November 2017

I wish to dedicate this thesis to my parents Symeon Poursaitidis and Maria Poursaitidou, my late grandma Theofania Mpostantzi and my wonderful significant other Paraskevi (Vivian) Dimou.

As you set out for Ithaka, hope your road is a long one, full of adventure, full of discovery. Laistrygonians, Cyclops, angry Poseidon—do not be afraid of them: you will never find things like that on your way as long as you keep your thoughts raised high, as long as a rare excitement stirs your spirit and your body. Laistrygonians, Cyclops, wild Poseidon—you won't encounter them unless you bring them along inside your soul unless your soul sets them up in front of you.

Hope your road is a long one. May there be many summer mornings when, with what pleasure, what joy, you enter harbours you see for the first time; may you stop at Phoenician trading stations to buy fine things, mother of pearl and coral, amber and ebony, sensual perfume of every kind— as many sensual perfumes as you can; and may you visit many Egyptian cities to learn and go on learning from their scholars.

Keep Ithaka always in your mind. Arriving there is what you are destined for. But do not hurry the journey at all. Better if it lasts for years, so you are old by the time you reach the island, wealthy with all you've gained on the way, not expecting Ithaka to make you rich.

Ithaka gave you the marvellous journey. Without her, you would not have set out. She has nothing left to give you now.

And if you find her poor, Ithaka will not have fooled you. Wise as you will have become, so full of experience, you will have understood by then what these Ithakas mean.

Ithaka -C. P. CAVAFY

Table of contents

I. ABSTRACT

To promote survival and proliferation cancer cells re-programme their metabolism, altering both uptake and utilisation of extracellular nutrients. To examine correspondences between nutrient supply and viability, in order to identify targetable requirements, I individually depleted amino acid nutrients from diploid Human Mammary Epithelial (HME) isogenic cells expressing commonly activated oncogenes. Cystine deprivation was found to induce massive-oxidative stress associated-cell death of HME cells expressing an activated epidermal growth factor receptor (EGFR). Cell death occurred via an iron-dependent mode, known as ferroptosis associated with increased generation of reactive oxygen species and lipid peroxidation. Pharmacological inhibition of EGFR or mitogen-activated protein kinase/extracellular regulated kinase (MAPK/ERK) signalling was found to block ferroptosis and ROS production and was associated with increased expression of glutathione peroxidase 4 (GPX4). Suppression of GPX4 expression in wild-type or gefitinib-treated HME-EGFR cells was sufficient to sensitise cells to ferroptosis. Importantly, MAPK signals were also important in suppressing cell-cell contact and communication that was found to provide an essential line of defence against ferroptosis induction and spread. In this way, microscopic observation of ferroptosis in wild-type HME cells identified a cell death spread phenotype that is consistent with necrosis phenotypes observed in ischemic models. Inhibition of ROS generation and lipid peroxidation effectively blocked the progression of necrosis indicating that counteracting lipid peroxidation might be beneficial for degenerative conditions where lipid peroxidation is evident. Additional therapeutic application of my findings was modelled using non-small lung cancer cell (NSCLC) lines with overactive ERK signalling. These cells were found to be sensitive to ferroptosis following deprivation

of cystine in vitro as well as in vivo where in systemic deprivation of cystine was achieved in xenografted mice following administration of a cystine-degrading enzyme. Taken together, my results show that the presence of common oncogenic mutations can render cells sensitive to the depletion of a specific nutrient, and further suggest potentially novel anti-cancer therapies based on the inability of some MAPK-driven cancer cells to overcome oxidative stress following nutrient depletion, as well as therapies to limit the spreading phenotype of ferroptosis in cells associated with other diseases such as Alzheimer's Disease, or that occur in normal cells in response to ischemic reperfusion and acute kidney injuries.

II. ACKNOWLEDGEMENTS

First of all, I would like to thank my supervisors; Dr Richard F. Lamb, for his guidance and for giving me the opportunity to work in his research group and Dr Joseph R. Slupsky, who patiently supervised me and supported me throughout my writing efforts, helping me to significantly improve my writing skills. Your support has been invaluable in completing this thesis.

I would also like to thank all the members of the “Lamb group” and particularly Ms Xiaomeng Wang and Mr Thomas Crighton who provided me with a lot of assistance in this work. Moreover, I would like to thank everyone working in the Cancer Research Centre (CRC) of Liverpool for always being helpful and nice to me. Special thanks to Dr Carlos Rubbi who introduced me to the magical world of microscopy and video time-lapse imaging and endured my endless questions. I would also like to thank my good friend Dr Shankar Varadarajan, with whom we have shared a lot of great discussion, many reagents and a lot of food and good times. I am also very grateful to our collaborators in the USA, Dr Everett Stone, Dr Scott Rowlinson and their team for kindly providing their cystine degrading enzyme and for performing the animal work included in this thesis. I could also not forget to thank Dr Christiaan Labuschange who provided assistance with the steady state amino acid measurements and Dr David Mason for kindly providing me with software code that allowed me to analyse my time-lapse videos. And of course, I am indebted to Cancer Research UK and the NIHR PBRU (Pancreas Biomedical Research Unit) for the financial support of my studies.

Finally, I would like to heartfully thank my family for their love and support throughout my academic studies. I would also like to commemorate my beloved late grandma,

Theofania Mpostanzti, the person who raised me up and whose passion for learning shaped my character and personality from a very young age. Saving the best for the end, I would like to thank from the bottom of my heart my lovely, fantastic significant other, (also soon-to-be Dr) Vivian (Paraskevi) Dimou, the person who has stood by my side and believed in me throughout this PhD, the one who has supported me and loved me through my hardest times, the one with whom I have shared all those endless conversations on our PhDs and the one who shares the same passion for science as I do.

Thank you all.

III. DECLARATION

This thesis is a result of my own work performed during the course of my studies in the Department of Molecular and Clinical Cancer Medicine, Institute of Translational Medicine, University of Liverpool, between October 2013 and September 2017. The material contained in this thesis has not been presented, nor is currently being presented, either wholly or in part for any degree or qualification. All work described was performed by me except where clearly indicated. The thesis was written wholly by me under guidance of my supervisors Dr. Richard F. Lamb and Dr. Joseph R. Slupsky.

Ioannis Poursaitidis

November 2017

IV. LIST OF FIGURES

V. LIST OF TABLES

VI. ABBREVIATIONS

3PG 3-glycerolphosphate

3PHP 3-phosphohydroxypyruvate

4E-BP1 eIF4E-binding protein-1

4HNE 4-hydroxynonenal

5mTHF 5-methyltetrahydrofolate

AAV adeno-associated-virus

ADI arginine deiminase

ADP adenosine diphosphate

AECase cysteinase

AJ adherens junctions

AKI acute kidney injury

ALL Acute lymphoblastic leukemias

Arg arginine

ASL argininosuccinate lyase

Asp aspartate

ASS argininosuccinate synthase

ATF4 activating transcription factor 4

ATG13 autophagy-related protein 13

ATP adenosine triphosphate

BRCA BReast CAncer susceptibility gene

BSA bovine serum albumin

BSO buthionine sulfoximine

CARS cysteinyl-tRNA synthetase

CBX carbenoxolone

CuOOH Cumene hydroperoxide

Cys cystine

DHA Dihydroartemisinin

DISC death-inducing signalling complex

DMEM Dulbecco's Modified Eagle's Medium

DNMT DNA methyltransferases

DTNB 5,5′-Dithiobis (2-nitrobenzoic acid)

ECM extracellular matrix

EGF epidermal growth factor

EGFR epidermal growth factor receptor

eIF eukaryotic initiation factor

ER endoplasmic reticulum

ER- oestrogen receptor negative

ERK extracellular regulated kinase

ES embryonic stem

FACS Fluorescence-activated cell sorting

FBS Fetal bovine serum

Fer1 Ferrostatin1

GAP GTPase-activating protein

GCN2 General control non-derepressable 2

GDP guanosine diphosphate

GEF guanosine exchange factor

GFPT glutamine-fructose-6-phosphate aminotransferase (

GJ gap junctions

GJIC gap junctional intracellular communication

Gln Glutamine

GLS glutaminase

Glu Glutamate

GLUD1 or GDH glutamate dehydrogenase

Gly glycine

GOT aspartate transaminase

GPX glutathione peroxidase

GPX4 glutathione peroxidase 4

GR glutathione reductase

GSH glutathione, reduced L-g-glutamyl-L-cysteinylglycine

GSK3 glycogen synthase kinase-3

GSSG glutathione, oxidised

GST glutathione s-transferase

GTP guanosine triphosphate

His histidine

HME Human Mammary Epithelial

HME-BRAF HME cells with BRAF (V600E)

HME-EGFR HME cells with EGFR (delE746-A750)

HME-KRAS HME cells with KRAS (G13D)

HME-PIK3CA HME cells with PIK3CA (H1047R)

HRI haem-regulated eIF2α kinase

Ileu Isoleucine

InR insulin receptor

IPTG Isopropyl β-D-1-thiogalactopyranoside

IRI ischemia-reperfusion injury

IRS insulin receptor substrate

ISR integrated stress response

LAA linoleamide alkyne

Leu Leucine

Lip1Liproxstatin1

LKB1 liver kinase beta1

Lys Lysine

MAPK mitogen-activated protein kinase

MAT methionine adenosyltransferase

MDA malondialdehyde

MDH1 malate dehydrogenase

MDSCs myeloid-derived suppressor cells

ME malic enzyme

MEK MAPK/ERK kinases

Met Methionine

MLKL mixed lineage kinase domain-like

MNK MAPK-interacting serine/threonine kinase

MS methionine synthase

mTORC Mechanistic target of rapamycin Complex

NAD+ oxidised nicotinamide adenine dinucleotide

NADH reduced nicotinamide adenine dinucleotide

NADP+ oxidised nicotinamide adenine dinucleotide phosphate

NADPH reduced nicotinamide adenine dinucleotide phosphate

NO nitric oxide

NOS nitric oxide synthase

NOX NADPH oxidase

NQO1 NADPH: quinone oxidoreductase 1

Nrf2 Nuclear factor like 2

NSCLC non-small lung cancer cell

OAA oxaloacetate

PARP poly ADP-ribose polymerase

PC phase contrast

PDAC pancreatic ductal adenocarcinomas

PDK1phosphoinositide-dependent kinase-1

PERK PKR-like endoplasmic reticulum kinase

PH pleckstrin-homology

Phe Phenylalanine

PHGDH phosphoglycerate dehydrogenase

PI3K phosphatidylinositol 3-kinase

PIP2 phosphatidy-linositol-4,5-bisphosphate

PIP3 phosphatidylinositol-3,4,5-bisphosphate

PKB protein kinase beta

PKM2pyruvate kinase m2

PKR protein kinase R

PSAT1 phosphoserine aminotransferase 1

PSCs Pancreatic stellate cells

PSPH phosphoserine phosphatase

PTEN phosphatase and tensin homolog deleted on chromosome ten

RBD RAS-binding domain

RCD regulated type of cell death

Rheb Ras homolog enriched in brain

RIPK receptor-interacting protein kinase

RNS reactive nitrogen species

ROS reactive oxygen species

RPMI 1640 Roswell Park Memorial Institute 1640 medium

RSK ribosomal protein S6 kinase

RSL RAS synthetic lethal molecules

RTK receptor tyrosine kinases

SAHC S-adenosylhomocysteine

SAHCH S-adenosylhomocysteine hydrolase

SAM S-adenosyl methionine

SD standard deviation

Ser Serine

SH2 Src homology 2

SHIP SH2 domain-containing inositol 5'-phosphatase

SHMT1 serine hydroxymethyltransferase1

siRNA small interfering RNA

SSP serine synthesis pathway

TCA tricarboxylic acid

TDH threonine dehydrogenase

TGF-α transforming growth factor alpha

THF tetrahydrofolate

Thr Threonine

TNB 5′-thio-2-nitrobenzoic acid

TNFR tumour necrosis factor receptor

Trp Tryptophan

TRX thioredoxin

TSC2 tuberous sclerosis complex 2

Tyr Tyrosine

ULK1 Unc-51-like kinase

Val Valine

WT wild-type

α-KG α-ketoglutarate

γ-GT γ-Glutamyl transpeptidase

1. CHAPTER 1: GENERAL INTRODUCTION

1.1 Targeting the vulnerabilities of cancer cells.

During tumour development cancer cells obtain genetic and epigenetic characteristics that provide them with an evolutionary proliferative and survival advantage over their normal counterparts. These advantages are often called the hallmarks of cancer because they endow abilities such as evading cell death, unlimited proliferative capacity, constitutive mitogenic signals and induction of tumour angiogenesis to ensure adequate supply of oxygen and nutrients (Hanahan and Weinberg, 2000, 2011). However, these advantages can come at a cost because they can endow cancer cells with particular and often unanticipated vulnerabilities. It is thought that by systematically identifying such vulnerabilities novel cancer therapies might be developed (De Raedt et al., 2011). Currently, most cancer therapies instead rely on chemotherapeutic agents that target the rapid cell division of cancer cells (Chabner and Roberts, 2005). However, single agent treatment is often insufficient to prolong long-term survival and patients frequently undergo relapse of disease (Brognard et al., 2001; Li et al., 2008). Moreover, it is now recognised that tumours often consist of multiple clones of malignant cells with different characteristics that can influence responses to treatment (Swanton, 2012). Finally, the large doses of chemotherapeutic agents used are often accompanied with significant toxicity to normal cells leading to alopecia, diarrhoea and cardiac damage (Pearce et al., 2017). Therefore, there is clinical demand for multi-agent treatments that simultaneously or sequentially exploit cancer cell vulnerabilities to provide patient benefit.

1.1.1 Oncogene addiction and synthetic lethality.

Illustrations of how such novel therapeutic strategies might be developed are through the identifications of both oncogene addiction and synthetic lethal genetic relationships between cancer-causing and normal genes (Hartwell et al., 1997). Tumour cells that are oncogene-addicted display continual dependence on the presence of an oncogene. For example, melanoma cells typically express mutant BRAF in more than 60% of patient cases from early stages of melanoma development (Davies et al., 2002) and recent development of BRAF inhibitors such as vemurafenib (Tsai et al., 2008), which specifically targets BRAF with a $V^{600}E$ mutation (Joseph et al., 2010), have shown good clinical results (Chapman et al., 2011). However, despite initial promising results using targeted BRAF inhibitors resistance was found to develop in approximately half of the patients (Sosman et al., 2012). In the majority of the cases tumours established alternative compensatory mechanisms that induced activation of MAPK pathway (Paraiso et al., 2010) highlighting the underlying addiction of these tumours to hyperactivation of this pathway. To effectively target the development of resistance in patients, combined treatment with inhibitors of MEK have been used instead of vemurafenib monotherapy (Long et al., 2014).

Another example of oncogene addiction is found in pancreatic ductal adenocarcinomas (PDAC) where 90% of tumours bear KRAS mutations leading to constitutive mitogenic signalling (Smit et al., 1988) and continued dependence upon KRAS during tumour development (Collins et al., 2012). The important role of KRAS and the other homologs in pancreatic and a variety of other cancers has been extensively studied with the hope of developing agents that could specifically target

and block mutant KRAS inhibiting its activity and kill KRAS-mutant tumour cells. However, little progress has been achieved despite multiple attempts, primarily due to the lack of good inhibitor binding pockets in RAS proteins and the very high affinity of KRAS for guanine nucleotides (McCormick, 2015). The failure to produce an effective inhibitor has attributed the characterisation “undruggable” to the RAS proteins (Cox et al., 2014). Efforts have since focused on “synthetic lethality” screens to identify features of malignancy that the presence of activating RAS mutation confers on cancer cells and could be exploited therapeutically (Downward, 2015).

“Synthetic lethality” describes the relationship between two genes whose concomitant loss or inhibition together but not individually impairs cell survival (Dobzhansky, 1946; Lucchesi, 1968). In malignancies such relationships can be challenged by pharmacologically inhibiting a normal gene product which works together with a mutated cancer gene and that promotes cell survival/proliferation of mutant cells (Rehman et al., 2010). An example of such a relationship with clinical relevance is found in familial breast cancer between poly adenosine diphosphate (ADP)-ribose polymerase (PARP), and mutations in the BReast CAncer susceptibility genes (*BRCA) BRCA1* and *BRCA2* (Bryant et al., 2005). Tumours bearing mutations in either *BRCA1* or *BRCA2* lack the ability to repair DNA damage via homologous recombination and are sensitive to inhibition of PARP because these tumours are dependent upon base-excision repair mechanisms for genomic integrity (Bryant et al., 2005; Farmer et al., 2005). This synthetic lethality relationship could be expanded to other alterations that generate phenotypes similar to BRCA gene loss of function, a feature termed “BRCAness” (Lord and Ashworth, 2016; McCabe et al., 2006). Synthetic lethal relationships can be identified by both genetic and drug-

based screening platforms and can provide novel insights into the essential requirements of cancer cells (Barbie et al., 2009; Possik et al., 2014; Scholl et al., 2009).

To conclude there is an increasing interest in identifying cancer cell vulnerabilities, particularly with respect to pancreatic and other cancers where treatment options are limited, and patient survival is poor (De Raedt et al., 2011; Huhn et al., 2013). It is hoped that knowledge of such vulnerabilities could ultimately be used in the design of novel therapeutics that are used either alone, or in combination with existing treatments, to improve patient survival. Insight into the functional consequences of oncogenic transformation could provide new directions in the search for such targetable dependencies.

1.2 The role of EGFR signalling and its downstream RAS-RAF-MEK-ERK MAPK kinase and PI3K-AKT pathways in cancer.

The EGFR protein belongs to the family of receptor tyrosine kinases (RTK), signalling molecules that are activated through ligand interaction and transduce signals to downstream intracellular targets (Schlessinger, 2000). The interaction of EGFR with its corresponding ligand epidermal growth factor (EGF) or transforming growth factor alpha (TGF-α) promotes receptor dimerization and subsequent phosphorylation on the receptor intracellular domains (Schlessinger and Ullrich, 1992). Phosphorylation of the intracellular part of the EGFR protein occurs in a conserved domain within the C-terminus of the protein, and is recognised by proteins with a conserved domain called Src homology 2 (SH2) domains (Moran et al., 1990). Such SH2 domains are required for interaction of the EGFR protein with adaptor proteins that aid in downstream signal transduction through activation of downstream effector proteins (Pawson and Schlessinger, 1993). In this way proliferative signals from EGFR initiate multiple signalling cascades with the most notable examples being the MAPK and PI3K-AKT pathways (Raymond et al., 2000).

Hyperactivation of EGFR signalling has been reported in several cancers, and particularly in non-small cell lung cancers (NSCLCs) where 20% of the cases have a mutation or amplification of the gene leading to higher downstream activation levels (Shigematsu et al., 2005). The most common mutations found in NSCLCs on the EGFR gene are a deletion of exon 19 and a single mutation in exon 21 that leads to substitution of leucine to arginine at codon 858 (L858R), (Shigematsu and Gazdar, 2006). In both of these cases the receptor is constitutively activated independently of EGF binding (Greulich et al., 2005). Effective inhibition of EGFR mediated-signalling

in NSCLC requires inhibition of the two downstream pathways of MAPK and AKT suggesting their central role in EGFR-driven oncogenesis (Ono et al., 2004).

1.2.2 RAS-RAF-MEK-ERK MAPK pathway.

The mitogen-activated protein kinases (MAPK) are crucial regulatory elements of eukaryotic cells responding to a variety of extracellular stimuli such as growth factors, hormones and cytokines (Krishna and Narang, 2008). There are four distinct MAPK pathways (ERK1/2, P38α/β/γ/δ, JNK1/2/3, and ERK5), each one comprising of a unique kinase cascade involving 3 different kinases (Roberts and Der, 2007). The most well-studied MAPK signalling pathway is the ERK1/2 MAPK pathway, due to its critical role in many types of cancer and functions in cell growth, proliferation, survival, differentiation and motility (Yoon and Seger, 2006).

Activation of the EGFR following ligand interaction leads to a cascade of phosphorylation of the elements involved in this pathway. Phosphorylated tyrosine residues on EGFR allow interaction with the SH2 domain of GRB2, an adaptor protein (Lowenstein et al., 1992) responsible for recruitment and activation of SOS, a protein with guanosine exchange factor (GEF) function for RAS, in the plasma membrane (Egan et al., 1993). RAS proteins are small GTPases, proteins with an ability to bind and hydrolyse GTP, which catalyse activation of downstream proteins when binding GTP, but are in an inactive confirmation when binding GDP (Bourne et al., 1991). RAS proteins are lipidated and associated with the plasma membrane (Seabra, 1998). Recruitment of SOS to the plasma membrane following interaction with the EGFR-GRB2 complex brings it in close proximity with RAS proteins to promote nucleotide exchange of GDP to GTP allowing activation of its downstream targets (Egan et al., 1993). Therefore, mitogenic stimuli through the EGFR pathway

lead to activation of RAS and its downstream effectors (Buday and Downward, 1993).

The family of RAS genes in mammalians is comprised of three highly homologous genes termed HRAS, KRAS and NRAS (Lowy and Willumsen, 1993). RAS genes were initially identified as viral oncogenes found in Rat Sarcoma tumours that could induce oncogenic transformation (Noda et al., 1985). These viral oncogenes originated from mutated genes obtained by viruses from hosts (Barbacid, 1987). The molecular function of RAS proteins is characterised as a signalling switch that controls the transduction of external stimuli to activation of cellular functions. Alterations and aberrant activity of RAS signalling is often associated with oncogenic transformation, highlighting the central role of these proteins and their connected pathways in oncogenesis (Downward, 2003)

The best characterised effectors of RAS are proteins of the RAF family of serine/threonine protein kinases that consists of three members, ARAF, BRAF and CRAF (Wellbrock et al., 2004) (Shaw and Cantley, 2006). Members of the RAF family interact directly with the active GTP-bound form of RAS through a RAS-binding domain (RBD) located in their N-terminal regulatory domain (Vojtek et al., 1993). RAF kinases are responsible for the phosphorylation and activation of the dual specificity MAPK/ERK kinases 1/2 (MEK1/2), which are found downstream in this signalling cascade (Kyriakis and Avruch, 2001). MEK1/2 are responsible for activation of the extracellular signal-regulated kinases (ERK) ERK1/2 (Crews et al., 1992). The ERK1/2 kinases have a very wide variety of substrates found in both the cytoplasm and the cell nucleus where the protein translocates to following activation (Pouyssegur et al., 2002). Notable examples include transcription factors, such as

ELK1 and MYC, enhancing the gene expression of the downstream target genes, as well as downstream kinases like p90 ribosomal protein S6 kinase (RSK) and MAPK-interacting serine/threonine kinase (MNK) (Yoon and Seger, 2006) .

Oncogenic mutations within RAS genes tend to cluster in particular codons and render it in a conformation that is constitutively active (Bos, 1989). The overall incidence of these mutations in cancer is considered to be around 20%, with certain tumour types demonstrating higher mutation incidence, indicative of oncogenic dependence on these genes (Bos, 1989). The most striking example is found in PDACs where mutations on the KRAS gene are present in more than 90% of cases (Smit et al., 1988). High levels of incidence are also commonly reported in colon, thyroid and lung cancers, as well as in myeloid leukemias (Lowy and Willumsen, 1993).

Hyperactivation of MAPK signalling is not solely dependent on RAS mutations. For example, RAS mutations account for only 15% of melanoma tumours, whereas mutation within the downstream BRAF gene is recorded in 66% of these tumours (Bos, 1989; Davies et al., 2002). The majority of BRAF mutations are located within the kinase domain of the protein, with the substitution of valine in codon 600 for glutamic acid (V600E) accounting for 80% of cases (Davies et al., 2002). Activation of the MAPK pathway is highly elevated in the presence of BRAF activating mutations independently of RAS activity, and is sufficient to promote oncogenesis (Wan et al., 2004). Inhibition of oncogenic BRAF activity can inhibit tumour growth, suggesting the addiction of these cancer cells to the constitutively active BRAF. Effective Inhibitors of BRAF have been developed and employed in the clinic, demonstrating significant anti-tumour responses, at least initially (Chapman et

al., 2011). However, in many patients resistance quickly develops as cancer cells establish alternative signalling pathways to induce MAPK activation (Nazarian et al., 2010; Paraiso et al., 2010) .

1.2.3 PI3K/AKT signalling

Aside from downstream activation of the MAPK pathway, EGFR can also induce activation of phosphatidylinositol 3-kinases (PI3Ks) and their downstream pathways. Activation of the PI3K-AKT pathway can promote several cellular processes, including cell survival, cell growth, proliferation, migration, and metabolism (reviewed in (Cantley, 2002; Luo et al., 2003)). Class I PI3Ks are lipid kinases that phosphorylate phosphatidyinositol-4,5-bisphosphate (PIP2) to phosphatidylinositol-3,4,5-trisphosphate (PIP3), a lipid that acts to recruit proteins bearing pleckstrin-homology (PH) domains to the plasma membrane. PI3Ks have crucial roles in oncogenesis and are found mutationally activated in some cancers (Zhao and Vogt, 2008a). PI3Ks members of class Ia consist of two subunits, a regulatory known as p85 and a catalytic subunit termed p110 (Yuan and Cantley, 2008). The regulatory p85 subunit contains an SH2 domain that binds to phosphorylated tyrosine residues within the C-terminus of EGFR, and then forces a conformational change within the p110 subunit to render it catalytically active (Carpenter et al., 1993). The function of PI3K proteins is counteracted by the tumours suppressor phosphatase and tensin homolog deleted on chromosome ten (PTEN), that dephosphorylates phosphatidylinositol-3,4,5-trisphosphate to phosphatidyinositol-4,5-bisphosphate (Myers et al., 1998), and by SH2 domain-containing inositol 5'-phosphatase (SHIP) which removes the 5’ phosphate of PIP3 to yield phosphatidyinositol-3,4-bisphosphate (Damen et al., 1996).

PIP3 is responsible for activation of protein kinase beta (PKB), also known as AKT due to homology to the viral oncogene v-AKT, and is recognised as the main downstream kinase effector of the PI3K pathway (Lawlor and Alessi, 2001). AKT is brought to the plasma membrane through interaction of its PH domain with PIP3, and is phosphorylated by phosphoinositide-dependent kinase-1 (PDK1) on threonine 308 (Alessi et al., 1997). PDK1 recruitment to the cell membrane is similar to that of AKT, and regulated by PIP3 interaction with its PH domain (Currie et al., 1999). A second phosphorylation on serine 473, thought to be catalysed mainly by mTORC2, stabilises AKT in its active form and allows dissociation from the plasma membrane (Sarbassov et al., 2005). Cell growth is promoted by AKT by phosphorylation and inactivation of TSC2, which has the effect of enhancing mTORC1 activity (Manning et al., 2002) and stimulating cell growth. Cell survival is supported by a role of AKT in stimulating the NF-κB pathway (Ozes et al., 1999), in facilitating the ability of MDM2 to ubiquitinylate p53 and mark it for downregulation (Trotman and Pandolfi, 2003), or preventing apoptosis by phosphorylating Bad and the proapoptotic transcriptional factor FOXO (Datta et al., 1999). Cell cycle progression is stimulated by AKT through its ability to phosphorylate and inhibit Glycogen synthase kinase-3 (GSK3) to eventually negatively regulate cyclin accumulation and progression to the S phase (Diehl et al., 1998).

Activation of the PI3K pathway can be additionally controlled by other factors. Other RTK proteins such as the insulin receptor (InR) induce activation of PI3K through interaction with the adaptor proteins insulin receptor substrate (IRS1/2) (Shepherd et al., 1998). Other receptors rely on tyrosine phosphorylated scaffold proteins such as CD19 in B cells. Active RAS facilitates PI3K activity via direct

binding to the Ras-binding domain within the p110 catalytic subunit (Rodriguezviciana et al., 1994). Mutations or deletions that inhibit the PTEN gene are associated with higher levels of PIP3, ultimately resulting in the generation of signals that are similar to active RTK signalling induced by growth factors (Stambolic et al., 1998). Such alterations are found in many human tumours and are often associated with poor outcomes and aggressive tumour phenotypes (Keniry and Parsons, 2008; Saal et al., 2007; Steck et al., 1997). Several cancers, including breast, ovarian, colorectal and hepatocellular cancers often accumulate mutations or amplifications in PIK3CA, the gene that codes for the p110α catalytic subunit (Bader et al., 2006). Some of these mutations confer a gain of function by either affecting the ability of p85 to inhibit p110 function or conferring constitutive kinase activity to p110 (Bader et al., 2006). For example, PIK3CA with mutations in exon 9 lead to a p110α protein that is no longer inhibited by p85 interaction. On the other hand, exon 20 mutations which results in substitution of histidine 1047 to arginine (H1047R) leads to a constitutively active p110α protein which leads to elevated levels of PIP3 (Zhao and Vogt, 2008b).

1.3 Cancer cells adapt their metabolism to their nutritional microenvironment.

One of the newly-appreciated hallmarks of cancer is the capacity that tumour cells have to re-programme their metabolism to support their biosynthetic and survival requirements (Hanahan and Weinberg, 2011). All eukaryotic cells require nutrients for homeostasis and growth. This applies particularly to rapidly-dividing neoplastic cells, and forces them to adapt their metabolism in order to fuel their growth and survival (Heiden et al., 2009; Vander Heiden, 2013). Additionally, it is thought that tumours are characterised by altered requirements for various nutrients in order to meet their increased biosynthetic needs (Hsu and Sabatini, 2008). It is hoped that by understanding the mechanisms responsible for such metabolic differences between normal and cancer cells novel therapeutics targeting cancer metabolism can be developed (Habrook and Lyssiotis, 2017; Vander Heiden, 2013).

1.3.1 Pancreatic cancer provides examples of metabolic adaptations

One such example of a tumour demonstrating metabolic adaptation is found in pancreatic ductal adenocarcinoma (PDAC) (Poursaitidis and Lamb, 2017). PDAC is characterised by a pronounced desmoplastic reaction, generating a stromal component that can account for the majority of the tumour mass (Provenzano et al., 2012). The surrounding stroma consists of pancreatic stellate cells (PSCs), immune cells and endothelial cells embedded in collagen, hyaluronan and other extracellular matrix (ECM) proteins. PSCs are fibroblast-like cells found in the healthy pancreas as well as PDAC lesions, and have an important role in the stromal desmoplastic reaction found in PDAC (Feig et al., 2012). Under physiological conditions, PSCs regulate the turnover of the ECM through regulation of expression and degradation of matrix-associated proteins such metalloproteases (Apte and Wilson, 2012). In

PDAC lesions PSCs are found in large numbers and in an activated state, in which they produce excessive quantities of stromal components (Haber et al., 1999). Accumulation of ECM components, generates excessive interstitial fluid pressure that is responsible for the collapse of the local vasculature (Jacobetz et al., 2013). Lack of developed blood vessels in PDAC tumours, is responsible for limiting the supply of both nutrients and oxygen to PDAC cancer cells (Feig et al., 2012). These adverse conditions force the metabolic adaptation of the PDAC cells, allowing them to grow and proliferate in a nutritionally poor microenvironment.

Although the extent of these metabolic adaptations is not completely understood, there are several mechanisms that have been characterised providing these cells with an evolutionary advantage. One such feature of pancreatic cancer cells within PDAC tumours is their high rate of macropinocytosis, a process through which cells engulf and degrade extracellular proteins in order to generate nutrients they lack (Commisso et al., 2013; Kamphorst et al., 2015). One recent report highlights the significance of PSC-generated collagen which PDAC cells can utilise through macropinocytosis, as a supply of required amino acids, particularly proline (Olivares et al., 2017). PDAC cells and PSCs are thought to establish a bilateral signalling network regulating each other's properties, promoting the survival of the former (Tape et al., 2016). In conditions of nutrient scarcity PDAC cells also promote autophagy in neighbouring PSCs, which then excrete the nutrient amino acid alanine. PDAC cells are then able to import and utilise alanine for biosynthetic needs (Sousa et al., 2016).

1.4 Cancer cells have increased requirement for glucose.

Elevated requirement of cancer cells for glucose was first observed by Otto Warburg, and recorded in a series of studies that were published beginning in the 1930's (Warburg, 1930). In these studies, Warburg demonstrated that cancer cells growing in the presence of oxygen produce their energy mainly through high levels of glycolysis followed by lactic acid production, rather than by the relative lower levels of glycolysis followed by oxidation of pyruvate that takes place in normal cells growing under similar conditions (Warburg, 1930, 1956a, b). Why cancer cells preferentially utilise glycolysis and lactic acid fermentation is likely because this produces metabolic intermediates useful for biosynthesis and critical for proliferation (Ward and Thompson, 2012). The lower adenosine triphosphate (ATP) yield from this process is thought to be compensated for by increased glucose uptake and utilization.

The reprogramming of cell metabolism results from both the presence of activating mutations in oncogenes, and by the loss-of-function of tumour suppressor genes (Hsu and Sabatini, 2008). Major oncogenic signalling pathways are also responsible for altering the function of mitochondria in a manner that supports anabolic processes (Ward and Thompson, 2012). For example, constitutive activation of the PI3K/AKT pathway is known to facilitate the Warburg effect in cells by promoting aerobic glycolysis (Elstrom et al., 2004). Moreover, enhanced glucose uptake and glycolysis are also observed in cancer cells bearing activating mutations in the RAS-MAPK pathway (Ying et al., 2012). Pharmacological inhibition of glycolysis and of glucose uptake is demonstrating promising results as novel forms

of cancer therapy, which, in combination with existing agents, may improve patient survival (Zhao et al., 2013).

1.5 Selective requirements for nutrient amino acids

In addition to an increased requirement for glucose, cancer cells in a variety of human malignancies have increased steady state levels of most amino acid nutrients compared to their untransformed counterparts in normal tissue (Hirayama et al., 2009; Kami et al., 2013). In this way, cancer cells may demonstrate an increased general requirement for nutrient amino acids. However amino acid needs may be more selective in some situations. For example, analysis of conditioned media from pancreatic cancer cell lines has revealed that some amino acids are preferentially taken up in favour of others (Wang and Permert, 2002). Thus, it is possible that restriction of certain nutrients might selectively compromise the viability of PDAC and other cancer cells.

1.5.1 Sensing plenitude and limitation of amino acid nutrients.

In order to understand the requirements of cancer cells for certain amino acids it is important to know how cells more generally sense their presence or absence, and how they then respond to such changes. Nutrient amino acids are required for essential cell processes but can also act as signalling molecules (Efeyan et al., 2015). This aspect is manifest in cells by development of mechanisms that allow them to sense the availability of amino acids, and thereby regulate their growth and metabolism accordingly (Lamb, 2012). In the absence of amino acid nutrients cells inhibit anabolic processes such as protein synthesis (Klionsky, 2007), and promote catabolic processes like autophagy as adaptive measures until amino acid levels are restored (Pain, 1994).

In mammalian cells amino acids signal through Mechanistic Target Of Rapamycin Complex 1 (mTORC1) to induce activation of S6 kinases (S6K1 and S6K2) as well as dissociation of the eukaryotic initiation factor 4E (eIF4E)-binding protein-1 (4E-BP1) from eIF4E through phosphorylation (Hara et al., 1998). TOR was first described in yeast as the target molecule of the immunosuppressant rapamycin (Heitman et al., 1991). TOR can form two different complexes, termed mTORC1 and mTORC2, and that, in mammalian cells, control distinct cell functions (Saxton and Sabatini, 2017). The mTORC1 complex comprises of mTOR, Raptor and mLST8 whereas the mTORC2 complex comprises of mTOR, Rictor, SIN1 and mLST8 (Jacinto et al., 2006; Kim et al., 2002; Kim et al., 2003; Loewith et al., 2002; Sarbassov et al., 2004; Wullschleger et al., 2006).

Although the exact mechanism through which amino acids regulate mTORC1 activation is unclear, several aspects are known. mTORC1 is recruited to the lysosomal surface for activation through interaction with the Rag GTPases (Sancak et al., 2010; Sancak et al., 2008). There are four Rag-family GTPases, RagA, RagB, RagC and RagD with functional similarity between RagA and RagB, and between RagC and RagD. These GTPases form heterodimers consisting of RagA with either RagC or RagD, or of RagB with either RagC or RagD (Kim et al., 2008; Sancak et al., 2008). These heterodimers are tethered to lysosomes by binding to Ragulator, a pentameric complex that consists of p18, p14, MP1, C7orf59 and HBXIP proteins (Bar-Peled et al., 2012; Sancak et al., 2010). The GTP loading status of the Rag GTPases has been implicated in the binding of mTORC1 and its subsequent activation. (Bar-Peled et al., 2013; Bar-Peled et al., 2012; Petit et al., 2013; Tsun et al., 2013).

Another requirement for activation of mTORC1 is the presence of the small GTPase Ras homolog enriched in brain (Rheb) in its GTP loaded form (Inoki et al., 2003). Rheb is under negative regulation by the GTPase-activating protein (GAP) activity of the tuberous sclerosis complex (TSC1-2) that is comprised of TSC1, TSC2 and the recently described TBC1D7 (Dibble et al., 2012). The TSC complex acts as a GAP for Rheb to promote the hydrolysis of GTP and render Rheb inactive (Zhang et al., 2003). The protein kinase AKT, stimulated by insulin and other growth factors, is thought to play a role in maintaining Rheb activation through an ability to phosphorylate and in some way inactivate TSC1-2 (Inoki et al., 2002; Manning et al., 2002).

mTORC1 activation controls cell growth through activation of several eukaryotic translation initiation factors and initiation of cap dependent protein translation. eIF4E can directly bind to the 5’ cap structure on eukaryotic mRNAs and recruit the eIF4F complex to initiate translation (Gingras et al., 1999). Active mTORC1 directly phosphorylates 4EBP1 leading to its dissociation from eIF4E, and also further contributes to translation through activation of eukaryotic translation initiation factors eIF4A and eIF4B via activation of S6K (Zoncu et al., 2011).

Aside from inducing mRNA translation mechanisms within the cell, mTORC1 actively inhibits scavenging processes that cells only require when starved of nutrients. Autophagy (also termed macroautophagy) is such a scavenging mechanism allowing optimal utilisation and recycling of nutrients. Autophagy is a multi-step regulated process through which cells recycle their own proteins and organelles through lysosomal degradation (Rabinowitz and White, 2010). Autophagy is also important for homeostatic recycling of defective organelles or misfolded

proteins, and can also provide missing nutrients to nutrient-starved cells (Mizushima and Komatsu, 2011). The autophagic process involves the formation of the autophagosome, a membranous structure incorporating the cell components targeted for degradation. Autophagosomes fuse with lysosomes to allow proteolysis of targeted proteins/organelles. Under nutrient replete conditions mTORC1 inhibits autophagy through phosphorylation of autophagy-related protein 13 (ATG13) and Unc-51-like kinase (ULK1), two proteins essential for the formation of the autophagosome (Hosokawa et al., 2009). However, withdrawal of amino acids inhibits mTORC1 and induces activation of autophagy (Ravikumar et al., 2004). Restoration of amino acids by autophagic flux reinstates mTORC1 activity and terminates any further autophagy (Yu et al., 2010).

It is apparent that regulation of mTORC1 signalling is crucial for cell homeostasis. Therefore, it is not surprising that mTORC1 is commonly found deregulated in many cancers through constitutive activation of key signalling pathways such as the Ras-MAPK and/or the PI3K pathways (Menon and Manning, 2008). Such deregulated mTORC1 signalling can uncouple cells from the requirement of mitogenic stimuli to promote growth and proliferation of malignant cells (Menon and Manning, 2008).

General control non-derepressable 2 (GCN2, EIF2AK4) is a serine/threonine kinase responsible in eukaryotic cells for the phosphorylation of eIF2α, a subunit of the eukaryotic initiation factor 2 (eIF2) (Hinnebusch, 2005). eIF2 is responsible for transferring the first methionine charged tRNA to the ribosome and initiate mRNA translation (Sonenberg and Hinnebusch, 2009). GCN2, along with three other kinases (haem-regulated eIF2α kinase (HRI, EIF2AK1), protein kinase R (PKR,

EIF2AK2) and PKR-like endoplasmic reticulum kinase (PERK, EIF2AK3)), interpret different signals and induce the activation of the integrated stress response (ISR) pathway, that involves several distinct cellular responses (Baird and Wek, 2012). All these kinases sense different stimuli; nutrient amino acid deprivation by GCN2, endoplasmic reticulum (ER) stress by PERK, deprivation of heme by HRI and viral infection through PKR (Baird and Wek, 2012). Despite their unique regulation from different factors they share a conserved kinase domain, and, collectively, they converge on phosphorylation of Ser51 on eIF2α. Phosphorylation of eIF2α blocks the GEF activity of eIF2B leading to inhibition of eIF2 function, and ultimately blocking the initiation of general mRNA translation (Hinnebusch, 2005). At the same time p-eIF2α promotes the translation of activating transcription factor 4 (ATF4), a transcription factor responsible for regulating gene expression in response to stress (Harding et al., 2003).

The mechanism of GCN2 activation during periods of amino acid starvation has been well-studied (Hinnebusch, 2005). GCN2 contains a domain homologous to histidyl-tRNA synthetases, and binding uncharged tRNA molecules induces activation of the kinase (Wek et al., 1989). Thus, tRNA binding causes GCN2 autophosphorylation which then forces a conformational change to the protein transforming it to an active state that allows binding and phosphorylation of eIF2α (Baird and Wek, 2012). This mechanism can be influenced by mTORC1 because pharmacological inhibition of this kinase under amino acid replete conditions induces activation of GCN2 (Wengrod et al., 2015). However, GCN2 activation imposes inhibition of mTORC1 through both ATF-driven and -independent pathways (Averous

et al., 2016; Ye et al., 2015). Thus, there is evidence of significant crosstalk between the mTORC1 and GCN2 amino acid-sensing pathways.

The pathways of mTORC1 and GCN2 activation are tightly regulated, and both provide cells with the ability to regulate processes that control amino acid utilisation in the face of nutrient scarcity(Lamb, 2012; Yan and Lamb, 2012). Cells can inhibit their metabolic activity and growth through inhibition of mTORC1 and limit protein synthesis via activation of GCN2, minimising nutrient utilisation until their nutrient sources are replenished (Carroll et al., 2015; Gonzalez and Hall, 2017) Failure to regulate these pathways could be catastrophic for cells. For example, melanoma cancer cells having hyperactive Ras-MAPK pathway activation maintain high levels of mTORC1 signalling even in the absence of the essential amino acid leucine. As a consequence, this constant activation of mTORC1 fails to inhibit cell growth and activate autophagy and results in widespread apoptosis of the cells (Sheen et al., 2011).

1.5.2 Asparagine restriction in acute lymphoblastic leukemias.

The clinical relevance of nutrient restriction is well described in Acute lymphoblastic leukemias (ALLs). The malignant cells of ALL do not express asparagine synthase, an enzyme required for asparagine synthesis, and ALL cells rely on the provision of exogenous asparagine for their survival (Broome, 1968). Clinically this reliance can be exploited by administration of a formulation of asparaginase to lower circulating asparagine levels which induces selective apoptosis of the malignant cells (Holleman et al., 2003; Tallal et al., 1970). Whether a similar approach can be applied to solid tumours, such as PDAC, remains to be

determined. Conceivably, such an approach requires identification of particular amino acids key to malignant cell survival in each case.

1.5.3 Glutamine addiction and anaplerosis.

Many cancer cell lines display a dependence upon glutamine, despite it being a non-essential amino acid that some cells have the capacity to synthesise (Lacey and Wilmore, 1990). Glutamine is the most abundant amino acid found in plasma, and, in cells, it is used for protein synthesis, as a precursor for biosynthetic molecules and as an energy source for adenosine triphosphate (ATP) generation (Bergstrom et al., 1974). As a precursor for biosynthetic molecules, glutamine acts as a nitrogen donor by providing amine groups for the synthesis of other non-essential amino acids (NEAA) and nucleotides. As an energy source for ATP, glutamine provides carbon molecules through incorporation of its metabolites into the tricarboxylic acid (TCA) cycle via a process known as anaplerosis (Hensley et al., 2013).

Glutamine is imported into cancer cells mainly via the Slc1a5 [ASCT2] transporter (Bode et al., 1995; Collins et al., 1998). Elevated protein levels of ASCT2 have been reported in a wide range of cancers, possibly reflecting the increased need of many malignant cells for glutamine (Fuchs and Bode, 2005; Hassanein et al., 2013). ASCT2 expression is upregulated by the c-Myc oncogene (Gao et al., 2009; Wise et al., 2008) whose own expression is upregulated/deregulated in many cancers (Dallafavera et al., 1982; Schwab et al., 1983).

Glutamine uptake by ASCT2 can also be controlled by the abundance of glucose due to the role of both nutrients in glycosylation (Wellen et al., 2010). Glycosylation is a post-translational modification essential for the correct localisation and function of some membrane proteins (Kornfeld and Kornfeld, 1985; Ohtsubo and

Marth, 2006). Glucose and glutamine converge on the hexosamine biosynthesis pathway that controls the synthesis of glucosamine, a critical building block used for protein glycosylation (Hanover, 2001). Due to the role of glycosylation in the localisation of the glutamine transporter itself the availability of glucose and thereby glucosamine can inhibit the uptake of glutamine (Wellen et al., 2010).

The initial reaction in the catabolism of glutamine is the deamination of glutamine to glutamate (Figure 1). Enzymes like glutamine-fructose-6-phosphate aminotransferase (GFPT) 1 and 2 are amidotransferases that transfer the amide group from glutamine to glucose and generate glucosamine (Broschat et al., 2002; Slawson et al., 2010). Alternatively, glutaminases such as those encoded by the GLS1 and GLS2 genes catalyse glutaminolysis whereby glutamine is converted to glutamate and ammonia (Mates et al., 2013). Interestingly, GLS1 up-regulation is often found in rapidly dividing cells, unlike the p53-driven expression of GLS2 which is correlated with enhancing the redox potential of normal quiescent cells (Hensley et al., 2013).

Glutamate is used itself for the synthesis of glutathione (GSH), which is the most prevalent antioxidant within cells (Lu, 2013). Alternatively, it can be further catabolised by either glutamate dehydrogenase (GLUD1 or GDH), or alanine and aspartate transaminases to generate α-ketoglutarate (α-KG), a component of the TCA cycle (Shashidharan et al., 1994). Under nutrient replete conditions, transaminase enzymes transfer the amine group from glutamate on to newly synthesised NEAAs like serine, glycine, alanine, and aspartate (Yang et al., 2009). However, when cells experience nutrient stress, glutamate is directly deaminated by GLUD1 to quickly provide α-KG that is shuttled into the TCA cycle (Yang et al.,

2009). Incorporation of α-KG into the TCA cycle can also be exploited for ATP production through oxidative phosphorylation (Reitzer et al., 1979). Additionally, it provides the carbon skeleton to replenish the intramitochondrial pool of oxaloacetate (OAA) to counterbalance the negative equilibrium of other components such as citrate, being used for biosynthetic purposes (DeBerardinis et al., 2007). Aside from a source of energy and carbon, α-KG is also a substrate of dioxygenases that play an important role in epigenetic regulation of gene expression (Son et al., 2013).

Requirement for glutamine can also be predicated by the presence of activated oncogenes. Activating mutations in KRAS increase the requirement of the malignant cells in PDAC for glutamine (Son et al., 2013). In these cells mutant KRAS suppresses expression of GLUD1 leaving the mitochondrial aspartate transaminase GOT2 free to transfer the amine group of glutamate to oxaloacetate and convert it to aspartate. This is then transferred to the cytosol to be converted back to OAA by the cytosolic homolog of aspartate transaminase GOT1, whose transcription is enhanced by mutant KRAS (Son et al., 2013). Subsequently, OAA is reduced to malate by malate dehydrogenase (MDH1) while oxidising reduced nicotinamide adenine dinucleotide (NADH) to oxidised (NAD+). The last step in this pathway involves the conversion of malate by the malic enzyme (ME) to produce pyruvate and reduce oxidised nicotinamide adenine dinucleotide phosphate (NADP+) to reduced (NADPH). This pathway of glutamate usage is important for pancreatic cancer cells because they depend on it to generate NADPH and maintain their redox capacity. PDAC cells cannot make NADPH by the oxidative pentose phosphate pathway because it is downregulated (Ying et al., 2012), a feature that makes them vulnerable to changes in the availability of glutamine.

It is clear that glutamine has diverse roles as a nutrient, and that targeting the supply of this amino acid could be exploited therapeutically to inhibit the growth and oncogenicity of addicted cells. An example of such targeting is inhibition of GLS with small molecules that can inhibit cancer cell growth in a variety of *in-vivo* and *in-vitro* models (Robinson et al., 2007; Wang et al., 2010). The potencies of these inhibitors can be maximised and their side effects minimised when they are used in conjunction with reactive oxygen species (ROS)-inducing molecules such as Dihydroartemisinin (DHA) (Wang et al., 2016), inhibitors of NADPH:quinone oxidoreductase 1 (NQO1) (Chakrabarti et al., 2015) and chemotherapeutic agents (Chen et al., 2016).

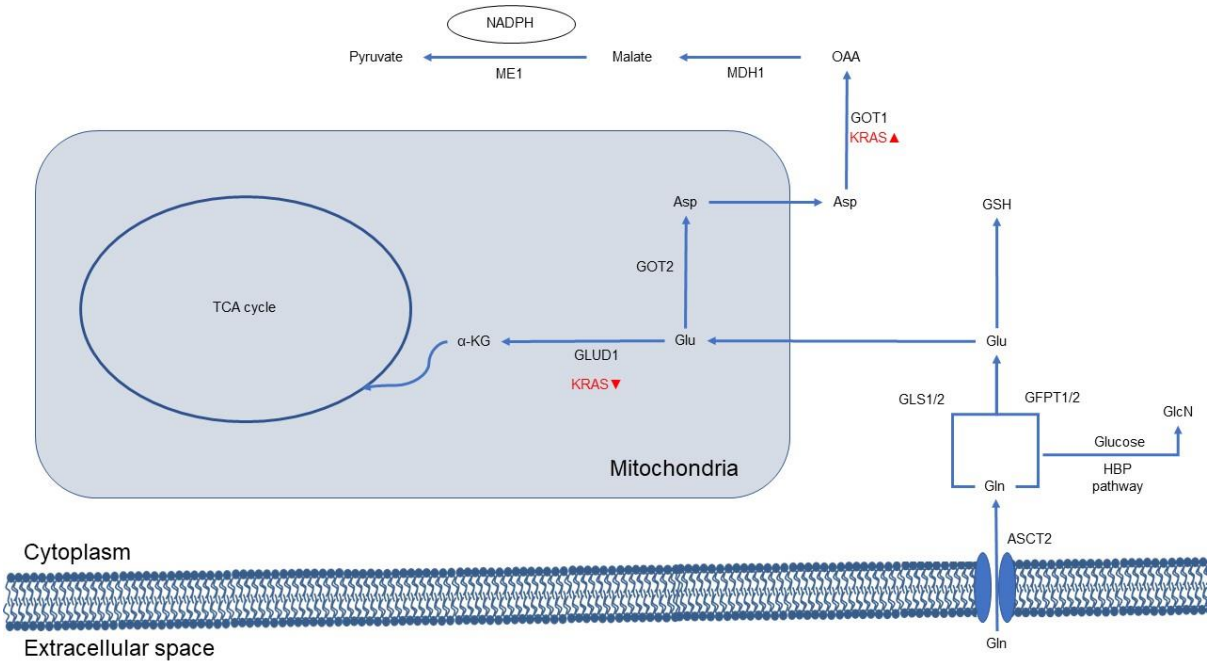

Figure 1.1 Glutamine utilisation pathways.

Glutamine (Gln) uptake in epithelial and cancer cells lines is mainly facilitated via Slc1a5 (ASCT2). Glutamine inside cells is then converted to glutamate (Glu) by acting as an amine donor like in glucosamine (GlcN) production via the HBP or by enzymatic degradation from the glutaminase enzymes GLS1 and GLS2. The derived Glu can be used for GSH production or, when energy is required, glutamate can be converted to α-ketoglutarate (α-KG) by GLUD1 and used as an anaplerotic source for the TCA cycle. Activating KRAS mutations inhibit the function of GLUD1 and glutamate is converted to aspartate (Asp) via GOT2 inside the mitochondria. Asp can exit the mitochondria and generate cytoplasmic oxaloacetic acid (OAA) via the function of GOT1, a cytoplasmic transaminase that is upregulated by the oncogenic signalling of KRAS. Cytoplasmic OAA can be converted to malate by malate dehydrogenase (MDH1) and then to pyruvate by the malic enzyme (ME1), a step that generates NADPH and is required to maintain the cellular redox balance.

1.5.4 The requirement of cancer and immune cells for arginine and nitric oxide.

Arginine is a positively charged non-essential amino acid, and yet many cancer cells appear to be sensitive to its depletion. Sensitivity to depletion of arginine is often correlated with reduced expression of the enzymes involved in the biosynthesis of this amino acid (Patil et al., 2016). Arginine is synthesised from its precursor citrulline by argininosuccinate synthase (ASS) and argininosuccinate lyase (ASL) (Albaugh et al., 2017). ASS has been shown to be downregulated in a variety of tumours including melanoma (Feun et al., 2012), lymphoma (Delage et al., 2012) mesothelioma (Szlosarek et al., 2006) and pancreatic cancer (Bowles et al., 2008). In contrast, downregulation of ASL has been reported thus far only in glioblastoma (Syed et al., 2013).

Sensitivity to arginine depletion has been explored also as an anti-cancer therapy. Engineered enzymes like human arginase and arginine deiminase (ADI) from mycoplasma can lower systemic levels of arginine and inhibit malignant cell growth in various tumour models, including pancreatic, melanoma, small cell lung cancer and hepatocellular carcinoma (Phillips et al., 2013). Both enzymes have the potential to reduce serum levels of arginine, with ADI being more effective than arginase (Patil et al., 2016). Arginine loss can induce either cycle arrest, followed by apoptosis, or in other settings a strong autophagic response that can lead to autophagic cell death (Wang et al., 2014). However, these approaches have caveats, because resistance can quickly be developed. The most common resistance mechanism involves upregulation of ASS expression, restoring innate arginine biosynthesis (Tsai et al., 2009). A further resistance mechanism involves induction of an immunogenic response where antibodies are developed against the

enzymes, and in particular ADI because of its derivation from mycoplasma, that inhibit their activity (Szlosarek et al., 2013).

The importance of arginine is associated with its special role in the generation of nitric oxide (NO) (Fukumura et al., 2006). NO is generated by nitric-oxide synthase (NOS) enzymes during oxidation of the guanidine nitrogen of arginine to convert it to citrulline (Fukumura et al., 2006). Citrulline can subsequently be recycled by ASS and ASL to regenerate the intracellular pool of arginine. The released NO is important in angiogenesis, and loss of arginine has demonstrated inhibitory effects on VEGF-induced vascularisation of tumours (Fukumura et al., 2001; Thomas et al., 2002).

Arginine deprivation however is a double-edged sword as it can act both to suppress tumour growth in arginine-dependent tumours but in other cases can provide promote tumour survival . In animal models of breast cancer, lower levels of arginine in the tumour microenvironment, correlate with higher levels of malignant cell growth which can be reversed by re-supplementation (Cao et al., 2016). This phenomenon was attributed to the role of arginine and NO in promoting anti-tumoural innate immune responses within the tumour microenvironment (Kirk et al., 1992). T-cells and macrophages require arginine for activation and can target cancer cells (Bronte and Zanovello, 2005). In addition, immunosuppressive myeloid-derived suppressor cells (MDSCs) also produce high levels of arginase as an adaptive mechanism to reduce local levels of arginine in the tumour microenvironment and block immune responses (Cao et al., 2016)

1.5.5 Serine requirements in cancer.

Serine is a non-essential amino acid with a significant role in one-carbon metabolism, a biosynthetic process that takes carbon molecules from serine and glycine and redirects them into pathways such as the folate and methionine biosynthesis pathways (Yang and Vousden, 2016). Despite the capacity of cells to *de-novo* synthesise serine, rapidly proliferating cells preferably utilise dietary serine for one-carbon metabolism (Jain et al., 2012; Maddocks et al., 2013). Serine is particularly useful as a one-carbon donor to the folate pathway because of ubiquitous expression of serine hydroxymethyltransferase1 (SHMT1) an enzyme that transfers a β-hydroxymethyl group to tetrahydrofolate (THF), converting serine to glycine (Yang and Vousden, 2016).

Cells have two main mechanisms to generate serine (Figure 1.2). The first is termed the serine synthesis pathway (SSP). This pathway branches from glycolysis at the point were 3-glycerolphosphate (3PG) is generated (Yang and Vousden, 2016). In the first step of the SSP pathway 3PG is converted to 3-phosphohydroxypyruvate (3PHP), a serine precursor, by phosphoglycerate dehydrogenase (PHGDH). This reaction results in the reduction of oxidised nicotinamide adenine dinucleotide (NAD+) to its reduced form NADH. Subsequently, 3PHP is transaminated into phosphoserine by phosphoserine aminotransferase 1 (PSAT1) with a concomitant conversion of glutamate to α-KG. Finally, phosphoserine is dephosphorylated to serine by phosphoserine phosphatase (PSPH) (Yang and Vousden, 2016). The second pathway for serine generation occurs through the bilateral action of the enzyme SHMT1. This enzyme can catalyse a reverse reaction

transferring the hydroxymethyl group from folate back to glycine to convert it to serine. However, this second pathway is not favoured because it exhausts the availability of one carbon units (Labuschagne et al., 2014).

Cancer cells defective in p53 function appear to be dependent upon provision of exogenous serine, likely because of the importance of this amino acid in generating the antioxidant GSH. Mechanistically, deprivation of serine has been shown to inhibit pyruvate kinase m2 (PKM2), allowing accumulation of 3PG due to the blockade of glycolysis (Chaneton et al., 2012). Accumulated 3PG is then converted by SSP pathway to serine, replenishing intracellular levels of serine (Chaneton et al., 2012). The reduction in glycolysis due to blockade of PKM2 however leads to a decrease in ATP levels (Mazurek, 2011). However, cells can counterbalance ATP depletion by activation of oxidative phosphorylation which in turn leads to higher levels of ROS. Increased ROS in turn requires an increase in GSH synthesis to maintain redox balance (Chaneton et al., 2012). This is provided by glycine, generated from exogenous serine for GSH as well as nucleotide synthesis (Maddocks et al., 2013). Thus, deprivation of serine results in lower levels of GSH and nucleotides which activates p53 in order to arrest cycle progression and inhibit cell growth in a p21-dependent manner (Deng et al., 1995; Linke et al., 1996). Loss of p53 or downstream p21 expression is associated with failure to induce this protective metabolic adaptation. Cells do not arrest, and as result they use up the derived glycine in anabolic processes like nucleotide synthesis instead of GSH synthesis (Maddocks et al., 2013). As a result, viability of p53 null cells is compromised due to a high burden of ROS and inability to adapt to the new conditions.

Despite the fact that glycine and not serine is the metabolite used in the above biosynthetic pathways, exogenous glycine alone cannot protect the viability of these cells (Labuschagne et al., 2014). This appears due to the role of serine in generating one carbon units for the folate pathway (Tibbetts and Appling, 2010). Supplementing cells growing in serine-free media with formate, an alternative one carbon donor, allows utilisation of exogenous glycine in biosynthetic pathways for nucleotide synthesis (Labuschagne et al., 2014). Serine addiction has recently been exploited in a therapeutic model whereby serine and glycine-free diets have been shown to impair the growth of $p53^{null}$ xenograft tumours in mice (Maddocks et al., 2017). However, in contrast serine and glycine-free diets do not inhibit KRAS-driven pancreatic tumours in a mouse model. This appears due to higher levels of serine synthesis within these tumours (Maddocks et al., 2017). High levels of serine synthesis have also been observed in human tumours, including breast cancers negative for oestrogen receptor (ER-) (Possemato et al., 2011), melanoma with chromosome 1p amplifications (Locasale et al., 2011) and pancreatic cancers with loss of liver kinase B1 (LKB1) (Kottakis et al., 2016) where enzymes within the SSP have been shown to be overexpressed. In these models, downregulation of the SSP enzymes have been shown to compromise malignant cell viability, demonstrating the dependence of some malignant cells on de novo serine synthesis (Possemato et al., 2011). Overall, the varied responses to serine depletion indicates that the requirement for exogenous serine, or for serine biosynthesis, is both oncogene- and cell-dependent.

Therapeutically, serine dependence may be exploitable. An inhibitor of PHGDH, the first enzyme in the SSP pathway, has been recently developed (Pacold

et al., 2016). This inhibitor has been shown to block the growth of not only tumours that rely on *de-novo* serine synthesis, but also tumours with high serine uptake (Pacold et al., 2016).

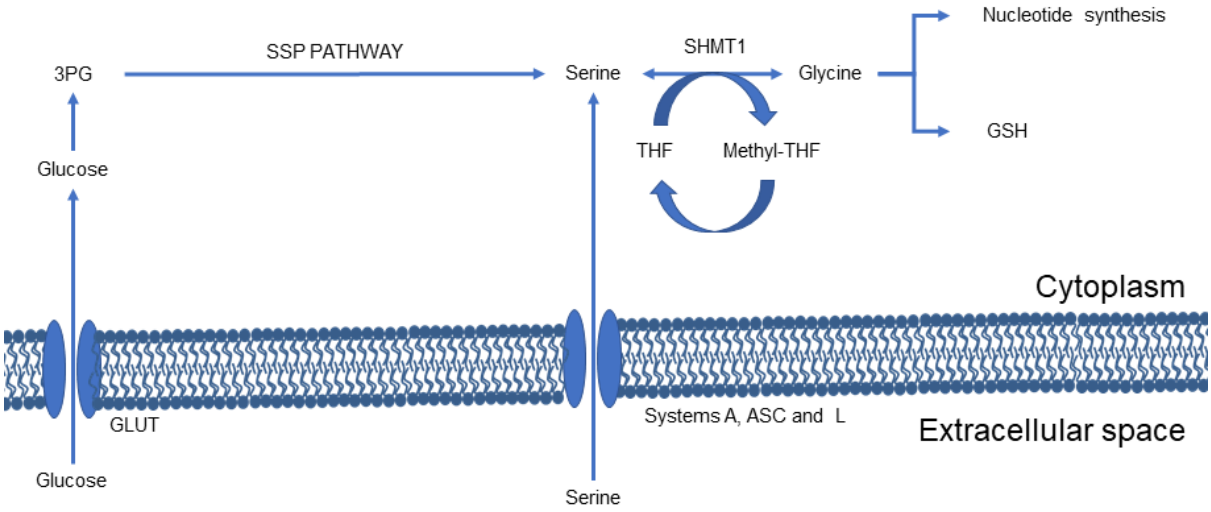

Figure 1.2 Serine uptake and biosynthesis.

Cells can obtain serine from dietary sources or synthesise it. Serine is fundamental for cell survival as it provides one carbon molecules on THF, a component of the folate cycle, and generates glycine that cells use for the biosynthesis of nucleotides and GSH. For serine synthesis cells utilise two main pathways: the SSP a pathway that utilises 3-PG generated from glycolysis to generate serine and the other one through the bilateral function of SHMT1 that can generate serine from glycine albeit in the expense of one carbon donors.

1.5.6 Methionine has a fundamental role in epigenetic regulation.

Methionine is an essential amino acid, and, aside from its role in protein synthesis, has additional roles that appear important for cancer cell survival. Methionine is the main donor of methyl groups for posttranslational modification of proteins and for DNA methylation important for epigenetic regulation of gene expression (Mato et al., 2002). These methyl groups are derived from the conversion of methionine to S-adenosylmethionine (SAM) by methionine adenosyltransferase (MAT) and by the demethylation of SAM into S-adenosylhomocysteine (SAHC) by protein and DNA methyltransferases (Yi et al., 2000) (Figure 1.3).

Within the methionine cycle, SAHC is hydrolysed to homocysteine by S-adenosylhomocysteine hydrolase (SAHCH) and can then be either used within the transulfuration pathway to generate cysteine, or be remethylated back to methionine (Toohey, 2006). Re-methylation of homocysteine utilises 5-methyltetrahydrofolate (5mTHF) as a one-carbon donor, vitamin B12 as a cofactor and is catalysed by methionine synthase (MS) (Toohey, 2006). SAM is also important because it can be incorporated into the polyamine synthesis pathway to generate adenosine, spermine and spermidine, prior to being recycled back to methionine (Pegg, 2009).

A feature of some cancer cell lines is that they are auxotrophic for methionine (Cavuoto and Fenech, 2012; Cellarier et al., 2003). In normal cells depletion of methionine can be rescued by provision of homocysteine, 5mTHF and vitamin B12 (Kreis et al., 1980; Kreis and Goodenow, 1978). However, cancer cell lines auxotrophic for methionine often have lower levels in expression of MS leaving them unable to effectively recycle methionine and maintain growth even when

supplemented with homocysteine, 5mTHF and vitamin B12 (Ashe et al., 1974; Halpern et al., 1974).

To induce methionine restriction therapeutically, recombinant enzymes that degrade methionine, termed methionases, have been developed. L-methionine-α-deamino-γ-mercaptomethane-lyase from *Pseudomonas putida* was the first enzyme to be used for this purpose (Tan et al., 1997) , but its use is limited because it induces an immunogenic response that inactivates the enzyme (Tan et al., 1998). The immunogenicity of methionases has been mitigated with the development of a humanised version of this enzyme engineered from cystathionine γ-lyase that selectively degrades methionine (Stone et al., 2012).

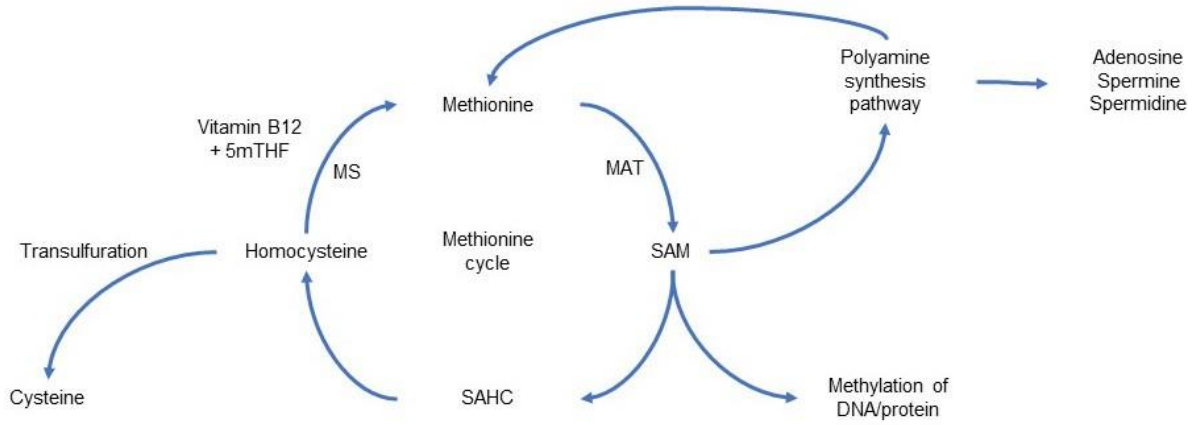

Figure 1.3 The methionine cycle provides methyl donors, polyamines and cysteine.

Methionine (Met) metabolism begins with conversion of Met to SAM. SAM can be incorporated in the polyamine synthesis pathway or be used by methyltransferase enzymes for DNA/protein modifications. Following, transfer of the methyl-group SAM is converted to SAHC and then to homocysteine. Homocysteine can be recycled back to methionine through the function of MS and the presence of vitamin B12 and a one carbon donor in the form of 5mTHF. Alternatively, homocysteine can be used for cysteine synthesis through the transulfuration pathway.

1.5.7 Serine and one carbon metabolism are responsible for recycling of methionine.

An important consideration of amino acid dependency is interconnection of the metabolic pathways which generate/use amino acids for cell metabolism. For example, cells which show a dependence on serine, exogenous or otherwise, appear unable to provide one-carbon intermediates to recycle methionine (Maddocks et al., 2016), potentially making these cells susceptible to methionine depletion that cannot be rescued by the presence of homocysteine. Serine can participate in methionine recycling due to its function as a one carbon donor to the folate pathway (Maddocks et al., 2016). Moreover, in PDAC cells with activated KRAS where LKB1 is lost, increased expression of DNA methyltransferases (DNMT) DNMT1 and DNMT3A augments the requirement of these cells for SAM with the consequence that expression of the components of the SSP are upregulated as the cell's requirement for serine as a one-carbon donor increases (Kottakis et al., 2016). This latter example demonstrates how subversion of the methionine metabolic pathway for epigenetic methylation and cancer cell pathogenesis results in co-opting the serine metabolic pathway to ensure malignant cell survival. In this way, a synthetic lethality requiring different amino acid nutrients might also be envisioned.

1.5.8 Threonine requirement for mouse embryonic stem cells is associated with methionine metabolism and epigenetic regulation.

Another example of the interconnection between amino acid metabolic pathways and nutrient dependence is observed in undifferentiated mouse embryonic stem (ES) cells (Wang et al., 2009). These cells are dependent upon threonine for viability and proliferation whilst they remain pluripotent because of their requirement

for methionine to maintain DNA methylation prior to the beginning of differentiation (Shyh-Chang et al., 2013). Mouse ES cells express the enzyme threonine dehydrogenase (TDH) which selectively breaks down threonine to generate glycine and Acetyl-CoA (Wang et al., 2009). Glycine provides one carbon donors to the folate pathway for the regeneration of methionine within the cycle donating methyl groups for DNA methylation (Shyh-Chang et al., 2013). Despite that this deficiency does not apply to human ES cells as they do not have the TDH enzyme, potentially other mechanisms might operate in cancer cells given the extensive range of differentiation and aberrant DNA methylation patterns that occur in these.

1.5.9 Cysteine requirement of cancer cells and ferroptosis

Cysteine, together with methionine, are the only two sulphur-containing amino acids incorporated into proteins within mammalian cells, where they function as the only source of sulphur for biosynthetic purposes (Cooper, 1983). Whereas methionine is essential because it can only be obtained through the diet, cysteine is considered semi-essential since it can also be synthesised endogenously from methionine through the intermediate, homocysteine, in a process known as transulfuration (Cooper, 1983). However, in certain circumstances, such as in during embryonic development, cysteine becomes essential because of lack of expression of transulfuration enzymes such as cystathionine-γ-lyase required for this conversion (Sturman et al., 1970). Cysteine is available in two forms; a reduced state with a reactive sulfhydryl group (Cys-SH), or an oxidised form, known as cystine, where two molecules of cysteine form a disulphide bridge across the sulfhydryl groups (Cys-S-S-Cys). Within cells cysteine is prevalent due to the reductive environment found there, but extracellularly, due to its high reactivity, cysteine is rapidly oxidised to cystine (Crawhall and Segal, 1967).

Several amino acids transporters for cysteine and cystine have been described. Cysteine can be imported directly into cells through A, ASC and L subfamily amino acid transporter systems as a neutral amino acid (Bannai, 1984). However, due to its prevalence extracellularly, cells require mechanisms of uptake of the reduced cystine. Cellular take up of cystine is mediated primarily by the glutamate-cystine antiporter system X_{c-}, which is a Na^+-independent anionic bidirectional transporter that mediates cystine influx and glutamate efflux (Bannai

and Kitamura, 1980). Exchange is promoted by high intracellular concentrations of glutamate and high extracellular concentrations of cystine (Bannai and Kitamura, 1980). Glutamate availability can affect uptake of cystine because when concentrations of glutamate in the growth media are high, uptake of cystine is inhibited (Bannai, 1984; Bannai and Kitamura, 1980). Conversely, when cystine is absent from the media, efflux of glutamate is impaired (Bannai and Kitamura, 1980). Upon uptake by cells cystine is readily reduced to cysteine by either glutathione, or through the thioredoxin–thioredoxin reductase system which generates cysteine for the synthesis of glutathione and/or proteins (Figure 1.) (Bannai and Kitamura, 1980; Mandal et al., 2010b).

The majority of intracellular cysteine is utilised for the synthesis of glutathione (Meister and Anderson, 1983). Glutathione (L-γ-glutamyl-L-cysteinylglycine, GSH) is a tripeptide with a fundamental role in the antioxidant capacity of cells (reviewed in (Griffith, 1999; Lu, 2013)). GSH is synthesised in two sequential steps that require energy in the form of ATP. The first step in this pathway is formation of γ-glutamylcysteine through the function of glutamate-cysteine ligase or γ-glutamylcysteine synthetase (Yan and Meister, 1990). The second step is catalysed by GSH synthetase and includes the addition of glycine on to γ-glutamylcysteine to form GSH (Oppenheimer et al., 1979). Cysteine is the rate-limiting component for the synthesis of GSH (Lu, 1999) and a decrease in the levels of cysteine lowers the GSH pool (Griffith, 1999).

As with cysteine/cystine, glutathione can be found in a reduced (GSH) and an oxidised (GSSG) form, the latter comprising two glutathione molecules connected by a disulphide bridge between opposing cysteine residues. GSH has the reductive

capacity to neutralise a variety of toxic ROS as well as reactive nitrogen species (RNS) (Griffith, 1999). Following neutralisation of these free radicals GSH is oxidised to GSSG, and can be recycled back to its reduced form through the function of glutathione reductase which uses NADPH as a reducing equivalent (Kehrer and Lund, 1994). Under physiological conditions the GSH pool is predominantly in its reduced form and GSH is generally found in 100-fold greater concentration than oxidised GSSG (Akerboom et al., 1982). Accumulation of GSSG due to oxidative stress leads to its transport out of cells to avoid disrupting the redox balance within cells (Griffith, 1999). Extracellular GSSG and GSH can subsequently be recycled through the γ-Glutamyl cycle whereby these peptides are degraded by γ-Glutamyl transpeptidase (γ-GT) and the individual amino acids transported back into the cell (Meister and Anderson, 1983).

Glutathione can react with ROS either alone, or via two classes of enzymes: glutathione peroxidases (GPXs) and glutathione S-transferases (GSTs). GPX enzymes are selenoproteins that contain selenocysteine, a unique amino acid whose structure is similar to that of cysteine but contains selenium instead of sulphur in the active site of the enzyme (Brigelius-Flohe and Maiorino, 2013; Lu and Holmgren, 2009). The selenhydryl group (-SeH) of selenocysteine is more nucleophilic than the sulfhydryl group of cysteine endowing this class of enzymes with greater reducing capability against ROS (Gromer et al., 2003). Glutathione is used in this context to recycle GPX enzymes back to their active reduced state. In contrast to GPX enzymes, GST enzymes do not contain selenocysteine but catalyse the transfer and conjugation of GSH in order to neutralise free radicals or reactive intermediates (Sharma et al., 2004).

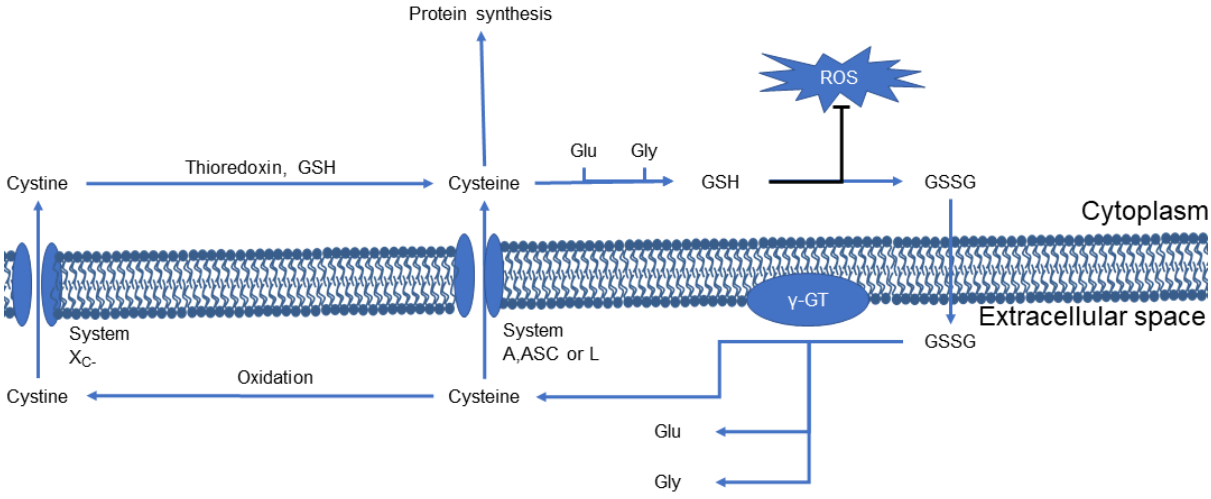

Figure 1.4 Cystine uptake, synthesis of GSH and GSH recycling via the γ-GT cycle.

Cysteine is not stable and is quickly oxidised to cystine disulphide in the environment. Cells have two different mechanisms to mediate uptake of both forms of this amino acid. Cysteine is taken up by systems A, ASC and L similarly to most amino acids. Cystine on the other hand could only be transferred by the function of the system X_{C-} that functions as an antiporter of cystine and glutamine. Once taken up cystine is reduced to cysteine as the intracellular reductive environment favours this form. Cysteine can be incorporated in protein synthesis but the bulk of it is used in the synthesis of the tripeptide GSH that is the major antioxidant found in cells. Neutralisation of ROS by GSH oxidises it to GSSG which is secreted by the cells. Cells have the ability to recycle extracellular GSSG via the function of γ-GT that breaks down GSH to its comprising amino acids which can then be taken up back by the cells.

1.5.10 Ferroptosis a novel form of regulated cell death in in response to deprivation of cystine.

Ferroptosis is a recently-characterised iron-dependent regulated form of necrotic cell death (Dixon et al., 2012). Ferroptosis occurs upon accumulation of lipid peroxides in cellular membranes, and is therefore an oxidative type of cell death (Dixon et al., 2012; Yang et al., 2014). This process was first characterised in pharmacological screens of small molecules that target cancer cells with activating RAS mutations (Dixon et al., 2012). It was found that these compounds, known as RAS synthetic lethal molecules (RSL), trigger a non-apoptotic, iron-dependent form of cell death (Yagoda et al., 2007; Yang and Stockwell, 2008). Erastin is an RSL originally described as an inhibitor of voltage-dependent anion channels (VDAC) VDAC2/3 (Yagoda et al., 2007), but which was later found to additionally inhibit the X_{c-} system-mediated uptake of cystine (Dixon et al., 2012). Treatment of cells with erastin leads to loss of intracellular glutathione and accumulation of ROS, particularly lipid peroxides (Dixon et al., 2012). In this situation iron is likely required to catalyse the Fenton reaction which is responsible for the formation of hydroxyl moieties within lipid molecules (Doll and Conrad, 2017). The importance of iron and the Fenton reaction in the process of ferroptosis is demonstrated by experiments showing that chelation of iron blocks the formation of lipid peroxides and induction of cell death (Dixon et al., 2012; Yang and Stockwell, 2008).

In order to effectively detoxify lipid peroxides cells depend upon GPX4, a glutathione peroxidase enzyme with selectivity for detoxification of lipid peroxides (Brigelius-Flohe and Maiorino, 2013). GPX4 requires glutathione as a cofactor to recycle its enzyme active site (Brigelius-Flohe and Maiorino, 2013), and loss of GSH

impedes the capacity of GPX4 to neutralise target lipid peroxides leading to their accumulation (Yang et al., 2014). A role for GPX4 in ferroptosis was demonstrated by genetic knockdown experiments (Friedmann Angeli et al., 2014) and by experiments where the novel compound RSL3 was used to inhibit the activity of this enzyme (Yang et al., 2014). These experiments showed that such manipulation allowed lipid peroxides to accumulate and resulted in ferroptosis, even when cystine was present. These data therefore indicate that control of the intracellular levels of lipid peroxidation is crucial to the prevention of ferroptotic cell death.

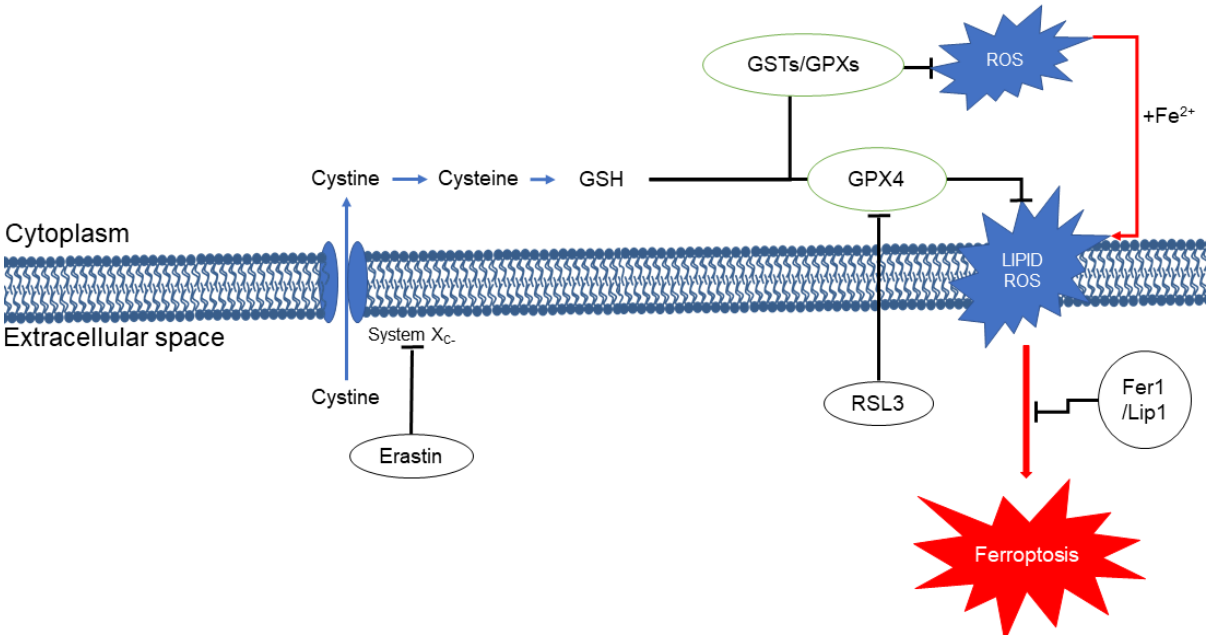

Figure 1.5 The mechanism of Ferroptosis.

Ferroptosis occurs due to accumulation of lipid peroxides in the cell membrane. Inhibitors Fer1 and Lip1 have the ability to scavenge lipid peroxides preventing accumulation. GPX4 is a selenoprotein with a similar intracellular function to neutralise lipid peroxides and inhibit ferroptosis. Lipid peroxides occurs as a by-product of the Fenton reaction that generates hydroxyl radicals from hydrogen peroxide and ferrous iron. GSH is synthesised by intracellular cysteine and is required for the neutralisation of ROS and lipid peroxides (Lipid ROS) through the function of GST and GPX enzymes. Ferroptosis occurs following inhibition of GPX4 either by pharmacological inhibition with RSL3 or following depletion of the required cofactor GSH that is essential for the recycling of the enzyme. Loss of glutathione occurs following deprivation of cystine either due to absence from the extracellular media or following inhibition of the system X_{C-} by small molecules such as erastin.

Ferroptosis is considered as a regulated type of cell death (RCD), but it still differs significantly from other forms of RCD. Unlike ferroptosis, RCDs like apoptosis and the newly described necroptosis and pyroptosis are mediated by activation of an executioner protein or a protein complex that facilitates the cell death process (Fearnhead et al., 2017).

Apoptosis is the best characterised and most extensively-studied form of cell death as it was considered for many years the only form of RCD. Apoptotic cell death can be triggered either intrinsically as a response to cellular stress and DNA damage or extrinsically following activation of death receptors (Elmore, 2007). The apoptotic process is mediated by the function of proteolytic enzymes known as caspases. Caspases are cysteine proteases that cleave endogenous proteins and are the main mediators of apoptosis (Cohen, 1997). The intrinsic response to apoptosis is mediated through the release of cytochrome C from the mitochondria which is regulated by the Bcl-2 family of proteins (Green and Reed, 1998; Reed, 1994). Cytochrome C release promotes the formation of the apoptosome, by facilitating the interaction of Apaf-1 with caspase-9 (Cain et al., 1999; Zou et al., 1999). The apoptosome activates through proteolytic cleavage, caspases 3 and 7, the executioner caspases of apoptosis (Cecconi et al., 1998). Caspase activation can also be mediated by the extrinsic pathway following activation of death receptors tumour necrosis factor receptors TNFR and FAS Nagata (Nagata, 1997). Interaction of the death receptors with their corresponding ligands leads to the formation of the death-inducing signalling complex (DISC) which includes pro-caspase 8 (Kischkel et al., 1995). Self-induced proteolysis of pro-caspase 8 leads to generation of the active

caspase 8 which is responsible for further downstream proteolysis of caspase 3 and induction of apoptosis (Scaffidi et al., 1998).

Inhibition of caspase activity inhibits downstream cleavage and blocks apoptosis. Such inhibition can be achieved either through pharmacological inhibition of caspases by small molecules such as z-VAD-fmk, a pan-caspase inhibitor (Cain et al., 1996), or through the involvement of viral proteins(Ray et al., 1992). Inability of cells to undergo apoptosis and inhibition promote an alternative pathway of RCD known as necroptosis (Vandenabeele et al., 2010).

Similar to apoptosis, necroptosis occurs following death receptor-ligand interaction with downstream activation of receptor-interacting protein kinases 1 and 3 (RIPK1/3)(Holler et al., 2000; Vercammen et al., 1998; Zhang et al., 2009). Under physiological conditions RIPK1 and RIPK3 kinases are proteolytically digested by caspase 8 following formation of the DISC complex (Cho et al., 2009). However, in the absence of caspase 8 activity, intact RIPK1 and RIPK3 interact inducing auto- and cross-phosphorylation of each other promoting formation of the necrosome (Declercq et al., 2009). RIPK3 binds and phosphorylates the pseudokinase mixed lineage kinase domain-like (MLKL) protein (Sun et al., 2012), which is an essential mediator/executioner in the induction of necroptosis (Murphy et al., 2013; Zhao et al., 2012).MLKL has been shown to oligomerise and translocate in the membrane inducing influx of sodium and calcium ions which generate osmotic stress which facilitates cell membrane rupture (Cai et al., 2014; Chen et al., 2014).

Unlike those forms of RCD ferroptosis does not involve the involvement of an executioner molecule that promotes the cell death process. Rather than that, the death occurs due to the excessive accumulation of lipid peroxidation (Skouta et al.,

2014; Yang et al., 2014; Yang and Stockwell, 2016). The increased levels of lipid peroxides occur as a consequence of reduced anti-oxidant capacity due to loss of intracellular cysteine and glutathione or due to impaired capacity of GPX4 to inhibit lipid peroxidation (Gaschler and Stockwell, 2017). It is however regulated by the presence of certain important proteins like system X_C- that controls uptake of cystine, and GPX4 that is responsible for removing dangerous lipid peroxides. Ferroptosis, despite recognised as a form of RCD it has been further characterised as by some a form of cellular sabotage instead of a cellular suicide (Green and Victor, 2012) . Similar to ferroptosis, other forms of RCD have been characterised as that, such as mitotic catastrophe where cell division fails due to chromosomal damage or segregation (Vakifahmetoglu et al., 2008) or parthanatos where death is induced due to overactivation of PARP1 (Andrabi et al., 2008).

1.5.11 Ferroptosis and human disease.

The generation and accumulation of lipid peroxidation may play a role in several aging and neurodegenerative diseases including Alzheimer's, Parkinson's and Huntington's diseases as well as motor neuron degeneration (Chen et al., 2015; Guiney et al., 2017; Hambright et al., 2017; Yoo et al., 2010). Accumulation of lipid peroxides in these diseases suggests that cell degeneration may occur by ferroptosis. Glutamate-induced neurotoxicity (oxytosis) partially involves ferroptosis due to inhibition of X_{C-} system by extracellular glutamate, but in contrast to oxytosis, ferroptosis is independent of glutamate receptor-mediated calcium influx (Yang and Stockwell, 2016). Additionally, recent evidence highlights the importance of ferroptosis in disease processes such as ischemia-reperfusion injury (IRI), as

demonstrated in murine models of hepatic IRI and acute kidney injury (AKI) (Friedmann Angeli et al., 2014; Linkermann et al., 2014). Ferroptosis has also been reported to occur in response to liver acetaminophen toxicity, alongside other forms of cell death such as necroptosis, due to drug-induced depletion of GSH and subsequent GPX4 inhibition (Lorincz et al., 2015).

Some specific inhibitors of ferroptosis have been developed. These include Ferrostatin1 (Fer1) (Dixon et al., 2012) and Liproxstatin1 (Lip1) (Friedmann Angeli et al., 2014). Those molecules have the ability to inhibit ferroptosis by acting as free radical-trapping antioxidants that can block the oxidation of lipids in the presence of iron (Zilka et al., 2017). Despite their antioxidant role these compounds protect specifically from ferroptosis as they cannot protect cells from hydrogen peroxide oxidative cell death (Dixon et al., 2012).

Several oncogenes have been found to be involved in mediating sensitivity to ferroptosis. The presence of an mutated constitutively active RAS induces activation of the downstream RAF-MEK-ERK pathway and sensitises cells to ferroptosis following erastin treatment (Yagoda et al., 2007). Moreover, these cells express higher levels of transferrin receptor 1 and lower levels of transferrin, leading to an increase in the labile iron pool that may also contribute to ferroptosis-sensitivity (Yang and Stockwell, 2008). The tumour suppressor p53 has also been found to suppress expression of xCT, one of the subunits that comprise system Xc- cystine transporter. Loss of p53 function leads to upregulation of the receptor and allows for enhanced uptake of cystine (Jiang et al., 2015). A similar upregulation on xCT expression is observed through the function of the known redox-controlling gene Nuclear factor like 2 (Nrf2) (Fan et al., 2017).

The requirement for cystine and the induction of ferroptosis is associated with other metabolic requirements and functions. A recent report highlights that glutaminolysis may be important for induction of ferroptosis and its inhibition can block ferroptosis (Gao et al., 2015). Finally, inhibition of cysteinyl-tRNA synthetase (CARS) induces activation of methionine transulfuration enzymes to compensate for cystine loss and can be protective against ferroptosis (Hayano et al., 2016). It becomes therefore apparent that metabolic networks are interconnected and requirements for certain nutrients might also be associated with the presence and metabolism of other amino acids.

1.6 Work presented in this thesis.

Those observed differences highlight the need for more systematic analyses to elucidate whether amino acid requirements operate oncogene-selectively and to identify novel amino acid requirements in different genetic and cellular contexts. So I have set out to examine if the presence of a common activated oncogene predicates an increased requirement for one or more extracellular amino acid nutrients. In chapter 3 I demonstrate that hTERT-HME1 cells with an activating mutation in EGFR are particularly dependent on cystine and withdrawal of this amino acid leads to ferroptosis. In chapter 4 I elucidate the underlying mechanism through which EGFR-mediated activation of MAPK pathway regulates the levels of ferroptosis regulator GPX4. In the same chapter I demonstrate that an enzymatic approach using a modified human enzyme that degrades cystine can induce ferroptosis in both in cultured cells as well as in a xenograft model. Finally, in chapter 5 I study the necrotic spread observed in hTERT-HME1 cells undergoing ferroptosis as well as the involvement of cell adhesion in this spreading process.

2. CHAPTER 2: MATERIALS AND METHODS

2.1 Cell Culture and treatments

The hTERT-HME cell line (Wild-type) and its isogenic KI cell line counterparts (EGFR (delE746-A750), KRAS (G13D), BRAF (V600E), PIK3CA (H1047R)) were a kind gift from Prof. Alberto Bardelli (Institute for Cancer Research and Treatment, IRCC, Candiolo, Torino, Italy). Cells were grown in Dulbecco's Modified Eagle's Medium (DMEM) (Life Technologies, 31966047) with 10% Fetal bovine serum (FBS) (Life Technologies), 1% PenStrep (Life Technologies), 20 ng/mL human hEGF (Peprotech), 10 µg/ml bovine insulin (Sigma), and 100 µg/ml hydrocortisone (Sigma) as described (Di Nicolantonio et al., 2008).

NSCLC lines, listed in Table 1, were obtained from the University of Liverpool Institute of Translational Medicine Authenticated cell line repository, or from Professor Michael J. Seckl (Imperial College, London, UK). NSCLC lines were grown either in Roswell Park Memorial Institute (RPMI) 1640 medium (Gibco) supplemented with 10% FBS (Life Technologies), 1% PenStrep (Life Technologies), or in DMEM (Gibco) also supplemented with supplemented with 10% FBS (Life Technologies), 1% PenStrep (Life Technologies).

Name	Obtained from	Growth media	Origin
hTERT-HME1 WT	Professor Alberto Bardelli	HME media	Human mammary epithelia
hTERT-HME1 EGFR	Professor Alberto Bardelli	HME media	Human mammary epithelia
hTERT-HME1 KRAS	Professor Alberto Bardelli	HME media	Human mammary epithelia
hTERT-HME1 BRAF	Professor Alberto Bardelli	HME media	Human mammary epithelia
hTERT-HME1 PIK3CA	Professor Alberto Bardelli	HME media	Human mammary epithelia
A549	ITM Authenticated Cell Line Repository	DMEM	NSCLC
Calu6	ITM Authenticated Cell Line Repository	DMEM	NSCLC
H1975	ITM Authenticated Cell Line Repository	RPMI	NSCLC
H1650	ITM Authenticated Cell Line Repository	RPMI	NSCLC
H727	ITM Authenticated Cell Line Repository	RPMI	NSCLC
H460	ITM Authenticated Cell Line Repository	RPMI	NSCLC
H322	ITM Authenticated Cell Line Repository	RPMI	NSCLC
H3255	Professor Michael Seckl	RPMI	NSCLC
PC9	Professor Michael Seckl	RPMI	NSCLC

Table 2.1 Human cell lines used in this thesis.

Name	Target-Function	Company	Concentration used
α-tocopherol	Vitamin E(ROS scavenger)	Sigma	30μM
AECase	Cyst(e)ine degrading enzyme	Aeglea Biotherapeutics	165nM
Auranofin	thioredoxin reductase (TrxR)	Santa Cruz	1μM
BSO	γ-GCS inhibitor	Santa Cruz	200μM
C11 BODIPY	Lipid peroxide marker	Molecular Probes	2μM
Carbexonolone	Cell junctions inhibitor	Sigma	100μM
Catalase	Purified enzyme targeting hydrogen peroxide	Sigma	1000U/ml
CMDCFDA	Total ROS marker	Molecular Probes	10μM
Deferroxamine	Iron chelator	Sigma	100μM
Erastin	System Xc- inhibitor/ inducer of Ferroptosis	Cayman Chemicals	2.5ug/ml
Ferrostatin1	Ferroptosis inhibitor	Sigma	2μM
Gefitinib	EGFR inhibitor	Tocris Bioscience	1μM
GKT136901	NOX1/4 inhibitor	Aobious	20μM
Idebenone	Co-Q10 analog (ROS scavenger)	Sigma	1μM
Oxidised GSSG	Purified GSSG (oxidised)	Sigma	Various
PD0325901	MEK inhibitor	SelleckChem	1μM
PD184352	MEK inhibitor	Sigma	10μM
Reduced GSH	Purified GSH (reduced)	Sigma	Various
S4PG	System Xc- inhibitor	Santa Cruz	100μM
Selumetinib	MEK inhibitor	SelleckChem	5μM
Superoxide dismutase	Purified enzyme targeting superoxide	Sigma	100U/ml
Sytox Green	Death marker	Invitrogen	0.5μM
Trolox	water soluble Vitamin E analog(ROS scavenger)	Sigma	5μM
U0126	MEK inhibitor	Calbiochem	10μM
Wortmannin	PI3K inhibitor	Sigma	1μM
z-VAD-fmk	Pan-caspase inhibitor(apoptosis inhibitor)	SelleckChem	50μM

Table 2.2 **List of reagents used in this thesis**

2.2 Transfection of cultured cells

2.2.1 siRNA interference

Lipofectamine 2000 (Invitrogen, ThermoFisher) was used for small interfering RNA (siRNA) transfection of HME cells according to the manufacturer's instruction. 500,000 cells were plated in 6-well plates and either mock-transfected (where lipofectamine was used with no siRNAs), or were transfected with either siCtrl or siGenome Smartpool siRNAs (Dharmacon, GE Lifesciences) to GPX1, GPX2, GPX3 and GPX4 (Table 3) used at a final concentration of 50nM. A day after transfection, cells were trypsinised and seeded into a 12-well plate well with 250,000 cells/well, or a 96-well plate wells with 25,000 cells per well. 3 days post transfection cells in the former were used for immunoblotting, whilst cells in the latter were used in viability assays.

2.2.2 Expression vectors

For GPX4 overexpression 500.000 HME-EGFR cells were transfected in 3cm dishes with 2.5µg/ml (5 of µg in 2ml) of p442-PL1 Flag-Strep-HA-GPX4 , a kind gift from Professor Marcus Conrad (Mannes et al., 2011), or control vector using Lipofectamine 2000 (Invitrogen, ThermoFisher). 48h after transfection wild-type or transfected cells were trypsinised and 20,000 cells/well were re-plated in a 96 well format , deprived of cystine for 16h and measure the viability using Cell titre Glo

2.2.3 Recombinant protein production

Human glutathione S-transferase alpha isozyme 4-4 (hGSTA4-4) was expressed as recombinant proteins using the pET30a(+)-hGSTA4-4 expression vector (Cheng et al., 2001) ,a kind gift from Professor Sanjay Awasthi (Department of Medical Oncology, Texas Tech University Health Sciences Center, Lubbock, TX 79430,

USA) , in BL21 competent E. coli. Bacterial cultures were incubated with 0.1mM Isopropyl β-D-1-thiogalactopyranoside (IPTG, Sigma) to induce protein expression for 4h prior to lysis. The overexpressed GSTA4-4 was isolated using agarose beads conjugated with glutathione (Sigma) and subsequently eluted using reduced glutathione solution (Sigma). Simply blue Safe stain (ThermoFisher) was used to determine protein quantity against BSA standards

A)

siRNAs				
Name	Gene	Company	Concentration	Product code
siNon-targeting Control	Non-Targetting	Dharmacon	50nM	D-001810-01-50
siGenome Smartpool siGPX1	GPX1	Dharmacon	50nM	M-008982-00-0005
siGenome Smartpool siGPX2	GPX2	Dharmacon	50nM	M-011675-00-0005
siGenome Smartpool siGPX3	GPX3	Dharmacon	50nM	M-006485-01-0005
siGenome Smartpool siGPX4	GPX4	Dharmacon	50nM	M-011676-01-0005

B)

siRNA sequences	Product code	Sequence
siControl	D-001810-01	UGGUUUACAUGUCGACUAA
GPX1	D-008982-01	GCAAGGUACUACUUAUCGA
	D-008982-02	UGAAUUCCCUCAAGUACGU
	D-008982-03	GGAGAACGCCAAGAACGAA
	D-008982-04	GCAACCAGUUUGGGCAUCA
GPX2	D-011675-01	GAACGAGCAUCCUGUCUUC
	D-011675-02	GAAGGUAGAUUUCAAUACG
	D-011675-03	CAGGAGAACUGUCAGAAUG
	D-011675-04	GCAGGGCCGUGCUGAUUGA
GPX3	D-006485-01	GUACGGAGCCCUCACCAUU
	D-006485-02	GGAUGUCAAUGGAGAGAAA
	D-006485-03	AGGAAGAGCUUGCACCAUU
	D-006485-04	GAGGCUUUGUCCCUAAUUU
GPX4	D-011676-01	CAACGUGGCCUCCCAGUGA
	D-011676-02	GUAACGAAGAGAUCAAAGA
	D-011676-03	CGUCAAAUUCGAUAUGUUC
	D-011676-04	GCUGCGUGGUGAAGCGCUA

C)

Plasmid vectors				
Name	Gene	Obtained from	Concentration	Tags
p442-PL1 Flag-Strep-HA-GPX4	GPX4	Dr. Marcus Conrad	2.5ug/ml	FLAG, HA, Strep
pET30a(+)-hGSTA4-4	GSTA4-4	Professor Sanjay Awasthi .	Recombinant protein vector	-

Table 2.3 Lists of siRNA and plasmids used in this thesis.

2.3 Amino acid depletion

Individual amino acid stocks (Sigma) made at 50X the concentrations used in DMEM in water. These stocks were used to generate complete DMEM media (+AA) were all amino acids were used, or individual DMEM amino acids were omitted to generate single amino acid deficient media. For the initial screen of amino acid sensitivity 30,000 cells were initially plated per well in a 96-well microtitre plate (NUNC, ThermoFisher) in complete DMEM media, that was then switched the following day to selectively depleted amino acid media. Cells under these conditions were cultured for a further 72 hours.

2.3.1 Cystine titration

For the cystine titration experiment cells were plated in triplicate cells at a final concentration of 30,000cells/well in a 96-well format (NUNC, ThermoFisher). The following day complete synthetic media containing or lacking EGF was serially diluted with DMEM lacking cysteine to achieve a range of decreasing cystine concentrations.

2.4 Viability assays

Viability was assessed using two different assays; one using Calcein AM (Molecular Probes, ThermoFisher), or, two, using the CellTitre-Glo assay (Promega). For viability measurements using Calcein (only used for the initial screen), cells were incubated with 1μM Calcein-AM for 2h followed by fixation with 4% paraformaldehyde for 15 mins prior to analysis on a Tecan Genios plate reader using an excitation wavelength of 485nm and measuring emission at 535nm. Viability measurement using the CellTitre-Glo assay was performed according to the manufacturer's instruction. Briefly, an equal volume of CellTitre-Glo reagent (to the

existing cell culture media) was added to the cell culture plate using a multichannel pipette. Plates were then vortexed at 1000 rpm for 2 minutes to allow cell lysis, and then luminescence was measured using a Tecan Genios plate reader. Cell viability of each cell line in test situations were normalised to that of each cell line grown in complete DMEM (the control condition). Experiments were performed in triplicate and one standard deviation has been used for error bars.

2.5 Microscopy

2.5.1 Time-lapse microscopy

For time lapse microscopy, a Nikon TE-300 microscope equipped with a 10X phase contrast (PC) objective and motorised with Sutter filter wheels and a Conix block changer, was used. The microscope was encased in a Perspex 37°C incubation chamber with an insert for multi-well plates. The incubation chamber was flushed with humidified air containing 5% CO_2. Green fluorescence was acquired through a Nikon B-2A block, and images were collected through a Hamamatsu Orca AG camera, using MicroManager software (Edelstein et al., 2010). Conversion of time series to an ImageJ readable format was performed using in-house software kindly provided by Dr Carlos Rubbi, Department of Molecular and Clinical Cancer Medicine. To perform each experiment, cells were plated in a 6-well plate at 500,000 cells per well, and then grown for 3 days prior to media switch to cysteine-deprived media. At this point Sytox Green nuclear stain (Molecular Probes, ThermoFisher) was added to a final concentration of 0.5μM. The plates were then transferred to the microscope stage within the incubator and maintained at 37°C with 5% CO_2. Individual frames were obtained every 5 minutes in phase contrast (PC) and green fluorescence channels for detection of nonviable cells. Measurements of Sytox green-positive

cells were performed using ImageJ (Schneider et al., 2012). An image-analysis algorithm to assist with fluorescence measurements was kindly generated by Dr. David Mason, Centre for Cell Imaging, Institute for Integrative Biology, University of Liverpool, allowing measurements of the rate of cell death spread.

2.5.2 Immunofluorescence and detection of LAA adducts using confocal microscopy.

For immunofluorescence experiments studying adherens junctions and for the detection of LAA adducts cell images were obtained at 63X magnification using a confocal laser scanning microscope (Zeiss 3I LSM 800). Confluent wild-type HME and HME-EGFR cells were plated in 13mm round glass coverslips. Following treatment, cells were fixed with 4% PFA/PBS and permeabilised with 0.2% Triton X-100/PBS. In order to block unspecific interactions coverslips were incubated in Odyssey blocking buffer (LICOR) in PBS (1:1 ratio). Coverslips were incubated with primary antibody overnight at 4°C, incubated with labelled secondary goat anti-Mouse Alexa Fluor 594 antibody (ThermoFisher) for 1 hr at room temperature, and mounted using Dako mounting medium (Agilent).

Lipid peroxidation adducts were detected using the Click-iT lipid peroxidation imaging kit as per manufacturer's instructions (Molecular Probes, ThermoFisher) were similarly visualised using a confocal laser scanning microscope (Zeiss 3I LSM 800). Cumene hydroperoxide (CuOOH, Sigma) was used as a positive control. Hoechst 33342 (ThermoFisher) was used as nuclear staining dye.

2.5.3 Phase contrast and fluorescence photographs for GJIC scrape loading Lucifer Yellow assay

For single phase contrast and fluorescent images an AMG EVOS FL digital inverted microscope was used. Images were obtained at 4x or 20x magnifications. Measurement of the total area of fluorescent-positive cells for cell death or for GJIC scrape loading assay was performed using ImageJ (Schneider et al., 2012).

Confluent cultures of wild-type HME cells were treated with the specified inhibitors or vehicle DMSO for 30h. Following cell treatment with the vehicle or the specified inhibitors cells were washed in Dulbecco's PBS (DPBS) without calcium and transferred to loading solution, which was composed by PBS containing 0.5mg/mL Lucifer yellow (Sigma), 0.5 mg/mL rhodamine-dextran (Molecular Probes) and either DMSO (100μM) or carbenoxolone (CBX, 100μM). For dye loading a wound was performed using a pipette tip and the cells were incubated for 15 minutes at 37^{o}C. Following incubation, the loading solution was removed, and cells were washed in PBS and subsequently fixed in 4% paraformaldehyde (PFA)/PBS. Areas close to the wound margin were imaged for green and red fluorescence at 20X magnification to demonstrate the infiltration of Lucifer Yellow dye into the monolayer. Rhodamine Dextran incorporation was limited in the wound margin as the dye cannot pass through gap junctions and was used a loading control for cell wounding.

2.6 Fluorescence-activated cell sorting (FACS) analysis

For the detection of intracellular ROS 200,000 cells were plated into 6-well plates (Greiner Bio-one). Following 3 days of culture in complete media, the supernatant was removed and cell were switched to cysteine deprived media in which they were cultured for a further 12 hours. The cells were then washed with PBS, and then

incubated in DPBS containing either CMDCFDA (10μM) or C11 BODIPY (2μM) (both from Molecular Probes, ThermoFisher) for 30min. After this final incubation, cells were removed from culture plates by trypsinisation with 0.25% Trypsin-EDTA (Gibco, ThermoFisher), and then resuspended in PBS with 1% FBS. Cells were then analysed using an Attune NxT flow cytometer (ThermoFisher). Both dyes were excited using a blue 488nm laser and emission was measured on BL1 (530/30). Data was collected for a minimum of 5,000 cells per sample.

2.7 GSH/GSSG quantification

For the quantification of cellular reduced (GSH) and oxidised (GSSG) glutathione the method described by Rahman et al (Rahman et al., 2006) was used. This method depends on the reaction of GSH with 5,5′-Dithiobis (2-nitrobenzoic acid)(DTNB) to generate 5′-thio-2-nitrobenzoic acid (TNB), a chromophore whose concentration can be measured at 412nm (Tietze, 1969). $1x10^6$ cells were plated in 6-well plates (Greiner) and cultured overnight. On the following day cell cultures were either treated with 200μM of BSO, or had their media switched to cystine deficient media and then further cultured for 8h. Cells were then washed in cold PBS, trypsinised and resuspended in 0.2ml of ice-cold extraction buffer (0.1% Triton-X and 0.6% sulfosalicylic acid in 0.1 potassium phosphate buffer with 5 mM EDTA, pH 7.5 (KPE)). The lysed cells were then subjected to 4 freeze-thaw cycles (liquid nitrogen - 37°C water bath), and this was followed by centrifugation at 3000g for 5 min at 4 °C. Supernatants were collected, and the protein concentrations within were measured using a Bradford assay (Bradford, 1976) in order to express GSH and GSSG levels as nM/mg of total protein.

Total glutathione (Total[GSH] = [GSH] + 2 × [GSSG]) within the supernatants was determined by first reducing GSSG to GSH with the addition of glutathione reductase (GR, Sigma) and DTNB (Sigma) followed by addition of 240μM β-Nicotinamide adenine dinucleotide 2′-phosphate (β-NAPDH, Sigma) and the rate of TNB formation was calculated by measuring absorbance at λ_{415nm} in a Tecan Genios plate reader every 30sec. Total glutathione within cell lysates was quantitated against a standard curve generated using GSH standards of known concentration made from stock GSH (Sigma).

For measurement of GSSG, 2-vinylpyridine (Aldrich) is added to cell lysates to a final concentration of 18.5mM, which were then incubated for 1h at RT. 2-vinylpyridine covalently binds to GSH to allow measurement of GSSG. Excess 2-vinylpyridine was neutralised with the addition of 75mM triethanolamine (Sigma) for 30 min (Griffith, 1980). However, derivatisation of GSH with 2-vinylpyridine could have lead to overestimation of the GSSG content in these cells and therefore addition of N-ethylmaleimide is suggested an approach that could yield more accurate measurements (McGill and Jaeschke, 2015)

Following derivatisation, levels of GSSG were determined by first reducing it to GSH by addition of GR as described above, and then measuring the rate of TNB formation following the addition of DNTB. Reduced glutathione (GSH) in cell lysates could be then determined by this formula: (Total[GSH] = [GSH] + 2 × [GSSG]). All measurements were done in triplicate. Glutathione synthesis inhibitor buthionine sulfoximine (BSO, Santa Cruz Biotechnologies) was used at 200μM.

2.8 Western Blotting

Cells were lysed in lysis buffer (50 mM Tris-HCl, pH 7.5, 1mM EGTA, 1 mM EDTA, 1% Triton X-100, 1mM Na_3VO_4, 50 mM NaF, 50 mM β-glycerolphosphate, 0.27M sucrose, 0.1% beta-mercaptoethanol, Complete protease inhibitors (Roche)). Cell lysates were centrifuged at 10,000xg for 30min at 4°C, and supernatants were taken for protein concentration determined by Bradford assay (Bradford, 1976) using Bradford reagent Biorad and measuring absorbance at 595nm using a SpectraMax Plus 384 Microplate Reader. 25 µg of total cellular protein was loaded per sample on to a SDS-PAGE gel, and proteins separated using 10% acrylamide gels. Separated proteins were electroblotted to PVDF membranes, which were then probed with the list of antibodies found in Table 2.4

Antibody target	Company	Product code	Species	Clonality	Application
pEGFR Y1068	Cell signalling Technologies	#3777	rabbit	Monoclonal	WB
EGFR	Cell signalling Technologies	#2232	rabbit	Polyclonal	WB
pAKT S473	Cell signalling Technologies	#9271	rabbit	Polyclonal	WB
AKT	Upstate EMD Millipore	#07-416	rabbit	Polyclonal	WB
ppERK T202/Y204	Cell signalling Technologies	#4370	rabbit	Monoclonal	WB
ERK1/2	Santa Cruz Biotech	sc-94	rabbit	Polyclonal	WB
GCN2-P T899	Epitomics Abcam	#2425-1	rabbit	Monoclonal	WB
GCN2	Cell signalling Technologies	#3302	rabbit	Polyclonal	WB
GPX1	R&D systems, Biotechne	AF3798	goat	Polyclonal	WB
GPX2	R&D systems Biotechne	MAB5470	mouse	Monoclonal	WB
GPX4	Abcam	ab125066	rabbit	Monoclonal	WB
COX2	Cayman Chemicals	#160112	mouse	Monoclonal	WB
RSK T359	Cell signalling Technologies	#8753	rabbit	Monoclonal	WB
RSK1/RSK2/RSK3	Cell signalling Technologies	#9355	rabbit	Monoclonal	WB
b-catenin	BD, Transduction Labs	C19220	mouse	Monoclonal	IF
COX2	Abcam	ab15191	rabbit	Polyclonal	IHC

Table 2.3 List of antibodies used in this thesis

2.9 In vivo mice models.

NCI-H1650 tumours were allowed to form in 1:1 in Matrigel: PBS (100 mL) where 250,000 cells were inoculated. Tumours were transferred to eight non-obese diabetic

(NOD) severe combined immunodeficiency (SCID) gamma male mice by subcutaneous injection. Prior to treatment, tumours were allowed to establish for 18 days and were then administered interperitoneally with two different concentrations 30 or 100 mg/kg cyst(e)inase (AECase) or PBS control for 20 days and left for 10 more days without any treatment prior to necropsy.

For WB and IHC samples derived from in vivo tumours, the tumors were allowed to engraft for 30 days (tumor volume averaged ~200 mm3) followed by intraperitoneal (i.p.) injection with 100 mg/kg cyst(e)inase or 100 mg/kg heatinactivated cyst(e)inase (n = 4 ea.) on day 30, with a second dose given on day 33. Mice were necropsied 24 hr after the second dose. For determination of COX2 using immunohistochemistry (IHC),half of the excised tumors were preserved in 10% neutral buffered formalin, while the remaining half was frozen in liquid nitrogen and then pulverised with morter and pestle inside a classII biological safety hood. The procedure of IHC was carried out and evaluated by Precision Pathology using an anti-COX2 antibody from Abcam (ab15191) with DAB detection.

2.10 LC-MS for amino acid steady state levels

For the measurement of steady state levels of amino acids within wild-type and HME-EGFR cells, 500,000 cells were seeded in 10cm dishes. The next day cells were washed 3 times using DPBS and switched to cystine lacking media, or complete The metabolites were extracted using a polar solvent (50% methanol, 30% acetonitrile, 20% water) with 1ml used per 1,000,000 cells. Sample were then mixed first on arocking plate and then on Thermomixer (Thermomixer comfort, Eppendorf AG, Hamburg, Germany) and then centrifuged at 16,100 x g for 10 minutes, with all procedures taking place at 0-4°C. Hydrophilic Interaction Liquid Chromatography

was performed by Dr. Christiaan Labuschange using a Sequant ZIC-pHILIC column (2.1 × 150 mm, 5 µm) (Merck) to separate amino acids before detection with high-resolution, accurate-mass (HR/AM) Mass Spectrometry using an Orbitrap Exactive in line with an Accela autosampler and an Accela 600 pump (Thermo Scientific). The elution buffers used to elute the analytes were Acetonitrile (ACN) for A and 20 mM (NH4)2CO3, 0.1% NH4OH in H2O for B. A linear gradient was programed starting from 80% A and ending at 20% A after 20 min at a flow rate of 200ul/min, followed by wash (20% A) and re-equilibration (80% A) steps at a flow rate of 400 µl/min. An Electrospray Ionization (ESI) probe was used to achieve ionization and the mass spectrometer operated in full-scan and polar-switching mode with the positive voltage at 4.5 kV and negative voltage at 3.5 kV. Metabolite identification and data analysis were done using TraceFinder TM software (Thermo Scientific).

3. CHAPTER 3. IDENTIFYING ONCOGENE-SELECTIVE DIFFERENTIAL EFFECTS OF SPECIFIC AMINO ACID DEPRIVATION IN HUMAN MAMMARY EPITHELIAL CELLS.

3.1 Introduction

The main aim of my study was to investigate whether the concept of synthetic lethality (Rehman et al., 2010) could be applied to the requirements of cancer cells harbouring specific oncogenic mutations for specific nutrient amino acids. To investigate this question, I performed a “drop-out” screen in which synthetic media were prepared that lacked each of the 20 amino acids found in DMEM media.

The cell model I chose was a panel of hTERT-immortalised Human mammary epithelial (hTERT-HME1) cell lines that had been gene-edited to express five of the most common oncogenic mutations found in human tumours but present an otherwise isogenic genomic background. These cells have a normal diploid karyotype and were immortalised via retroviral transfection of human telomerase enzyme (Yi et al., 1999). Gene editing of the parental wild-type hTERT-HME (HME) cell line was performed by adeno-associated-viral (AAV) mediated homologous recombination to introduce the following common oncogenic mutations: EGFR (delE746-A750) (HME-EGFR), KRAS (G13D) (HME-KRAS), BRAF (V600E) (HME-BRAF), and PIK3CA (H1047R) (HME-PIK3CA) (Di Nicolantonio et al., 2008). Unlike tumour cell lines these cells have a normal genetic background and a diploid karyotype providing an excellent system to dissect the specific effects of the highlighted oncogenes (Di Nicolantonio et al., 2008). On the contrary, a model of isogenic cancer cell lines could potentially be more complex due to the presence of mutations accumulated during their oncogenic transformation. Moreover, these cell

lines, except for HME-BRAF, cannot grow in an anchorage-independent manner and none of them have tumorigenic properties (Di Nicolantonio et al., 2008).

3.2 HME cells with activating EGFR and BRAF mutations require the nutrient amino acid cystine to maintain viability.

3.2.1 Screen for oncogene-selective requirements of individual amino acids

To define effects upon viability in wild-type and mutant hTERT-HME cells I firstly prepared DMEM media deficient in individual amino acid nutrients. This media was used to culture the above cells for 72h, after which viability was measured using Calcein-AM labelling.

When cystine was omitted from the media, all cell lines demonstrated some loss of viability in the range of 40% to >80%. The cell lines that exhibited the highest loss in viability were those with a mutated allele for EGFR and BRAF where only <20% of the cells survived (Figure 3.1). However, some other differences were also observed. Thus, deprivation of Gln led to around 50% loss of viability for all cell lines irrespective of their mutational status. Similarly, Arg and Val deficiency also reduced the viability of cultured cells regardless of mutational status, but to a lesser extent than that found with deprivation of Gln. Finally, Met deficiency also caused some variable reduction in cell line viability. Deficiency of the other amino acids found in DMEM media did not markedly affect cell viability.

A)

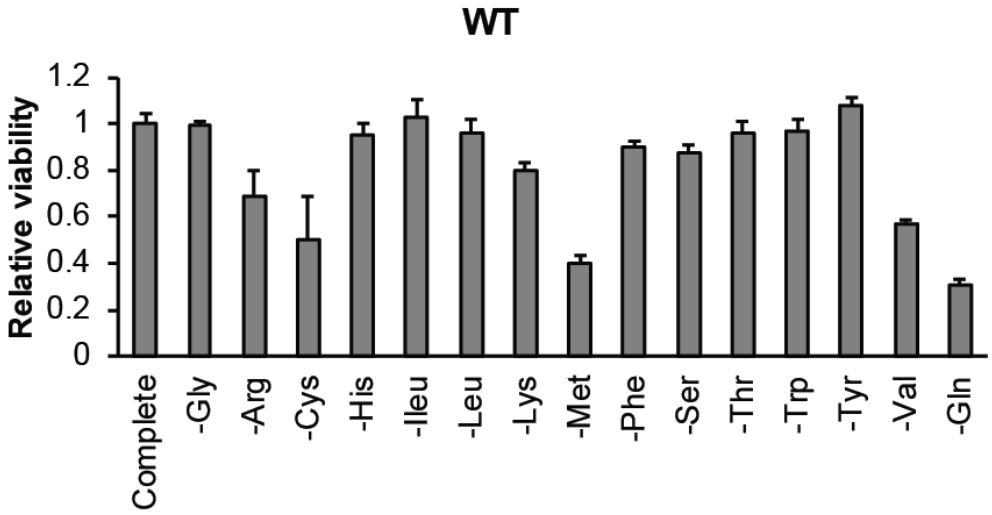
WT
Relative viability
1.2
1
0.8
0.6
0.4
0.2
0
Complete
-Gly
-Arg
-Cys
-His
-Ileu
-Leu
-Lys
-Met
-Phe
-Ser
-Thr
-Trp
-Tyr
-Val
-Gln

B)

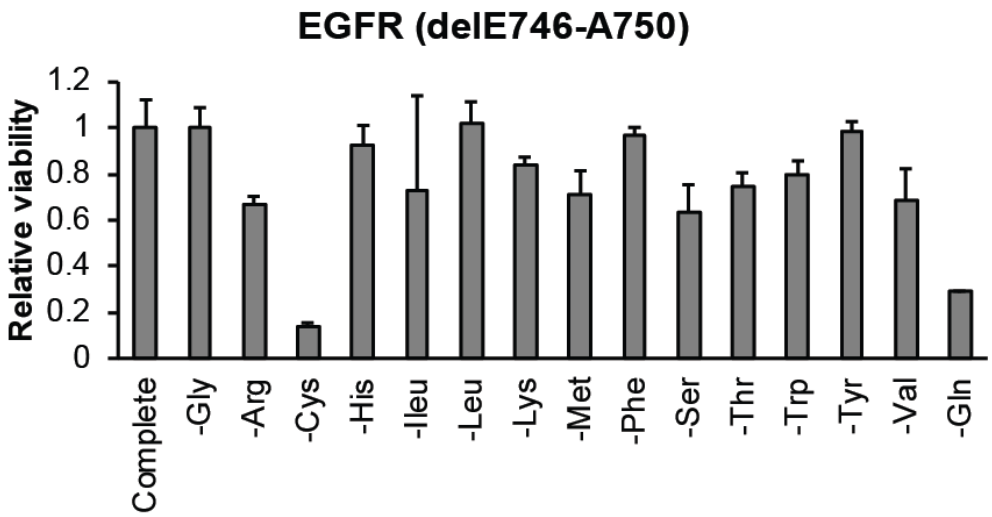
EGFR (delE746-A750)
Relative viability
1.2
1
0.8
0.6
0.4
0.2
0
Complete
-Gly
-Arg
-Cys
-His
-Ileu
-Leu
-Lys
-Met
-Phe
-Ser
-Thr
-Trp
-Tyr
-Val
-Gln

C)

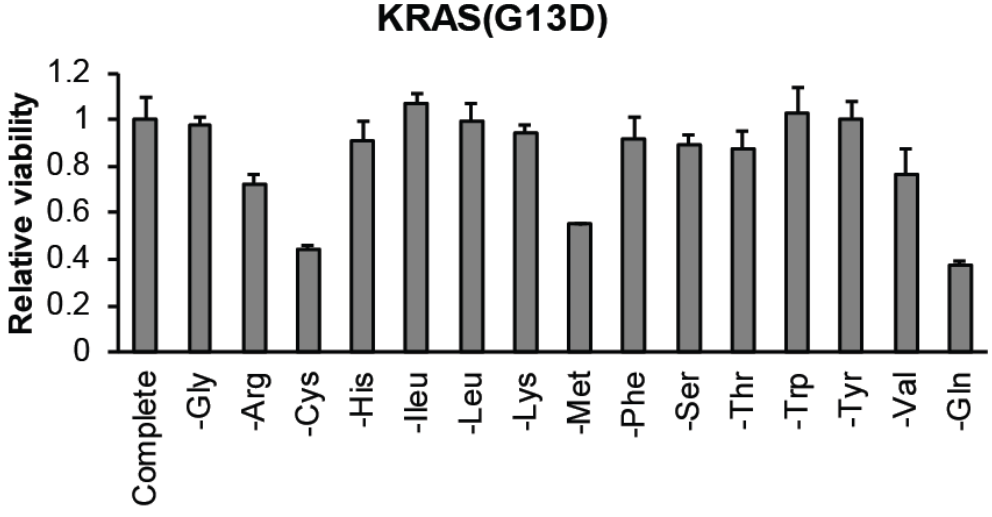
KRAS(G13D)
Relative viability
1.2
1
0.8
0.6
0.4
0.2
0
Complete
-Gly
-Arg
-Cys
-His
-Ileu
-Leu
-Lys
-Met
-Phe
-Ser
-Thr
-Trp
-Tyr
-Val
-Gln

D)

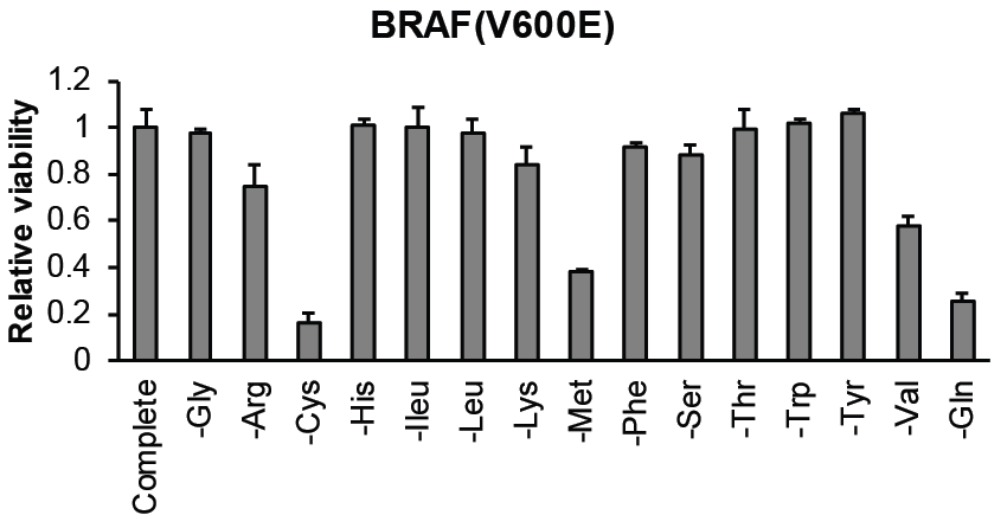

E)

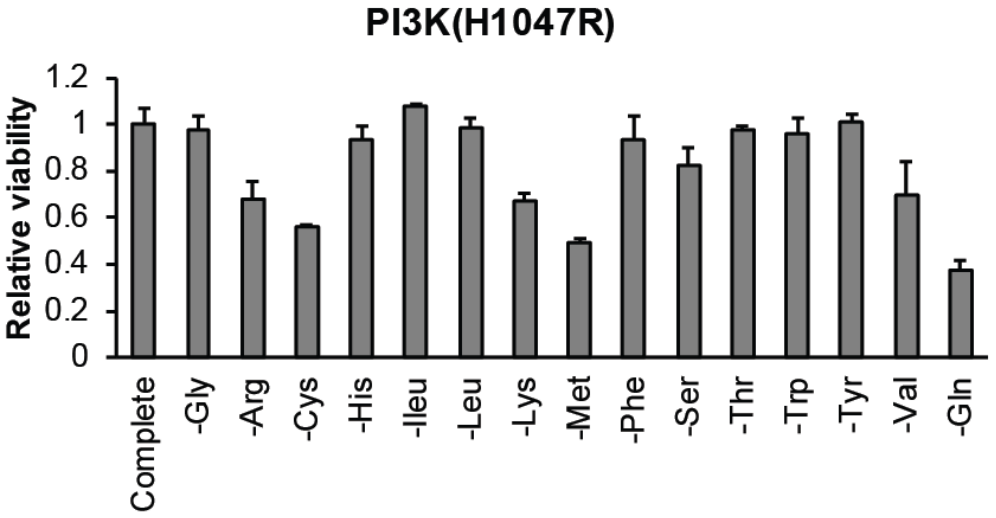

Figure 3.1 Cell survival assay for individual amino acid depletions in HME cell lines.

Viability of each individual cell line was measured by fluorescence intensity from incorporated Calcein-AM used for labelling and was normalised to viability in complete media assigned an arbitrary value of 1. Each graph represents the average viability ± standard deviation (SD) of three biological replicates. Parts A – E indicate experiments performed on the indicated cell line (WT, wild-type HME cells).

3.2.2 HME-EGFR cells demonstrate the strongest requirement among the other cell lines for cystine.

To further determine the specificity of the observed effect of cystine deprivation I assayed cells under different conditions of confluency. Wild-type HME cells along with HME-EGFR and HME-BRAF were plated in conditions that allowed them to reach complete (100%) or partial confluence (50%). All cell lines appeared partly sensitive under conditions of low confluency (Figure 3.2A). However, when allowed to reach complete confluency wild-type and HME-BRAF cells were protected from cystine deprivation-induced cell death, whereas cells with an activating EGFR mutation remained highly sensitive (Figure 3.2B). These observations demonstrate that cell-cell contact, for as yet unknown reasons, can partially overcome the death-inducing effect of cystine depletion in wild-type and HME-BRAF cells, but not in HME-EGFR cells. This suggests greater dependence of the latter cells upon cystine, and allows the use of HME-EGFR cells to model the mechanism of cell death that is induced when cystine is depleted. From this point forward, all experiments were performed using confluent cell cultures.

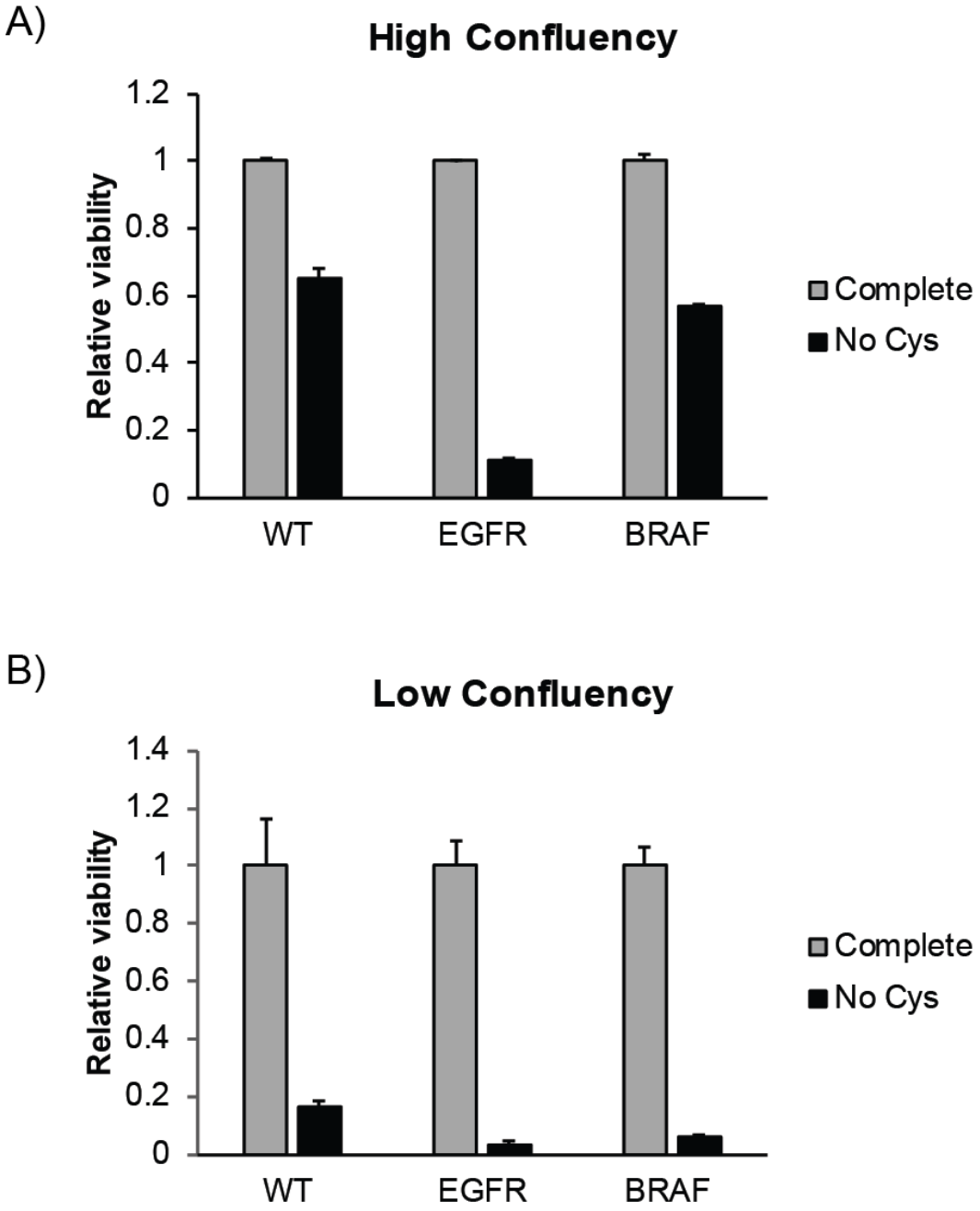

Figure 3.2 Cell survival assay for deprivation of cystine under conditions of high and low confluence in wild-type HME (WT), HME-EGFR and HME-BRAF cell lines.

Viability of each individual cell line was measured by luminescence using the Cell-titre Glo assay and was normalised to viability in complete media. Each graph represents the average viability ± standard deviation (SD) of three biological replicates. Panel A indicates viability under conditions of high confluence (~100%) whereas panel B displays the results obtained from lower confluence experiments (~50-70%).

3.2.3 HME-EGFR cells have an active requirement for L-cystine but not D-cystine to maintain viability.

To determine the minimum requirement of wild-type and EGFR-mutant cell lines for the presence of exogenous cystine, I next cultured confluent cells in a range of decreasing cystine concentrations. Two different media formulations were prepared, one including EGF and a second one where it was omitted. Under these conditions wild-type HME cells maintained their viability regardless of cystine concentration, the exception was when cystine was completely removed and cell viability of the EGF-cultured cells was reduced to around 80% (Figure 3.3A). In contrast, HME-EGFR cells exhibited a markedly elevated requirement for cystine, with loss of 50% viability (IC50) occurring at 2μM concentration in the presence of EGF and 1μM concentration when EGF was omitted (Figure 3.3A). These results suggest an active requirement for exogenous cystine by HME-EGFR cells.

I next examined the possibility that supplementation of D-cystine (the enantiomer of L-cystine) could prevent cell death. Figure 3.3B shows that addition of D-cystine to either complete media or to media lacking L-cystine had no effect on the viability of wild-type HME or HME-EGFR cells. Importantly, there was no rescue from cell death of HME-EGFR cells when L-cystine was replaced with an equivalent concentration of D-cystine, indicating that the requirement of these cells is enantiomer specific, likely as a result of specificity the System X_{c-} for uptake of L- but not D-cystine (Patel et al., 2004).

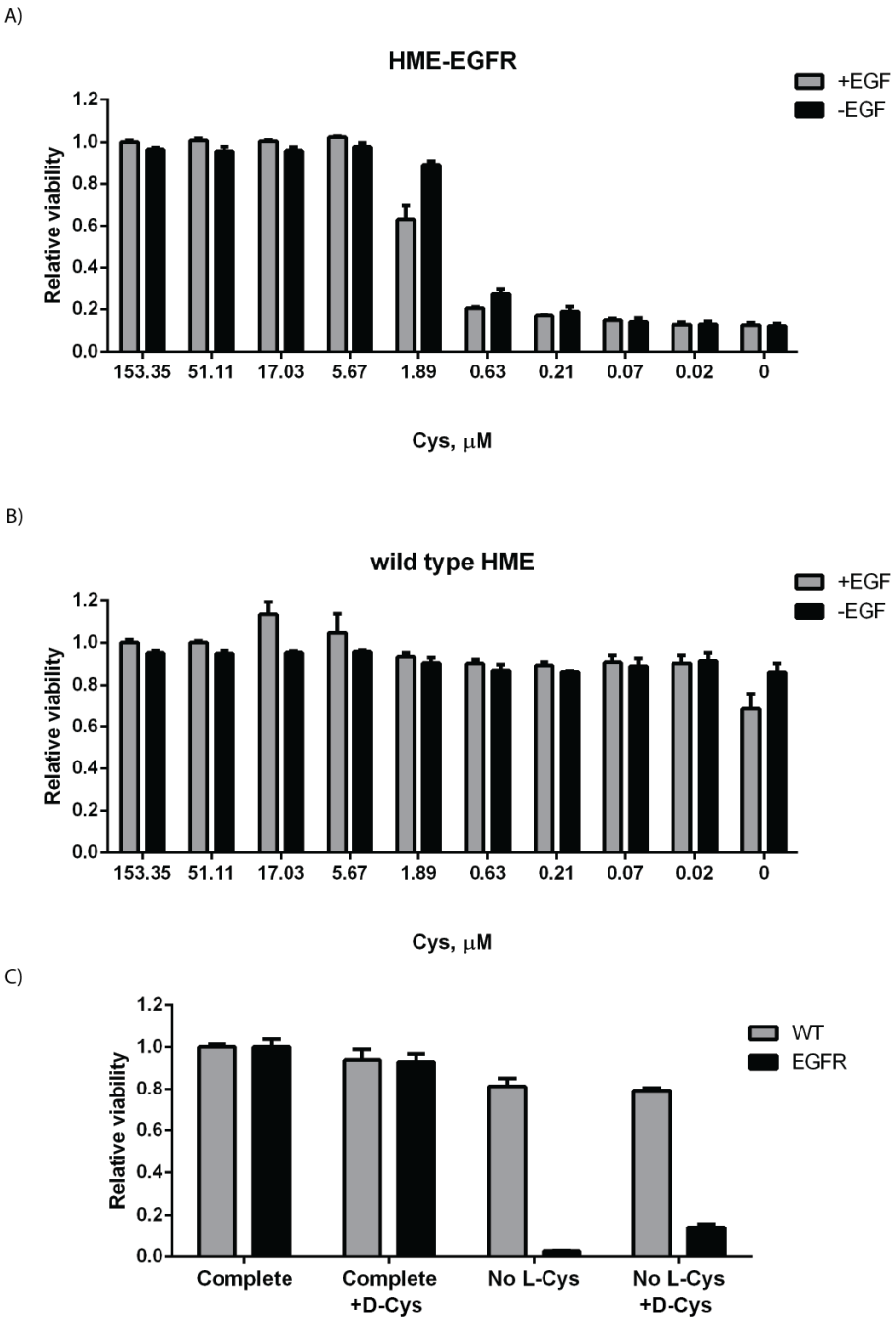

Figure 3.3 HME-EGFR cells have an active requirement for exogenous L-, but not D-cystine.

A and B Cell viability assay for wild-type HME and HME-EGFR cell lines grown in media containing different concentrations of L-Cystine. Panel C Cell viability assay for wild-type and HME-EGFR cell lines cultured in complete or L-cystine-deprived media testing the effect of supplementation with (153μM) D-Cystine. Viability of each individual cell line was measured by luminescence using the CellTitre-Glo assay and was normalised to viability in complete media. Each graph represents the average viability ± standard deviation (SD) of three biological replicates.

3.3 Deprivation of cystine leads to oxidative cell death and loss of the glutathione pool.

3.3.1 Cystine withdrawal results in production of reactive oxygen species in HME-EGFR cells which lead to oxidative cell death.

The majority of cystine in cells is used to produce glutathione, the most abundant antioxidant within cells (Lu, 2013). Given the importance of glutathione as a major antioxidant within cells, I next examined wild-type and HME-EGFR cells for evidence of oxidative stress during cystine deprivation. Figure 3.4A shows that total ROS increased in confluent cultures of HME-EGFR cells but not in cultures of wild-type HME cells following 12h of cystine deprivation as detected using FACS analysis with the DCFDA probe. Further exploration of more specific indicators of ROS in cystine-deprived cell cultures revealed increased levels of lipid ROS within membranes of HME-EGFR cells compared with wild-type HME cells (Figure 3.4 B). Thus, cystine deprivation leads to increased levels of ROS in cultures of HME-EGFR, but not wild-type HME cells.

Next, I investigated the role of ROS in facilitating cell death in HME-EGFR cells. I treated HME-EGFR cells with two different ROS scavengers, idebenone and α-tocopherol. Idebenone is a short-chain benzoquinone, a synthetic analogue of coenzyme Q10, with antioxidant activity against a variety of different radical species (Mordente et al., 1998). Idebenone is less lipophilic than coenzyme Q10, making it more readily available by allowing for its localisation in the cytoplasm as well as inside mitochondria (Gueyen et al., 2015). α-tocopherol is a naturally-occurring homologue of vitamin E, and acts as a potent lipophilic antioxidant within biological membranes (Brigelius-Flohe, 2009). Treatment with either of these antioxidants

rescued HME-EGFR cells from cystine deprivation-induced cell death (Figure 3.5). The differential mechanisms of how these compounds work to lower ROS indicates that rescue is not due to the individual properties of each compound, rather it is their collective ability to negate oxidative stress generated by cystine deprivation.

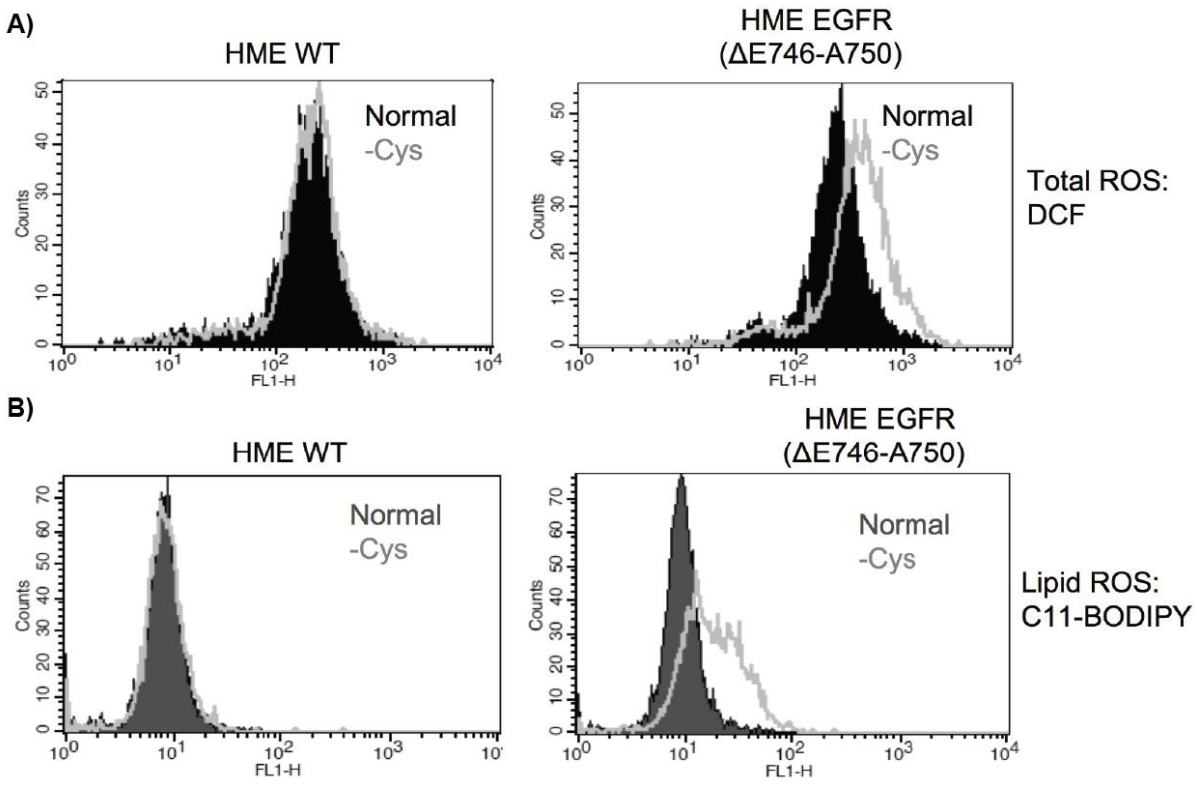

Figure 3.4 FACS analyses of total ROS and lipid peroxidation in wild-type and HME-EGFR cell lines.

Total ROS was measured using the DCFDA probe following 12h of cystine deprivation in wild-type (top left) and HME-EGFR (top right) and using FL1-H channel for detection. Lipid ROS was measured using the C11-BODIPY probe following 12h of cystine deprivation in wild-type (bottom left) and HME-EGFR (bottom right) and using FL1-H channel for detection. Each histogram shows the spread of a population of minimum 5000 events of cells in complete medium (dark graphs) or in medium lacking cystine (light outline).

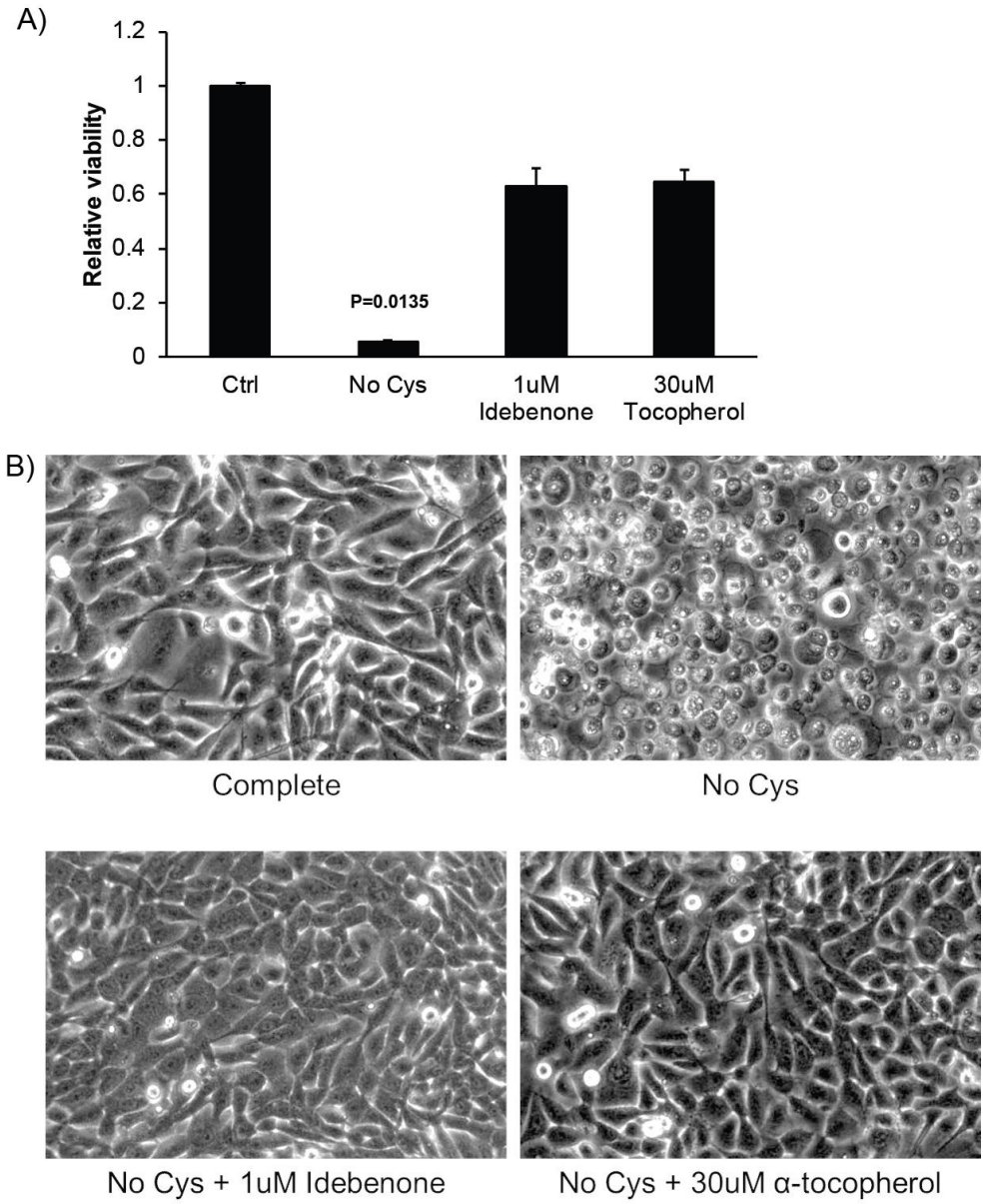

Figure 3.5 Treatment with ROS scavengers protects HME-EGFR cells from oxidative cell death caused by cystine depletion.

Confluent HME-EGFR cells were cultured in complete or cystine deprived media in the presence or absence of idebenone (1μM) or α-tocopherol (30μM) for 24h. A, viability assay using the Cell-titre Glo reagent. Viability of cells in cystine-deprived media was normalised to that of cells in complete media that was given the arbitrary value of 1. Statistical analysis was performed using a Kruskal Wallis non-parametric with Dunn's post hoc test (p=0.0135). Each graph represents the average viability ± standard deviation (SD) of three biological replicates. B, 20X phase-contrast images depicting HME-EGFR cells cultured in complete media (top left), in cystine-deprived media (top right), in cystine-deprived media supplemented with 1μM idebenone (bottom left) and in cystine-deprived media supplemented with 30μM α-tocopherol (bottom right).

3.3.2 HME cells experience activation of a nutrient stress response and loss of intracellular cystine levels following deprivation of cystine.

Having established that ROS was generated within confluent HME-EGFR cells when cystine is absent from the growth media, and was associated with the induced cell death, it was therefore important to determine if the intracellular levels of cystine corresponded to the deprivation of the nutrient from the growth media. To address this question, I deprived cells of cystine and performed an immunoblotting experiment to detect induction of GCN2 phosphorylation, a general sensor of amino acid depletion which becomes activated when phosphorylated (Hinnebusch, 2005). Both wild-type and EGFR mutant HME cells, demonstrated strong activation of GCN2 that peaked at 4h and remained high until after 20h later (Figure 3.6 A), indicating that the two cell lines responded to cystine deprivation in a similar way.

In these experiments the steady state levels of cystine levels were also measured using liquid chromatography–mass spectrometry (LC-MS), showing that the basal levels of this amino acid within wild-type and EGFR mutant HME cells were similar and declined equivalently following extracellular cystine depletion (Figure 3.6B).

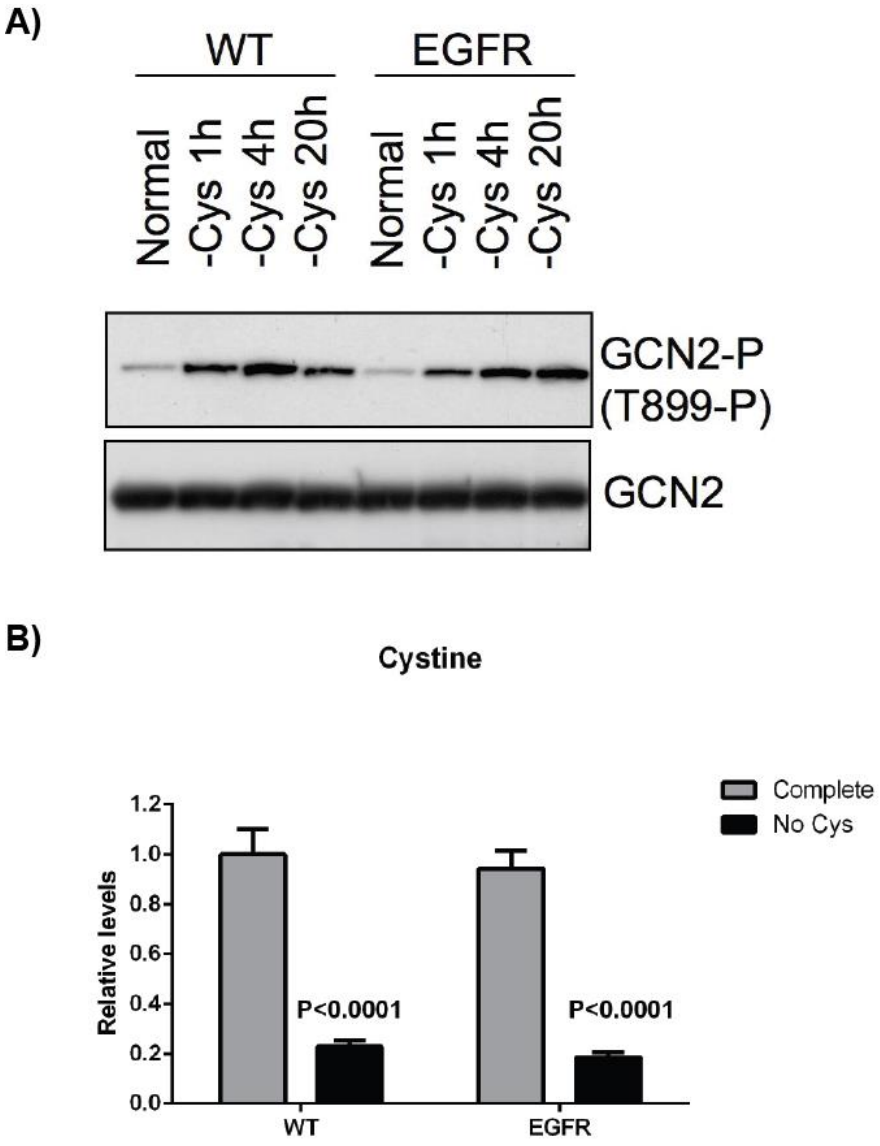

Figure 3.6 Culture of HME cells in the absence of cystine stimulates GCN2 and results in loss of the intracellular cystine pool.

A, immunoblot analysis of phosphorylated GCN2 in wild-type HME and HME-EGFR cells cultured in complete or cystine-deprived media for 1h, 4h and 20h, B, Amino acid analysis of steady-state levels of cystine, measured by LC-MS in wild-type and EGFR (delE746-A750) cells cultured in complete media (grey bars) or media lacking cystine (black bars) for 8 hours. Bar plots represent the average values ± standard deviation (SD) of three biological replicates with the viability in complete media for wild-type HME cells assigned the arbitrary value of 1. Statistical analysis comparing differences between complete and cystine deficient media was performed using a student's T-test. Amino acid analysis with LC-MS was performed by Dr Christiaan Labuschange.

3.3.3 Depletion of glutathione pools occurs due to cystine restriction.

Having established that levels of cystine within cells decline in response to deprivation of cystine and that ROS accumulation occurs, it was therefore important to determine whether this was occurring as a result of decreased glutathione levels. To achieve this aim I examined the total levels of glutathione within cultures of wild-type and HME-EGFR cell lines. Basal levels of total glutathione, and of both reduced (GSH) and oxidised glutathione (GSSG) were found to be higher in HME-EGFR cells compared to wild-type cells (Figure 3.6). Cystine deprivation however decreased the levels of glutathione to a similar degree in both cell types following 8h and 12h culture under these conditions. With respect to GSSG, while HME-EGFR cells initially had increased levels compared to wild-type HME cells, by 8h of culture in the absence of cystine the levels declined equivalently. Thus, decreased levels of glutathione are unlikely to be the cause of increased ROS production associated with cell death in HME-EGFR cells following cystine depletion.

As a positive control to affect glutathione depletion, I treated cells with BSO a potent inhibitor of γ-glutamylcysteine synthetase (Griffith and Meister, 1979). Treatment of both cell types in complete media with BSO for 12 h decreased equivalently the levels of all glutathione pools to levels similar to those observed in cells cultured under conditions of cysteine deprivation (Figure 3.7). To investigate whether loss of the glutathione pools explained the cell death resulting from cystine depletion I assayed cell viability following BSO treatment. However, despite the similarity between BSO and cystine deprivation in affecting the levels of the glutathione pool (Figure 3.7), treatment with BSO failed to induce cell death of either wild-type or HME-EGFR cells after 24h of treatment (Figure 3.8, panel A). Moreover, BSO also failed to induce accumulation of total or lipid-associated ROS in

either cell type (Figure 3.8, panels B and C). These data therefore indicate that the effect of cystine deprivation on glutathione levels is unlikely to be the causative agent inducing cell death of HME-EGFR cells.

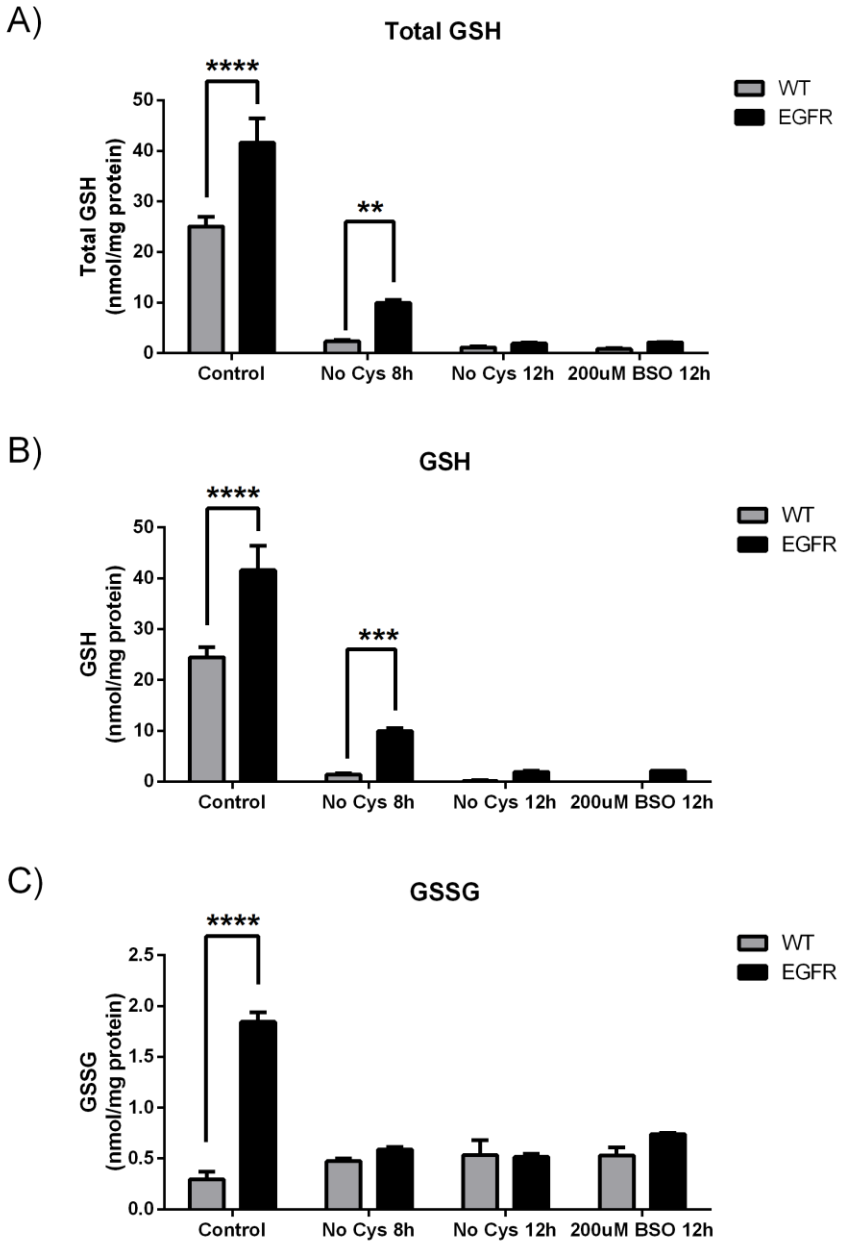

Figure 3.7 Cystine deprivation induces equivalent glutathione depletion in wild-type and HME-EGFR cells.

Total, reduced and oxidised glutathione in confluent cultures of wild-type HME (WT, dark grey bars) and HME EGFR cells (black bars) investigating the effect of cystine deprivation. A, bar graph of total glutathione levels (GSH+2GSSG). B), bar graph of reduced glutathione (GSH) levels. C, bar graph of oxidised glutathione (GSSG) levels. Measurements were performed on cells cultured in complete media for 12 hours (Complete) or in media lacking cystine for 8 and 12 hours. As a positive control BSO (200μM for 12h h) was added to cells cultured in complete media, and measurement of the glutathione pool performed. Measurements are mean ±SD of three biological replicates. Statistical analysis was performed using a two-way ANOVA with a Bonferroni post hoc test.

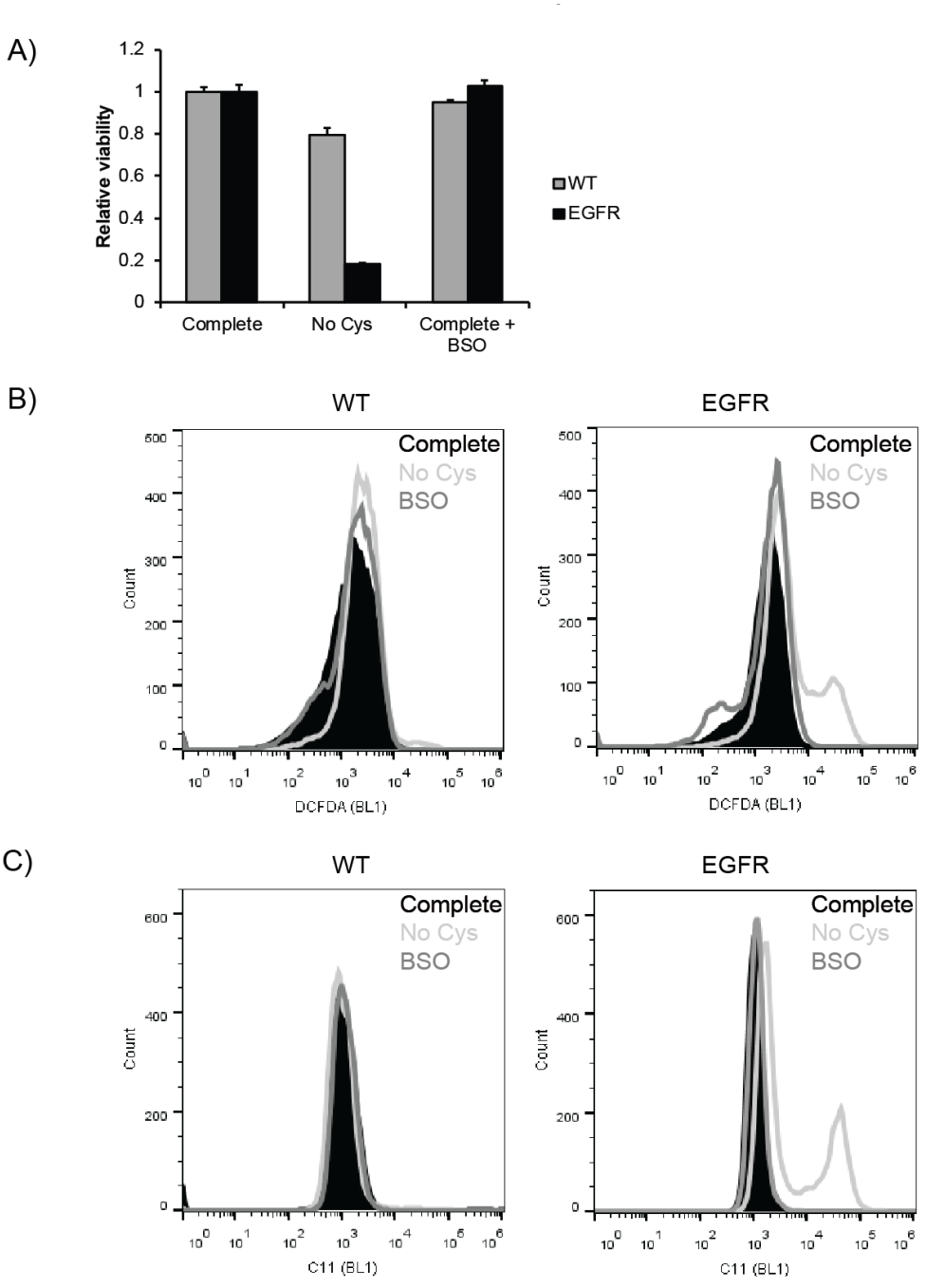

Figure 3.8 BSO treatment does not induce cell death nor induce total or lipid ROS, unlike deprivation of cystine.

A, viability of wild-type HME cells (gray bars) and HME-EGFR cells (black bars). Viability of cells cultured for 24 hours in complete media (light bars), or media lacking cystine or complete media containing 200μM BSO (BSO) for 24 h with viability measured using CellTitre Glo. Bar plots represent the average values ± standard deviation (SD) of three biological replicates with the level in complete media assigned the arbitrary value of 1. B, FACS analyses of total ROS; and C, FACS analyses or lipid ROS in wild-type (left) and HME-EGFR (right) cells cultured in complete (black traces) or media lacking cystine for 12h (light grey) or complete media following treatment with BSO (dark grey).

3.4 Deprivation of cystine induces cell death by ferroptosis.

3.4.1 Ferrostatin and Deferroxamine protect HME-EGFR cells from cystine deprivation-induced cell death unlike the pan-caspase inhibitor z-VAD-fmk.

The requirement for cystine to regulate oxidative stress suggested that HME-EGFR cells may undergo ferroptosis, an iron-dependent form of non-apoptotic cell death (Dixon et al., 2012). Ferroptosis is an oxidative type of cell death that occurs due to accumulation of lipid peroxides via a process that requires the presence of iron (Dixon et al., 2012). The significance of iron may be attributed to its role of in the Fenton reaction and its chelation is sufficient to prevent induction of lipid peroxidation(Yang and Stockwell, 2008). Additionally, an inhibitor of ferroptosis, Fer1 has been developed (Dixon et al., 2012). Fer1 is a potent radical trapping antioxidant when present in phospholipid membranes that can react with and neutralise lipid peroxides, thereby acting as an inhibitor of ferroptosis (Zilka et al., 2017). This hypothesis is strengthened by observations that HME-EGFR cells accumulate lipid ROS following cystine deprivation (Figure 3.4).

The notion that ferroptosis is the modality of cell death was tested by culturing HME-EGFR cells in the presence of the iron chelator Deferroxamine (DFO) or Fer1 under conditions of cystine deprivation. The presence of these compounds fully rescued HME-EGFR cells from cystine deprivation-induced cell death (Figure 3.9 A). In contrast, treatment of HME-EGFR cells with Z-VAD-FMK, a broad-spectrum caspase inhibitor that can effectively inhibit apoptosis (Cain et al., 1996; Cohen, 1997), had no effect on cell death induced by cystine deprivation. Importantly, treatment of HME-EGFR cells with Z-VAD-FMK rescued staurosporine (STS)-induced apoptotic cell death (Figure 3.9 B). Next, I investigated the effects of DFO

and Fer1 on cysteine deprivation-associated lipid peroxidation. Figure 3.9 C shows that treatment of cells DFO and Fer1 blocks the formation of lipid ROS in HME-EGFR cells under conditions of cystine deprivation. Taken together, rescue from cell death, and inhibition of lipid ROS accumulation by DFO and Fer1 treatment strongly suggests that cystine deprivation of these cells results in induction of ferroptosis. This phenomenon was not isolated to just HME-EGFR cells, but extended to the other hTERT-HME1 cell lines used in this study as Fer1 also provided protection against the variable loss of viability resulting from cystine deprivation of these cells (Figure 3.10).

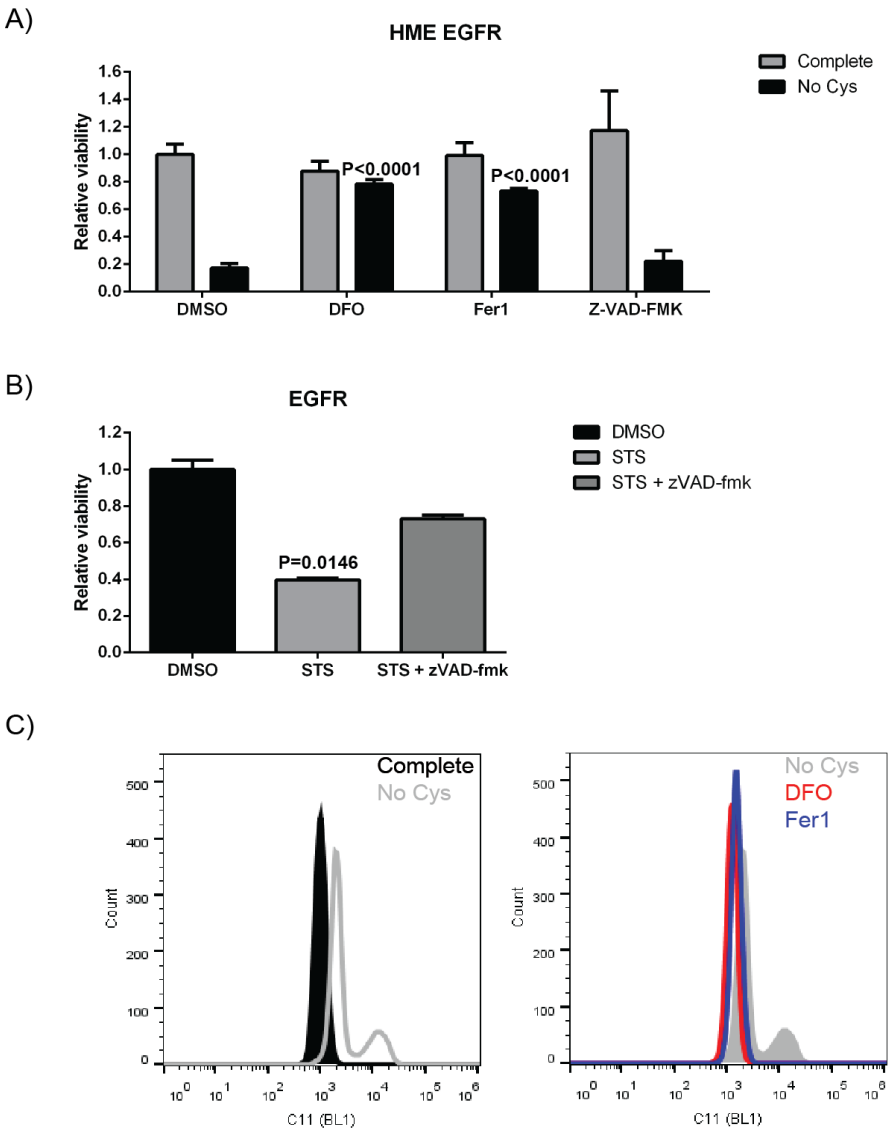

Figure 3.9 DFO and Fer1 protect HME-EGFR cells from cell death and generation of lipid ROS.

A, viability of HME-EGFR cells. Bar plots are average viability ± SD cells cultured in complete media (grey bars, DMSO assigned an arbitrary value of 1) or media lacking cystine for 24 hr (black bars) in the presence of DMSO as a control or DFO (100µM), Fer1 (2µM), or z-VAD-FMK (50µM). Statistical analysis was performed using a two-way ANOVA with a Bonferroni post hoc test. n = 3 per each group. B, viability of HME-EGFR cells. Bar plots are average viability ± SD cells cultured in control media with DMSO as a positive control (black bar, assigned an arbitrary value of 1) or 1µM of STS in untreated or pre-treated cells with 50µM z-VAD-FMK. Statistical analysis was performed using a Kruskal Wallis non-parametric test with a Dunn's post hoc test. n = 3 per each group. C, lipid ROS in HME-EGFR cells. Left histogram shows an overlay of cells cultured in complete (black) or media lacking cystine (grey) for 12 hr. On the right histogram all cells were grown in media lacking cystine in the absence (grey) or presence of DFO (100µM, red line) or Fer1 (2µM, blue line) for 12 hr.

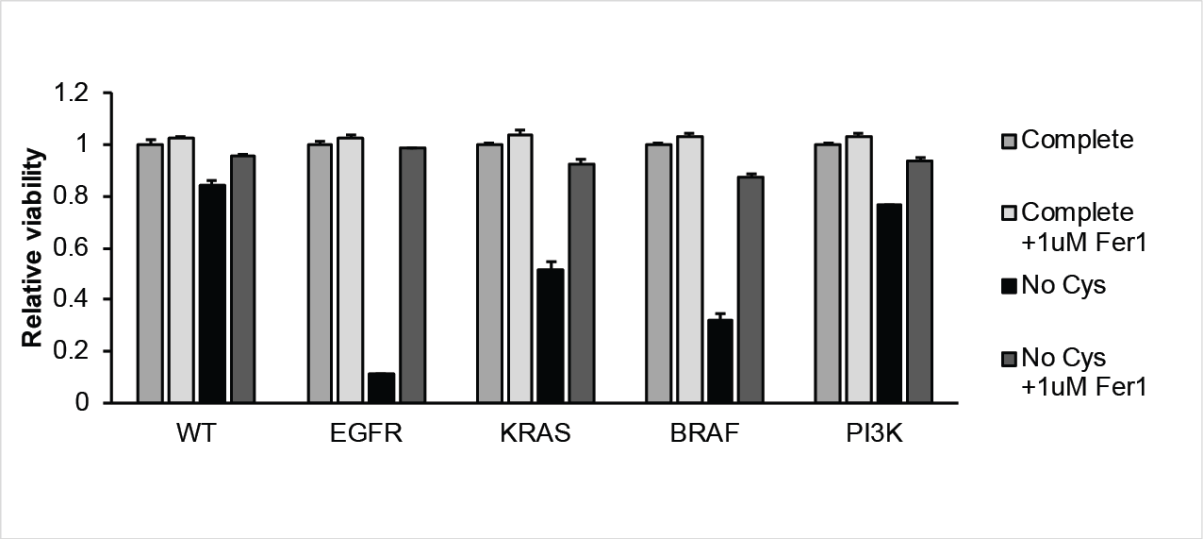

Figure 3.10 The variable loss of viability in HME cell lines following cystine depletion occurs by ferroptosis.

Cell viability of all HME1 cell lines in complete or cystine depleted media in the presence or absence of Fer1. Bar plot represents the average viability ± SD of cells normalised to the average viability of each cell line in complete media being 1. Viability was measured using the CellTitre-Glo assay.

3.4.2 Treatment with Erastin induces a similar differential loss of viability in HME-EGFR cells as cystine deprivation.

Erastin is a small molecule inhibitor that has been shown to induce ferroptosis in RAS mutant cell lines (Dixon et al., 2012). Despite being originally identified as an inhibitor of VDAC2 and VDAC3 (Yagoda et al., 2007), erastin is now thought to act primarily by inhibiting cystine uptake via the Xc system, a cystine/glutamate-antiporter (Dixon et al., 2012). Thus, I reasoned that erastin treatment should act equivalently to artificial removal of cystine from the cell culture media and lead to selective loss of viability of HME-EGFR cells. I treated both wild-type HME and HME-EGFR cells with erastin in normal media and measured cell viability. Erastin treatment led to a greater than 70% loss of viability in HME-EGFR cells, but did not cause any loss of viability in wild-type HME cells (Fig 3.11A). Moreover, HME-EGFR cells could be protected from loss of viability following either cystine deprivation and erastin treatment when supplemented with Fer1 (Figure 3.11). Thus, either blockade of cystine import or depletion of cystine from the cell culture media leads to a selective loss of viability of HME-EGFR cells.

A)

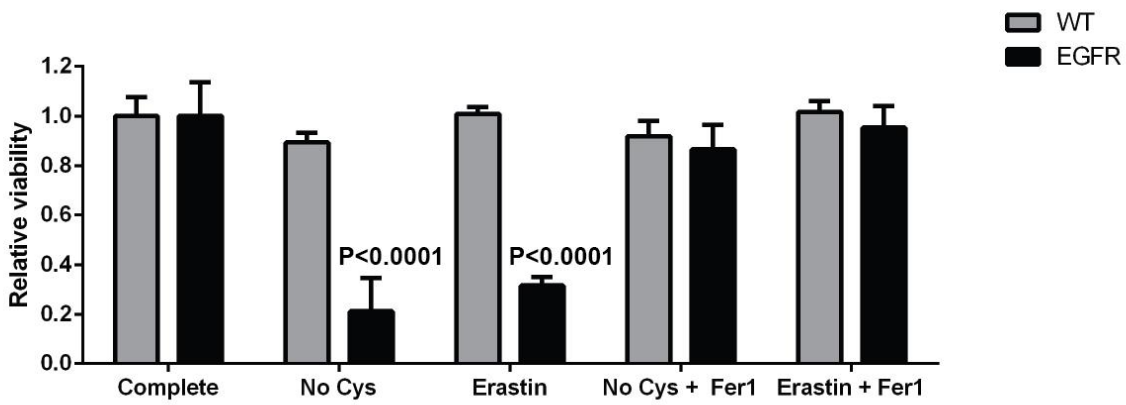
WT
EGFR
Relative viability
1.2
1.0
0.8
0.6
0.4
0.2
0.0
P<0.0001
P<0.0001
Complete
No Cys
Erastin
No Cys + Fer1
Erastin + Fer1

B)

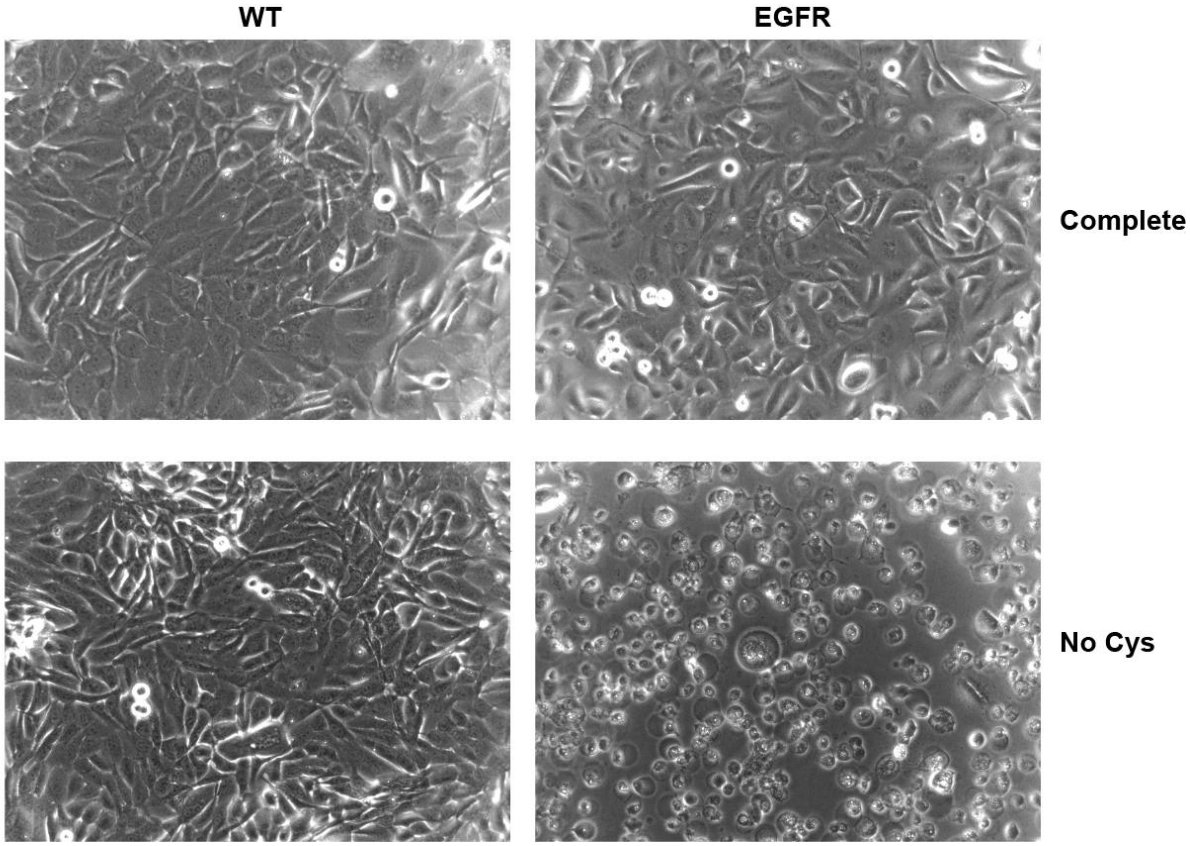
WT
EGFR
Complete
No Cys

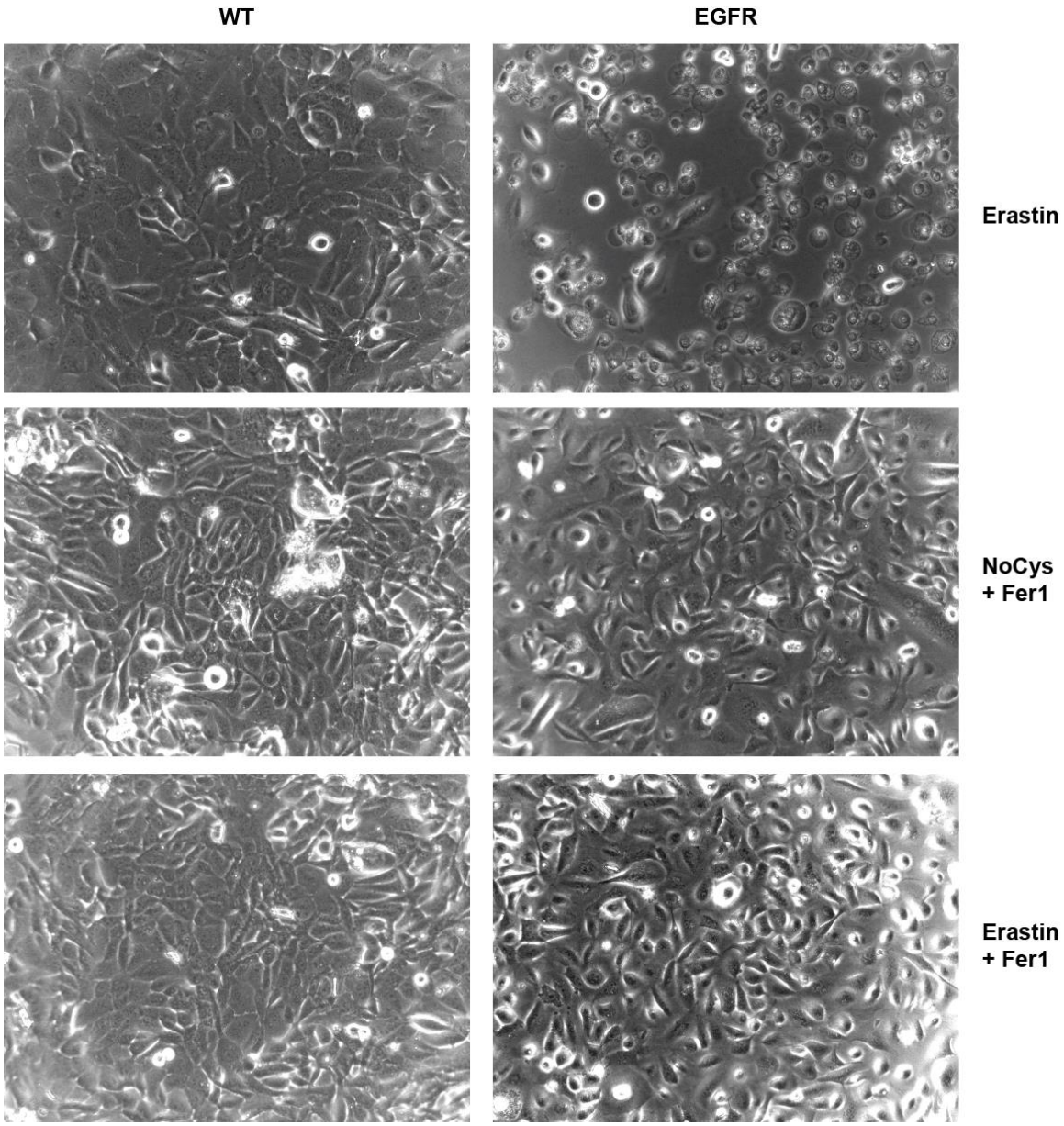

Figure 3.11 Erastin induces a differential ferroptotic response in HME-EGFR cells.

A, viability of wild-type HME (WT, gray bars) or HME-EGFR (black bars) cells. Bar plots represent the average viability ± SD cells cultured in normal media, media lacking cystine or normal media with Erastin (2.5μg/ml) for 24 hr in the presence or absence of Fer1. Viability was measured using the CellTitre-Glo assay and viability was normalised to the average viability of cells in complete media. Statistical analysis was performed using a two-way ANOVA with a Bonferroni post hoc test. n = 3 per each group. B, 20X phase-contrast images depicting wild-type (left) and HME-EGFR cells (right) cultured in complete media, in cystine-deprived media or normal media with Erastin for 24 hr in the presence or absence of Fer1.

3.4.3 Loss of intracellular cysteine leads to ferroptosis

The previous section showed that inhibition of X_{c-} system-mediated uptake of cystine using erastin generates a similar effect to deprivation of cystine from the growth media, with marked ferroptosis being observed in cultures of HME-EGFR cells. Although intracellular cystine is required for GSH synthesis, lack of GSH is not the cause of ferroptosis in these cells as shown in Figure 3.8. Nevertheless, cystine deprivation does cause reduction in intracellular cystine levels (Figure 3.6B), suggesting that cystine itself is required to prevent ROS formation, and that cysteine, generated by thioredoxin (TRX)-mediated reduction of cystine (Mandal et al., 2010a), is responsible for mediating this prevention. To test this hypothesis, I used auranofin, an inhibitor of TRX reductase (Gromer et al., 1998). Treatment of HME-EGFR cells with 1μM auranofin or 200μM BSO had no effect on cell viability or induction of lipid peroxidation (Figure 3.12). However, when combined, these two compounds induced ferroptosis in HME-EGFR cells to a similar extent as is observed under conditions of cystine deprivation, with viability of cells being reduced and accumulation of lipid peroxides being evident (Figure 3.12) The next experiment involved pre-treatment of HME-EGFR cells with BSO to effectively diminish GSH levels, then adding either Erastin or S-4-PG, two inhibitors of the X_{c-} system, or culturing the cells under conditions of cystine deprivation. In all cases, prior inhibition of GSH synthesis with BSO resulted in accelerated cell death (Figure 3.13). Taken together, these data demonstrate the central importance of cysteine within cells, acting to counteract either directly or as a precursor to GSH synthesis the formation of lipid peroxides that cause ferroptosis.

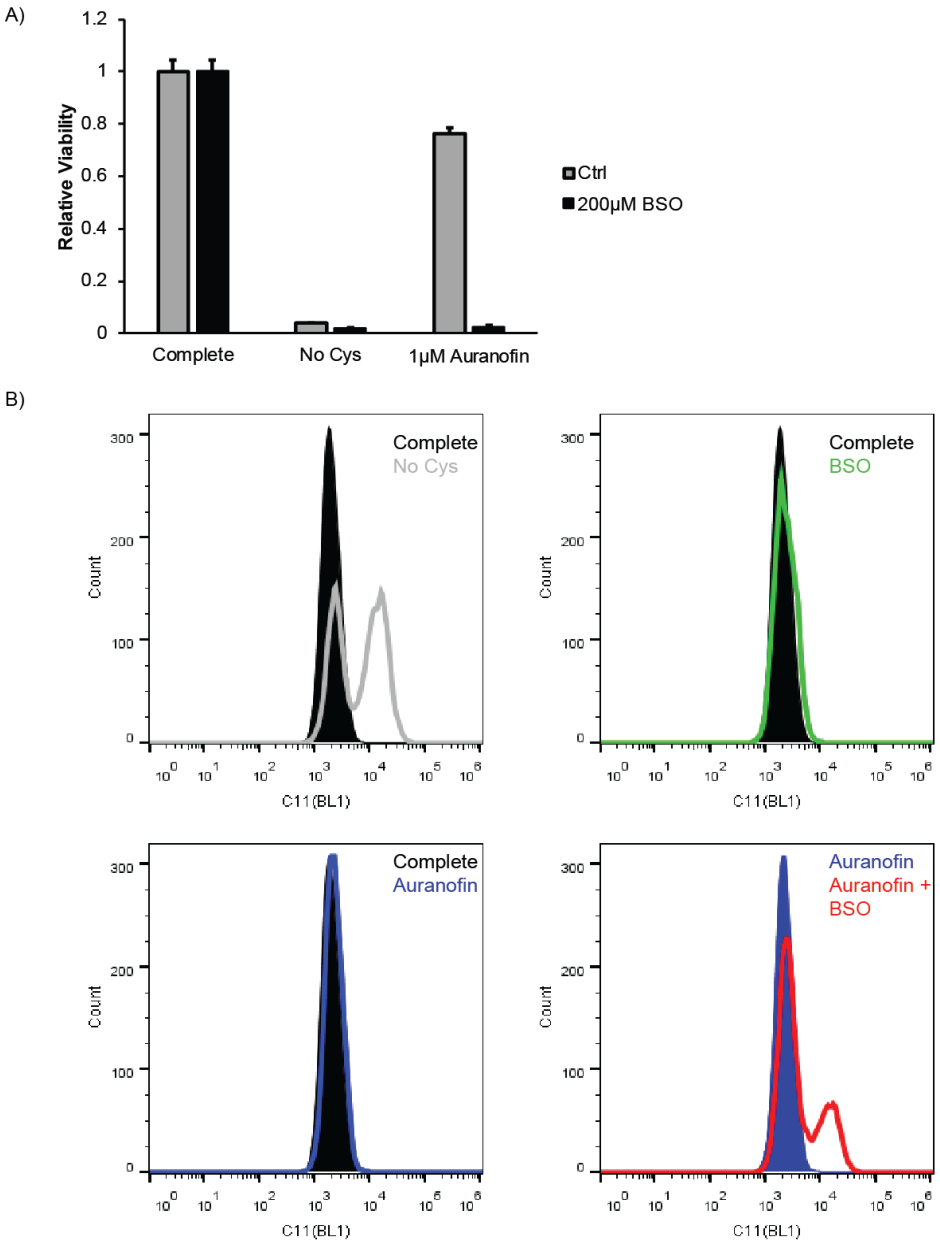

Figure 3.12 BSO and auranofin act synergistically to induce loss of reductive cysteine and lead to ferroptosis.

A, viability of HME-EGFR cells following 18h of DMSO (grey bars) or BSO (200μM, black bars). Bar plots represent the average viability ± SD cells cultured in complete media, media lacking cystine for 24h and complete media with auranofin (1μM) for 24 hr. Viability was measured using the CellTitre-Glo assay and normalised to the average viability of cells in complete untreated media. Statistical analysis was performed using a two-way ANOVA with a Bonferroni post hoc test. n = 3 per group. B, corresponding lipid ROS in HME-EGFR cells with the same treatments. Panels 1-3 show histograms of complete media (black) overlaid against cystine deprived media (gray) or single treatment histograms of BSO-treated cells (green) or auranofin-treated cells (blue). Panel 4 show a histogram overlay between mono-treatment of cells with auranofin (blue) or double-treatment with BSO and auranofin together (red).

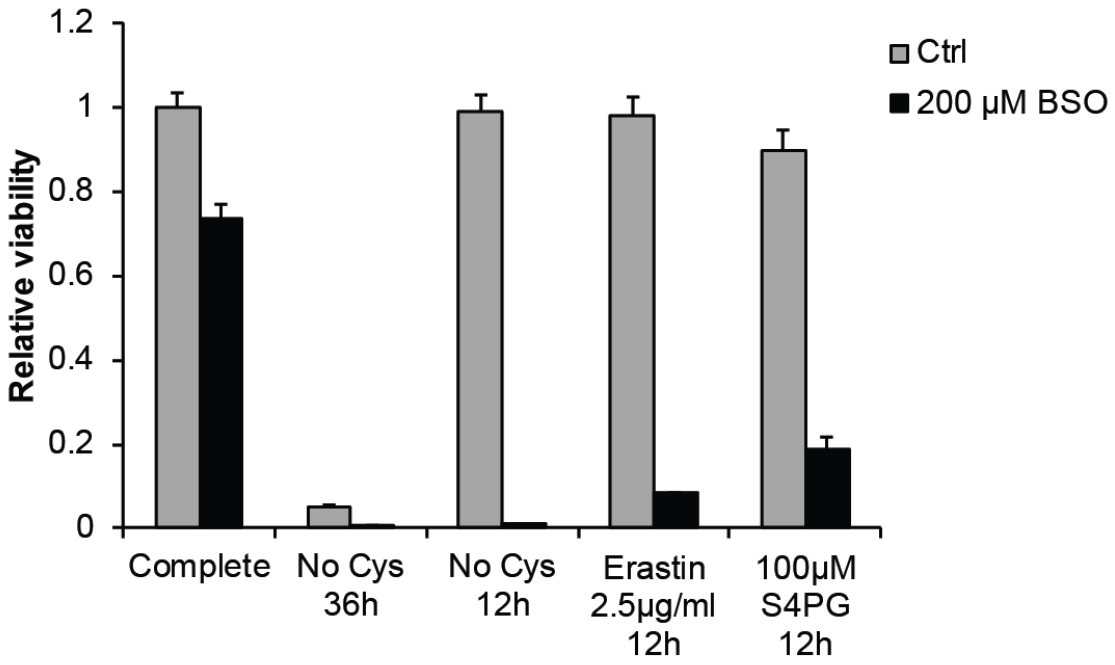

Figure 3.13 HME-EGFR cells undergo rapid ferroptosis after deprivation of cystine or inhibition of X_C- mediated cystine uptake when glutathione is diminished.

A, viability of HME-EGFR cells following pre-treatment with DMSO (grey bars) or 200µM BSO (black bars) for 24h. Bar plots represent the average viability ± SD cells cultured in complete media, media lacking cystine for 36h or 12h and complete media with Erastin (2.5µg/ml) or S4PG (100µM) for 12 hr. Viability was measured using the CellTitre-Glo assay and viability was normalised to the average viability of cells in complete untreated media. Statistical analysis was performed using a two-way ANOVA with a Bonferroni post hoc test. n = 3 per each group.

3.4.4 Glutaminolysis is not involved in ferroptosis occurring in HME-EGFR

Previous reports have indicated an important role for Gln and glutaminolysis in the process of ferroptosis (Gao et al., 2015). Measurement of glutamine and glutamate in order to determine if glutaminolysis was contributing to the induction of cystine deprivation cell death as is reported(Gao et al., 2015) showed that intracellular levels of the former were equivalent and unaffected by deprivation of cystine, whereas levels of the latter seemed to increase under these conditions (Figure 3.14). This increase in glutamate is likely due to the inhibitory effects that cystine deprivation has on the Xc- (Bannai, 1984). Taken together, these data indicate that glutaminolysis is not affected by cystine deprivation in the HME-EGFR cells used and is therefore unlikely to contribute to ferroptosis. Instead, a rapid loss of intracellular cystine is observed and is responsible for the induction of the ISR through GCN2 activation.

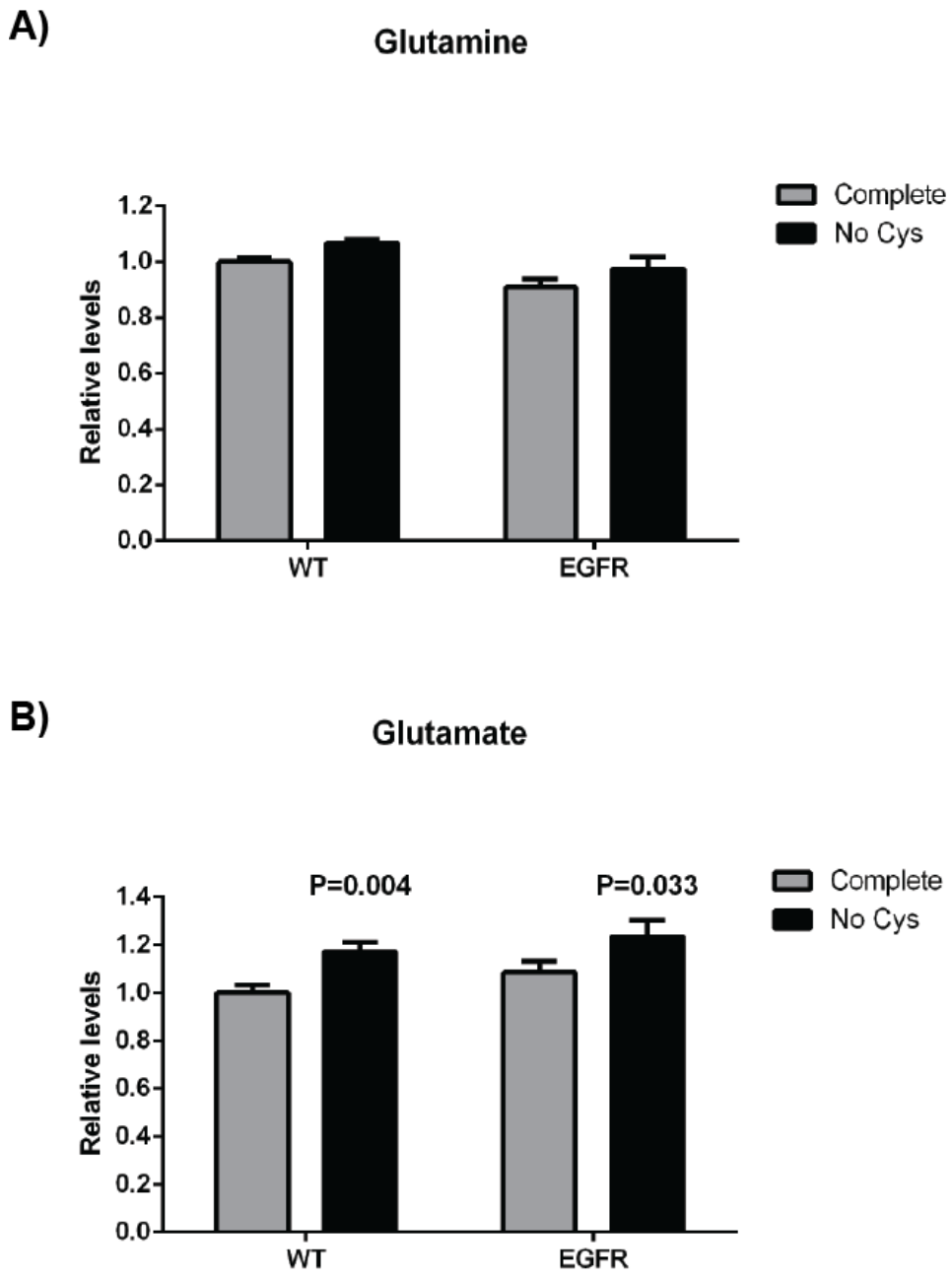

Figure 3.14 Steady state levels of Gln and Glu do not suggest involvement of glutaminolysis in modulation of ferroptosis in HME cells.

Amino acid analysis of steady-state levels of glutamine (A) and glutamate (B) measured by LC-MS in wild-type HME and EGFR (delE746-A750) cells cultured in complete media (grey bars) or media lacking cystine (black bars) for 8 hours. Bar plots represent the average values ± standard deviation (SD) of three biological replicates with the viability in complete media for wild-type HME cells assigned the arbitrary value of 1. Statistical analysis comparing differences between complete and cystine deficient media was performed using a Student's T-test. Amino acid analysis with LC-MS was performed by Dr Christiaan Labuschange.

3.5 Conclusions

This chapter reports the finding that cystine is essential for survival of HME cells with an activating EGFR mutation. This finding is the result of a viability screen whereby wild-type HME or EGFR-, BRAF-, KRAS- and PI3K-mutant HME cells were grown in media lacking individual amino acids. All of the cell lines used demonstrated some loss of viability following removal of cystine from growth media, but the cell lines containing EGFR and BRAF mutations were most sensitive to this condition. However, when allowed to grow to confluence, only the EGFR mutant HME cells remained fully sensitive to cystine deprivation.

Confirmation of the essential requirement of HME- EGFR- cells for cystine was achieved in experiments titrating the addition of this amino acid to growth media. These experiments showed a requirement for a minimal concentration of 2μM L-cystine that could not be rescued with the D-cystine. This result shows that HME-EGFR cells have a specific requirement for L-cystine. This is likely due to the stereoselectivity of the X_{c-} system transporter for L-cystine and not its enantiomer, D-cystine.

Cystine taken up by cells is reduced to cysteine for biosynthetic purposes (Bannai and Kitamura, 1980). To determine if the ISR is induced following restriction of cystine I measured the phosphorylation of GCN2, the EIF2AK4 that senses loss of individual amino acids and activates phosphorylation of eIF2α (Hinnebusch, 2005), and found that both cell lines experience similar levels of kinase activation and thereby presumably similar levels of intracellular cystine depletion. This conclusion was further strengthened using LC-MS to quantify the intracellular levels of cystine, which did not differ significantly and declined equivalently after deprivation of cystine.

The majority of intracellular cysteine is utilised by cells primarily for glutathione synthesis, and only a smaller proportion is incorporated into proteins (Lu, 2013). To address if the differential response observed in EGFR-HME1 cells is due to lower levels of glutathione following cystine deprivation, I measured the levels of reduced and oxidised glutathione. My results demonstrate that wild-type and EGFR-HME1 cells experience a similar decrease in their total levels of glutathione when they are cultured in the absence of cystine. However, induction of cell death in HME-EGFR cells is not the result of reduced glutathione levels alone because pharmacological inhibition of glutathione synthesis (with BSO) was ineffective in killing cells despite inducing loss of the glutathione pool. These results suggest that HME-EGFR cells require cysteine/cystine to compensate for loss of glutathione in the maintenance of their survival.

Glutathione in cells is responsible for opposing ROS (Lu, 2013). Thus, cell lines generating increased levels of ROS will be sensitive to decreased glutathione levels. Analysis of wild-type HME and HME-EGFR cells showed increased comparative levels of total ROS as well as lipid peroxides, a secondary product of ROS that affects membrane lipids, in the latter. The probable role of ROS in the loss of viability induced in EGFR-HME1 cells by cystine deprivation was confirmed in experiments where addition of ROS scavengers, compounds that neutralise produced oxygen radicals, protected the cells from the death response. Taken together, these observations indicate that uncontrolled oxidative stress is the underlying cause of loss of viability.

Ferroptosis is an iron-dependent regulated form of necrotic cell death that results from the accumulation of lipid peroxidation in cell membranes. Characteristic

features of this mechanism of cell death are a requirement for cystine and a phenotype of lipid ROS accumulation. HME-EGFR cells cultured in the absence of cystine show evidence of oxidative stress, suggesting that they undergo ferroptosis. To confirm this hypothesis experiments were carried out testing the effects of the ferroptosis-selective inhibitor Fer1 and the iron chelator DFO. Culture of HME-EGFR cells with these inhibitors protected them from accumulation of lipid peroxides and subsequent loss of viability under conditions of cystine deprivation, whereas treatment with z-VAD-fmk, an inhibitor of caspase-mediated apoptosis had no effect. Further evidence of ferroptosis was provided using Erastin, a compound that effectively blocks the X_{c-} system, a cystine-glutamate antiporter that transfers cystine inside cells in exchange for intracellular glutamate. (Dixon et al., 2012). Treatment of wild-type and HME-EGFR cells with Erastin induced a selective cell death response undistinguishable from that observed under conditions of cystine deprivation. Finally, I confirmed that cystine itself is the important component that protects cell from ferroptosis acting either as a precursor of GSH or in combination with thioredoxin when GSH synthesis is impaired. Moreover, measuring intracellular levels of glutamine and glutamate that again did not differ between the two cells lines I was able to rule out any possible involvement of glutaminolysis in ferroptosis as other reports had suggested (Gao et al., 2015).

In summary, the results presented in this chapter indicate that loss of cystine induces a ferroptotic cell death response in HME-EGFR cells. This observation could be extended to the other hTERT-HME1 cell lines to different degrees because Fer1 treatment also inhibited the variable loss of viability under cystine deprivation conditions in all HME cell lines tested. The striking feature of my findings is the

exquisite sensitivity of HME-EGFR cells to cystine deprivation, suggesting that the constitutive signals generated by the mutant EGFR (delE746-A750) endow a selective requirement for cystine. The next chapter of this thesis investigates the elements of this signalling pathway with the aim of determining why HME-EGFR cell survival depends upon cystine.

4. CHAPTER 4: EGFR SIGNALLING SENSITISES CELLS TO FERROPTOSIS.

4.1 Introduction

In the previous chapter I identified an active requirement for the amino acid cystine in maintaining viability of hTERT-immortalised HME cells expressing a mutationally-active EGFR oncoprotein. The EGFR protein is member of a receptor tyrosine kinase (RTK) protein family that transduces extracellular signals resulting in intracellular responses of cells (Pines et al., 2010). Activation of EGFR under physiological conditions is dependent upon the presence of ligands such as EGF or TGF-α. Ligand binding leads to receptor dimerization allowing cross-phosphorylation of tyrosine residues within the EGFR intracellular domains (Seshacharyulu et al., 2012). Activated receptors then trigger multiple downstream signalling cascades including activation of the MAPK and PI3K-AKT pathways (Figure 4.1) (Raymond et al., 2000).

In the cell system studied in this thesis, the mutation that was introduced in the *EGFR* gene is deletion of exon 19, which is the most common *EGFR* mutation found in NSCLC, followed by an exon 21 mutation, L858R (Shigematsu and Gazdar, 2006). Both mutations lead to an active protein kinase that is not strictly dependent upon ligand binding for activity, although retaining some responsiveness to EGF binding (Greulich et al., 2005). Response to EGFR signalling inhibition in cell lines of NSCLC origin is dependent on activation of MAPK and AKT pathways highlighting their importance in EGFR-driven oncogenesis (Ono et al., 2004).

Since the presence of a mutant *EGFR* allele sensitises HME cells to ferroptosis it became pertinent to inhibit EGFR and its downstream targets and determine whether this response was strictly dependent upon EGFR activation. Such

an approach would allow me to determine the mechanism through which the presence of an EGFR mutation determines sensitivity to ferroptosis. To block EGFR signalling I used gefitinib, an FDA-approved EGFR-inhibitor for the management of NSCLC (Baselga and Averbuch, 2000). Gefitinib can inhibit both wild-type and mutant (delE746-A750 and L858R) EGFR by binding to the ATP-binding cleft (Yun et al., 2007). Gefitinib has demonstrated clinical efficacy in the treatment of NSCLC with EGFR mutations, particularly those patients with EGFR deletions of exon 19 (Paez et al., 2004; Riely et al., 2006).

To determine if the signals that confer sensitivity are mediated through the MAPK signalling cascade I selected selumetinib, an allosteric ATP-non-competitive MEK inhibitor that blocks downstream activation of ERK (Yeh et al., 2007). To inhibit activation of PI3K I employed wortmannin an inhibitor that acts by covalently binding to the active site of the catalytic subunit of PI3K (Arcaro and Wymann, 1993; Wymann et al., 1996).

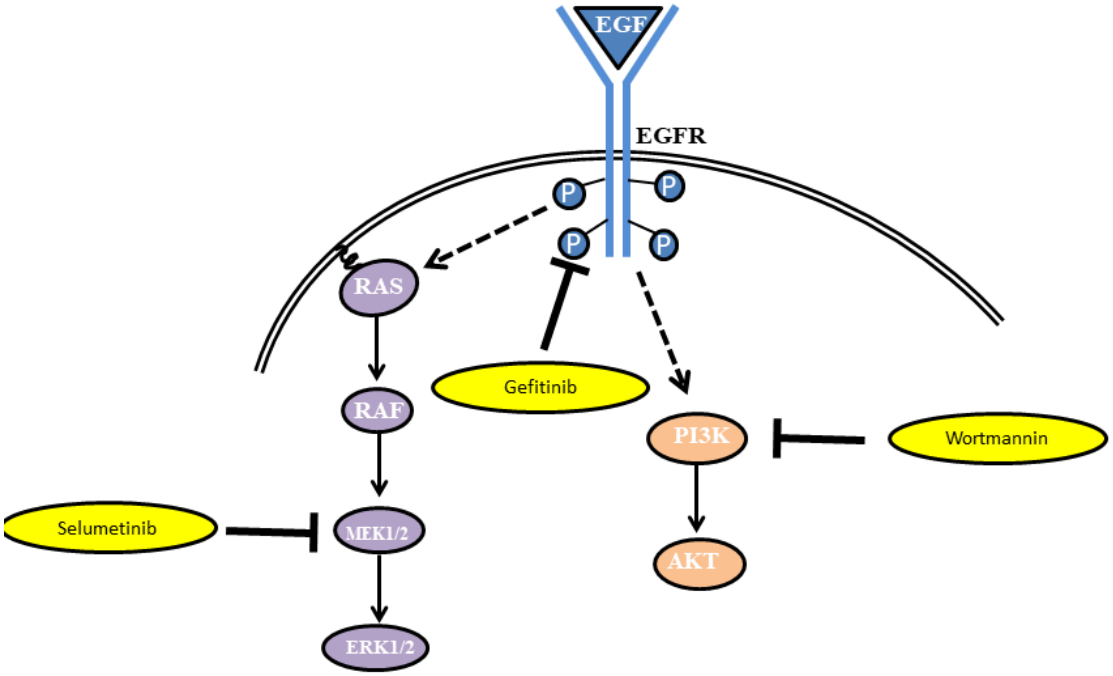

Figure 4.1 Schematic representation of EGFR pathway and its downstream pathways PI3K and MAPK pathway.

Following interaction with its ligand, EGF, the EGFR dimerises facilitating cross-phosphorylation of specific tyrosine residues within the intracellular domain. Activated EGFR signalling can lead to activation of the MAPK pathway via the signalling cascade of RAS-RAF-MEK-ERK, or activation of the AKT pathway through activation of PI3K. To identify the downstream components of this signalling pathway that confer sensitivity to ferroptotic cell death three different inhibitors were used. Gefitinib (Iressa) which inhibits the kinase activity of the EGFR itself; selumetinib which inhibits the MAPK pathway via inhibition of MEK, and wortmannin which inhibits activation of the AKT pathway by blocking the catalytic activity of PI3K.

4.2 Inhibition of EGFR-mediated MAPK activation rescues cells from ferroptosis.

The first step in understanding the mechanism whereby constitutively active EGFR signalling drives sensitivity to ferroptosis was through inhibition of the downstream signalling pathways. To determine the effectiveness of gefitinib, selumetinib and wortmannin, respective inhibitors of EGFR, MEK and PI3K within the EGFR-induced signalling pathway, an immunoblotting experiment was performed after treatment of HME-EGFR cells. Treatment of HME-EGFR cells with 1μM gefitinib for 30 hours effectively blocked phosphorylation of EGFR and downstream phosphorylation of ERK1/2 (Fig. 4.2A). Surprisingly, phosphorylation of AKT was unaffected by treatment of the cells with gefitinib but was blocked when cells were treated with 1μM wortmannin suggesting that AKT activation in HME-EGFR cells is independent of EGFR activity. Finally, treatment of HME-EGFR cells with 5μM selumetinib effectively inhibited ERK1/2 phosphorylation. Similar results were obtained when HME-EGFR cells were cultured in the absence of cystine for 12h, with the exception that ERK1/2 phosphorylation *was* enhanced following deprivation of cystine. Taken together, these data demonstrate that gefitinib, selumetinib and wortmannin are effective inhibitors of their respective targets within HME-EGFR cells.

These inhibitors were then tested to investigate their effect upon cystine deprivation-induced ferroptosis. Ferroptosis of HME-EGFR cells was reversed when the cells were pre-treated with gefitinib and, to a lesser extent, selumetinib for a total of 30 hours (Figure 4.2 B). In contrast, the PI3K inhibitor wortmannin did not inhibit ferroptosis, following cystine deprivation (Figure 4.2 B). Taken together with

observations showing that HME-EGFR cells are particularly sensitive to cystine deprivation compared to wild-type HME cells, these observations indicate that constitutive signals from EGFR to the MAPK pathway play a critical role in ferroptosis when the availability of cystine is restricted. In contrast, the PI3K pathway appears not to be involved in promoting sensitivity to ferroptosis in these cells.

The rescuing effect following sustained gefitinib or selumetinib treatment was also observed in control of cellular morphology. By phase-contrast microscopy HME-EGFR cells pre-treated with the EGFR or MEK inhibitors appeared flattened and demonstrated more well-defined cell-cell borders (Fig. 4.3). Following deprivation of cystine cells treated with DMSO and wortmannin demonstrated features of ferroptosis as observed previously, with swollen plasma membranes and condensed nuclei. In contrast, cells in which the MAPK pathway was inhibited by prior treatment with selumetinib did not undergo ferroptosis and cells remained flattened with well-defined cell-cell borders as observed by phase-contrast microscopy (Fig. 4.3, bottom right panel).

In Chapter 3 I showed that cystine deprivation increased ROS levels within cells, particularly lipid ROS. To investigate the role of MAPK pathway in generating ROS a flow cytometry experiment was performed. Pre-treatment of HME-EGFR cells with gefitinib and selumetinib blocked the formation of total ROS (Figure 4.4) and lipid ROS (Figure 4.5) in cells cultured under conditions of cystine deprivation in HME-EGFR cells. In contrast, inhibition of PI3K with wortmannin had no effect on induction of total ROS or lipid ROS in HME-EGFR cells. These results suggest a critical role for the MAPK pathway in generating ROS involved in the process of ferroptosis in these cells.

A)

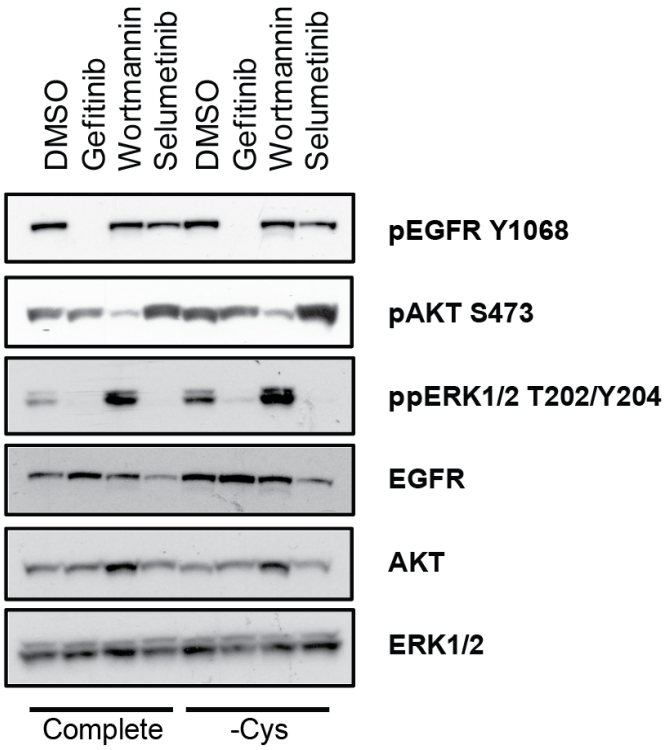

B)

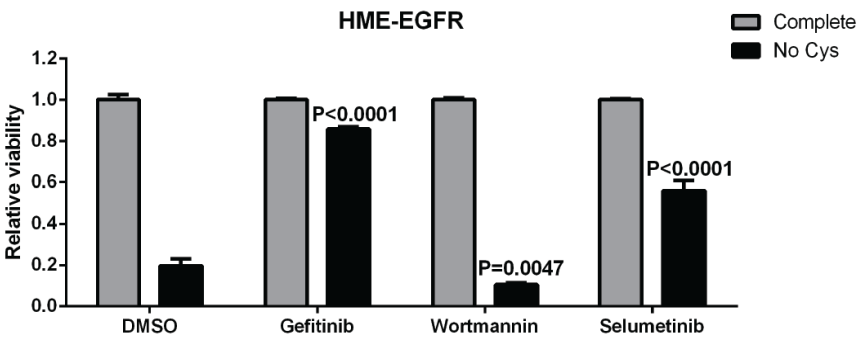

Figure 4.2 Inhibition of EGFR signalling in HME-EGFR cells.

HME-EGFR cells were cultured in complete media (Complete) or media lacking cystine (-Cys) for 12h in the presence of DMSO, 1μM Gefitinib, 1μM Wortmannin, or 5μM Selumetinib added for a total of 30h. A, immunoblot analysis of HME-EGFR cell lysates probed to detect phosphorylated EGFR, AKT, and ERK. B, viability assay examining the effect of the indicated inhibitors following deprivation of cystine for 24h. Each bar represents mean ± SD of three biological replicates of cells cultured in complete media (grey bars) or media lacking cystine for 24 hr (black bars). All measurements are expressed relative to the viability of HME-EGFR cells grown in complete media (assigned the arbitrary value of 1). Statistical analysis was performed using a 2-way ANOVA test with a Bonferroni's post hoc comparing each treatment effect following cystine deprivation with the DMSO treated control.

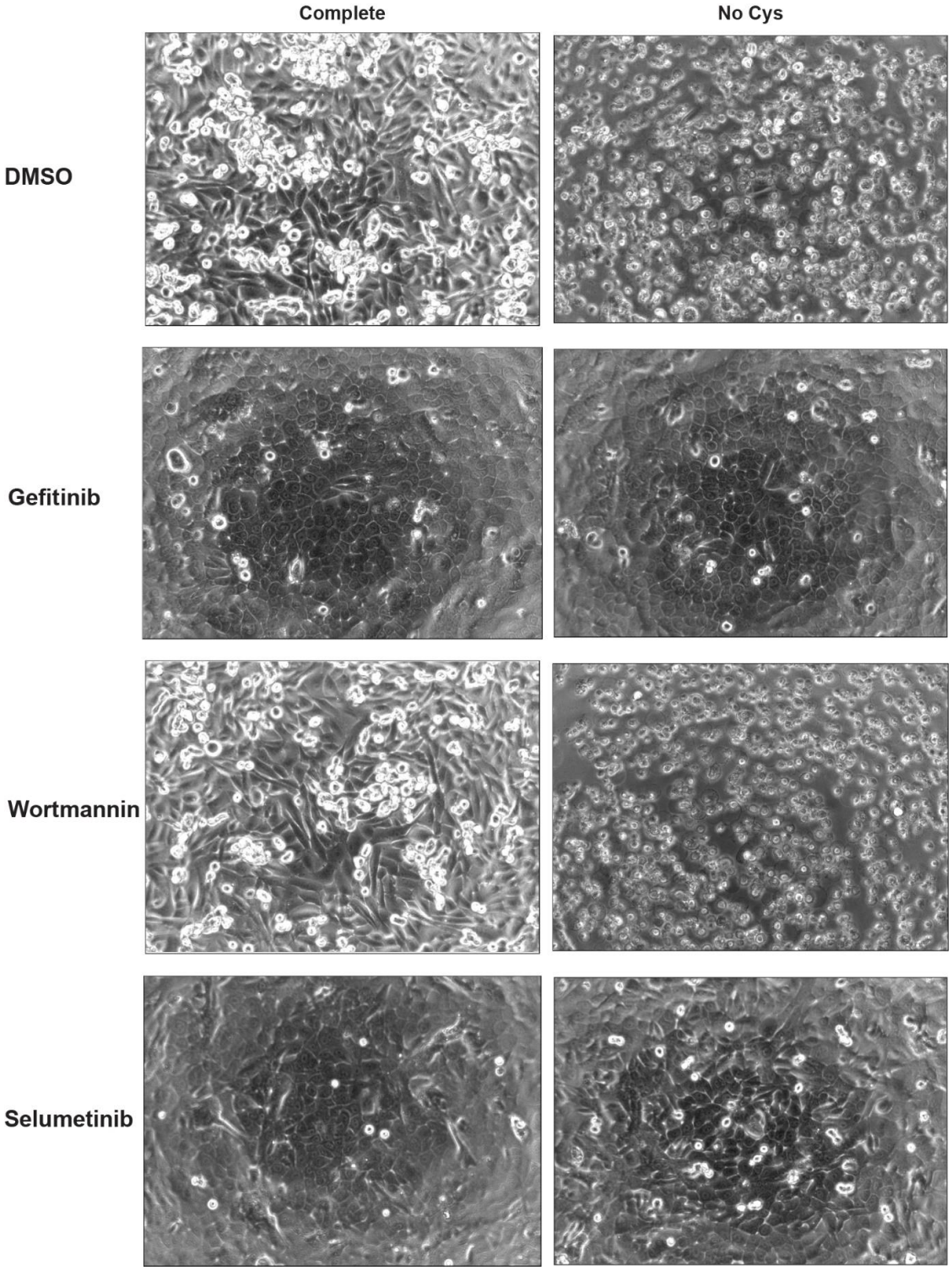

Figure 4.3 Inhibition of EGFR and MAPK signalling in HME-EGFR cells protects cells from ferroptosis and induces morphological changes.

20X phase-contrast images showing HME-EGFR cells cultured in complete media (Complete, left panels) or media lacking cystine for 24 hr (No Cys, right panels) following treatment with DMSO control or inhibitors 1μM Gefitinib, 1μM Wortmannin, or 5μM Selumetinib for a total of 30h.

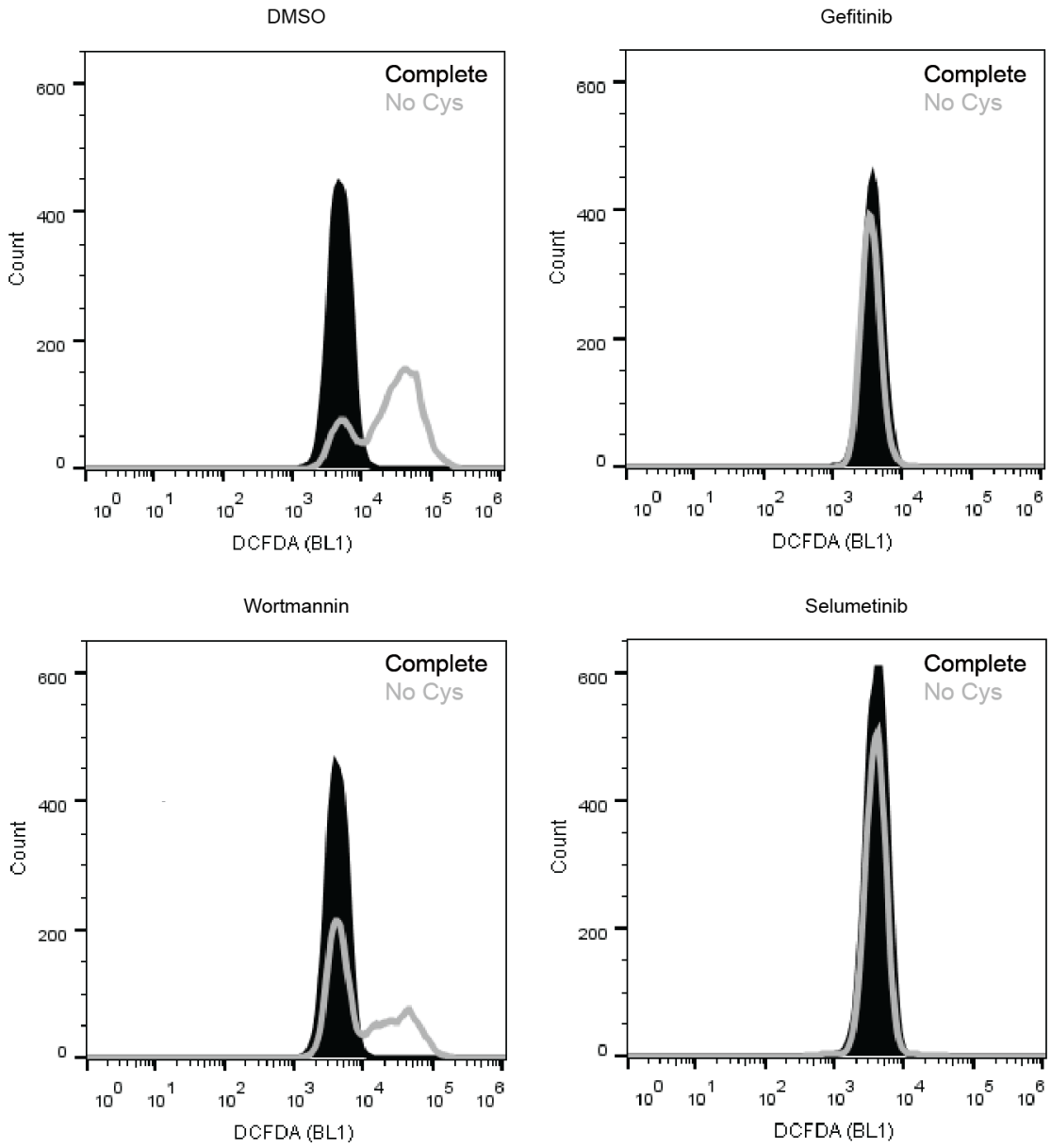

Figure 4.4 Accumulation of reactive oxygen species is reversed following EGFR and MEK inhibition in protects cells from ferroptosis cells.

FACS analyses of total ROS for HME-EGFR cells cultured in the presence or absence of inhibitors (DMSO as control, 1μM Gefitinib, 1μM Wortmannin, 5μM Selumetinib, with cells treated for a total of 30h using the DCFDA probe (10μM) and detected using the BL1 channel. Each histogram shows the spread of a population of minimum 5000 events of cells cultured in complete medium (black graphs) or in medium lacking cystine (grey outline) for 12h.

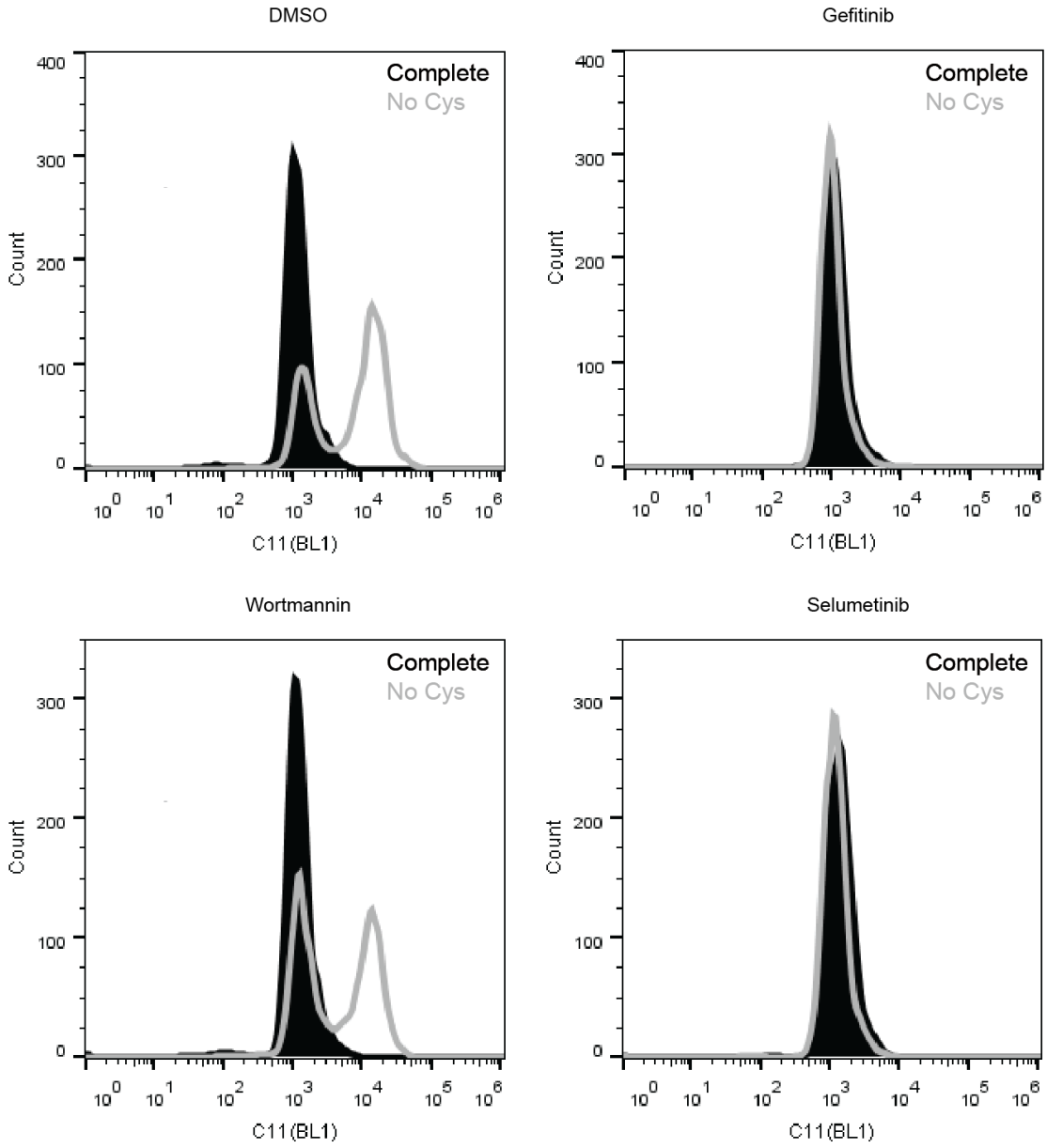

Figure 4.5 Lipid ROS is attenuated following treatment of cells with Gefitinib and Selumetinib.

FACS analyses of lipid peroxides in HME-EGFR cells cultured for 12h in complete medium (black graphs) or in medium lacking cystine (grey outline) prior to using the C11 probe (2μM) and flow cytometry to detect lipid peroxides. Each panel represents overlaid histogram plots to show the effects of treatment with DMSO, 1μM Gefitinib, 1μM Wortmannin and 5μM Selumetinib for a total of 30h.

To further substantiate the association between inhibition of MAPK signalling and resistance to ferroptosis three additional MEK inhibitors (U0126, PD184352, PD0325901) and two inhibitors of ERK1/2 (GDC-0994, SCH772984) were also tested for their effect on rescuing cell viability and inhibiting ROS accumulation following cystine deprivation of HME-EGFR cells. The effectiveness of these inhibitors was first evaluated by Western blot analysis using phosphorylation of RSK as a readout, as RSK is a known downstream target of ERK1/2 (Yoon and Seger, 2006). All the inhibitors tested, including gefitinib and selumetinib, effectively blocked phosphorylation of RSK by ERK1/2 (Figure 4.6 A). Next, I used these inhibitors in cell viability assays. All inhibitors of MEK or ERK1/2 effectively inhibited ferroptotic cell death following cystine deprivation in HME-EGFR cells (Figure 4.6 B, C). These inhibitors also blocked both total (Figure 4.7) and lipid ROS (Figure 4.8) following cystine deprivation. Taken together, these results point to a critical role of active MAPK kinase pathway signalling in the cell death mechanism induced in HME-EGFR cells when cells are deprived of cystine.

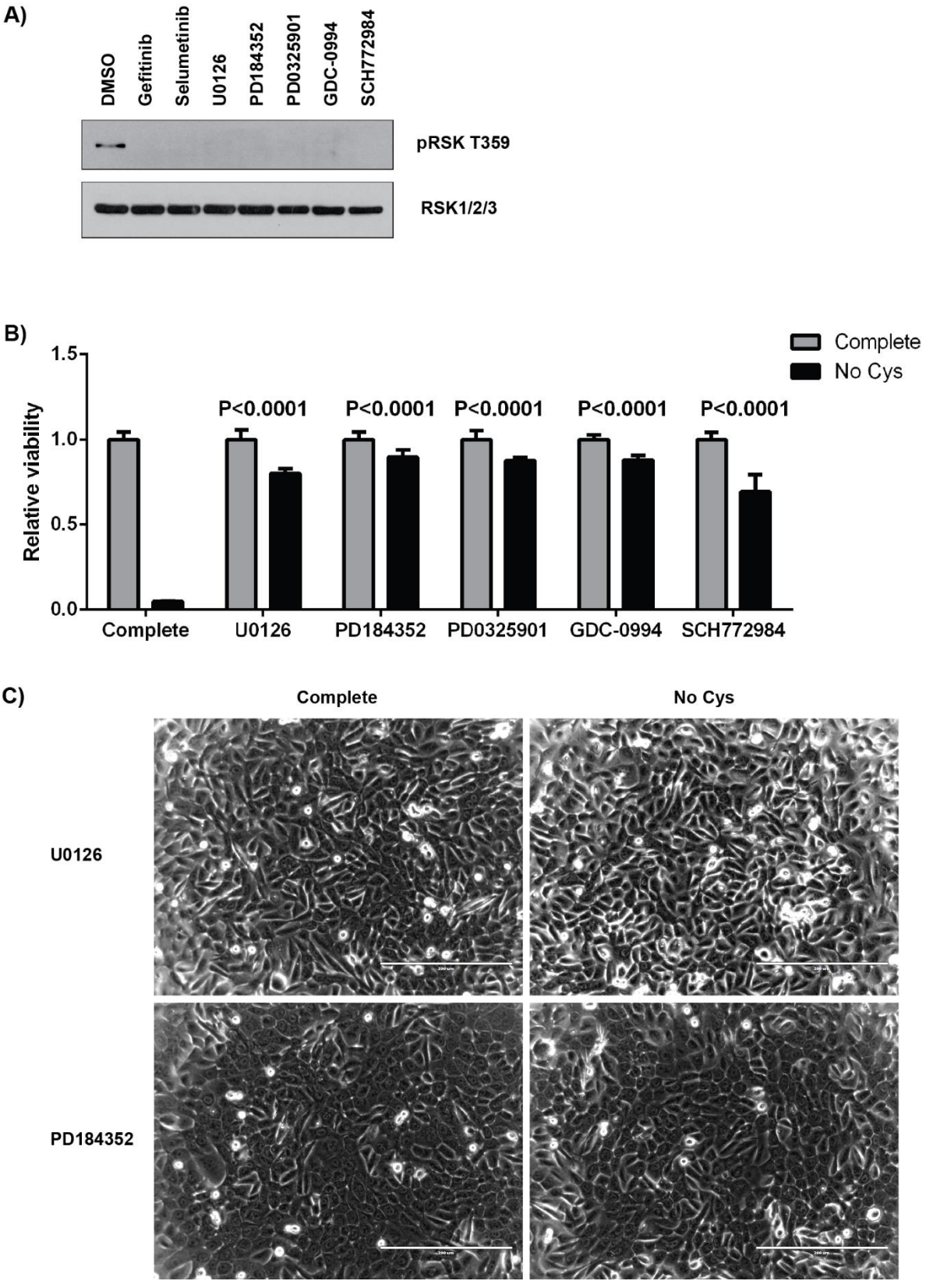
A)
DMSO
Gefitinib
Selumetinib
U0126
PD184352
PD0325901
GDC-0994
SCH772984
pRSK T359
RSK1/2/3
B)
Complete
No Cys
Relative viability
1.5
1.0
0.5
0.0
P<0.0001
P<0.0001
P<0.0001
P<0.0001
P<0.0001
Complete
U0126
PD184352
PD0325901
GDC-0994
SCH772984
C)
Complete
No Cys
U0126
PD184352

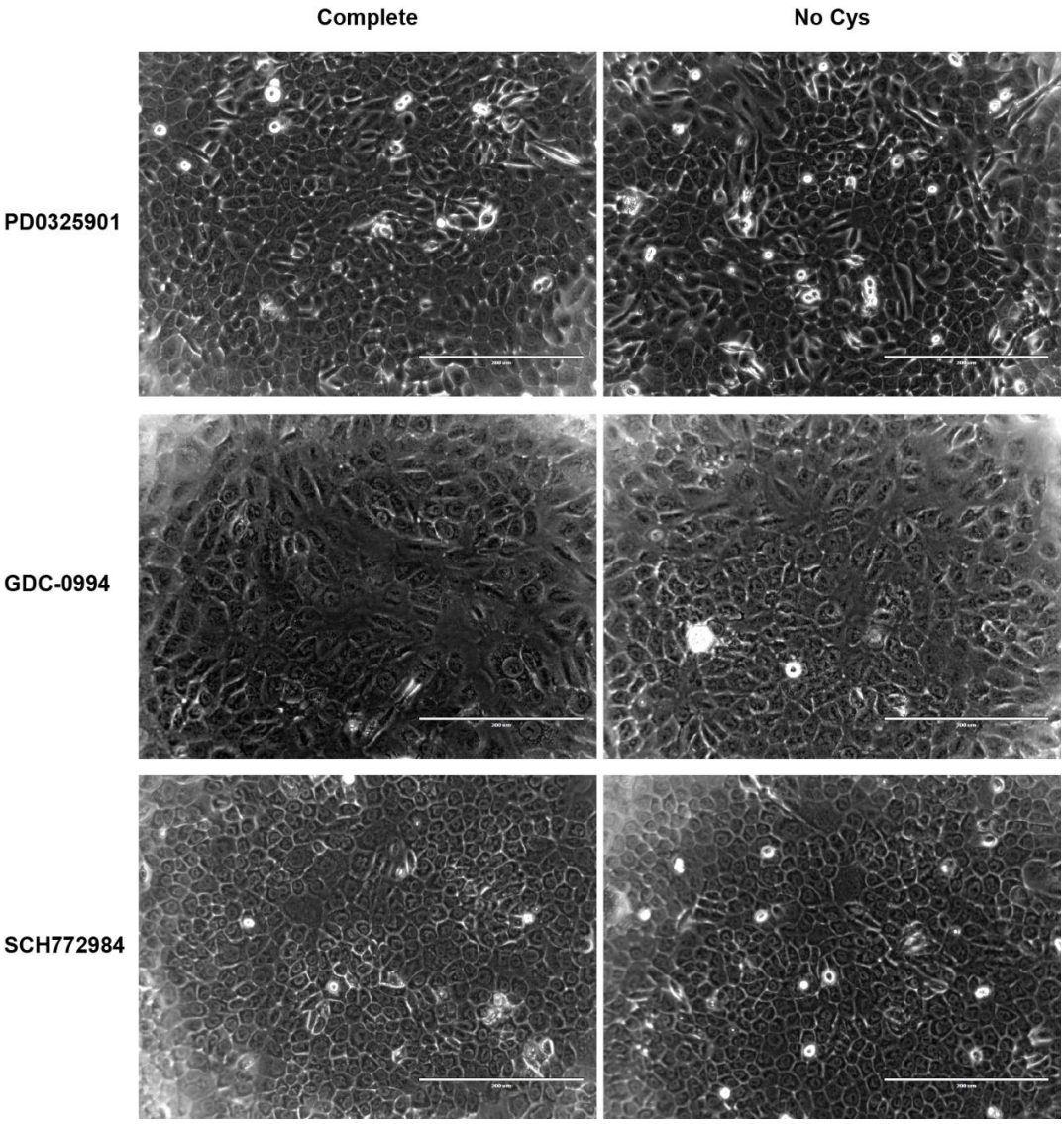

Figure 4.6 Inhibition of MEK and ERK signalling HME-EGFR cells.

HME-EGFR cells were cultured in normal media or media lacking cystine (No Cys) in the presence of inhibitors (DMSO as control, 1μM Gefitinib, 5μM Selumetinib, 10μM U0126, 10μM PD184352, 1μM PD0325901, 5μM GDC-0994, 5μM SCH77294) for a total of 30h A, immunoblot analysis of HME-EGFR cell lysates probed to detect phosphorylated RSK with total RSK detected as a loading control. B, viability assay examining the effect of the indicated inhibitors using the Cell-titre Glo assay. Each bar represents mean ± SD of three biological replicates of cells cultured in complete media (grey bars) or media lacking cystine for 24 hr (black bars). All measurements are expressed relative to the viability of HME-EGFR cells grown in complete media (assigned the arbitrary value of 1). Statistical analysis was performed using a 2-way ANOVA test with a Bonferroni's post hoc C, 20X phase-contrast images showing HME-EGFR cells cultured in normal media (Complete, left panels) or media lacking cystine for 24 hr (no Cys, right panels) following treatment with the indicated inhibitors.

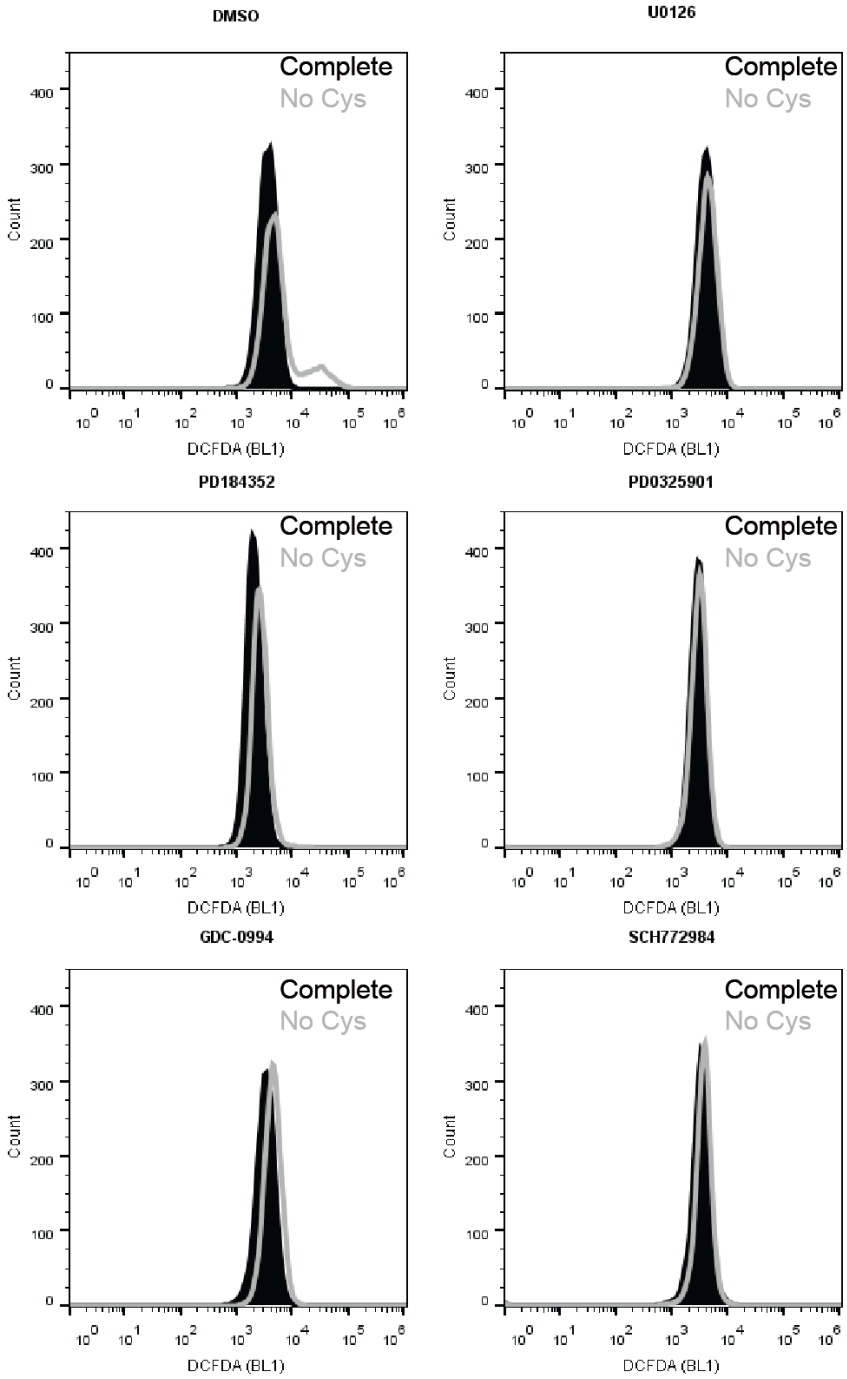

Figure 4.7 Accumulation of reactive oxygen species is reversed following MEK and ERK1/2 inhibition in HME-EGFR cells.

FACS analyses of total ROS for HME- EGFR cells cultured in the presence or absence of inhibitors (DMSO as control, 10μM U0126, 10μM PD184352, 1μM PD0325901, 5μM GDC-0994, 5μM SCH77294) for a total of 30h using the DCFDA probe (10μM) and detected using the BL1 channel. Each histogram shows the spread of a population of minimum 5000 events of cells in complete medium (black graphs) or in medium lacking cystine (grey outline) for 12h.

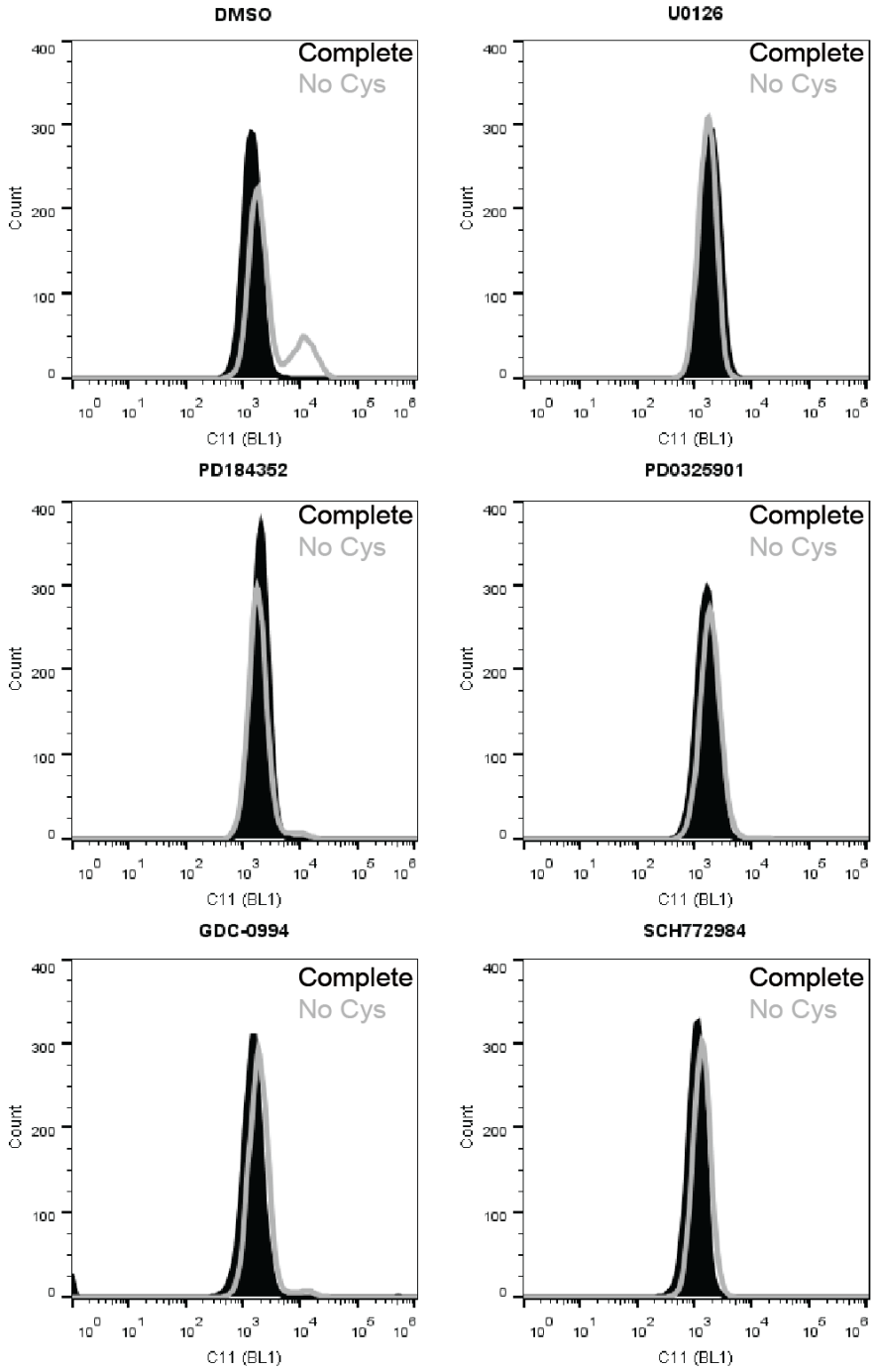

Figure 4.8 Lipid peroxidation is attenuated following incubation of HME-EGFR cells with MEK and ERK1/2 inhibitors.

FACS analyses of lipid peroxides for HME- EGFR cells cultured in the presence of inhibitors (DMSO as control, 10μM U0126, 10μM PD184352, 1μM PD0325901, 5μM GDC-0994, 5μM SCH77294) for a total of 30h, measured using the C11 probe (2μM) and detected using the BL1 channel. Each histogram shows the spread of a population of minimum 5000 events of cells in complete medium (black graphs) or in medium lacking cystine (grey outline) for 12h.

4.3 GPX4 modulates sensitivity to ferroptosis following cystine depletion.

4.3.1 EGFR-mutant cells have impaired oxidation of glutathione

The results from Chapter 3 suggest that HME-EGFR cells utilise GSH and cystine to oppose the effects of increased ROS, a conclusion that is supported by data showing that HME-EGFR cells cultured in complete media have higher levels of oxidised GSH (GSSG) than do wild-type HME cells (Figure 3.7). Considering the role of MAPK pathway signals in generating ROS in HME-EGFR cells, it was necessary to investigate how this pathway affected glutathione levels. Measurement of the ratio of GSSG/total GSH showed that oxidation of GSH to GSSG occurred faster in EGFR cells treated with gefitinib than in cells treated with DMSO control (Figure 4.9). This result suggests that MAPK pathway inhibition in HME-EGFR cells led to a more efficient oxidation of GSH, which would presumably facilitate increased neutralisation of ROS. Therefore, subsequent experiments focused on determining the mechanism(s) regulating GSH oxidation.

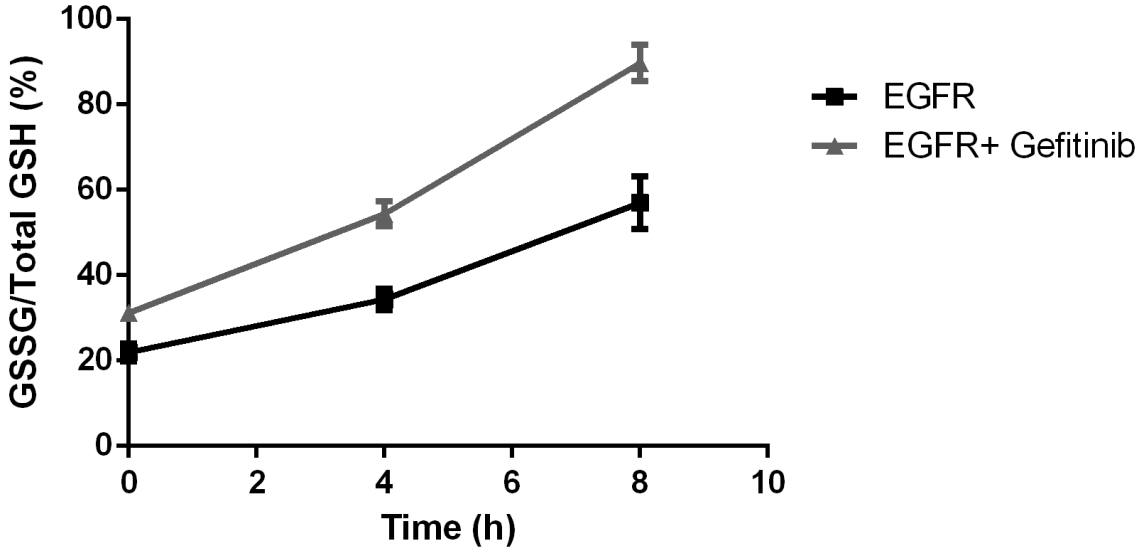

Figure 4.9 Inhibition of EGFR signalling improves oxidation of glutathione.

HME-EGFR cells in the absence (black, DMSO) or presence (grey) of gefitinib (1μM) for a total of 30h were grown in complete media (time 0h) followed by culture in media lacking cystine for 4 or 8 hours. Each point represents the mean percentage of oxidised glutathione ± standard deviation (SD) of three biological replicates.

4.3.2 GPX4 expression is downregulated in HME-EGFR cells by active MAPK signalling

Glutathione peroxidases are a family of enzymes that utilise available GSH to neutralise ROS, and therefore might potentially play roles in protecting cells from ferroptosis (Brigelius-Flohe and Maiorino, 2013). To investigate any role of these enzymes in our system, I performed immunoblotting experiments to assess the level of expression of the 4 main members of this family (GPX1 – 4) in wild-type and HME-EGFR cells (Figure 4.10). Neither cell line expressed detectable GPX2 or GPX3. Expression levels of GPX1 were similar between wild-type and HME-EGFR cells. However wild-type HME cells expressed around 2.5-fold higher levels of GPX4 than HME-EGFR cells (Figure 4.10 A). To determine whether reduced GPX4 expression was a result of elevated EGFR-MAPK signalling I again utilised EGFR and MAPK inhibitors. Treatment of HME-EGFR cells with the previously used inhibitors showed that GPX4 levels could be restored to levels comparable to those detected in wild-type HME cells following gefitinib or selumetinib treatment, but not following treatment with wortmannin (Figure 4.10 A). Importantly, such inhibitor treatments had no effect on expression of GPX1, whose expression remained constant in wild-type and HME-EGFR cells regardless of the inhibitor treatment used. Similar restoration of GPX4 expression was also observed when HME-EGFR cells were treated with other MAPK (MEK or ERK) inhibitors (Figure 4.10 B). These results, together with those generated using gefitinib and selumetinib, suggest that activation of the MAPK pathway suppresses the expression of GPX4.

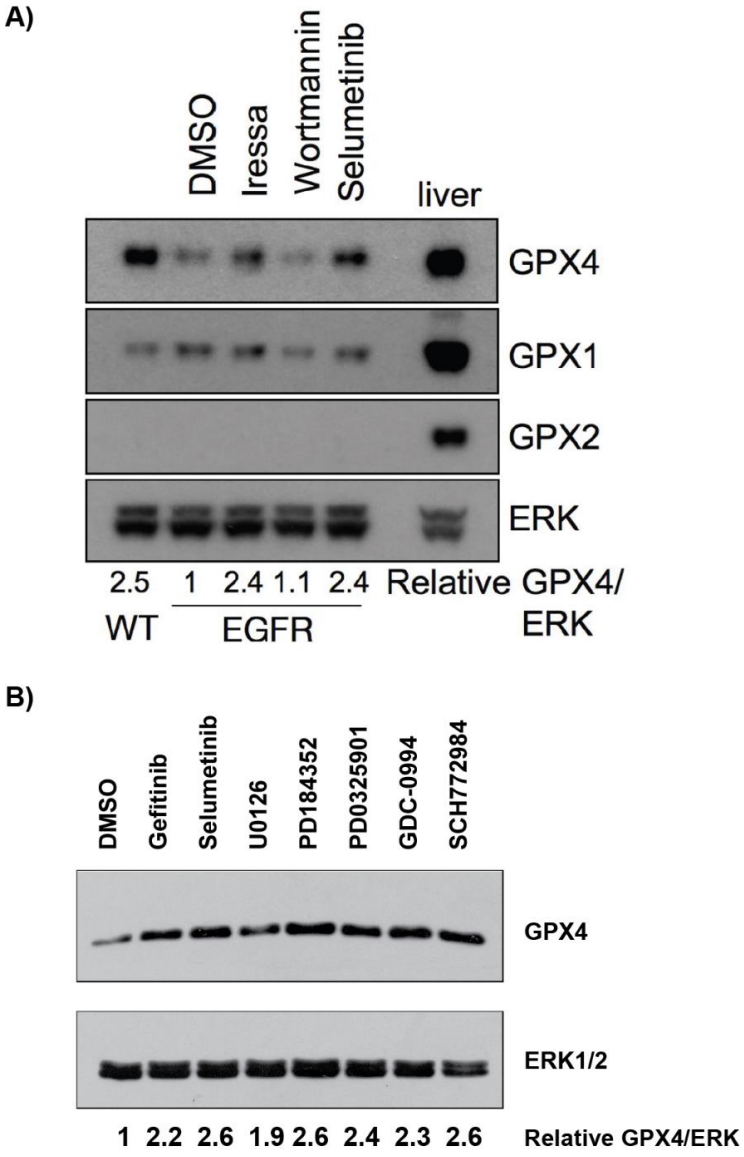

Figure 4.10 Inhibition of MAPK pathway increases GPX4 expression.

A, immunoblot analysis of wild-type HME (WT) and HME-EGFR cells cultured in the presence of inhibitors (DMSO as control, 1μM Gefitinib, 1μM Wortmannin, 5μM Selumetinib) for a total of 30h. Cell lysates were probed for GPX1, GPX2 and GPX4. ERK1/2 was used as a loading control and a mouse liver sample as a positive control. B, immunoblot analysis of HME-EGFR cell lysates probed for GPX4 in HME-EGFR cells the presence or absence of inhibitors (DMSO as control, 1μM Gefitinib, 5μM Selumetinib, 10μM U0126, 10μM PD184352, 1μM PD0325901, 5μM GDC-0994, 5μM SCH77294) for a total of 30h. ERK1/2 was used as a loading control. Quantification for both panels was performed using Image J and the ratio of GPX to HME-EGFR cells treated with DMSO was taken as an arbitrary value of 1. Immunoblot experiment in panel A was performed by Ms. Xiaomeng Wang.

4.3.3 Suppression of GPX4 expression reverses the protective effects of EGFR signalling inhibition on viability following cystine deprivation.

That GPX4 expression is negatively regulated by EGFR-MAPK-driven signalling is significant because this enzyme is thought to be the only member of the GPX family able to detoxify lipid ROS using GSH (Brigelius-Flohe and Maiorino, 2013). To determine the role of GPX4 within the mechanism protecting wild-type and inhibitor-treated HME-EGFR cells from cell death under conditions of cystine deprivation, I used siRNA to suppress GPX4 expression. For these experiments siRNAs targeting all four GPX proteins were employed, and immunoblotting first used to confirm knockdown of the respective GPX proteins. Expression of GPX1 and GPX4 were both effectively reduced following transfection of their respective siRNAs (Figure 4.11 A). Knockdown of GPX2 and GPX3 could not be measured in HME cell lysates because GPX2 is not expressed in these cells, and GPX3 is a secreted protein. It is noteworthy that GPX2 siRNA partially reduced expression levels of GPX1, presumably due to the high sequence similarity of these two proteins (Brigelius-Flohe and Maiorino, 2013). Moreover, downregulation of GPX4, but not GPX1, induced accumulation of total and lipid ROS following deprivation of cystine (Figure 4.11 B, C).

Next I used siRNA-treated HME cells in functional experiments measuring cell viability. Targeted reduction in expression of GPX enzymes 1-3 did not alter the viability of wild-type HME cells following deprivation of cystine (Figure 4.12). In contrast, knockdown of GPX4 in wild-type HME cells sensitised these cells to deprivation of cystine, inducing formation of lipid ROS (Figure 4.12 A) resulting in loss of viability (Figure 4.12 B). Knockdown of GPX4 also affected HME-EGFR cells

cultured under conditions of cystine deprivation that had been previously treated with gefintinib (Figure 4.13). These data demonstrate a key role for GPX4 in regulating sensitivity of wild-type HME cells to cystine deprivation, where expression of this glutathione peroxidase is downregulated through activation of MAPK pathway resulting from the constitutively-active mutant EGFR. This conclusion was further supported by experiments whereby GPX4 was ectopically overexpressed in HME-EGFR cells (Figure 4.14). HME-EGFR cells were transfected with a tagged GPX4 or control vector and subjected to cystine deprivation. GPX4-transfected cells were less sensitive than HME-EGFR cells transfected with an empty vector to cystine deprivation, and displayed a response similar to wild-type HME cells (Figure 4.14).

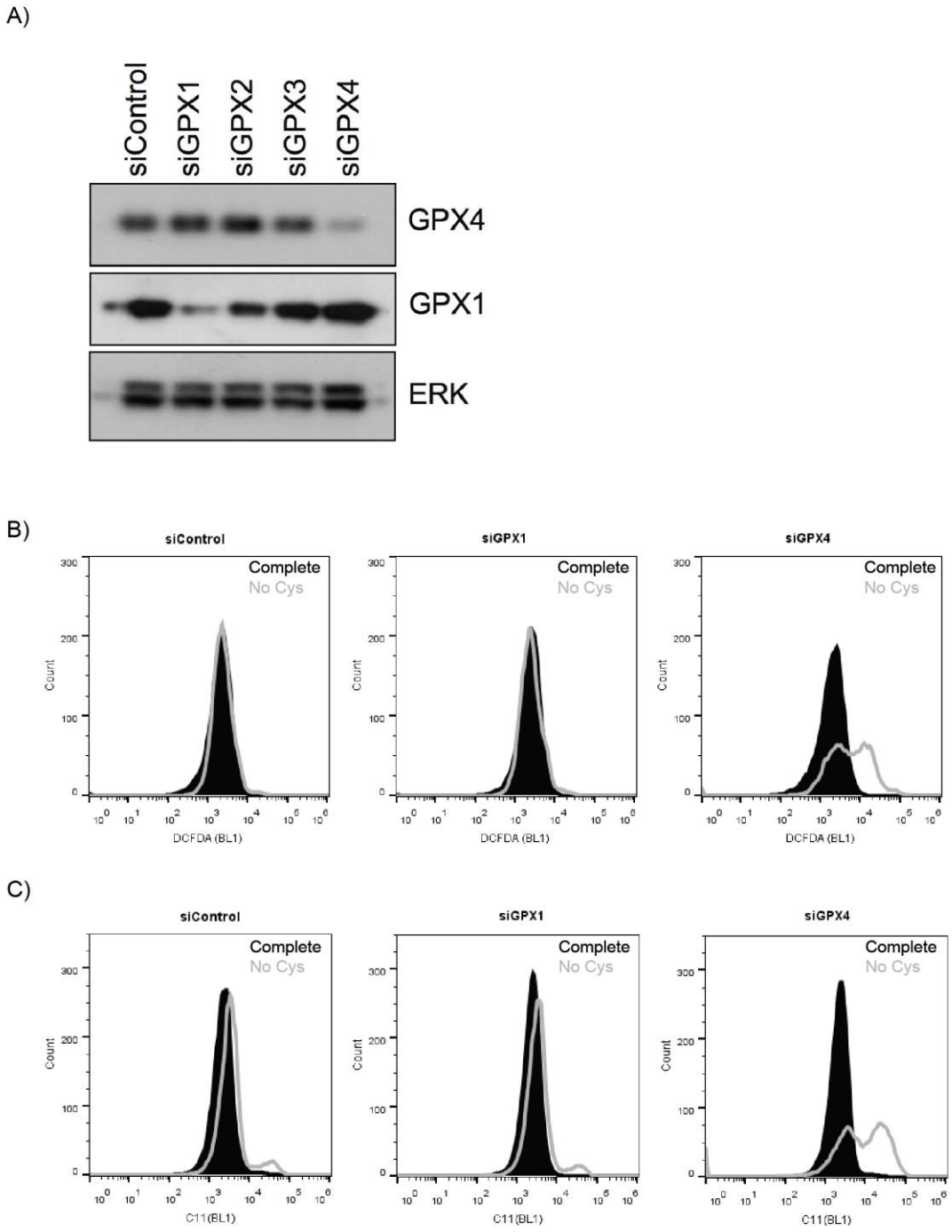

Figure 4.11 Knockdown of GPX family members in wild-type HME cells.

Wild-type HME were analysed 72h after transfection with control non-targeting siRNA (siCtrl) or siRNA Smartpools targeting each of the individual GPX proteins (siGPX1-4). A, immunoblot analysis of GPX1 and GPX4 after siRNA transfection targeting indicated proteins. ERK1/2 was used as a loading control. B, C FACS analyses of total ROS (B) and lipid ROS (C) for wild-type HME cells transfected with indicated siRNAs and measured using the DCFDA (10μM) and C11 probe (2μM) respectively, detected using the BL1 channel. Each histogram shows the spread of a population of minimum 5000 cells in complete medium (black) or in medium lacking cystine (grey) for 14h.

A)

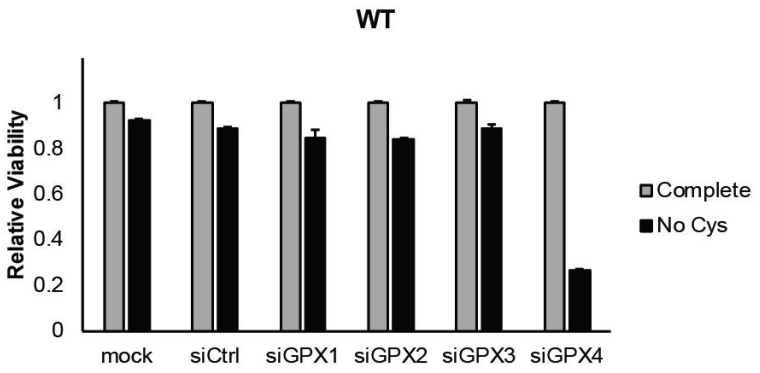

B)

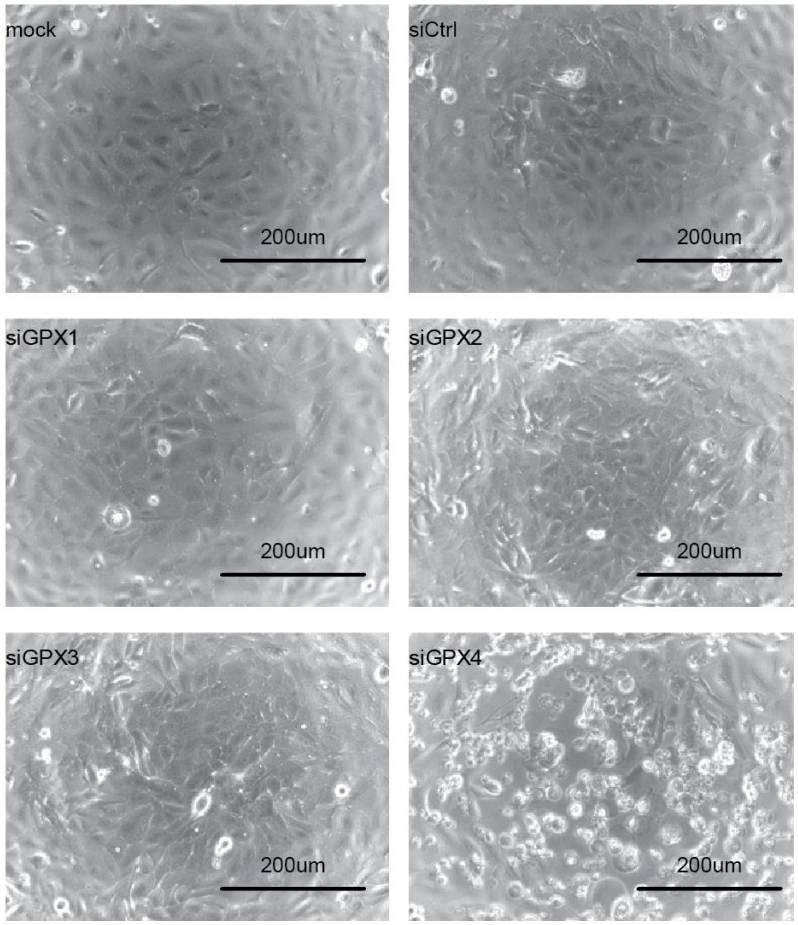

Figure 4.12 Knockdown of GPX family members in wild-type HME cells.

A, viability assay for wild-type HME cells following mock transfection or transfection with control non-targeting siRNA (siCtrl) or siRNAs targeting each individual of the 4 GPX proteins (siGPX1-4) for 72h followed by culture in normal media or media lacking cystine for 24 hr. Viability of each individual cell line was measured using the Cell-titre Glo assay. Results were expressed for each condition separately, with viability in normal media assigned the arbitrary value of 1. Each graph represents the average viability ± standard deviation (SD) of three biological replicates. B, 20X Phase-contrast micrographs of wild-type HME cells following transfection for 72h and culture in media lacking cystine for 24 hr.

A)

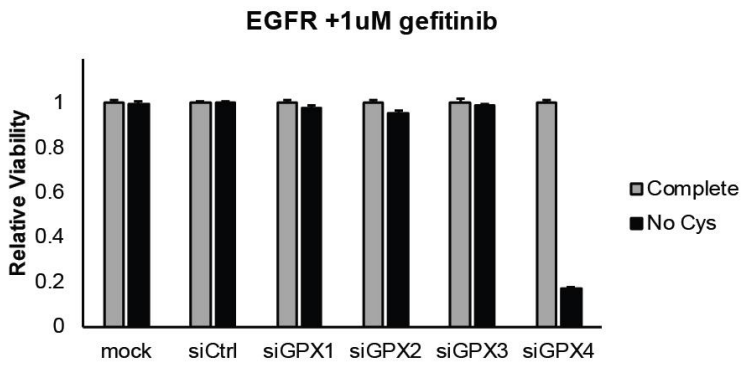

B)

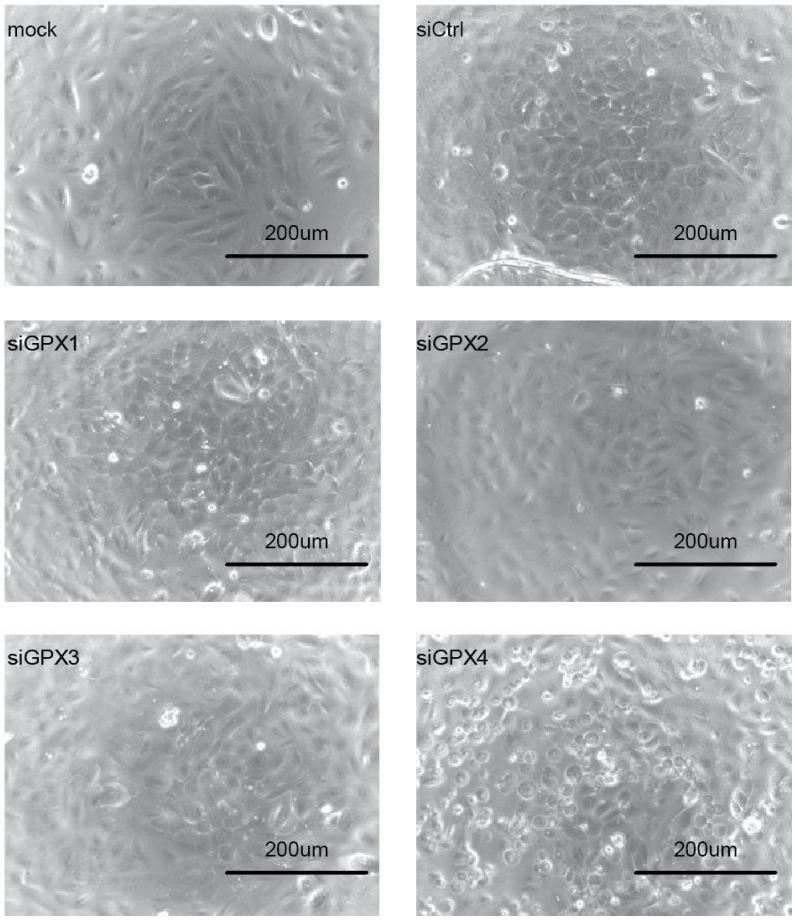

Figure 4.13 Knockdown of GPX4 in gefitinib-treated HME-EGFR cells induces sensitivity to ferroptosis.

A, viability assay for HME-EGFR cells following mock transfection or transfection with control non-targeting siRNA (siCtrl) or siRNAs targeting each individual of the 4 GPX proteins (siGPX1-4) for 72h followed by culture in normal media or media lacking cystine for 24 hr. Cells were treated with gefitinib (1μM) 24h after transfection. Viability of each individual cell line was measured using the Cell-titre Glo assay. Results were expressed for each condition separately, with viability in normal media assigned the arbitrary value of 1. Each graph represents the average viability ± standard deviation (SD) of three biological replicates. B, 20X phase-contrast micrographs of gefitinib-treated HME-EGFR cells following transfection for 72h and culture in media lacking cystine for 24 hr.

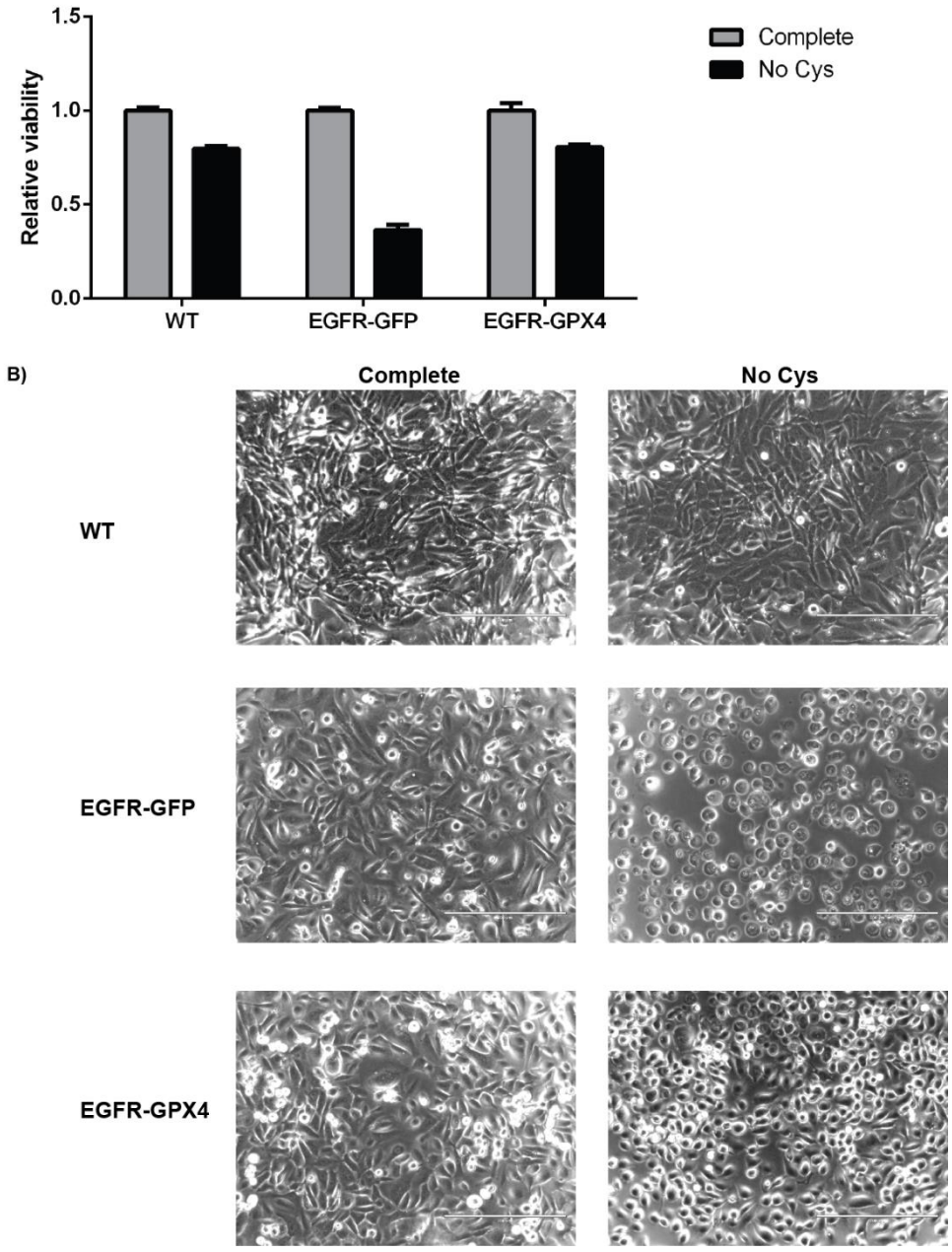

Figure 4.14 Overexpression of GPX4 in HME-EGFR cells rescues viability.

A, viability assay for wild-type and HME-EGFR cells transfected with eGFP as a control or FSH-GPX4, followed by culture in normal media or media lacking cystine for 24 hr. Viability of each individual cell line was measured using the Cell-titre Glo assay. Results were expressed for each condition separately, with viability in normal media assigned the arbitrary value of 1. Each graph represents the average viability ± standard deviation (SD) of three biological replicates. B, 20X Phase-contrast micrographs of cells cultured in normal media or media lacking cystine for 24 hr. Scale bar represents 200μm distance.

4.4 Responses of a Non-Small Cell Lung Cancer cell line panel to cystine deprivation indicate a general MAPK-driven sensitivity to ferroptosis.

The cell system used in this study to identify differential response of cells to deprivation of individual amino acid nutrients comes with certain limitations. hTERT-HME cells are diploid immortalised cells and even with an activating mutation in EGFR these cells are not oncogenic unlike *bone fide* cancer cells (Di Nicolantonio et al., 2008). It therefore became pertinent to test whether such responses could be replicated in cancer cell lines in order to potentially test the efficacy of cystine limitation as an anti-cancer therapy. A panel of nine Non-Small Cell Lung Cancer (NSCLC) cell lines were selected to further clarify correspondences between EGFR, MAPK and sensitivity to ferroptosis due to the presence of EGFR mutations in some fraction of NSCLC tumours and cell lines (Shigematsu and Gazdar, 2006) (Table 4.1).

Deprivation of cystine appeared to have distinct effects in the cell lines utilised (Figure 4.15 A). The viability of three of the cell lines (Calu-6, H1650, H3255) was significantly compromised following cystine depletion, to an extent similar to that observed in HME-EGFR cells (Figure 4.15 B). The H1650 and H3255 cell lines both have an activating mutation in the *EGFR* gene, with H1650 having the exon 19 deletion similar to HME-EGFR cells, and H3255 expressing an exon 20 L858R mutant EGFR. On the contrary Calu 6, are wild-type for *EGFR* but have an activating mutation Q61K in the *KRAS* gene promoting activation of the MAPK pathway (Bos, 1989). I next sought to investigate the potential biomarkers of sensitivity in these NSCLC cell lines. The first rational target to investigate as responsible for the observed sensitivity was expression of GPX4. However, lower expression of GPX4

in NSCLC cell lines did not appear to correspond to higher sensitivity to cystine deprivation (Figure 4.15 C). However, activation of the MAPK pathway, as measured by the ratio of ppERK/ERK, did correspond to sensitivity to ferroptosis, and was highly elevated in the three most sensitive NSCLC cell lines as well as HME-EGFR cells and lower in the most resistant cells (Figure 4.15 C).

	EGFR	KRAS	Other genes			Ferroptosis
H_1975	L858R, T790M	WT	PI3KCA G118D	CDKN2A E69*	TP53 R273H	resistant
H_1650	del E746-A750	WT	TP53 c.673-2A>G			sensitive
H_727	WT	KRAS G12V				resistant
H_460	WT	KRAS Q61H	PI3KCA E545K			resistant
H_322	WT	n/a	CDKN2A c.1_150del150			resistant
A_549	WT	KRAS G12S				resistant
Calu_6	WT	KRAS Q61K	TP53 R196*			sensitive
H_3255	L858R	n/a				sensitive
PC9	del E746-A750	n/a				resistant

Table 4.1 List of NSCLC cell lines and their mutational profile and their sensitivity to cystine deprivation.

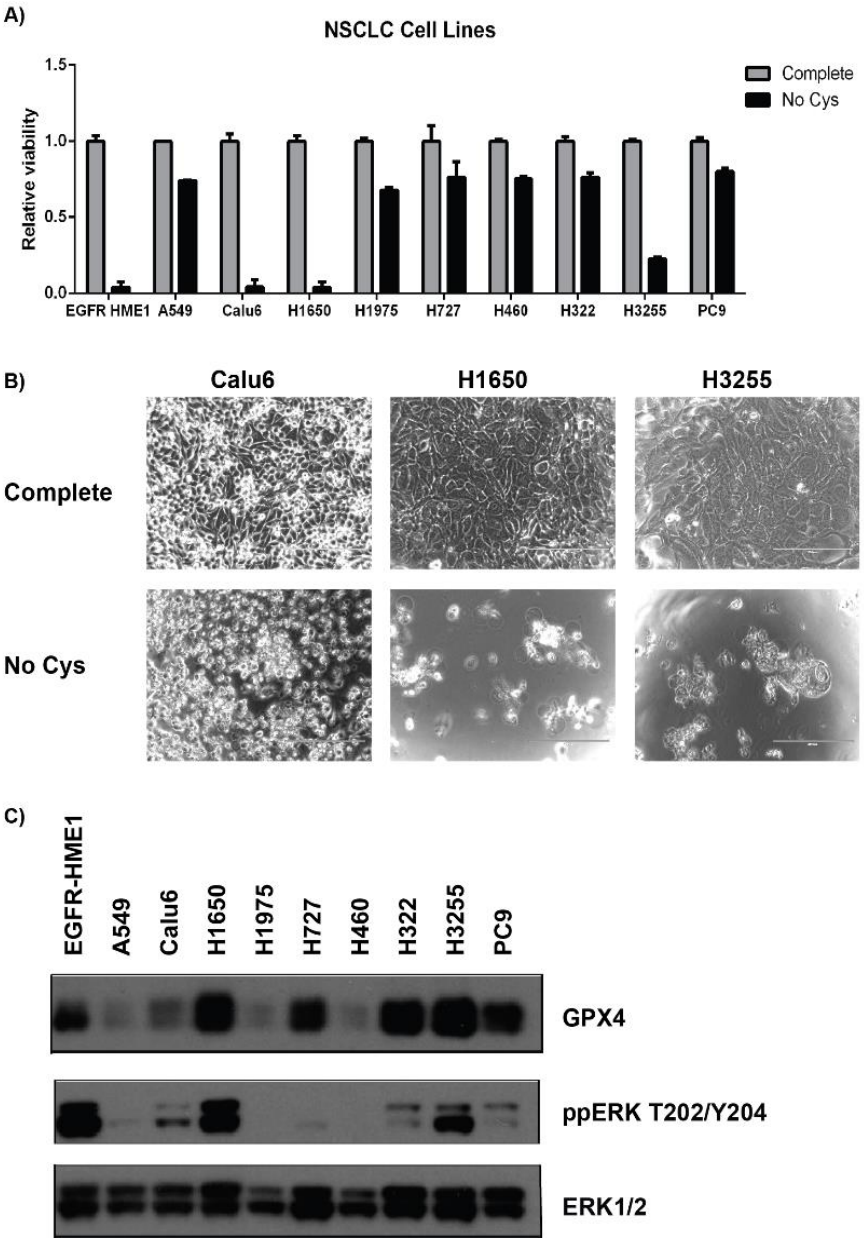

Figure 4.15 NSCLC cell lines with elevated MAPK activation are sensitive to ferroptosis following deprivation of cystine.

A, viability assay for indicated NSCLC cell lines cultured in normal media (grey bars) or media lacking cystine (black bars) for 48 hr. Viability of each individual cell line was measured using the Cell-titre Glo assay. Results were expressed for each cell line separately, with viability in normal media assigned the arbitrary value of 1. Each graph represents the average viability ± standard deviation (SD) of three biological replicates. B, 20X phase-contrast micrographs of responding cell lines Calu6, H1650 and H3255 cultured in normal media (Complete, top panels) or media lacking cystine (No Cys, bottom panels) for 48 hr. C, immunoblot analysis of NSCLC cell lines to detect ERK phosphorylation. Total ERK1/2 were detected as a loading control. Ms. Xiaomeng Wang has assisted with the immunoblot experiment

Given the strong association observed between sensitivity to ferroptosis and activation of the MAPK pathway observed in the responding NSCLC cell lines I investigated whether treatment with MAPK inhibitors could similarly protect NSCLC cells from ferroptosis following cystine depletion. In Calu6 cells which express a mutant KRAS oncoprotein I observed significant protection from cell death when cells were treated with either MEK and ERK inhibitors, whilst gefitinib treatment was without effect (Figure 4.16 A). In H3255 cells however, which express an activating L858R mutation in exon 20 of EGFR, viability was strongly protected by both MEK inhibitors (U0126 and PD0325901) and gefitinib (Figure 4.16 B). Taken together these data indicate that EGFR-MAPK signalling in NSCLC cells can sensitise cells to ferroptosis.

The EGFR-mutant cell lines H1650 that harbours the same EGFR mutation as found in HME-EGFR cells (deletion of exon 19) was found to be one of the most sensitive NSCLC lines to ferroptosis and additionally displayed the highest MAPK activation amongst the NSCLC cell lines tested. H1650 was therefore selected as a good candidate to study the effects of EGFR signalling in a cancerous cell line. To clarify whether cell death observed in H1650 occurred by ferroptosis, I treated these cells alongside HME-EGFR cells with Fer1, an antioxidant inhibitor of ferroptosis (Dixon et al., 2012) as well as with a known ROS antioxidant, α-tocopherol. Both antioxidants suppressed cell death following cystine depletion, indicating that H1650 cells, like HME-EGFR cells, underwent ferroptosis following cystine depletion (Figure 4.17).

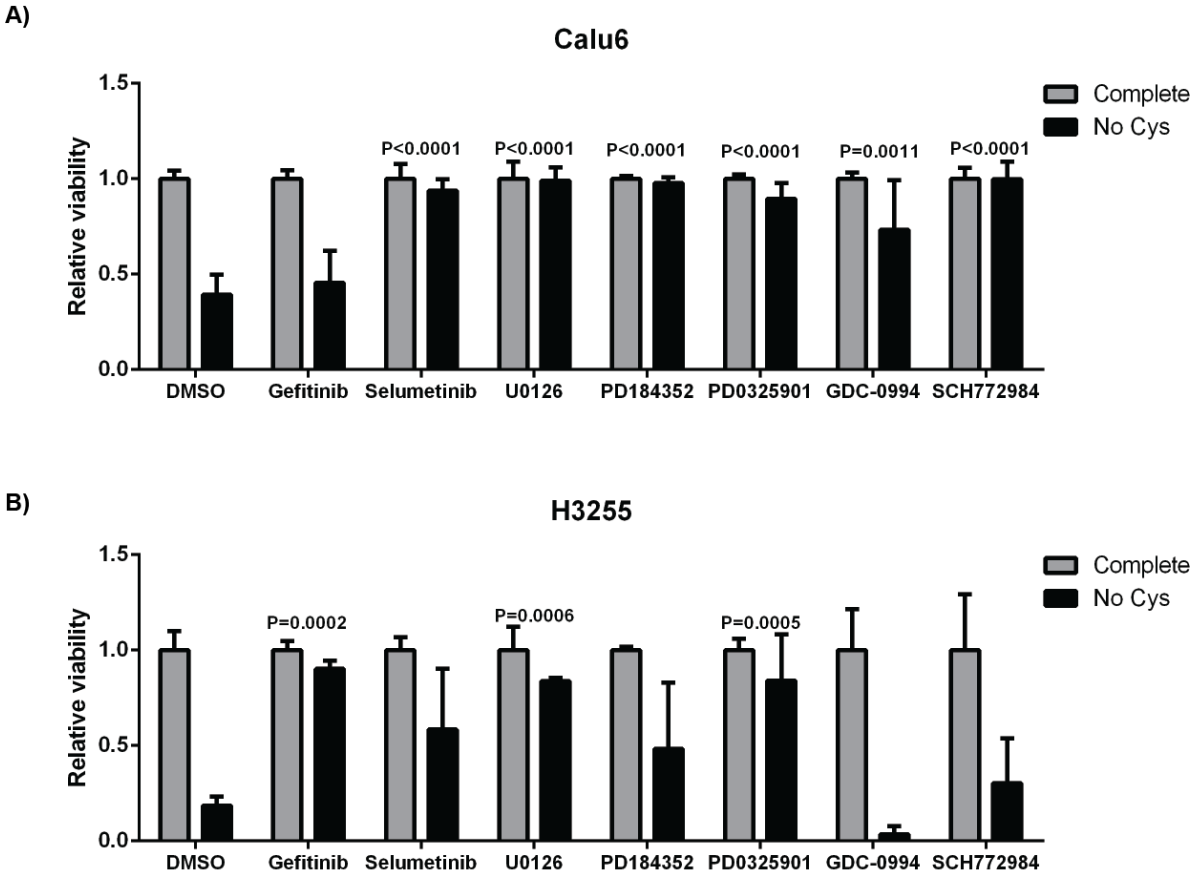

Figure 4.16 MAPK pathway inhibition reverses ferroptosis in ferroptosis-sensitive NSCLC cell lines.

Viability assays of Calu6 (A), H1650 and H3255 (B) cultured in complete media (grey bars) or media lacking cystine for 48 hr (black bars) in the presence or absence of MAPK pathway inhibitors (DMSO as control, 1μM Gefitinib, 5μM Selumetinib, 10μM U0126, 10μM PD184352, 1μM PD0325901, 5μM GDC-0994, 5μM SCH77294). Each bar plot represents mean ± SD of cell viability measured using Cell-titre Glo. Results were expressed for each condition separately, with viability in normal media assigned the arbitrary value of 1. Statistical analysis was performed using a 2-way ANOVA test and a Bonferroni post hoc test between different media of the same inhibitor treatment.

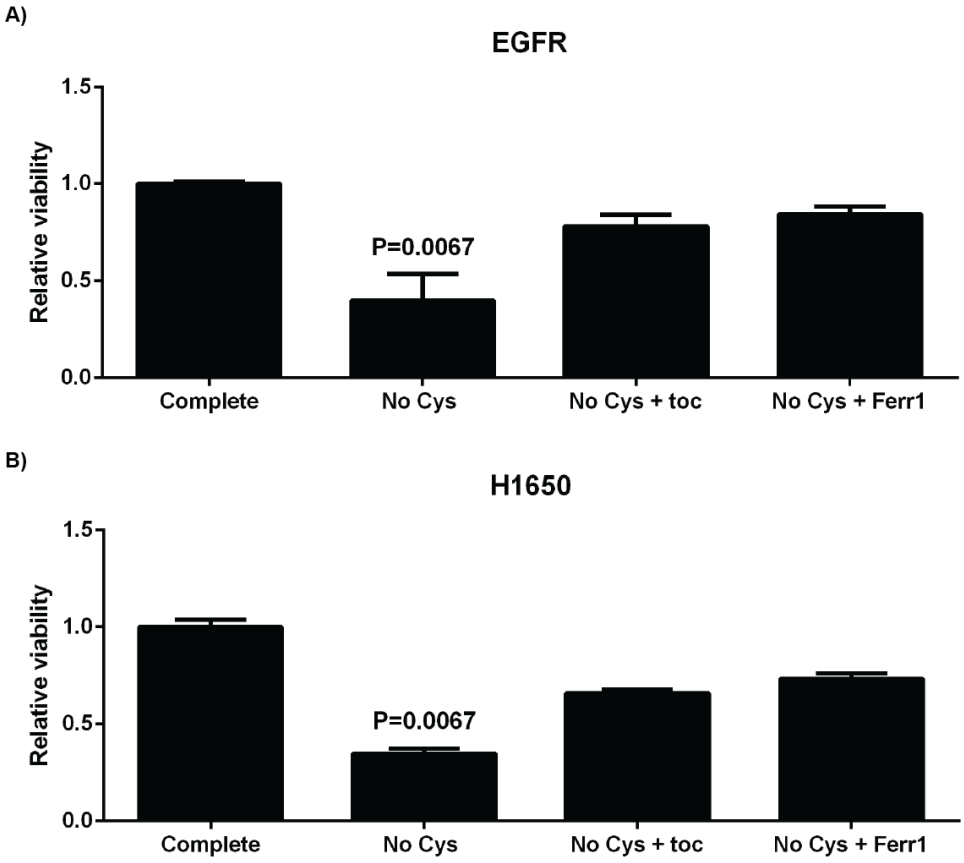

Figure 4.17 H1650 response to cystine deprivation is reversed by Fer1 and antioxidant α-tocopherol.

Cell viability assays of HME-EGFR (A) and H1650 (B) following treatment with Fer1 or a-tocopherol. Each bar plot represents mean ± SD of cells cultured in complete media (grey bars) or media lacking cystine in the absence or presence of tocopherol (30μM) and Fer1 (2μM). All measurements are expressed relative to the viability of HME-EGFR cells grown in complete media (assigned the arbitrary value of 1). Statistical analysis was performed using a Kruskal Wallis non-parametric test with a Dunn's post hoc test.

4.4.1 The enzymatic degradation of cystine in cell culture media mimics cystine depletion and results in ferroptosis.

A recent paper has described the mutational modification of a human enzyme, cystathionine-γ-lyase to create a cysteinase (AECase), an enzyme that can degrade and therefore deplete both cysteine and cystine (Cramer et al., 2017). We therefore wished to determine whether AECase treatment of cells also resulted in ferroptosis. Indeed, treatment of HME-EGFR cells or H1650 cells with AECase, but not its heat-inactivated form, efficiently killed the majority of both cell lines (by >90%) in a manner similar to deprivation of cystine, which was inhibited in the presence of Fer1, indicating that cell death occurred by ferroptosis (Figures 4.18 and 4.19). Following depletion of cystine, or following addition of AECase, nuclear accumulation of a marker of loss of membrane impermeability, Sytox Green, was evident within cell nuclei, whilst treatment with the heat-inactivated AECase was without effect (Figure 4.20).

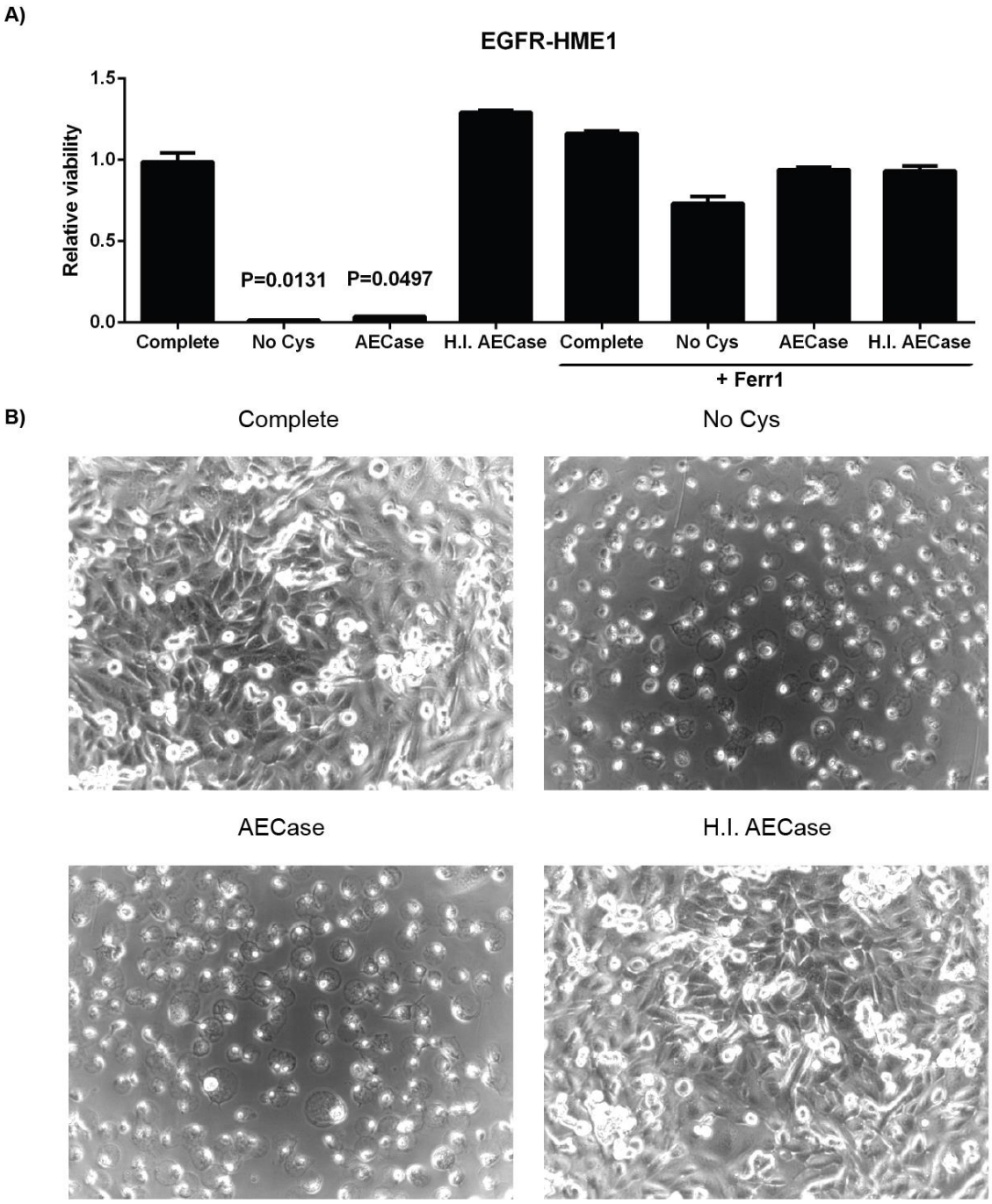

Figure 4.18 AECase induces ferroptosis in HME-EGFR cells.

A, viability assay for HME-EGFR cells following treatment with AECase. Each bar plot represents mean ± SD of cells cultured in complete media or media lacking cystine or media containing active or heat-inactivated AECase (125nM) in the absence or presence of Fer1 (2μM). All measurements are expressed relative to the viability of HME-EGFR cells grown in complete media (assigned the arbitrary value of 1). Statistical analysis was performed using a Kruskal Wallis non-parametric test with a Dunn's post hoc test. B, 20X phase-contrast micrographs of HME-EGFR cells following culture in complete media or media lacking cystine or media containing active or heat-inactivated AECase (125nM) for 24 hr.

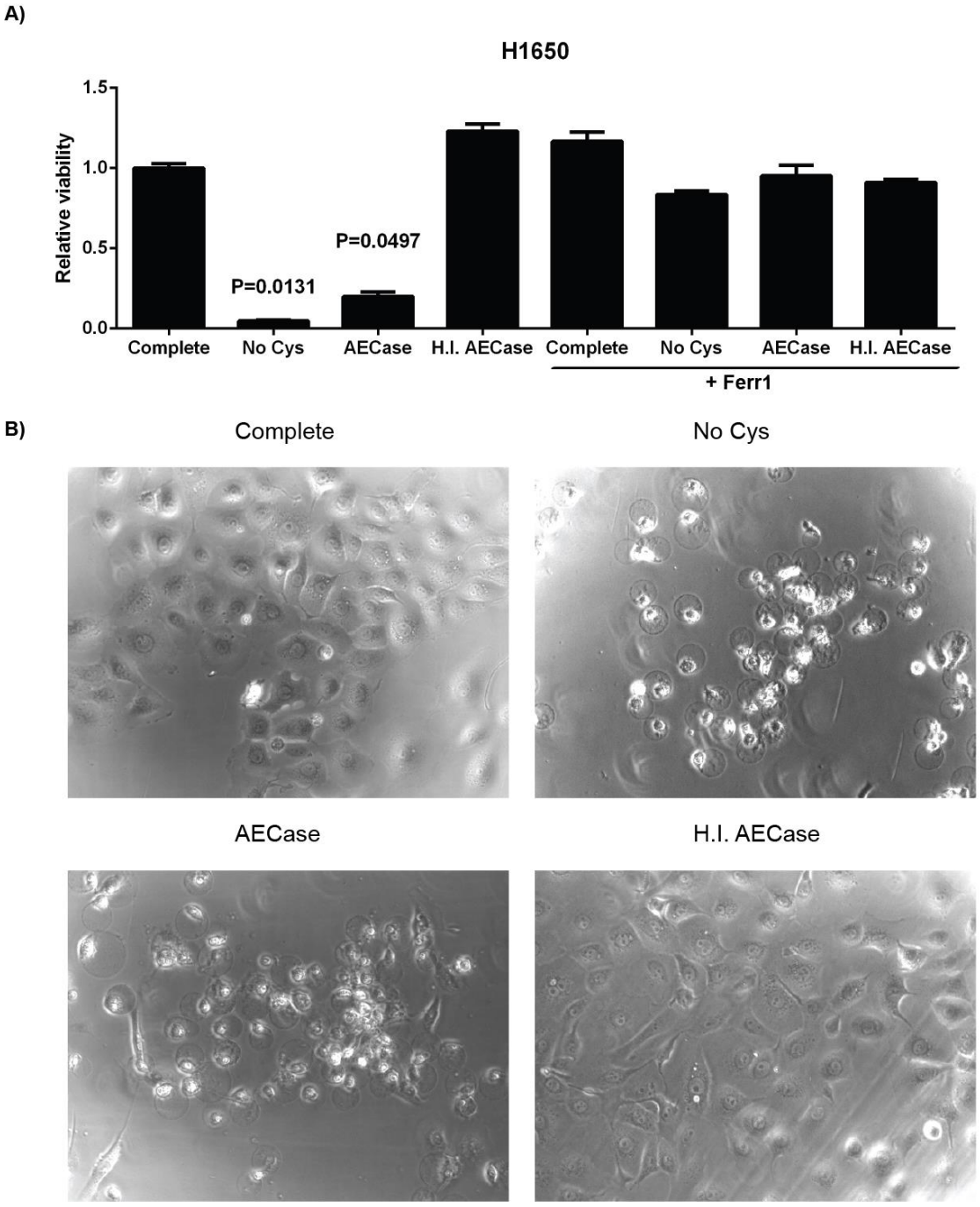

Figure 4.19 AECase also induces ferroptosis in H1650 cells.

A, viability assay for H1650 cells following AECase treatment. Each bar represents mean ± SD of cells cultured in complete media, media lacking cystine, or normal media containing active or heat-inactivated AECase (125nM) in the absence or presence of Fer1 (2μM). All measurements are expressed relative to the viability of H1650 cells grown in complete media (assigned the arbitrary value of 1). Statistical analysis was performed using a Kruskal Wallis non-parametric test with a Dunn's post hoc test. B, 20X phase-contrast micrographs of H1650 cells following culture in complete media or media lacking cystine or media containing active or heat-inactivated AECase (125nM) for 24 hr.

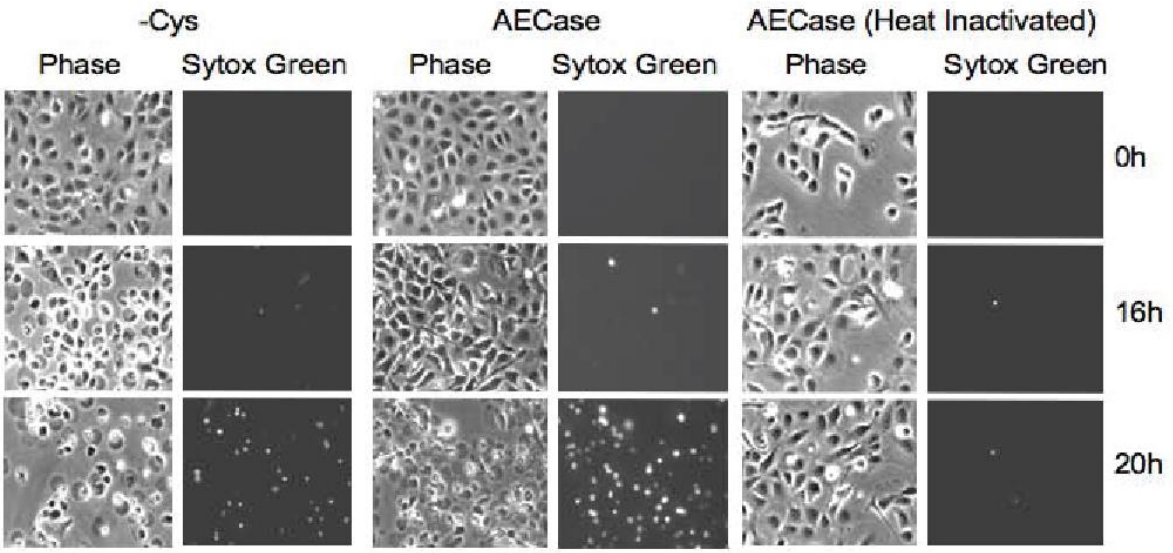

Figure 4.20 Ferroptosis in H1650 cells leads to loss of plasma membrane integrity.

Time-lapse 20X phase contrast photographs (Phase) together with epifluorescence capture of the non-permeable green fluorescent nuclear dye Sytox Green in H1650 cells cultured in media lacking cystine or media containing active or heat-inactivated formulations of AECase (125nM) at the indicated times following cystine depletion or enzyme addition.

4.4.2 Treatment of a mouse xenograft model with AECase indicates reduction of tumour growth associated with ferroptosis

In order to study the response of tumours *in vivo* to systemic cystine depletion elicited by AECase treatment we employed a mouse xenograft model using engrafted ferroptosis-sensitive H1650 cells. Immunocompromised mice were inoculated with H1650 cells to form xenograft tumours. Tumours were allowed to grow for 18 days prior to treament with two different concentrations of AECase or control for 20 days. Tumour growth was found to be significantly retarded in mice administered with the AECase enzyme, which also prolonged overall survival of the AECase-treated mice (Figure 4.21). To determine if ferroptosis was occuring within tumours from the AECase-treated mice, tumour sections were stained for COX2 a suggested indicator of ferroptosis (Yang et al., 2014) whilst tumour lysates were immunoblotted for COX2. Upregulation of COX2 expression was observed by IHC as well as by immunoblotting in AECase-treated tumours (Figure 4.22). These results taken together indicate that tumours sensitive to ferroptosis could potentially be targeted by modulation of plasma cystine levels using AECase.

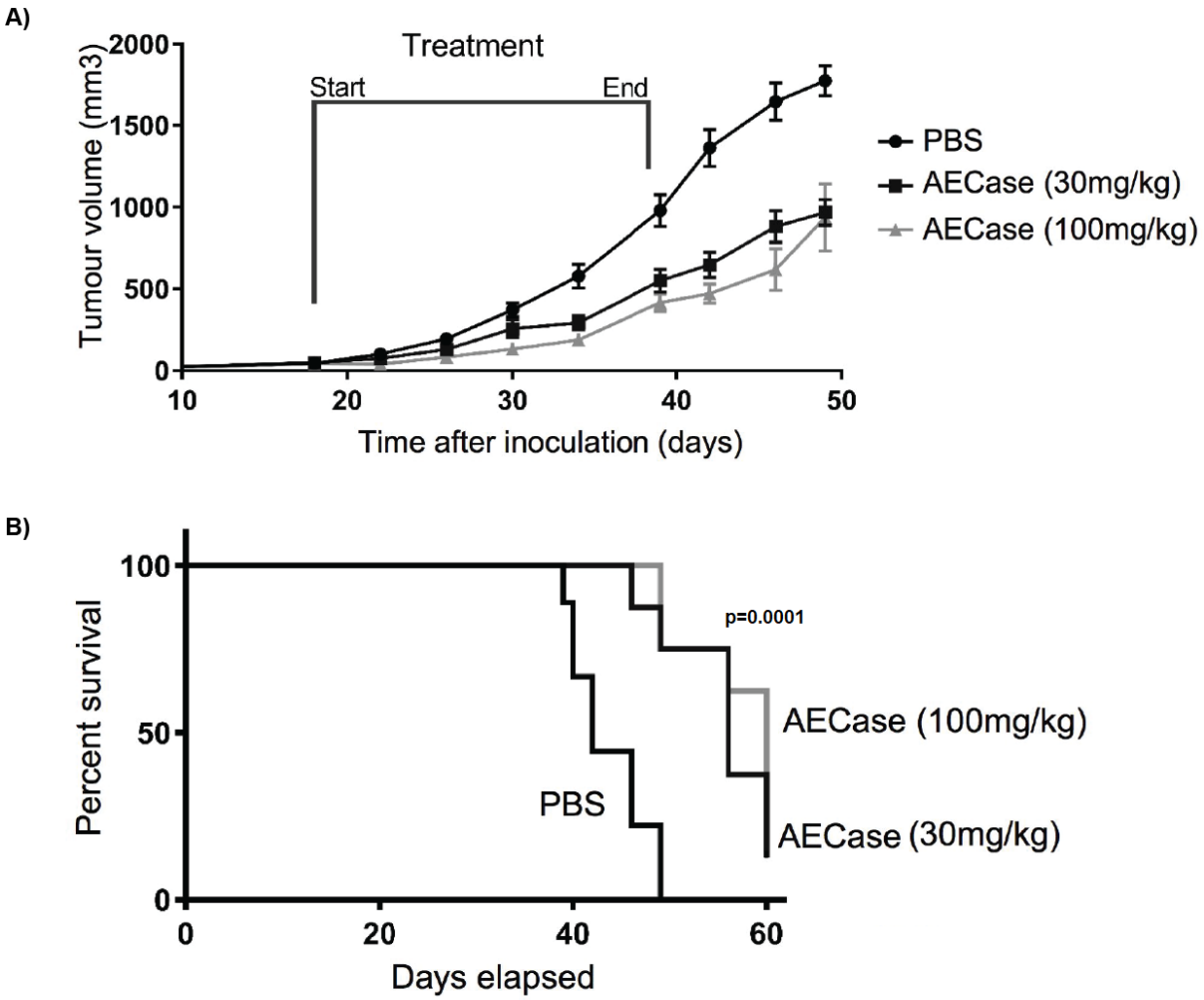

Figure 4.21 Cyst(e)inase (AECase) administration inhibits tumour growth in a NCI-NH1650 xenograft mouse model.

A, increase in tumour volume following i.p. administration of PBS control (dark circles) or 30 mg/kg (dark squares) or 100 mg/kg (light triangles) AECase. Start and end of treatment times are also shown. B, Kaplan-Meier plots of median survival times of PBS- or AECase-treated tumour-bearing mice. All animal experiments were performed by Ms. Shira L. Cramer and Ms. Kendra Triplett in The University of Texas at Austin, TX, USA.

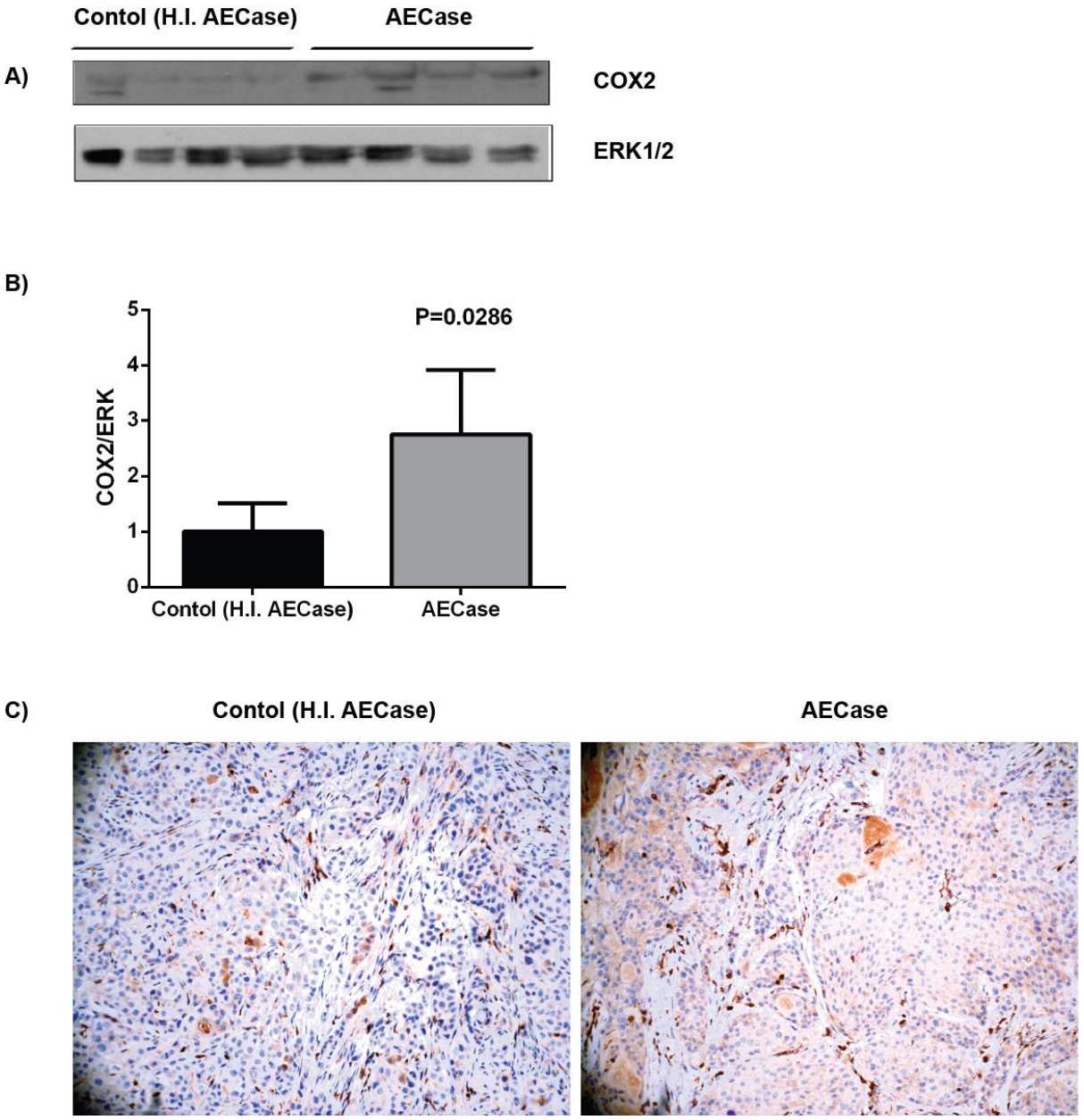

Figure 4.22 Induction of COX2 in H1650 xenograft tumours following treatment with AECase indicates ferroptosis.

A, immunoblot analysis of lysates from control (lanes 1–4) or AECase-treated (lanes 5–8) H1650 xenograft tumours probed to detect COX2. ERK1/2 was used as a loading control. B, quantification of relative COX2/ERK in control or AECase-treated groups. p = 0.0286; n = 4 using a student's t test. C, Images of IHC staining for COX2 in sections from control and AECase-treated tumours. Staining was performed and evaluated by Precision Pathology. Ms Xiaomeng Wang has assisted with the immunoblot experiment.

4.4 Conclusions

The results presented in this chapter provide an insight on the mechanisms through which activation of EGFR and subsequently MAPK pathway sensitises cells to ferroptosis. Inhibition of constitutive EGFR signalling using gefitinib was shown to be effective in reversing ferroptosis in HME-EGFR cells and blocked the formation of lipid ROS. Dissecting the downstream pathways active in the presence of the mutant EGFR, I demonstrated that sensitivity to ferroptosis was mediated by activation of the MAPK pathway through the RAS-RAF-MEK cascade. In contrast, activation of PI3K and its downstream effector AKT was independent of EGFR signalling, and appeared irrelevant to ferroptosis sensitivity. Further interrogation of the MAPK pathway using distinct MEK and ERK inhibitors yielded similar results and blocked cell death and ROS accumulation following deprivation of cystine.

An increased rate of glutathione oxidation was observed in wild-type HME cells and gefitinib-treated HME-EGFR cells that led me to investigate the role of the GPX family of enzymes in modulation of glutathione oxidation. Expression of GPX4 was found to be downregulated in HME-EGFR cells, an effect reversible upon inhibition of EGFR and downstream MAPK signalling. Inhibition of expression of GPX4 using an siRNA transient knockdown approach effectively sensitised both wild-type and gefitinib-treated HME-EGFR cells to deprivation of cystine to a degree comparable to untreated HME-EGFR cells. Inhibition of GPX4 expression was also shown to induce accumulation of lipid ROS in wild-type HME cells. Finally using a reconstitution approach, ectopic expression of GPX4 in HME-EGFR cells increased their resistance to ferroptosis following cystine depletion.

To establish the potential of nutrient modulation to induce ferroptosis in cancer cells I expanded my study to a panel of NSCLC cell lines. In these cells sensitivity to ferroptosis did not appear to strictly correlate with the levels of GPX4 but did show that MAPK activation determined sensitivity to ferroptosis. Inhibition of MAPK pathway in two of these cell lines correlated with restoration of cell viability. The H1650 cell line, which shares the same mutation as the one found in HME-EGFR cells, was shown to be sensitive to deprivation of cystine, inducing ferroptosis, which could be reversed following addition of Fer1 or tocopherol.

I have additionally shown that using an enzymatic approach to decrease the extracellular levels of cystine successfully induced ferroptosis in both HME-EGFR and H1650 cells, cell lines that share the same activating EGFR mutation (exon 19 deletion). This observation was supported by the ability of AECase to induce cell death that was reversible by treatment with a ferroptosis-specific antioxidant Fer1 and by α-tocopherol. Moreover, incubation of H1650 cells in cystine-deprived media or following treatment AECase compromised the integrity of the cell membrane. Finally, utilising an *in vivo* xenograft model provided evidence that cystine depletion in vivo could potentially provide a therapeutic benefit in some NSCLC tumours sensitive to ferroptosis. Given the previous observations on the importance of MAPK activation in determining sensitivity to ferroptosis, my results suggest that tumours with a high level of MAPK activation may be particularly good candidates to effect cystine depletion in a therapeutic setting.

5. CHAPTER 5. STUDYING THE PROPAGATION OF FERROPTOSIS IN HUMAN MAMMARY EPITHELIAL CELLS.

5.1 Introduction

The initial screen of amino acid sensitivity performed in Chapter 3 established that the requirement for cystine varies depending on the mutational status of each HME cell line used (Figure 3.1). Interestingly, cell confluence appeared to play an important role in rescue from ferroptosis; whereas sub confluent cultures of wild-type HME and HME-BRAF cells were as sensitive to cystine deprivation as were HME-EGFR cells, confluent cell cultures of the former cell types were significantly less so (Figure 3.2). These observations suggested that cell-cell contact may protect against ferroptosis in wild-type HME and HME- BRAF cells in a way that it did not in HME-EGFR cells.

These cells take on a characteristic balloon-like morphology during ferroptosis that was particularly apparent in confluent cultures of HME-EGFR cells where more than 90% of the cells took on this morphology. In contrast, confluent monolayers of wild-type HME cells largely appear normal in morphology and only a small proportion of dead cells were seen that appeared to accumulate in sporadic foci (see Section 5.2).

5.2 Ferroptosis occurs in a wave like manner.

Typical representations of the cell death occurring in confluent cultures of cystine-deprived wild-type HME and HME-EGFR cells are shown in Figure 5.1A. Cells that had undergone ferroptosis exhibit a characteristic balloon-like morphology (as indicated by red arrows in both images). Cultures of HME-EGFR cells displayed wide-spread cell death, whereas wild-type HME cultures showed more limited ferroptosis that seemed to accumulate in specific foci (indicated by the red border) that was surrounded by otherwise healthy cells.

The balloon-like morphology of cells that have undergone ferroptosis suggested a loss of plasma membrane integrity. This hypothesis was tested using Sytox Green staining. Sytox Green is a membrane impermeable nuclear cell dye that indicates cells in which the integrity of the plasma membrane is compromised. Sytox Green uptake is a widely used tool to indicate cell death by necrosis using time-lapse microscopy (Forcina et al., 2017; Wallberg et al., 2016). Figure 5.1B shows that cultures of wild-type HME cells developed sporadic foci of Sytox Green-positive cells when deprived of cystine for 72h. Time-lapse microscopic observation of wild-type HME cells showed that foci of Sytox Green-positive cells grew in size with time, with increasing numbers of cells adjacent to Sytox Green-positive cells losing membrane integrity in an apparent wave-like manner (Figure 5.2). Additionally, cells on the wave-front appeared to lose contact both with neighbouring cells and with the substratum prior to uptake of Sytox Green (Figure 5.3). Taken together, these data suggest that in wild-type HME cells, ferroptosis resulting from cystine deprivation occurs sporadically within the monolayer and progresses which is then propagated from cell to cell in a progressive, wave-like, manner.

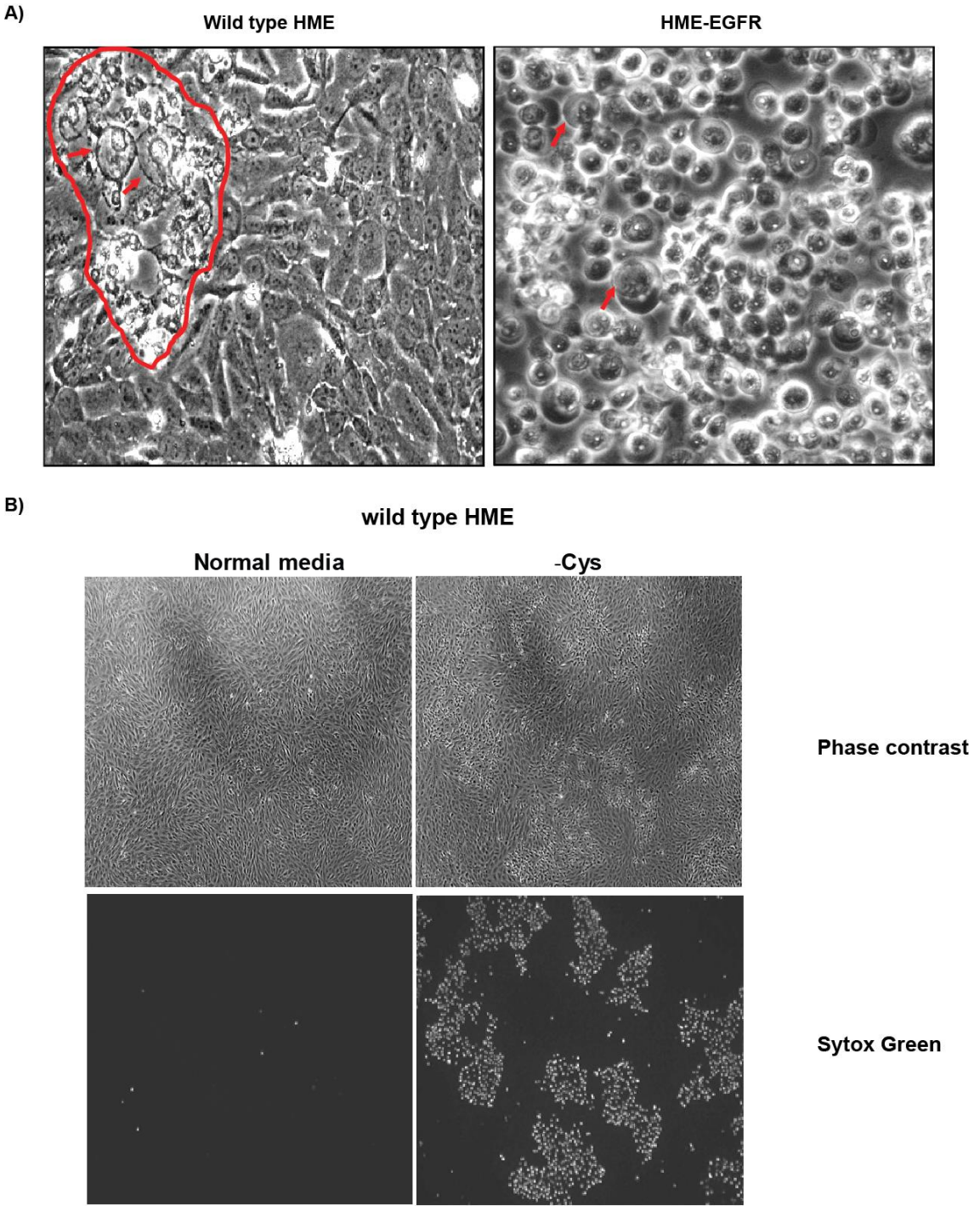

Figure 5.1 Ferroptosis initiated in confluent cultures of wild-type HME cells by cystine deprivation occurs in sporadic foci.

A, 20x phase-contrast image of confluent wild-type HME and HME-EGFR cells following culture in media lacking cystine for 24h. Area bounded in red is a necrotic foci, and arrows indicate characteristic balloon-like cells that have undergone ferroptosis. B, 4x phase-contrast (top panels) and green fluorescence (Sytox Green, bottom panels) images of confluent wild-type HME cells following culture in normal media (left panels) or media lacking cystine for 72h (right panels).

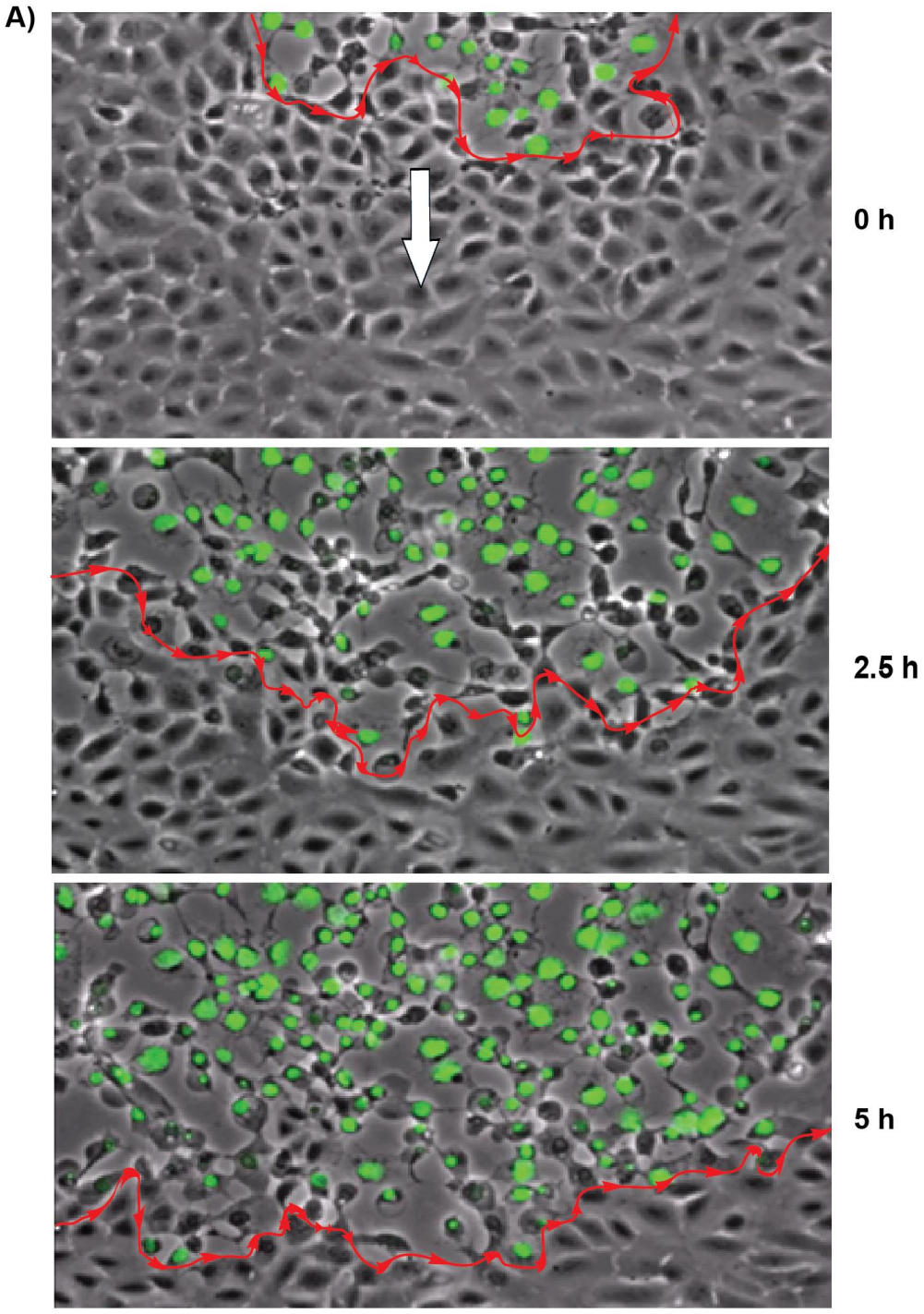

Figure 5.2 Ferroptosis is propagated in a wave-like manner in wild-type HME cells following cystine deprivation.

Wild-type HME cells were cultured in the absence of cystine for 24h and then observed by video time-lapse photography (20x magnification) for 5 hours following observation of initiation of a focus of ferroptotic cells using Sytox Green uptake as a marker. Phase-contrast and green fluorescence images of cultured cells were superimposed, the wave-front is highlighted by a red arrowed line to demonstrate the boundary between Sytox Green-positive (dead), and Sytox Green-negative (live) cells. White arrow indicates the direction of the wave of Sytox Green positivity.

.

A)

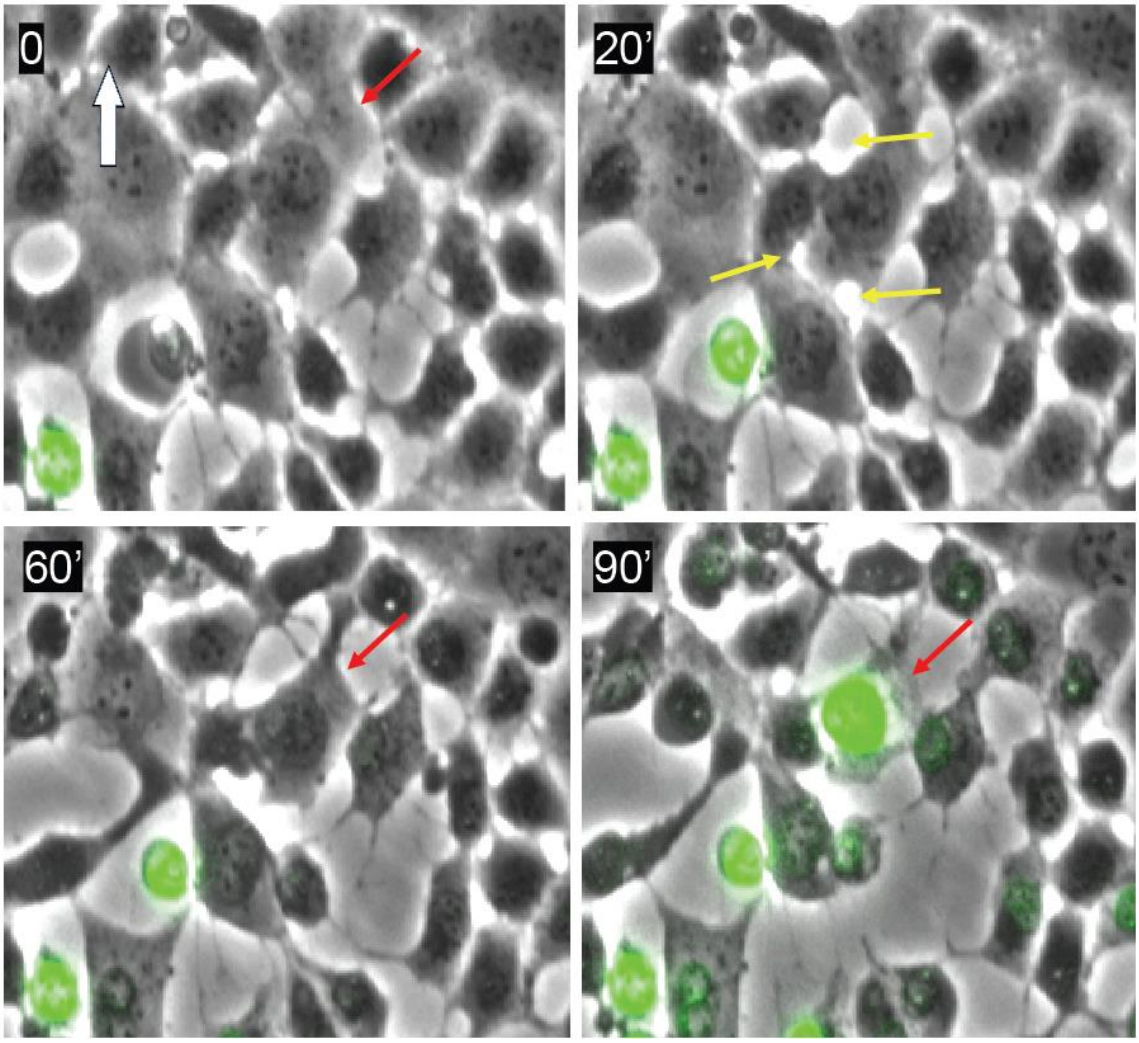

Figure 5.3 Cell detachment appears to precede loss of membrane integrity in wild-type HME cells cultured in the absence of cystine.

A, wild-type HME cells were cultured for 24h in the absence of cystine, then stained with Sytox green. Video time-lapse microscopy was performed and phase contrast/fluorescence images (20x magnification) recorded over a period of 90 minutes. The white arrow indicates the direction of the wave progression while the red arrow indicates a cell, proximal to neighbouring Sytox Green-positive cell (in green) and presented images track loss of cell-cell (yellow arrows) and cell-substratum contact prior to uptake of Sytox Green at 20, 60 and 90min.

.

5.3 Release of soluble H_2O_2 and involvement of NOX enzymes in ferroptosis.

In Chapter 3 I demonstrated that HME-EGFR cells cultured in the absence of cystine have higher levels of ROS than do wild-type HME cells, and that ferroptosis of the former cells is associated with accumulation of lipid peroxides. In Chapter 4 I demonstrated that lipid peroxide generation in HME-EGFR cells results from MAPK pathway-driven suppression of GPX4 expression and partly explains the rapid induction of ferroptosis in these cells. NADPH oxidase (NOX) enzymes may also promote ferroptosis because of their role in regulating ROS levels in cells (Dixon et al., 2012; Linkermann et al., 2014) through the production of hydrogen peroxide (H_2O_2) (Kamata, 2009). In this regard, NOX4 is of particular interest because of its role in direct generation of hydrogen peroxide (Takac et al., 2011) and because expression of this enzyme is known to be positively regulated by the MAPK pathway (Kodama et al., 2013; Ogrunc et al., 2014). Moreover, previous reports have indicated EGFR signalling promotes the accumulation of hydrogen peroxide (Bae et al., 1997).

To determine whether hydrogen peroxide and NOX1/4 have a role to play in the mechanism regulating ferroptosis of HME-EGFR cells, I added to cell culture media soluble catalase, an enzyme that breaks down H_2O_2 (Aebi, 1984) and GKT136901, an inhibitor of NADPH-oxidases 4 (NOX4) (Laleu et al., 2010). Both treatments protected HME-EGFR cells from ferroptosis following cystine deprivation (Figure 5.4 A), with the presence of GKT136901 additionally attenuating the formation of lipid ROS (Figure 5.4 B). These observations indicate that both generation and release of H2O2 contribute to ferroptosis following deprivation of cystine in HME-EGFR cells.

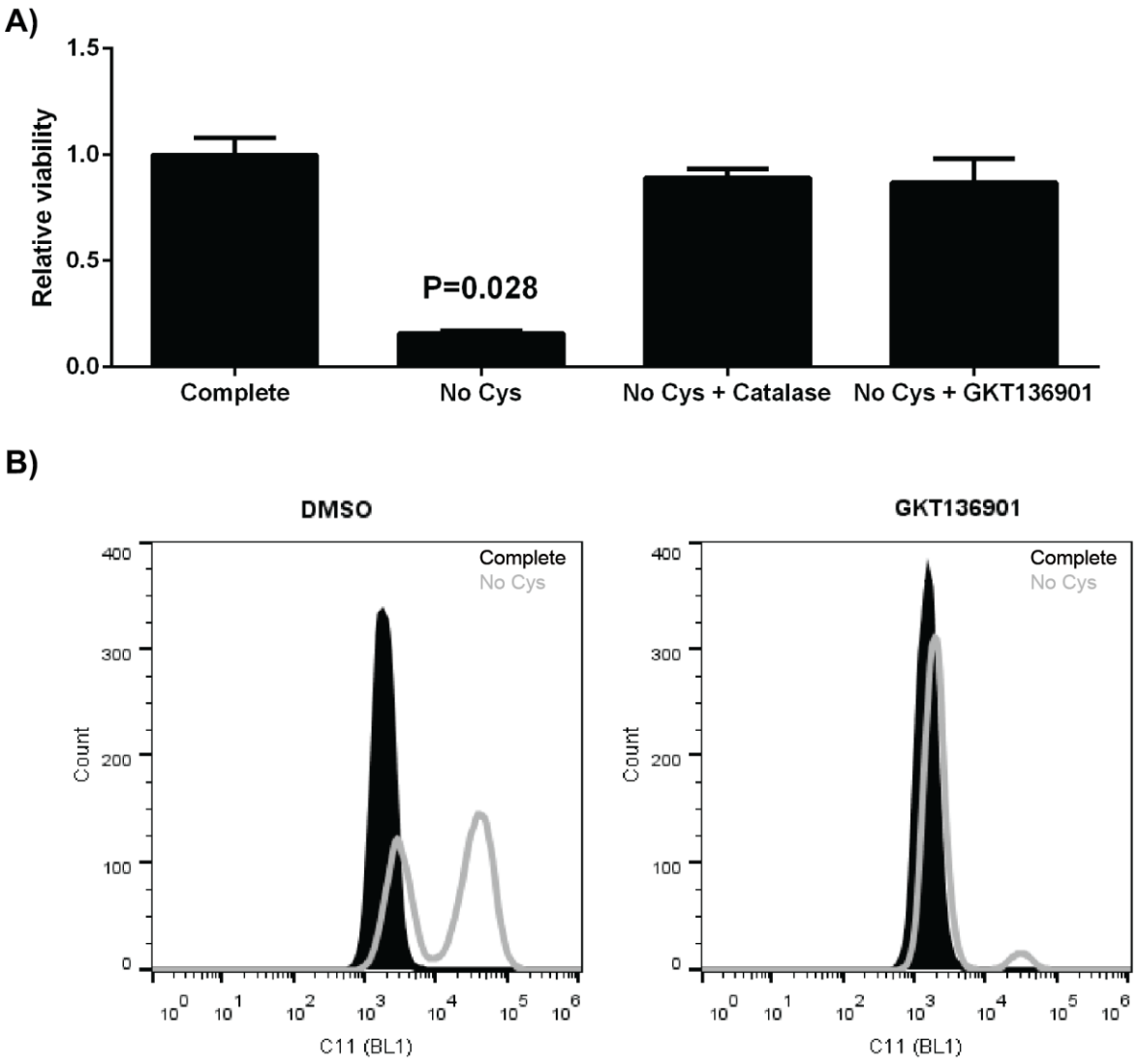

Figure 5.4 Involvement of hydrogen peroxide in ferroptosis in HME-EGFR cells.

A, viability assay for HME-EGFR cells cultured in complete media or media lacking cystine in the presence or absence of catalase (1000kU/ml) or NOX4 inhibitor, GKT136901 (20μM) for 24h. B, analyses of lipid ROS by FACS analysis in HME-EGFR cells cultured in complete media or media lacking cystine in the presence or absence of GKT136901 (20μM) using the C11 probe (2μM) detected using the BL1 channel. Each histogram shows the spread of a population of minimum 5000 events of cells in complete medium (black graphs) or in medium lacking cystine (grey outline) for 12h.

5.4 Cell-cell contact protects cells from ferroptosis.

5.4.1 The formation of well-defined adherence junctions protects cells from ferroptosis and is suppressed by activation of MAPK signalling.

Observations that wild-type HME cells are less sensitive to deprivation of cystine when confluent (Figure 3.2), that cell-cell contact is lost during ferroptosis propagation and a report that E-cadherin:β-catenin complexes that form adherens junctions (AJ) between cells are degraded in ischemic epithelia (Bush et al., 2000) all suggested an important role for cell-cell contact in regulating induction of ferroptosis. I next explored this possibility by examining AJs between cells in cultures of wild-type HME and HME-EGFR cells. Figure 5.5 shows confocal microscope images of wild-type HME and HME-EGFR cells stained with β-catenin to observe AJs. Examination of wild-type HME cells showed characteristic features of epithelial cells with distinct borders and linear AJs. In contrast, HME-EGFR cells stained for β-catenin exhibited inconsistent cell-cell borders, broken AJ and obvious spaces between cells. The role of EGFR-MAPK signalling in AJ disruption was tested next using inhibitors of EGFR (gefitinib) and MEK (selumetinib). Treatment of HME-EGFR cultures with these compounds (for 30 h) restored AJ connections to generate a staining pattern similar to that observed in cultures of wild-type HME cells. In contrast, inhibition of PI3K signalling in HME-EGFR cultures by treatment with wortmannin was without obvious effect on AJ straining. Together these data suggest a role for increased MAPK signalling in disruption of AJs in cultures of HME-EGFR cells. Considering that MAPK signals are responsible for sensitivity to ferroptosis (Figures 4.2-4.5), it seems probable that the protective effect of cell-cell contact in wild-type HME cells may be the result of reduced MAPK activation resulting in increased AJ formation.

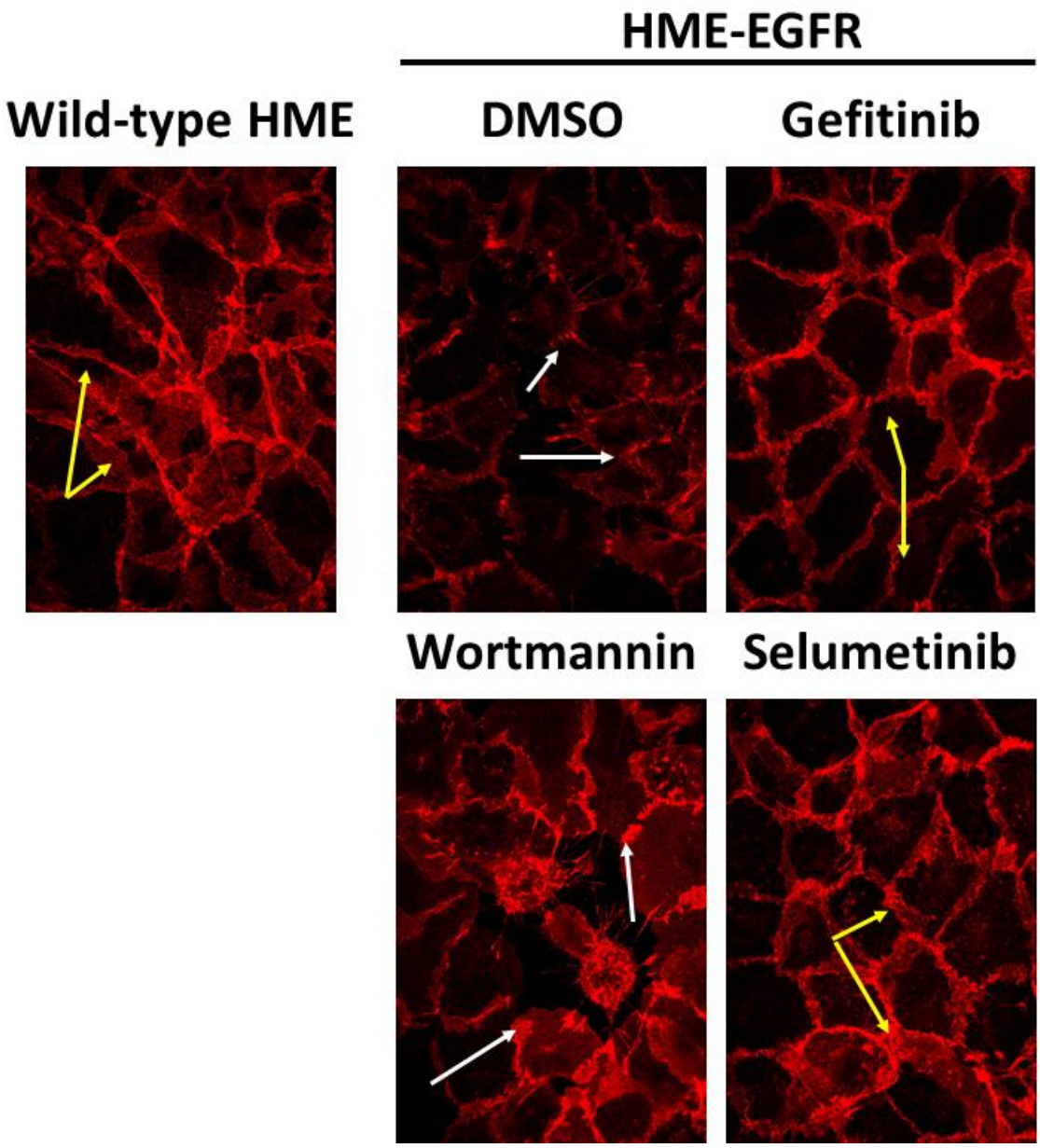

Figure 5.5 Wild-type and EGFR-mutant HME cells display differential distribution of intercellular AJ.

Confocal laser scanning microscope images of β-catenin immunofluorescent staining in wild-type HME and HME-EGFR cells. Wild-type cells were only treated with DMSO control (left panel) and HME-EGFR cells (right panels) were treated with either DMSO, 1μM Gefitinib, 1μM Wortmannin or 5μM Selumetinib for a total of 30h. Yellow arrows point to consistent linear β-catenin staining at adherens junctions (A, C and E) whereas white arrows are used to indicate discontinuous adherens junctions between cells (B and D). Experiment was performed by Mr Thomas Crighton.

5.4.2 Cell contact facilitates the formation of Gap junctional communication channels that have a protective effect in wild-type cells.

Following the observation that establishment of AJ was associated with a protective effect in cells from ferroptosis I next examined the role of Gap junctions (GJ). GJ are intercellular channels formed between cells that allow exchange of small molecules such as metabolites and enzyme cofactors (Nielsen et al., 2012). GJs can be found colocalised with AJs on cell borders, due to the instructive role that AJs have in the formation of GJs (Shaw et al., 2007). Moreover, both type of junctions have been found disrupted in ischemic models suggesting a potential role in regulation of subsequent cell death. To test whether GJs are important for the propagation of ferroptosis I initially employed carbenoxolone (CBX), an inhibitor of GJ intercellular communication (GJIC) (Davidson and Baumgarten, 1988). Notably, treatment of wild-type HME cells with CBX increased cell death in cystine-deprived cultures (Figure 5.6).

However, CBX is widely considered as a pharmacological agent with limited specificity (Connors, 2012) .To determine if the previously observed effect of CBX to accelerate ferroptosis in wild-type HME cells was dependent on GJIC I next examined GJIC in cultures of wild-type HME, while also examining GJIC in HME-EGFR cells. For this purpose, we used an assay that measures the transfer of Lucifer yellow dye from cells scrape loaded following monolayer wounding (Figure 5.7). This assay showed that CBX blocked GJIC in cultures of both wild-type HME and HME-EGFR cells. Quantitative comparison of Lucifer yellow dye transfer in cultures of wild-type HME and HME-EGFR cells showed reduced GJIC in HME-EGFR cells. I next investigated the role of MAPK signalling in impaired GJIC in HME-

EGFR cells. As with AJ formation, treatment of HME-EGFR cells with gefitinib (to inhibit EGFR) or selumetinib (to inhibit MEK signalling) for 30h restored GJIC to levels comparable to those observed in wild-type cells (Figure 5.7). These experiments therefore suggest that the MAPK pathway resulting from increased EGFR signalling plays a role in inhibiting GJIC formation, and that GJ are important in protecting wild-type HME cells from induction of ferroptosis. A potential mechanism could be hypothesised by the ability of GJIC to dilute the NOX-generated hydrogen peroxide in order to prevent its accumulation within a single cell which could be responsible for induction of ferroptosis.

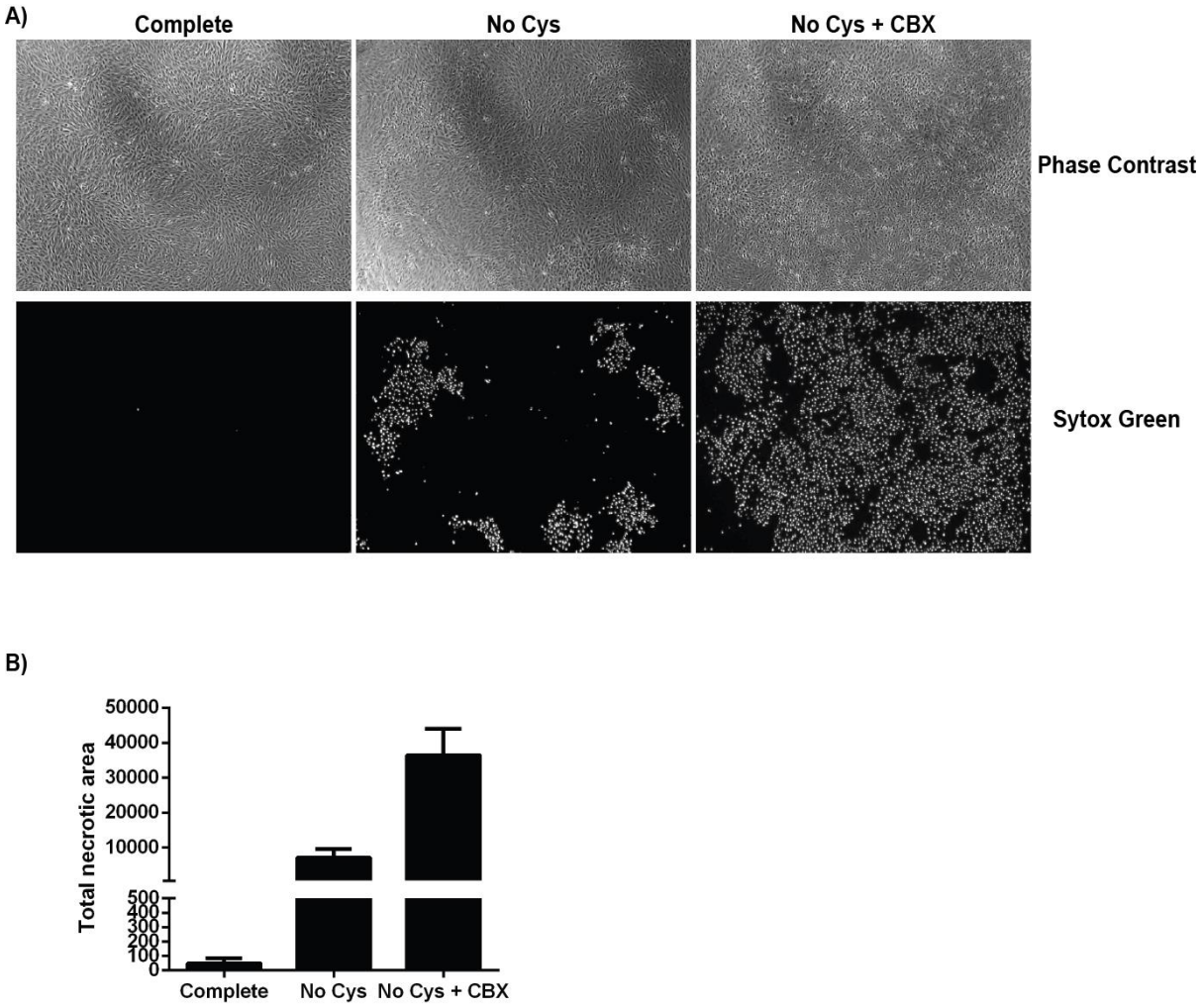

Figure 5.6 Inhibition of GJIC using carbenoxolone sensitises wild-type HME cells to ferroptosis.

A, 4x phase contrast (top panels) and green fluorescence (Sytox Green, bottom panels) of confluent wild-type HME cells taken 24h after change of media to either complete synthetic HME media or media deficient in cysteine with or without CBX (100μM). B, Graph shows quantification of total necrotic area observed in cells cultured for 24h in complete media, cystine-deficient media or cystine-deficient media with CBX (n=3). Results are typical of three independent experiments. Experiment was performed by Mr Thomas Crighton.

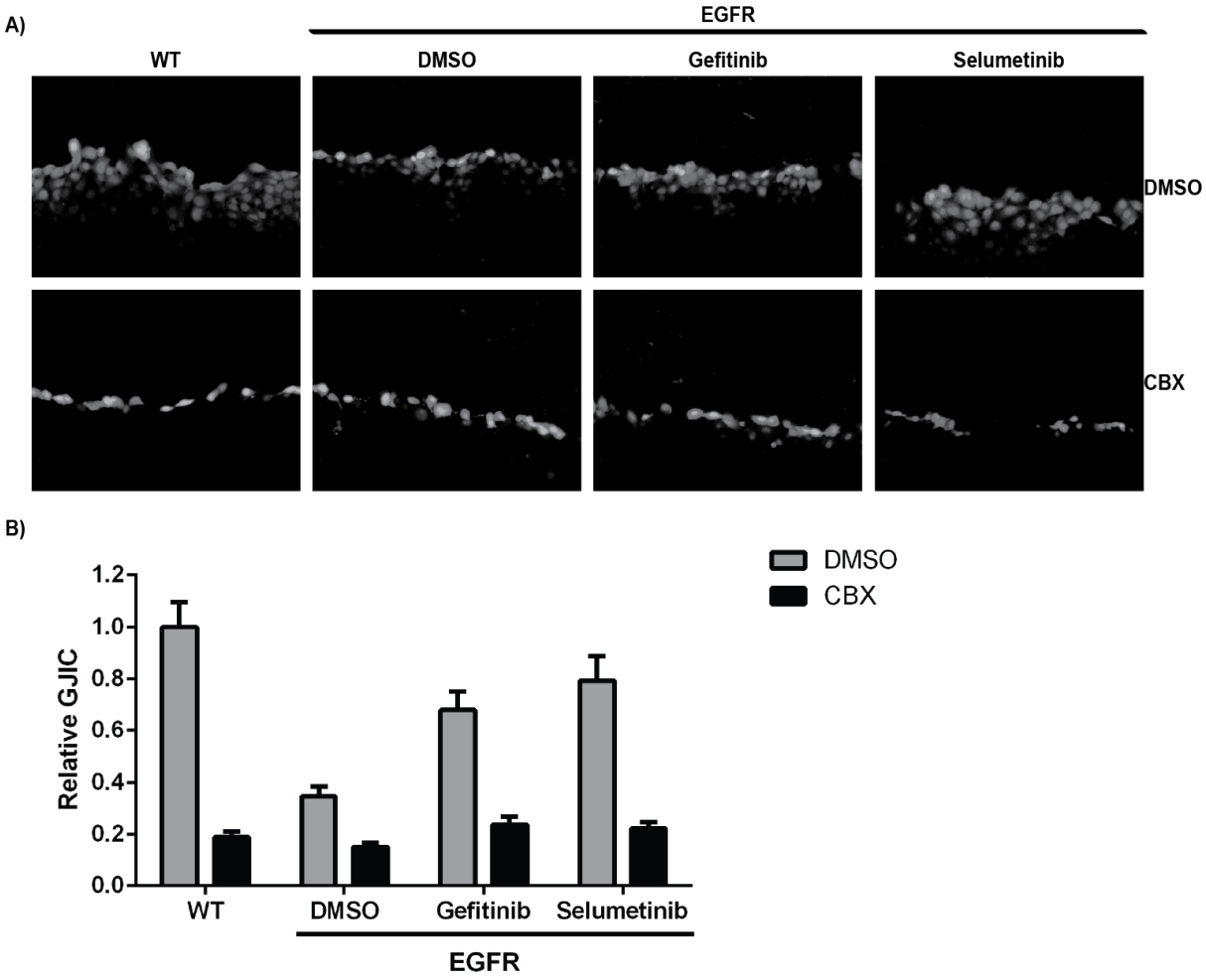

Figure 5.7 HME-EGFR cells demonstrate lower levels of GJIC that can be restored following MAPK inhibition.

A, 20x green fluorescence micrographs of lucifer yellow transfer in wild-type HME and HME-EGFR cells treated with DMSO control, Gefitinib (1μm) or Selumetinib (5μM) for a total of 30h in the presence or absence of CBX (100μM). B, Bar graph representing quantification of GJIC. Grey bars indicate DMSO-treated or drug-treated cells and black bars indicate CBX treated cells. For each condition 18 different fields in three biological replicates were analysed with the values shown representing the mean and SD and expressed relative to GJIC in wild-type HME cells assigned an arbitrary value of 1. Experiment was performed by Mr Thomas Crighton.

5.5 Ferroptotic cell spread occurs through extracellular products of lipid peroxidation.

My previous results suggest that ferroptosis within cultures of wild-type HME cells occurs in a wave-like manner, spreading from dead Sytox Green-positive cells to their neighbouring Sytox Green-negative cells in a way reminiscent of the synchronous pattern of necrotic spread previously reported in ischemic renal tubules undergoing ferroptosis (Linkermann et al., 2014). My results also show that GJIC protects HME cells against ferroptosis, but once this process is initiated it appears that proximity to Sytox Green-positive ferroptotic cells affects neighbouring cells firstly to disrupt their cell-cell and cell-matrix contacts and secondly to induce membrane permeabilization and cell death. This poses the question of whether a paracrine factor is responsible for the propagation of ferroptosis.

I first investigated whether the spread of ferroptosis was associated with generation of reactive oxygen species. Treatment with antioxidants Fer1, α-tocopherol (vitamin E) or Trolox [a water-soluble form of vitamin E (Davies et al., 1988) inhibited cell death propagation as measured by quantification of rate of increase of area of Sytox-Green-positivity determined by fluorescence time-lapse microscopy (Figure 5.8). Given the effectiveness of catalase in inhibiting ferroptosis in HME-EGFR cells following cystine deprivation, I next examined whether soluble H_2O_2 could be responsible for the propagation of ferroptosis in cultures of wild-type HME cells deprived of cystine. However, propagation of cell death was unaffected by the presence of soluble catalase (Figure 5.9) suggesting that local extracellular release of H_2O_2 was not responsible for the cell-cell spread of cell death. In contrast, addition of the NOX4 inhibitor GKT136901, involved in direct intracellular synthesis

of H_2O_2 effectively blocked ferroptosis propagation. Addition of BSA in similar quantity to the enzyme catalase was used as a positive control to exclude any possible effects of protein macropinocytosis and did not generate any effect on cell death transmission (Figure 5.9). Thus, H_2O_2, plays an important role in the propagation of ferroptosis but is unlikely to be the paracrine factor involved in cell-cell spread. Instead, a possible scenario is that hydrogen peroxide is responsible for the appearance of lipid peroxides through the Fenton reaction that is mediated by iron (Winterbourn, 1995).

To test whether soluble lipid peroxides were involved in ferroptotic spread I employed addition of recombinant GPX4, a GPX enzyme that can specifically neutralise lipid peroxides. Addition of soluble GPX4 to cultures of wild-type HME cells following initiation of ferroptosis significantly inhibited subsequent spread of ferroptosis (Figure 5.10). Next, I tested whether end-products of lipid peroxidation, such as 4HNE, were involved in ferroptotic spread. To detoxify 4HNE I employed a GST, recombinant GST4-4, which is known to detoxify 4HNE (Awasthi et al., 2004). Treatment with GST4-4 similarly inhibited spread of ferroptosis. 4HNE is known to react primarily with reactive cysteines within proteins (LoPachin et al., 2009). To further investigate the role of such lipid peroxidation-induced protein modifications in cell-cell spread of ferroptosis we utilised a linoleamide alkyne (LAA) assay which detects lipid peroxidation-induced protein modifications (Gong et al., 2016). Addition of Cumene hydroperoxide (CuOOH) to wild-type HNE cells was used as a positive control for such protein modifications due to its ability to generate lipid peroxides (Vanderkraaij et al., 1990). This experiment showed that strong DAPI-positive adherent cells proximal to morphologically distinct weak DAPI-positive cells that had

undergone ferroptosis exhibited strong LAA signals following deprivation of cystine (Figure 5.11) that diminished with distance. Thus, lipid peroxide-associated protein adducts, likely derived primarily from 4HNE, appear to be a likely promoter of cell-cell propagation of ferroptosis.

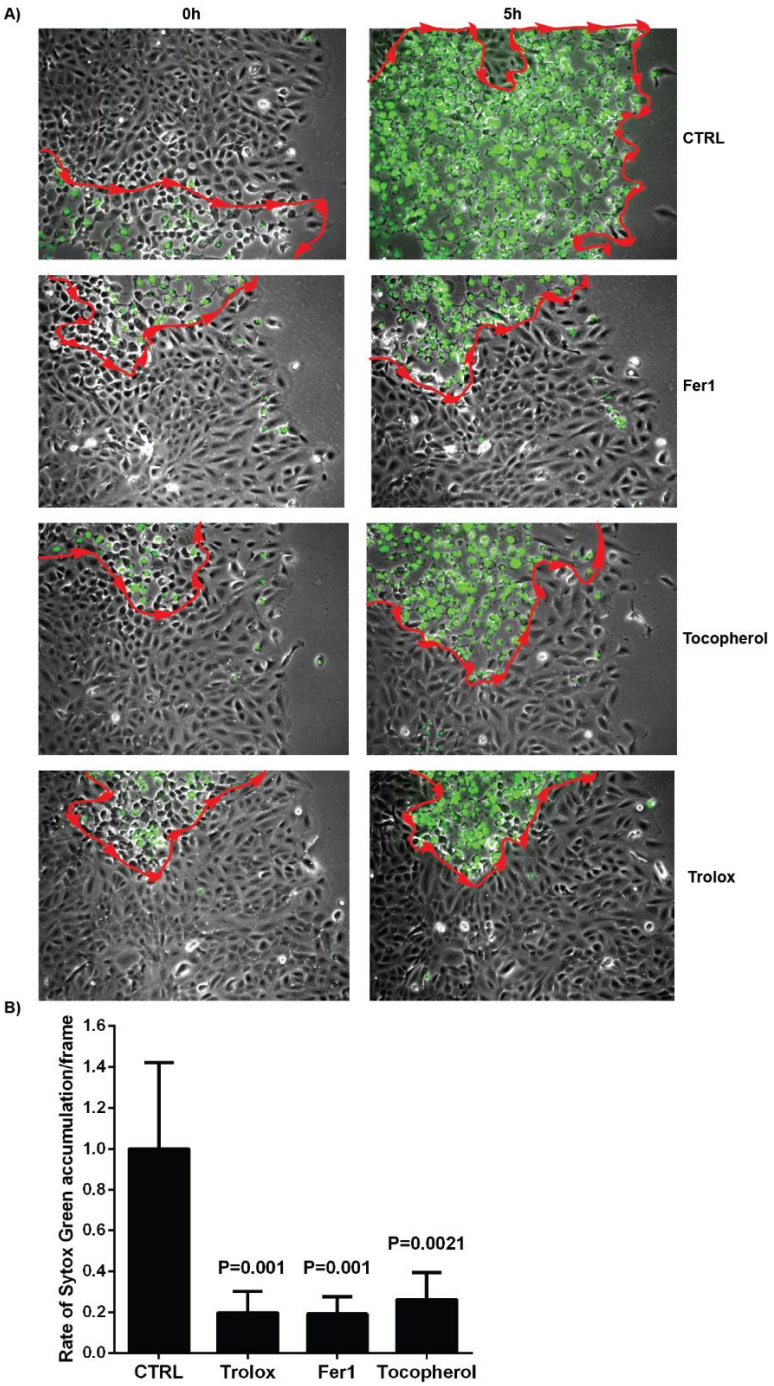

Figure 5.8 Propagation of ferroptosis can be inhibited by antioxidants and Fer1.

A, Dual phase-contrast/fluorescence images of Sytox Green stained cells captured by video time-lapse for 5 hours following culture in media lacking cystine for 24h hours in the presence of BSA, Fer-1 or antioxidants Trolox and α-tocopherol. Area of Sytox Green positivity is bounded in red. B, Quantification of the rate of increase of Sytox Green positivity in the presence of BSA (control), Trolox (1μM), Fer-1 (2μM) or α-tocopherol (30μM). For each condition four 10X fields were analysed and the values shown represent the mean and SEM relative to BSA supplemented media assigned an arbitrary value of 1. Statistical analysis was performed using ANOVA with a Bonferroni post hoc test. Mr Thomas Crighton has assisted in this experiment.

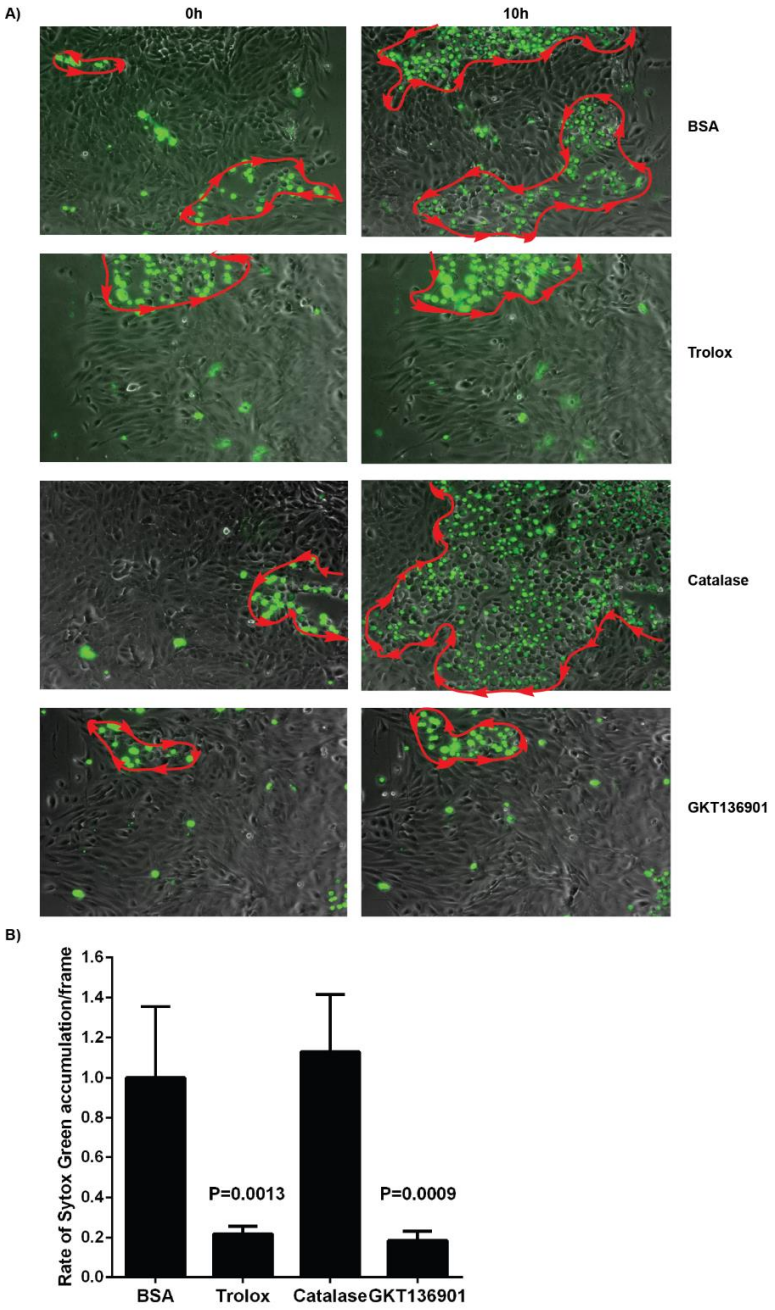

Figure 5.9 Inhibition of hydrogen peroxide generation, but not extracellular release, restricts propagation of ferroptosis.

A, Dual phase contrast/fluorescence images of video time-lapse for 10 hours following culture in media lacking cystine for 24h hours in the presence of BSA, antioxidant Trolox, catalase or the NOX4 inhibitor GKT136901. Area of Sytox Green positivity is bounded in red. B, Quantification of the rate of progression of ferroptosis (increase in Sytox Green positivity) in the presence of Trolox (5μM) or in the presence of BSA (0.3mg/ml), catalase (1000kU/ml) or NOX4 inhibitor GKT136901 (20μM). For each condition three 10X fields were analysed. Values shown represent the mean and SEM and rate of ferroptosis in BSA supplemented media assigned an arbitrary value of 1. Statistical analysis was performed using an ANOVA with a Bonferroni post hoc test. Mr Thomas Crighton has assisted in this experiment.

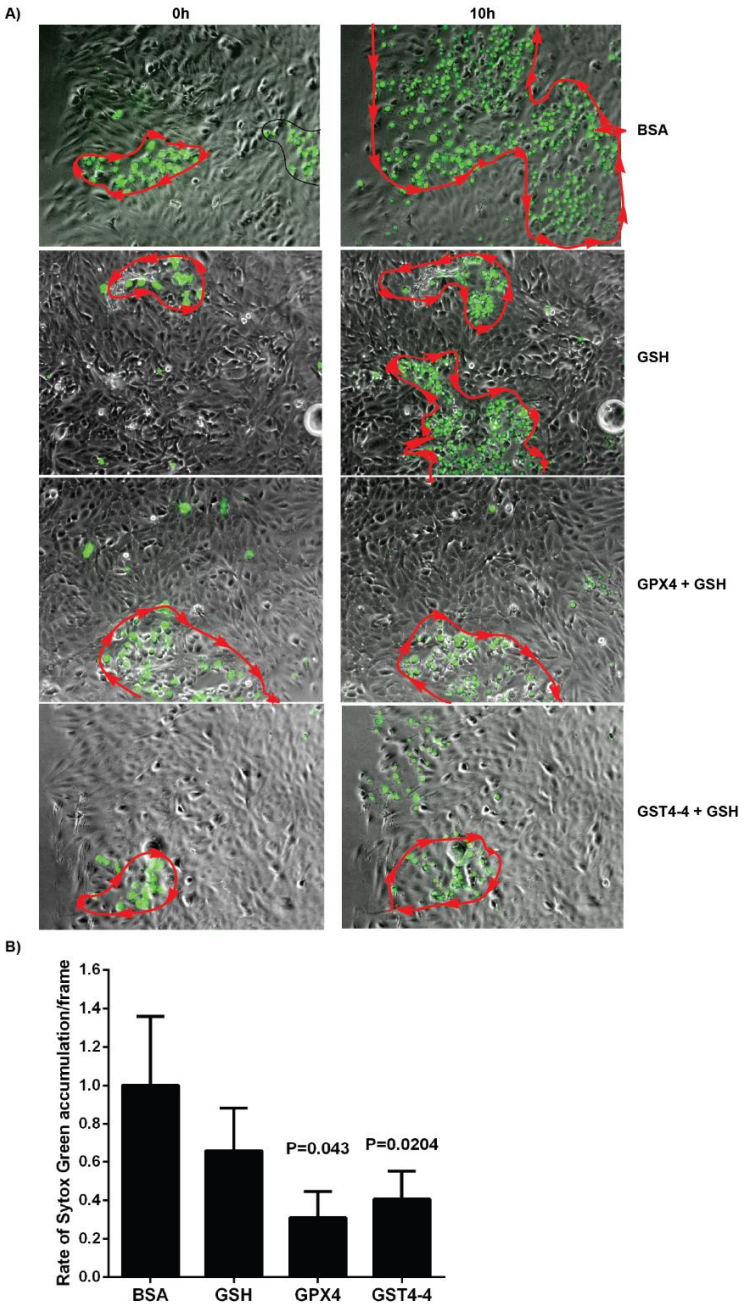

Figure 5.10 Detoxification of lipid peroxides or 4HNE inhibits ferroptotic spread.

A, dual phase contrast/fluorescence images of video time-lapse for 10 hours following culture in media lacking cystine for 24h hours in the presence of BSA, GSH alone or in the presence of GPX4 or hGSTA4-4. Area of Sytox Green positivity is bounded in red. B, quantification of the rate of progression of ferroptosis in the presence of BSA (10µg/ml), GSH (20µM) alone or in the presence of GSTA4-4 (10µg/ml enzyme /20µM GSH) or GPX4 (10µg/ml enzyme /20µM GSH). For each condition three 10X fields were analysed with and values shown represent the mean and SEM with the rate of ferroptosis in BSA supplemented media assigned the arbitrary value of 1. Statistical analysis was performed using an ANOVA with a Bonferroni post hoc test. Mr Thomas Crighton has assisted in this experiment.

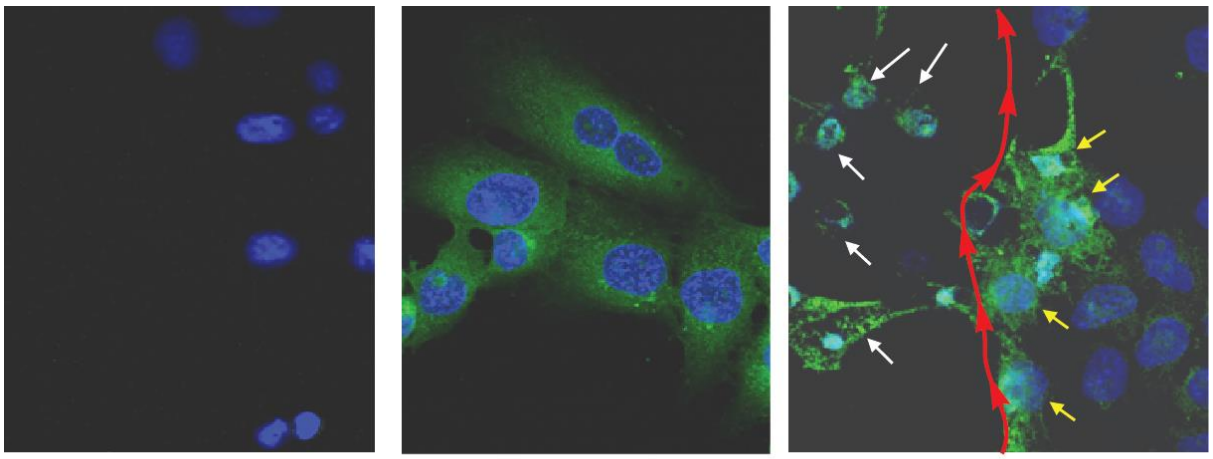

Figure 5.11 Lipid peroxidation-associated protein modification is detected adjacent to ferroptotic cells.

Confocal laser scanning microscope images of cells stained with LAA-azide and DAPI. Cells were treated with complete media as a negative control (left), or in complete media with addition of CuOOH (100μM, middle) as a positive control to induce lipid peroxidation or with media lacking cystine for 24h (right). White arrows point to necrotic cells that have undergone ferroptosis and yellow arrows indicate cells that are still adherent but with significant levels of lipid peroxidation. Red line indicates the borders of the wave front. Experiment was performed by Mr Thomas Crighton.

5.6 Conclusions

This chapter describes the cell-cell transmission and expansion of area of cell death by ferroptosis within epithelial cell monolayers of HME cells. Early observations of cell morphology following oxidative stress elicited by deprivation of cystine had previously revealed a distinctive necrotic phenotype, with the appearance of ruptured cells exhibiting a balloon-like appearance. In wild-type HME cells cell death following cystine deprivation occurred heterogeneously within discrete foci within the monolayer and was significantly slower than in HME-EGFR cells, where cell death was rapid and synchronous. Cells that had undergone ferroptosis could be distinguished from cells that had not by virtue of becoming permeable to membrane-impermeant nuclear die Sytox Green which allowed visualization of cell-cell transmission of ferroptosis and allowed me to quantify the rate of spread of cell death with time. Sytox Green-positive foci were observed to grow in size over time in a manner reminiscent of a wave, with Sytox Green positive cells inducing loss of cell-cell and cell-substratum contacts prior to attaining Sytox-Green positivity.

Two previous reports have highlighted the role of the NOX enzymes, that generate superoxide radicals and hydrogen peroxide, in the induction of ferroptosis (Dixon et al., 2012; Linkermann et al., 2014). In the cell system studied here, NOX4 inhibition using GKT136901 and extracellular addition of catalase to degrade extracellular hydrogen peroxide equally rescued the most-sensitive HME-EGFR cells from ferroptosis. It would be therefore possible that hydrogen peroxide acted as a paracrine factor inducing ferroptosis in cells adjacent to the focus margin.

Since loss of cell-cell contact of Sytox Green-negative cells was observed by fluorescence video time-lapse microscopy to be associated with proximity to Sytox Green-positive cells and subsequent death, I examined two distinct types of cell-cell junctions in wild-type and EGFR-mutant HME cells. In wild-type HME cells typical linear continuous adherens junctions detected by β-catenin staining were observed associated with robust gap junctional communication, determined by Lucifer Yellow dye transfer. In contrast, in HME-EGFR cells AJs were smaller and discontinuous, and gap junctional communication was weak relative to wild-type HME cells. To determine whether these features were dependent upon EGFR-MAPK signalling I again used small molecule inhibitors of these pathways. Inhibition of MAPK signalling effectively restored both AJ and GJ in HME-EGFR cells to levels similar to wild-type cells, corresponding with decreased sensitivity to ferroptosis. Thus, these observations indicate that differences in cell-cell contact and in cell-cell communication can influence sensitivity to ferroptosis. Given the role of AJ's in influencing GJIC (Shaw et al., 2007), one possibility is that robust GJIC is important in preventing local accumulation of hydrogen peroxide and other radicals within individual cells, thereby slowing the rate of progression of cell death by ferroptosis.

Addition of ferroptosis inhibitor Fer1 and antioxidants, trolox and α-tocopherol effectively inhibited death propagation in wild-type HME cells indicating that death spread is ROS-dependent. To determine the role of hydrogen peroxide in this process I used the NOX4 inhibitor GKT136901 to block hydrogen peroxide generation and addition of soluble catalase to cell culture media to break down extracellular hydrogen peroxide. Addition of the former effectively inhibited propagation of ferroptosis but catalase alone did not. Therefore, despite the critical

role that hydrogen peroxide generation plays in determining sensitivity to ferroptosis, it is unlikely to act as the paracrine factor that propagates ferroptosis within wild-type HME monolayers. Since lipid peroxidation is the distinctive feature of cell death by ferroptosis I determined whether extracellular lipid peroxides, or a major by-product of lipid peroxidation 4HNE, mediated ferroptosis propagation. To assess this possibility, I utilised addition to culture media of recombinant GPX4 or GST4-4, enzymes that detoxify lipid peroxides and 4HNE, respectively. Both enzymes effectively inhibited ferroptotic propagation, indicating that both lipid peroxidation and the generation of 4HNE are involved in spread of ferroptosis.

Together these observations indicate a previously undiscovered process of cell death spread that can occur in epithelial monolayers in which ferroptosis has been initiated. This process can be partially resisted by cell-cell contact, with cells that form better junctions more resistant to ferroptosis. Understanding of such mechanisms could potentially provide insight on how disease associated with ferroptosis affects healthy epithelial tissues, and how such processes might be modulated.

.

6. CHAPTER 6: GENERAL DISCUSSION

The results presented in this thesis demonstrate that HME cells require the amino acid cystine to prevent cell death by ferroptosis. Deprivation of cystine induces the accumulation of ROS and oxidative stress leading eventually to ferroptosis, a non-apoptotic necrotic cell death. Cystine deprivation-induced ferroptosis occurs to different extents and in different ways in the HME cell line series tested in this thesis (wild type HME cells and with those activating mutations in EGFR, BRAF, KRAS and PIK3CA). HME-EGFR cells demonstrated the highest dependence upon cystine to maintain cell viability through mechanisms involving MAPK pathway-driven changes in gene expression and increased sensitivity to ROS.

In wild type HME cells induction of ferroptosis once initiated was found to spread in a novel manner from the initiating cell to those in close proximity, leading to a “wave” of necrotic cell death within the epithelial monolayer (Section 5.2). Sensitivity of these cells to ferroptosis was also found to be associated with cell-cell contact and the establishment of strong adherens and gap junctions between cells. Finally, both ferroptosis initiation and subsequent spread and was found to be dependent upon hydrogen peroxide generation, likely due to its intracellular role in generating lipid peroxides. The results presented in this thesis further suggest that induction of ferroptosis may be exploitable as a therapeutic tool against MAPK-driven cancers. Indeed, experiments to degrade cystine using a recombinant cyst(e)inase effectively reduced the viability of EGFR-driven cancer cells *in vitro* and inhibited tumour growth *in vivo*, inducing ferroptosis in both cases.

6.1 Nutrient amino acid requirement screen for cells bearing oncogenic mutations.

The Chapter 3 of this thesis identifies cystine as an amino acid critically important for the survival of HME cells. This was determined using an amino acid dependency screen in HME cells (Figure 3.1) and is similar in principle to other studies using similar screens of nutrient dependency in cancer cells (Maddocks et al., 2013; Sheen et al., 2011). The initial aim of this work was a comparison of individual amino acid requirements between wild type HME cells and HME cells bearing activating mutations in the driver oncogenes EGFR, KRAS, BRAF and PIK3CA. I found that restriction of most amino acids generates small changes to the viability of the explored cell lines, consistent with a slowing of cell cycle progression in the absence of cell death (Figure 3.1). An exception is glutamine whose deprivation induced a strong loss of viability amongst all HME cell lines (Figure 3.1), consistent with previous findings (Wise and Thompson, 2010). The other notable exception was cystine where it was observed that cells with an activating mutation in EGFR or BRAF were particularly sensitive to removal of this amino acid (Figure 3.1). Conditions of higher confluency were also found to exert a protective effect upon cell viability in wild type HME and HME-BRAF, but not HME-EGFR cells (Figure 3.2). Overall these results indicate that the presence of an activating oncogene can alter a cell's nutrient requirements and their sensitivity to cell death by ferroptosis.

Titration experiments showed that HME-EGFR cells minimally require around 2μM of cystine in their growth media to ensure protection from ferroptosis (Figure 3.3). Moreover, HME-EGFR cells have an active requirement specifically for L-cystine because the presence of its enantiomer D-cystine did not protect HME-EGFR

cells from L-cystine deprivation-induced cell death (Figure 3.3). The enantiomer-specific selectivity of these cells for L- but not D-cystine may be attributed to the selectivity of the X_c^- system transporter which actively transfers the former but is inhibited by the latter (Patel et al., 2004).

A major question arising from my observations is why is cystine so critical as an amino acid nutrient to prevent cell death by ferroptosis? The requirement of some cultured cells for cystine, despite the ability to synthesise it from methionine, was initially observed in the early 1960s (Eagle et al., 1961). Later studies demonstrated that leukemic cells were auxotrophic for cystine, and therefore sensitive to deprivation of this amino acid (Foley et al., 1969; Iglehart et al., 1977; Ohnuma et al., 1971). Early attempts to take advantage of this requirement involved the administration of either rat cystathionine γ-lyase or cysteine desulfhydrase to lower the serum levels of cystine and cysteine in mice engrafted with L1210 leukemic cells to limit growth of the tumour (Uren and Lazarus, 1979; Uren et al., 1978). A more recent approach has proposed the use of recombinant human cystathionine γ-lyase enzyme that has been genetically engineered to degrade both cystine and cysteine (Cramer et al., 2017). Intermittent peritoneal injection of this recombinant cysteinase in mice with xenograft tumours of prostate and breast cancer origin, as well as in Tcl1-transgenic mice- which model human chronic lymphocytic leukaemia- was observed to inhibit tumour growth through induction of ROS and oxidative stress (Cramer et al., 2017).

Following uptake via the X_c^- system, cells need to reduce cystine to cysteine for further use in biosynthesis (Mandal et al., 2010a). Only a small fraction of intracellular cysteine is thought to be used in protein synthesis, with most of it is

utilised for the synthesis of the antioxidant glutathione (Lu, 2013). Glutathione is the major antioxidant defence of eukaryotic cells due to its capacity to neutralise ROS, and is found in high concentrations both intracellularly and in the extracellular milieu (Lu, 2013). Why then are HME-EGFR cells particularly sensitive to cystine-deprivation induced ferroptosis? Deprivation of cystine induces the accumulation of total ROS as well as lipid peroxidation, indicating that the cell death observed might be attributed to oxidative stress (Figure 3.4). Consistent with this notion, my experiments show that addition of ROS scavengers idebenone and α-tocopherol to cultures of cystine-deprived HME-EGFR cells rescues them from induction of cell death (Figure 3.5). Measurement of glutathione levels in wild type HME and HME-EGFR cells shows the latter have higher basal levels of both reduced (GSH) and oxidised (GSSG) glutathione (Figure 3.7). The similarity in glutathione depletion in both HME cell lines following deprivation of cystine is suggestive of a higher basal generation of ROS in HME-EGFR cells, and indeed activation of EGFR following ligand interaction had been previously shown to promote ROS induction (Bae et al., 1997). It would therefore not have been surprising that exposure to a basally higher ROS burden even in normal media was the underlying reason for the higher basal levels of glutathione in HME-EGFR cells. Why then did only HME-EGFR cells accumulate ROS when depleted of cystine and die by ferroptosis, whilst wild type cells did not? My studies point strongly to a failure of HME-EGFR cells to efficiently detoxify ROS, due in large part to a MAPK-driven programme, that leads to an increased sensitivity to ferroptosis following limitation of cystine. It seems to me a likely possibility that this could be a natural tumour suppressive mechanism that prevents cancer cells with elevated MAPK signalling from thriving under conditions of nutrient limitation.

This conclusion- that MAPK-activated cells are particularly ROS-sensitive and therefore susceptible to a form of death associated with damage to membranes- is supported by a number of my observations. Firstly, I could rule out any differences in intracellular cystine levels themselves as responsible for the differential increase in ROS and cell death. Thus, both wild type HME and HME-EGFR cells were found to respond to cystine deprivation with similar kinetics of activation of GCN2, a sensor for amino acid deficiency (Figure 3.6). Similarly, intracellular levels of cystine were found to diminish equivalently following cystine depletion in ferroptosis-sensitive or -resistant HME cells, as determined by LC-MS (Figure 3.6). This equivalent loss of intracellular cystine was associated with an equivalent reduction in levels of reduced and oxidised glutathione in wild type HME and HME-EGFR cells regardless of their basal levels in complete media (Figure 3.7). Thus, both cell lines require cystine to maintain levels of glutathione, and it is unlikely that cystine is preferentially maintained in ferroptosis-resistant wild type HME cells, for example via increased levels of transulfuration, a compensatory pathway that can synthesise cysteine from methionine (Stipanuk, 2004). Moreover, my results surprisingly indicate that intracellular cystine through reduction to cysteine, not only acts as an antioxidant by providing a component of the major cellular antioxidant glutathione, but also as an alternative antioxidant that can to some degree compensate for transient reductions in the glutathione pool. Thus, inhibition of glutathione synthesis following BSO treatment induced a similar reduction in glutathione levels as cystine depletion, but failed to induce cell death or accumulation of ROS or lipid peroxidation unless cysteine was co-depleted (Figure 3.8).

6.2 Ferroptosis is the modality of cell death in HME cells following deprivation of cystine.

How do EGFR-mutant HME cells die once ROS is generated to high levels during cystine depletion? Microscopically these cells appeared ruptured and burst, which suggested membrane damage was the main cause of death. By a variety of criteria the mechanism of the cell death that occurs in HME-EGFR cells, and to a lesser extent the other HME cell lines used in this thesis is indistinguishable from ferroptosis a form of cell death associated with lipid damage by ROS.

Previously it had been shown that ferroptosis was associated with the accumulation of lipid peroxides within cell membranes, and such ROS could be inhibited by chelation of iron using DFO (Yang and Stockwell, 2008). Ferroptosis has also been found to be inhibited by a lipophilic antioxidant, Fer1, a small lipophilic antioxidant that appears to specifically inhibit ferroptosis (Dixon 2012). Similarly, my data shows that both DFO and Fer1 also inhibit cystine-deprivation induced cell death in HME-EGFR cells (Figures 3.9 and 3.10).

The term “Ferroptosis” was first used to describe a non-apoptotic form of cell death resembling necrosis in a study where RAS-lethal small molecules were screened against cell lines with an activating RAS mutation (Yagoda et al., 2007). One such ferroptosis-inducing small molecule, erastin, was initially thought to target mitochondrial VDAC2/3 proteins (Yagoda et al., 2007), but was eventually shown to inhibit the X_C^- system and thereby prevent uptake of cystine (Dixon 2012). In the HME cell system treatment with erastin generated responses that were similar to cystine deprivation. Thus, ferroptosis was observed to occur in cultures of HME-EGFR treated with this compound and not in wild type HME cells (Figure 3.11).

A recent report has similarly demonstrated a requirement for cystine, but described necroptosis as the modality of cell death in cultures of renal cell carcinoma cells in response to cystine deprivation. However, in that setting the effect was dependent on loss of von Hippel-Lindau gene expression/function which enhanced TNFα signalling and induced RIPK1-mediated formation of the necrosome (Tang et al., 2016).

In the HME cell system I used cystine was found to be more important in preventing ferroptosis than simply providing substrates for glutathione synthesis. Reduction in glutathione levels following treatment with BSO was found to occur to the same extent to that elicited by cystine depletion, but failed to induce ferroptosis. Another report has found different results and demonstrated that BSO treatment, and subsequent inhibition of glutathione synthesis, can in some cells be sufficient to induce ferroptosis (Yang et al., 2014). However, my work confirms a previous study showing that cysteine can also function as an alternative antioxidant during glutathione deficiency (Mandal et al., 2010a). Such a role for cysteine requires the presence of both thioredoxin, which reduces intracellular cystine to cysteine, and upregulated expression and function of the X_c^- cystine transporter to facilitate increased cystine uptake. In my experiments individual treatments of HME-EGFR cells with BSO, to reduce total levels of GSH (Figure 3.8), or with auranofin, an inhibitor of thioredoxin reductase to limit the recycling of thioredoxin (Arner and Holmgren, 2000) induced neither cell death nor accumulation of lipid peroxides. However, the combination of both treatments in HME-EGFR induced both lipid peroxidation and ferroptosis (Figure 3.12). Moreover, prior glutathione depletion in HME-EGFR cells by BSO treatment sensitised these cells to cystine limitation

elicited by inhibition of X_c^- transporter using erastin or S4PG to more rapidly induce ferroptosis (Figure 3.13). Together, these results highlight the importance of cystine/cysteine as an alternative antioxidant to glutathione in HME-EGFR cells.

Insight from a previous study has suggested a role for transferrin and glutamine in the induction of ferroptosis within nutrient-starved mouse embryonic stem cells (Gao et al., 2015). This study demonstrated that the process of glutaminolysis, a process that generates glutamate from glutamine to be used in downstream metabolic pathways, is key for ferroptosis to occur in these cells, and that its inhibition was sufficient to restrict ferroptosis in an *ex vivo* model of ischemic heart injury (Gao et al., 2015). However, measurements of Gln and Glu steady state levels before and after cystine deprivation did not demonstrate any discernible alteration suggesting that glutaminolysis was not required for ferroptosis in the context of HME cells.

6.3 EGFR mediated activation of MAPK pathway is responsible for conferring sensitivity to cystine-deprivation induced ferroptosis through downregulation of GPX4 expression

Chapter 4 of this thesis is concerned with the elucidation of the mechanistic underpinnings of EGFR signalling that confer sensitivity of HME-EGFR cells to ferroptosis. I found that sustained inhibition of EGFR or MAPK was sufficient to block generation of ROS and thereby block ferroptosis. One underlying mechanism for this phenomenon is the role of MAPK signalling in downregulating GPX4 expression, an enzyme which specifically detoxifies lipid peroxides (Brigelius-Flohe and Maiorino, 2013; Yang et al., 2014).

The potential therapeutic benefit that cystine restriction might confer in a cancer treatment setting was examined using the NSCLC cell line H1650. In a xenograft mouse model systemic depletion of cystine, using an enzyme that specifically degrades cystine, reduced tumour cell growth (Section.4.4), suggesting that induction of ferroptosis through enzymatic depletion of cystine could be exploited therapeutically to target tumours with elevated MAPK signalling.

The mutation present within the *EGFR* gene engineered by gene editing in HME-EGFR cells was a deletion of exon 19 which leads to the generation of a protein which is ligand independent for activation of the EGFR signalling pathway (Greulich et al., 2005; Raymond et al., 2000). HME-EGFR cells were found to exhibit high levels of pAKT and ppERK (Figure 4.2), and treatment of these cells with gefitinib (EGFR inhibitor) or selumetinib (a MEK inhibitor) lowered ppERK levels, demonstrating the role of active EGFR in stimulating MAPK pathway activation. Interestingly, pAKT levels could only be lowered by treating HME-EGFR cells with wortmannin not gefitinib, indicating that PI3K activation of AKT was independent of EGFR in these cells (Figure 4.2). Importantly, activation of the MAPK pathway was responsible for the over-accumulation of ROS and lipid peroxidation I had previously observed in HME-EGFR cells following cysteine deprivation (Figures 4.4-4.8). Thus, MAPK pathway activation by active EGFR can be correlated with cell sensitivity to ferroptosis during conditions of cystine deprivation, and observation that agrees with previous work (Yagoda et al., 2007).

My observation that the rate of glutathione oxidation in HME-EGFR cells was enhanced following inhibition of EGFR signalling (Figure 4.9) indicated possible alterations in the activity of antioxidant enzymes, or generators of ROS, in HME-

EGFR cells that could account for ROS over-accumulation during cystine depletion. This difference could in part be attributed to reduced expression of the lipid ROS detoxification enzyme GPX4 in HME-ERGR cells, which, following inhibition of MAPK was found to be restored to levels found in wild type HME cells (Figure 4.10). Indeed, knock-down of GPX4 utilising an siRNA approach sensitised both wild-type HME and gefitinib-treated HME-EGFR cells to ferroptosis following cystine deprivation (Figure 4.11-4.13), whereas ectopic GPX4 overexpression in HME EGFR cells exerted a protective effect towards ferroptosis (Figure 4.14). Taken together, these results demonstrate a clear role for GPX4 in regulating ferroptosis in HME cells. This finding agrees with previous research highlighting the importance of GPX4 in ferroptosis (Friedmann Angeli et al., 2014; Yang et al., 2014). In particular, inhibition of GPX4 can induce ferroptosis independently of cystine sufficiency (Yang et al., 2014). Moreover, in some cells it is known that MAPK activation affects GPX4 expression. Thus, treatment of melanoma cells expressing mutant BRAF (V600E) with the BRAF inhibitor vemurafenib, which inhibits MAPK activation, had been found previously to increase GPX4 mRNA abundance (Parmenter et al., 2014). Thus, the findings of this thesis, combined with those of others, support a conclusion that MAPK pathway activation in HME-EGFR cells suppresses expression of GPX4 and thereby increases the accumulation of lipid ROS following cystine deprivation, leading ultimately to the loss of membrane integrity characteristic of cell death by ferroptosis.

6.4 Enzymatic induction of ferroptosis in lung cancer cell line models as a therapeutic approach.

The pro-ferroptotic effect of cystine deprivation on HME-EGFR cells was replicated in other NSCLC tumour cell lines. Of nine lines tested, three (Calu-6, H1650, H3255) were found to demonstrate marked sensitivity to ferroptosis when deprived of cystine. Two of these cell lines had activating mutations on EGFR (H1650, H3255) and one was mutant KRAS-driven (Calu-6). In contrast to my findings in HME cells, the levels of GPX4 expression within Calu-6, H1650, H3255 cells did not appear to predict sensitivity in these cells, indicating that despite the demonstrated role of this enzyme in protecting HME cells, it cannot generally be used a marker of sensitivity to ferroptosis (Figure 4.15). Nevertheless, inhibition of the MAPK pathway also protected against cystine-induced ferroptosis in NSCLC lines, further highlighting the general role of this pathway in determining sensitivity to ferroptosis (Figure 4.15) and implying the existence of alternative mediators of sensitivity downstream of MAPK.

Limitation of an individual amino acid or protein in general is possible through implementation of a isocaloric diet that provides all the required nutrients except those of interest (Horvath et al., 1996; Kalhan and Marczewski, 2012; Wu et al., 1999). While such an approach is feasible in mice, its application to human subjects would likely be problematic. An alternative approach to generate cystine depletion, or depletion of other amino acids in man is the use of genetically-modified enzymes that specifically degrade the amino acid nutrient of interest systemically. Such approaches have been used for the restriction of several amino acids such as arginine, glutamine and asparagine (Fernandes et al., 2017). Tumour-specific

targeting of such enzymes if it could be achieved, could conceivably also allow the effects of cystine depletion to be restricted to the tumour microenvironment, preventing potentially deleterious side-effects of systemic cystine depletion on normal tissues.

With respect to cystine, an enzyme that specifically degrades cystine and cysteine (AECase) was described and demonstrated to lower the systematic levels of cystine and cysteine in animals following intraperitoneal administration during the work presented in this thesis (Cramer et al., 2017). To test this approach, I first performed proof-of-principle experiments and showed that HME-EGFR cultures grown in complete media underwent ferroptosis following addition of AECase (Figure 4.20). In a similar manner the NSCLC cell line H1650 was found to be equally as sensitive to AECase treatment as cystine depletion (Figure 4.21). Importantly, the effects of AECase on HME-EGFR and H1650 cells were also reversible by Fer1 supplementation (Figure 4.21 and 4.22), indicating that the AECase-mediated cell death in these cultures was via ferroptosis. A model where immunocompromised mice were engrafted with H1650 cells was then used to test whether cystine restriction had therapeutic utility. Intermittent treatment of these mice in a xenograft therapeutic regime with AECase markedly decreased subsequent tumour growth and increased overall survival of tumour-bearing mice (Figure 4.23). In line with my observations of HME-EGFR and H1650 cells made *in vitro*, ferroptosis appeared to be occurring within the tumour xenografts as COX2 - which has been described as a marker of ferroptosis in vivo (Yang et al., 2014) was found to be upregulated following AECase treatment (Figure 4.24). Taken together, these observations indicate that implementation of cystine restriction in patients with NSCLC tumours

with activating EGFR mutations could potentially be therapeutically beneficial through induction of ferroptosis.

6.5 Wave-like propagation of ferroptotic cell death in wild type HME cells.

Chapter 5 of this thesis focused on the study of ferroptosis propagation in cultures of wild type HME cells. Ferroptosis in these cells initiated in foci and contained cells with a characteristic balloon-like morphology that stained positive with Sytox Green, a marker of loss of membrane integrity. By video time-lapse microscopy ferroptosis could be observed to spread from Sytox Green-positive to nearby Sytox Green-negative cells in an apparent wave-like manner.

My results show that cell-cell contact has a significant effect in conferring resistance to ferroptosis in wild type HME cells. In wild type HME cells I observed more mature AJ and a higher level of GJIC than in HME-EGFR cells. Both of these weakened junctional effects in HME-EGFR cells could be reversed by MAPK inhibition (Section 5.3). I also found that the generation of extracellular hydrogen peroxide, possibly through NOX4 activity, was important for mediating synchronous cell death in cultures of cystine-deprived HME-EGFR cells because addition of catalase or the NOX4 inhibitor GKT136901 (Laleu et al., 2010) prevented ferroptosis. However, extracellular hydrogen peroxide was not responsible for the wave of ferroptosis in cultures of cystine-deprived wild type HME cells as addition of catalase did not prevent propagation of ferroptosis (Section 5.5).

Despite being more resistant to ferroptosis than HME-EGFR cells, wild type HME cells demonstrated low levels of ferroptotic cell death when deprived of cystine (Figure 5.1). Dead cells in such cultures had a characteristic balloon-like morphology with loss of plasma membrane integrity, and these cells appeared to initiate

ferroptosis randomly and then expand in size over time (Figure 5.1). Once these foci formed, I found that the adjacent healthy cells very quickly lost cell and substratum adhesion prior to loss of membrane integrity, generating a domino-like spread of cell death (Figures 5.2 and 5.3). It seems possible that this wave phenomenon could be representative of the type of death observed when some normal epithelia experience extreme oxidative stress, as is the case during ischemic injury (Conrad et al., 2016).

Inhibition of ferroptosis spread was also achieved by the use of a NOX4 inhibitor, GKT136901. This inhibitor, along with extracellular catalase, were both found to be effective in protecting HME-EGFR cells from ferroptosis when added immediately with deprivation of cystine (Figure 5.7). This observation indicates the involvement of hydrogen peroxide in the process of ferroptosis. However, when assayed for their ability to inhibit the spread of cell death in wild-type HME cells, the NOX4 inhibitor GKT136901 prevented cell-cell spread of ferroptosis whereas catalase addition failed to (Figure 5.9). This difference may be attributed to the ability of catalase to neutralise extracellular hydrogen peroxide but not affect the intracellular formation of lipid peroxides. Hydrogen peroxide is known to have an important role in the Fenton reaction involving iron and the production of more damaging ROS species and therefore its accumulation could contribute to the accumulation of lipid peroxides typical of ferroptosis (Winterbourn, 1995). The ability of the NOX4 inhibitor to equally block initiation of ferroptosis and cell death spread indicates that the generation of hydrogen peroxide is also important for ferroptosis propagation. However, a recent report has indicated that this NOX4 inhibitor could potentially act as a scavenger of peroxynitrite, a radical that is formed by superoxide and nitric oxide (Schildknecht et al., 2014). Therefore, further studies are required to

determine if the observed protective effect of NOX4 inhibition is completely attributable to its ability to inhibit NOX4. Moreover, recent insights into the mechanisms of ferroptosis indicate the involvement of additional oxidising enzymes other than NOX4. Such an example is lipoxygenase (LOX) whose function is responsible for direct oxidation of phospholipids, and recent reports demonstrate that LOX-driven lipid oxidation can also contribute to induction of ferroptosis (Kagan et al., 2017; Yuan et al., 2016)

In my experiments cell-cell contact was also found to modulate induction of ferroptosis because confluent wild type HME and HME-BRAF cells maintained higher viability when deprived of cystine than did culture at lower density (Figure 3.2). My results suggest that this modulation may be due to the formation of strong AJ and GJIC between wild type HME cells as they reach confluence. Such connection did not occur between HME-EGFR cells regardless of the state of confluence unless the cells were treated with EGFR or MAPK inhibitors (Figure 5.4). GJIC was particularly important because inhibition of these channels in cultures of cystine-deprived wild type HME cells induced ferroptosis that was similar in extent and rapidity as was observed in similar cultures of HME-EGFR cells (Figure 5.5). Higher levels of GJIC could be restored in HME-EGFR cells following treatment with EGFR and MAPK inhibitors (Figure 5.6), suggesting that cell-cell adhesion and GJIC are impaired by oncogenic EGFR signalling. That AJ and GJ are important in my cell system is supported by evidence found in ischemic models where AJs are disrupted and the corresponding GJ are found mislocalised (Matsushita et al., 1999). The observation that ferroptosis is accelerated rather than inhibited by inhibition of GJIC presumably suggests that cell-cell spread of ferroptosis is not mediated by the so-

called “bystander effect”, a phenomenon describing toxic effects on cell viability of neighbouring cells, mediated partly through the function of GJs(Nagasawa and Little, 1992). However, a protective effect of GJIC had been previously identified in a glutamate-induced cell death that resembled ferroptosis in neuronal cells during ischemia (Nakase et al., 2003; Naus et al., 2001). These findings, along with my results, indicate the importance of GJIC not only as an additional line of defence against oxidative stress. Moreover, previous research highlights the regulation of GJIC by activation of EGFR and downstream MAPK signals in agreement with the changes we observed in our studies (Kanemitsu and Lau, 1993). Further research is need however to clarify how GJIC protects against ferroptosis in this system. This could be attributed for example to either an increased ability to share nutrients (Alexander and Goldberg, 2003), such as cystine or glutathione within the monolayer, thereby protecting individual cells from experiencing excessive ROS or in providing a buffering capacity against over-accumulation of ROS species such as hydrogen peroxide (Decrock et al., 2009; Kirchhoff et al., 2001).

I further observed that the propagation of ferroptotic cell death was inhibited by antioxidants, including Fer1 (Figure 5.8). Ferroptosis inhibitors Ferrostatin1 (Fer1) and Liproxstatin1 (Lip1) were discovered with the help of high-throughput screening (Dixon et al., 2012; Friedmann Angeli et al., 2014). Both compounds can act as radical trapping antioxidants and neutralise lipid peroxides within biological membranes (Skouta et al., 2014). Outside lipid membranes the ability of these compounds to counteract peroxyl radicals is not as potent as that of α-tocopherol. However, when these molecules operate within lipid membranes, their potency is higher due to the lipophilic nature of these compounds (Zilka et al., 2017). Lipid

peroxidation is thought to occur via a chain reaction, termed autoxidation, where lipid peroxides can interact with other lipids to generate further lipid radicals in the presence of molecular oxygen. Fer1 and Lip1 inhibit the autoxidation chain reaction as they neutralise the lipid radicals and inhibit further oxidative damage (Zilka et al., 2017). Such a phenomenon could potentially explain the ferroptosis wave spread, as lipid peroxidation is a continuous reaction that can be further propagated (Yin et al., 2011). Administration of these antioxidant molecules in *in vivo* models of renal and hepatic IRI has demonstrated protective effects from ferroptosis, indicating a future clinical potential (Friedmann Angeli et al., 2014; Linkermann et al., 2014).

The importance of GPX4 function as a critical regulator of ferroptosis indicates that excessive lipid peroxidation has a likely causative role in induction of ferroptosis (Yang et al., 2014). Increased levels of lipid peroxides in biological membranes induce loss of membrane bilayer stability and loss of water impermeability (Lis et al., 2011; Wong-Ekkabut et al., 2007). Such an effect could additionally explain the characteristic balloon phenotype of ferroptotic cells. It was therefore important to investigate if lipid peroxidation and its downstream by-products played a role in propagating cell death and affecting the viability of nearby cells. Accumulation of lipid peroxides is accompanied by the formation of other reactive electrophiles such as malondialdehyde (MDA) and 4HNE, which can create protein and DNA adducts and induce cell death (Awasthi et al., 2017; Del Rio et al., 2005). Addition of either recombinant GPX4 or recombinant GST4-4 both effectively inhibited death propagation, indicating that neutralisation of either lipid peroxides or 4HNE inhibits cell death propagation (Figure 5.10). Further indication of lipid peroxidation associated damage was supported from the accumulation of LAA staining in cells

adjacent to the wave front where lipid peroxidation by-product adducts were formed (Figure 5.11). Previous research on 4HNE has indicated a role in disruption of formed junctions as well as junctional communication (Radu and Moldovan, 1991; Usatyuk et al., 2006). Such evidence indicates a possible role for 4HNE as an important mediator in ischemic death spread where cell junctions are disrupted prior to ferroptotic cell death by accumulation of lipid peroxidation. If indeed 4HNE was released locally from cells that had undergone ferroptosis and inhibited GJIC in adjacent cells, one could envisage a scenario whereby those cells with impaired GJIC then fail to adequately buffer ROS species with neighbouring cells, thereby accelerating their accumulation of ROS damage and demise by ferroptosis.

As mentioned previously, ferroptosis is an oxidative type of cell death where generation and accumulation of ROS, particularly lipid peroxides, catalyse cell necrosis in an iron-dependent manner (Dixon et al., 2012). Lipid peroxidation has been previously implicated in a variety of human diseases, including neurological conditions, possibly due to the lipid content of neurons and high oxygen consumption (Gaschler and Stockwell, 2017). It is therefore possible that inhibition of ferroptosis might have a clinical potential and alleviate some neuronal diseases. In the context of acute kidney injury renal tubules appear also to die in a synchronous manner, with necrotic cell death spread within the kidney tubule (Linkermann et al., 2014). Similarly in an animal model of myocardial ischemia-reperfusion injury an analogous spreading wave front phenomenon of cell death has been observed that correlates with ischemia duration and increase in size of adjacent necrotic areas (Reimer et al., 1977). Therefore, the work I present in this Chapter may be important in designing novel ways of inhibiting myocardial cell death during ischemia-reperfusion injury.

What then might be released from cells that have undergone ferroptosis and lost membrane integrity that might mediate cell-cell spread of ferroptosis? My results suggest that both lipid peroxides and their by-products, such a 4HNE, generated within cystine-deprived wild type HME cells play a significant role in propagating death stimuli between cells.

6.6 Proposed model for ferroptosis progression

The first requirement to model the progression of ferroptosis in tissues is the generation of increased ROS. In our system this was generated by cystine depletion. In wild type HME cells it appears that with time some cells may generate sufficient ROS during cystine deprivation to induce ferroptosis sporadically. However in other situations this could be due to alterations in activity of enzymes that generate ROS such as NOX or LOX (Dixon et al., 2012; Kagan et al., 2017; Linkermann et al., 2014), depletion of glutathione as occurs during acetaminophen poisoning (Lorincz et al., 2015) or the high ROS accumulation that occurs following ischemia reperfusion (Conrad et al., 2016). Over-accumulation of ROS could then induce lipid peroxidation. Accumulation of lipid peroxidation may then be amplified through the autoxidation of lipids (Skouta et al., 2014; Zilka et al., 2017) until a critical threshold of lipid damage is reached and the permeability of the cell is compromised (Lis et al., 2011; Wong-Ekkabut et al., 2007) leading to ferroptosis. In a tissue such a process may then lead to a local increase in the levels of lipid peroxides or peroxidation by-products such as 4HNE. 4HNE may then promote propagation of ferroptosis through effects on junctional formation and communication (Radu and Moldovan, 1991; Usatyuk et al., 2006), which may accelerate ferroptosis in adjacent cells Such a cascade would then further propagate in a positive-feedback manner, inducing the wave expansion of cell death by ferroptosis I have characterised here (Figure 6.1).

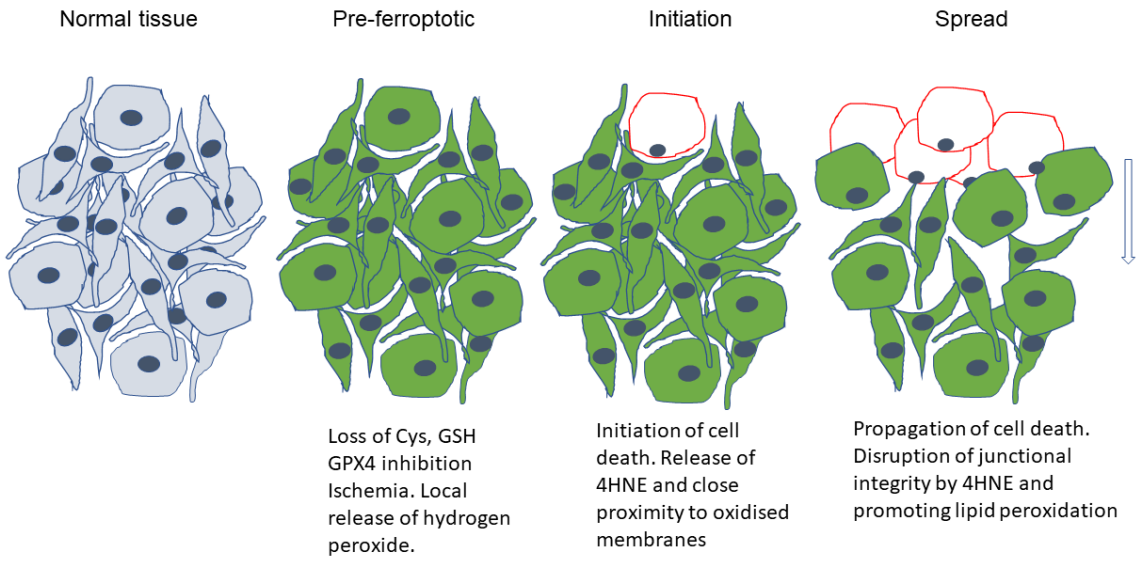

Figure 6.1 Model of ferroptosis progression.

Loss of antioxidant capacity induces a state of high oxidative stress. Ferroptosis initiation releases 4HNE and a local increase in the content of lipid peroxidation. Neighbouring cells are affected by 4HNE through disruption of adhesion and interruption of GJIC while the increase in lipid peroxidation promotes further oxidative stress. As a result, their threshold is surpassed, and adjacent cells die by ferroptosis affecting their own neighbours and promoting further cell death.

6.7 Future work and perspectives

The insights that my studies have provided as to the mechanisms controlling sensitivity to ferroptosis could be useful in understanding further the mechanisms and mediators of ferroptosis. Such knowledge could ultimately allow control over this process, whether that is inhibitory to prevent damage to normal tissues or stimulatory to kill tumour cells via systemic depletion of cystine. Moreover, overall knowledge over the field of ferroptosis has expanded significantly since its initial characterisation. Induction of this process is multifactorial and the mechanisms that mediate sensitivity are incompletely understood. The specific cellular and disease contexts in which ferroptosis operates *in vivo* constitute an emerging and expanding field. Understanding how ferroptosis is propagated from cell to cell, and whether this propagation also occurs *in vivo*, remain future avenues for further research.

8. REFERENCES

Aebi, H. (1984). CATALASE INVITRO. Methods Enzymol *105*, 121-126.

Akerboom, T.P.M., Bilzer, M., and Sies, H. (1982). THE RELATIONSHIP OF BILIARY GLUTATHIONE DISULFIDE EFFLUX AND INTRACELLULAR GLUTATHIONE DISULFIDE CONTENT IN PERFUSED-RAT-LIVER. Journal of Biological Chemistry *257*, 4248-4252.

Albaugh, V.L., Pinzon-Guzman, C., and Barbul, A. (2017). Arginine-Dual Roles as an Onconutrient and Immunonutrient. J Surg Oncol *115*, 273-280.

Alessi, D.R., James, S.R., Downes, C.P., Holmes, A.B., Gaffney, P.R.J., Reese, C.B., and Cohen, P. (1997). Characterization of a 3-phosphoinositide-dependent protein kinase which phosphorylates and activates protein kinase B alpha. Current Biology *7*, 261-269.

Alexander, D.B., and Goldberg, G.S. (2003). Transfer of biologically important molecules between cells through gap junction channels. Curr Med Chem *10*, 2045-2058.

Andrabi, S.A., Dawson, T.M., and Dawson, V.L. (2008). Mitochondrial and Nuclear Cross Talk in Cell Death Parthanatos. Mitochondria and Oxidative Stress in Neurodegenerative Disorders *1147*, 233-241.

Apte, M.V., and Wilson, J.S. (2012). Dangerous liaisons: Pancreatic stellate cells and pancreatic cancer cells. J Gastroenterol Hepatol *27*, 69-74.

Arcaro, A., and Wymann, M.P. (1993). WORTMANNIN IS A POTENT PHOSPHATIDYLINOSITOL 3-KINASE INHIBITOR - THE ROLE OF PHOSPHATIDYLINOSITOL 3,4,5-TRISPHOSPHATE IN NEUTROPHIL RESPONSES. Biochemical Journal *296*, 297-301.

Arner, E.S.J., and Holmgren, A. (2000). Physiological functions of thioredoxin and thioredoxin reductase. Eur J Biochem *267*, 6102-6109.

Ashe, H., Clark, B.R., Chu, F., Hardy, D.N., Halpern, B.C., Halpern, R.M., and Smith, R.A. (1974). N5-METHYLTETRAHYDROFOLATE - HOMOCYSTEINE METHYLTRANSFERASE ACTIVITY IN EXTRACTS FROM NORMAL, MALIGNANT AND EMBRYONIC TISSUE-CULTURE CELLS. Biochemical and Biophysical Research Communications *57*, 417-425.

Averous, J., Lambert-Langlais, S., Mesclon, F., Carraro, V., Parry, L., Jousse, C., Bruhat, A., Maurin, A.C., Pierre, P., Proud, C.G.*, et al.* (2016). GCN2 contributes to mTORC1 inhibition by leucine deprivation through an ATF4 independent mechanism. Sci Rep *6*, 10.

Awasthi, Y.C., Ramana, K.V., Chaudhary, P., Srivastava, S.K., and Awasthi, S. (2017). Regulatory roles of glutathione-S-transferases and 4-hydroxynonenal in stress-mediated signaling and toxicity. Free Radic Biol Med *111*, 235-243.

Awasthi, Y.C., Yang, Y.S., Tiwari, N.K., Patrick, B., Sharma, A., Li, J., and Awasthi, S. (2004). Regulation of 4-hydroxynonenal-mediated signaling by glutathione S-transferases. Free Radic Biol Med *37*, 607-619.

Bader, A.G., Kang, S.Y., and Vogt, P.K. (2006). Cancer-specific mutations in PIK3CA are oncogenic in vivo. Proceedings of the National Academy of Sciences of the United States of America *103*, 1475-1479.

Bae, Y.S., Kang, S.W., Seo, M.S., Baines, I.C., Tekle, E., Chock, P.B., and Rhee, S.G. (1997). Epidermal growth factor (EGF)-induced generation of hydrogen peroxide - Role in EGF receptor-mediated tyrosine phosphorylation. Journal of Biological Chemistry *272*, 217-221.

Baird, T.D., and Wek, R.C. (2012). Eukaryotic Initiation Factor 2 Phosphorylation and Translational Control in Metabolism. Adv Nutr *3*, 307-321.

Bannai, S. (1984). TRANSPORT OF CYSTINE AND CYSTEINE IN MAMMALIAN-CELLS. Biochimica Et Biophysica Acta *779*, 289-306.

Bannai, S., and Kitamura, E. (1980). TRANSPORT INTERACTION OF L-CYSTINE AND L-GLUTAMATE IN HUMAN-DIPLOID FIBROBLASTS IN CULTURE. Journal of Biological Chemistry *255*, 2372-2376.

Bar-Peled, L., Chantranupong, L., Cherniack, A.D., Chen, W.W., Ottina, K.A., Grabiner, B.C., Spear, E.D., Carter, S.L., Meyerson, M., and Sabatini, D.M. (2013). A Tumor Suppressor Complex with GAP Activity for the Rag GTPases That Signal Amino Acid Sufficiency to mTORC1. Science *340*, 1100-1106.
Bar-Peled, L., Schweitzer, L.D., Zoncu, R., and Sabatini, D.M. (2012). Ragulator Is a GEF for the Rag GTPases that Signal Amino Acid Levels tomTORC1. Cell *150*, 1196-1208.
Barbacid, M. (1987). RAS GENES. Annual Review of Biochemistry *56*, 779-827.
Barbie, D.A., Tamayo, P., Boehm, J.S., Kim, S.Y., Moody, S.E., Dunn, I.F., Schinzel, A.C., Sandy, P., Meylan, E., Scholl, C*., et al.* (2009). Systematic RNA interference reveals that oncogenic KRAS-driven cancers require TBK1. Nature *462*, 108-U122.
Baselga, J., and Averbuch, S.D. (2000). ZD1839 ('Iressa')(1,2) as an anticancer agent. Drugs *60*, 33-40.
Bergstrom, J., Furst, P., Noree, L.O., and Vinnars, E. (1974). INTRACELLULAR FREE AMINO-ACID CONCENTRATION IN HUMAN MUSCLE-TISSUE. Journal of Applied Physiology *36*, 693-697.
Bode, B.P., Kaminski, D.L., Souba, W.W., and Li, A.P. (1995). GLUTAMINE TRANSPORT IN ISOLATED HUMAN HEPATOCYTES AND TRANSFORMED LIVER-CELLS. Hepatology *21*, 511-520.
Bos, J.L. (1989). RAS ONCOGENES IN HUMAN CANCER - A REVIEW. Cancer Research *49*, 4682-4689.
Bourne, H.R., Sanders, D.A., and McCormick, F. (1991). THE GTPASE SUPERFAMILY - CONSERVED STRUCTURE AND MOLECULAR MECHANISM. Nature *349*, 117-127.
Bowles, T.L., Kim, R., Galante, J., Parsons, C.M., Virudachalam, S., Kung, H.J., and Bold, R.J. (2008). Pancreatic cancer cell lines deficient in argininosuccinate synthetase are sensitive to arginine deprivation by arginine deiminase. International Journal of Cancer *123*, 1950-1955.
Bradford, M.M. (1976). RAPID AND SENSITIVE METHOD FOR QUANTITATION OF MICROGRAM QUANTITIES OF PROTEIN UTILIZING PRINCIPLE OF PROTEIN-DYE BINDING. Analytical Biochemistry *72*, 248-254.
Brigelius-Flohe, R. (2009). Vitamin E: The shrew waiting to be tamed. Free Radic Biol Med *46*, 543-554.
Brigelius-Flohe, R., and Maiorino, M. (2013). Glutathione peroxidases. Biochim Biophys Acta-Gen Subj *1830*, 3289-3303.
Brognard, J., Clark, A.S., Ni, Y.C., and Dennis, P.A. (2001). Akt/protein kinase B is constitutively active in non-small cell lung cancer cells and promotes cellular survival and resistance to chemotherapy and radiation. Cancer Research *61*, 3986-3997.
Bronte, V., and Zanovello, P. (2005). Regulation of immune responses by L- arginine metabolism. Nat Rev Immunol *5*, 641-654.
Broome, J.D. (1968). STUDIES ON MECHANISM OF TUMOR INHIBITION BY L-ASPARAGINASE - EFFECTS OF ENZYME ON ASPARAGINE LEVELS IN BLOOD NORMAL TISSUES AND 6C3HED LYMPHOMAS OF MICE - DIFFERENCES IN ASPARAGINE FORMATION AND UTILIZATION IN ASPARAGINASE-SENSITIVE AND -RESISTANT LYMPHOMA CELLS. Journal of Experimental Medicine *127*, 1055-&.
Broschat, K.O., Gorka, C., Page, J.D., Martin-Berger, C.L., Davies, M.S., Huang, H.C., Gulve, E.A., Salsgiver, W.J., and Kasten, T.P. (2002). Kinetic characterization of human glutamine-fructose-6-phosphate amidotransferase I - Potent feedback inhibition by glucosamine 6-phosphate. Journal of Biological Chemistry *277*, 14764-14770.
Bryant, H.E., Schultz, N., Thomas, H.D., Parker, K.M., Flower, D., Lopez, E., Kyle, S., Meuth, M., Curtin, N.J., and Helleday, T. (2005). Specific killing of BRCA2-deficient tumours with inhibitors of poly(ADP-ribose) polymerase. Nature *434*, 913-917.
Buday, L., and Downward, J. (1993). EPIDERMAL GROWTH-FACTOR REGULATES P21(RAS) THROUGH THE FORMATION OF A COMPLEX OF RECEPTOR, GRB2 ADAPTER PROTEIN, AND SOS NUCLEOTIDE EXCHANGE FACTOR. Cell *73*, 611-620.
Bush, K.T., Tsukamoto, T., and Nigam, S.K. (2000). Selective degradation of E-cadherin and dissolution of E-cadherin-catenin complexes in epithelial ischemia. Am J Physiol-Renal Physiol *278*, F847-F852.

Cai, Z.Y., Jitkaew, S., Zhao, J., Chiang, H.C., Choksi, S., Liu, J., Ward, Y., Wu, L.G., and Liu, Z.G. (2014). Plasma membrane translocation of trimerized MLKL protein is required for TNF-induced necroptosis. Nature Cell Biology *16*, 55-+.
Cain, K., Brown, D.G., Langlais, C., and Cohen, G.M. (1999). Caspase activation involves the formation of the aposome, a large (similar to 700 kDa) caspase-activating complex. Journal of Biological Chemistry *274*, 22686-22692.
Cain, K., InayatHussain, S.H., Couet, C., and Cohen, G.M. (1996). A cleavage-site-directed inhibitor of interleukin 1 beta-converting enzyme-like proteases inhibits apoptosis in primary cultures of rat hepatocytes. Biochemical Journal *314*, 27-32.
Cantley, L.C. (2002). The phosphoinositide 3-kinase pathway. Science *296*, 1655-1657.
Cao, Y., Feng, Y.H., Zhang, Y.J., Zhu, X.T., and Jin, F. (2016). L-Arginine supplementation inhibits the growth of breast cancer by enhancing innate and adaptive immune responses mediated by suppression of MDSCs in vivo. BMC Cancer *16*, 11.
Carpenter, C.L., Auger, K.R., Chanudhuri, M., Yoakim, M., Schaffhausen, B., Shoelson, S., and Cantley, L.C. (1993). PHOSPHOINOSITIDE 3-KINASE IS ACTIVATED BY PHOSPHOPEPTIDES THAT BIND TO THE SH2 DOMAINS OF THE 85-KDA SUBUNIT. Journal of Biological Chemistry *268*, 9478-9483.
Carroll, B., Korolchuk, V.I., and Sarkar, S. (2015). Amino acids and autophagy: cross-talk and co-operation to control cellular homeostasis. Amino Acids *47*, 2065-2088.
Cavuoto, P., and Fenech, M.F. (2012). A review of methionine dependency and the role of methionine restriction in cancer growth control and life-span extension. Cancer Treatment Reviews *38*, 726-736.
Cecconi, F., Alvarez-Bolado, G., Meyer, B.I., Roth, K.A., and Gruss, P. (1998). Apaf1 (CED-4 homolog) regulates programmed cell death in mammalian development. Cell *94*, 727-737.
Cellarier, E., Durando, X., Vasson, M.P., Farges, M.C., Demiden, A., Maurizis, J.C., Madelmont, J.C., and Chollet, P. (2003). Methionine dependency and cancer treatment. Cancer Treatment Reviews *29*, 489-499.
Chabner, B.A., and Roberts, T.G. (2005). Timeline - Chemotherapy and the war on cancer. Nat Rev Cancer *5*, 65-72.
Chakrabarti, G., Moore, Z.R., Luo, X., Ilcheva, M., Ali, A., Padanad, M., Zhou, Y., Xie, Y., Burma, S., Scaglioni, P.P*., et al.* (2015). Targeting glutamine metabolism sensitizes pancreatic cancer to PARP-driven metabolic catastrophe induced by SS-lapachone. Cancer & metabolism *3*, 12-12.
Chaneton, B., Hillmann, P., Zheng, L., Martin, A.C.L., Maddocks, O.D.K., Chokkathukalam, A., Coyle, J.E., Jankevics, A., Holding, F.P., Vousden, K.H*., et al.* (2012). Serine is a natural ligand and allosteric activator of pyruvate kinase M2. Nature *491*, 458-+.
Chapman, P.B., Hauschild, A., Robert, C., Haanen, J.B., Ascierto, P., Larkin, J., Dummer, R., Garbe, C., Testori, A., Maio, M*., et al.* (2011). Improved Survival with Vemurafenib in Melanoma with BRAF V600E Mutation. New England Journal of Medicine *364*, 2507-2516.
Chen, L., Cui, H.M., Fang, J., Deng, H.D., Kuang, P., Guo, H.R., Wang, X., and Zhao, L. (2016). Glutamine deprivation plus BPTES alters etoposide- and cisplatin-induced apoptosis in triple negative breast cancer cells. Oncotarget *7*, 54691-54701.
Chen, L.J., Hambright, W.S., Na, R., and Ran, Q.T. (2015). Ablation of the Ferroptosis Inhibitor Glutathione Peroxidase 4 in Neurons Results in Rapid Motor Neuron Degeneration and Paralysis. Journal of Biological Chemistry *290*, 28097-28106.
Chen, X., Li, W.J., Ren, J.M., Huang, D.L., He, W.T., Song, Y.L., Yang, C., Li, W.Y., Zheng, X.R., Chen, P.D*., et al.* (2014). Translocation of mixed lineage kinase domain-like protein to plasma membrane leads to necrotic cell death. Cell Research *24*, 105-121.
Cheng, J.Z., Yang, Y.S., Singh, S.P., Singhal, S.S., Awasthi, S., Pan, S.S., Singh, S.V., Zimniak, P., and Awasthi, Y.C. (2001). Two distinct 4-hydroxynonenal metabolizing glutathione S-transferase isozymes are differentially expressed in human tissues. Biochemical and Biophysical Research Communications *282*, 1268-1274.

Cho, Y., Challa, S., Moquin, D., Genga, R., Ray, T.D., Guildford, M., and Chan, F.K.M. (2009). Phosphorylation-Driven Assembly of the RIP1-RIP3 Complex Regulates Programmed Necrosis and Virus-Induced Inflammation. Cell *137*, 1112-1123.
Cohen, G.M. (1997). Caspases: the executioners of apoptosis. Biochemical Journal *326*, 1-16.
Collins, C.L., Wasa, M., Souba, W.W., and Abcouwer, S.F. (1998). Determinants of glutamine dependence and utilization by normal and tumor-derived breast cell lines. Journal of Cellular Physiology *176*, 166-178.
Collins, M.A., Bednar, F., Zhang, Y.Q., Brisset, J.C., Galban, S., Galban, C.J., Rakshit, S., Flannagan, K.S., Adsay, N.V., and di Magliano, M.P. (2012). Oncogenic Kras is required for both the initiation and maintenance of pancreatic cancer in mice. J Clin Invest *122*, 639-653.
Commisso, C., Davidson, S.M., Soydaner-Azeloglu, R.G., Parker, S.J., Kamphorst, J.J., Hackett, S., Grabocka, E., Nofal, M., Drebin, J.A., Thompson, C.B.*, et al.* (2013). Macropinocytosis of protein is an amino acid supply route in Ras-transformed cells. Nature *497*, 633-+.
Connors, B.W. (2012). Tales of a Dirty Drug: Carbenoxolone, Gap Junctions, and Seizures. Epilepsy Currents *12*, 66-68.
Conrad, M., Angeli, J.P.F., Vandenabeele, P., and Stockwell, B.R. (2016). Regulated necrosis: disease relevance and therapeutic opportunities. Nat Rev Drug Discov *15*, 348-366.
Cooper, A.J.L. (1983). BIOCHEMISTRY OF SULFUR-CONTAINING AMINO-ACIDS. Annual Review of Biochemistry *52*, 187-222.
Cox, A.D., Fesik, S.W., Kimmelman, A.C., Luo, J., and Der, C.J. (2014). Drugging the undruggable RAS: Mission possible? Nat Rev Drug Discov *13*, 828-851.
Cramer, S.L., Saha, A., Liu, J., Tadi, S., Tiziani, S., Yan, W., Triplett, K., Lamb, C., Alters, S.E., and Rowlinson, S. (2017). Systemic depletion of L-cyst(e)ine with cyst(e)inase increases reactive oxygen species and suppresses tumor growth. Nat Med *23*, 120-127.
Crawhall, J.C., and Segal, S. (1967). INTRACELLULAR RATIO OF CYSTEINE AND CYSTINE IN VARIOUS TISSUES. Biochemical Journal *105*, 891-&.
Crews, C.M., Alessandrini, A., and Erikson, R.L. (1992). THE PRIMARY STRUCTURE OF MEK, A PROTEIN-KINASE THAT PHOSPHORYLATES THE ERK GENE-PRODUCT. Science *258*, 478-480.
Currie, R.A., Walker, K.S., Gray, A., Deak, M., Casamayor, A., Downes, C.P., Cohen, P., Alessi, D.R., and Lucocq, J. (1999). Role of phosphatidylinositol 3,4,5-trisphosphate in regulating the activity and localization of 3-phosphoinositide-dependent protein kinase-1. Biochemical Journal *337*, 575-583.
Dallafavera, R., Bregni, M., Erikson, J., Patterson, D., Gallo, R.C., and Croce, C.M. (1982). HUMAN C-MYC ONC GENE IS LOCATED ON THE REGION OF CHROMOSOME-8 THAT IS TRANSLOCATED IN BURKITT-LYMPHOMA CELLS. Proceedings of the National Academy of Sciences of the United States of America-Biological Sciences *79*, 7824-7827.
Damen, J.E., Liu, L., Rosten, P., Humphries, R.K., Jefferson, A.B., Majerus, P.W., and Krystal, G. (1996). The 145-kDa protein induced to associate with Shc by multiple cytokines is an inositol tetraphosphate and phosphatidylinositol 3,4,5-trisphosphate 5-phosphatase. Proceedings of the National Academy of Sciences of the United States of America *93*, 1689-1693.
Datta, S.R., Brunet, A., and Greenberg, M.E. (1999). Cellular survival: a play in three Akts. Genes & Development *13*, 2905-2927.
Davidson, J.S., and Baumgarten, I.M. (1988). GLYCYRRHETINIC ACID-DERIVATIVES - A NOVEL CLASS OF INHIBITORS OF GAP-JUNCTIONAL INTERCELLULAR COMMUNICATION - STRUCTURE-ACTIVITY-RELATIONSHIPS. J Pharmacol Exp Ther *246*, 1104-1107.
Davies, H., Bignell, G.R., Cox, C., Stephens, P., Edkins, S., Clegg, S., Teague, J., Woffendin, H., Garnett, M.J., Bottomley, W.*, et al.* (2002). Mutations of the BRAF gene in human cancer. Nature *417*, 949-954.
Davies, M.J., Forni, L.G., and Willson, R.L. (1988). VITAMIN-E ANALOG TROLOX-C - ELECTRON-SPIN-RESONANCE AND PULSE-RADIOLYSIS STUDIES OF FREE-RADICAL REACTIONS. Biochemical Journal *255*, 513-522.

De Raedt, T., Walton, Z., Yecies, J.L., Li, D.A., Chen, Y.M., Malone, C.F., Maertens, O., Jeong, S.M., Bronson, R.T., Lebleu, V.*, et al.* (2011). Exploiting Cancer Cell Vulnerabilities to Develop a Combination Therapy for Ras-Driven Tumors. Cancer Cell *20*, 400-413.
DeBerardinis, R.J., Mancuso, A., Daikhin, E., Nissim, I., Yudkoff, M., Wehrli, S., and Thompson, C.B. (2007). Beyond aerobic glycolysis: Transformed cells can engage in glutamine metabolism that exceeds the requirement for protein and nucleotide synthesis. Proceedings of the National Academy of Sciences of the United States of America *104*, 19345-19350.
Declercq, W., Vanden Berghe, T., and Vandenabeele, P. (2009). RIP Kinases at the Crossroads of Cell Death and Survival. Cell *138*, 229-232.
Decrock, E., Vinken, M., De Vuyst, E., Krysko, D.V., D'Herde, K., Vanhaecke, T., Vandenabeele, P., Rogiers, V., and Leybaert, L. (2009). Connexin-related signaling in cell death: to live or let die? Cell Death and Differentiation *16*, 524-536.
Del Rio, D., Stewart, A.J., and Pellegrini, N. (2005). A review of recent studies on malondialdehyde as toxic molecule and biological marker of oxidative stress. Nutr Metab Carbiovasc Dis *15*, 316-328.
Delage, B., Luong, P., Maharaj, L., O'Riain, C., Syed, N., Crook, T., Hatzimichael, E., Papoudou-Bai, A., Mitchell, T.J., Whittaker, S.J.*, et al.* (2012). Promoter methylation of argininosuccinate synthetase-1 sensitises lymphomas to arginine deiminase treatment, autophagy and caspase-dependent apoptosis. Cell Death & Disease *3*, 9.
Deng, C.X., Zhang, P.M., Harper, J.W., Elledge, S.J., and Leder, P. (1995). MICE LACKING P21(C/P1/WAF1) UNDERGO NORMAL DEVELOPMENT, BUT ARE DEFECTIVE IN G1 CHECKPOINT CONTROL. Cell *82*, 675-684.
Di Nicolantonio, F., Arena, S., Gallicchio, M., Zecchin, D., Martini, M., Flonta, S.E., Stella, G.M., Lamba, S., Cancelliere, C., Russo, M.*, et al.* (2008). Replacement of normal with mutant alleles in the genome of normal human cells unveils mutation-specific drug responses. Proceedings of the National Academy of Sciences of the United States of America *105*, 20864-20869.
Dibble, C.C., Elis, W., Menon, S., Qin, W., Klekota, J., Asara, J.M., Finan, P.M., Kwiatkowski, D.J., Murphy, L.O., and Manning, B.D. (2012). TBC1D7 Is a Third Subunit of the TSC1-TSC2 Complex Upstream of mTORC1. Molecular Cell *47*, 535-546.
Diehl, J.A., Cheng, M.G., Roussel, M.F., and Sherr, C.J. (1998). Glycogen synthase kinase 3 beta regulates cyclin D1 proteolysis and subcellular localization. Genes & Development *12*, 3499-3511.
Dixon, S.J., Lemberg, K.M., Lamprecht, M.R., Skouta, R., Zaitsev, E.M., Gleason, C.E., Patel, D.N., Bauer, A.J., Cantley, A.M., Yang, W.S.*, et al.* (2012). Ferroptosis: An Iron-Dependent Form of Nonapoptotic Cell Death. Cell *149*, 1060-1072.
Dobzhansky, T. (1946). GENETICS OF NATURAL POPULATIONS .13. RECOMBINATION AND VARIABILITY IN POPULATIONS OF DROSOPHILA-PSEUDOOBSCURA. Genetics *31*, 269-290.
Doll, S., and Conrad, M. (2017). Iron and Ferroptosis: A Still Ill-Defined Liaison. IUBMB Life *69*, 423-434.
Downward, J. (2003). Targeting ras signalling pathways in cancer therapy. Nature Reviews Cancer *3*, 11-22.
Downward, J. (2015). RAS Synthetic Lethal Screens Revisited: Still Seeking the Elusive Prize? Clin Cancer Res *21*, 1802-1809.
Eagle, H., Oyama, V.I., and Piez, K.A. (1961). BIOSYNTHESIS OF CYSTINE IN HUMAN CELL CULTURES. Journal of Biological Chemistry *236*, 1425-&.
Edelstein, A., Amodaj, N., Hoover, K., Vale, R., and Stuurman, N. (2010). Computer control of microscopes using Manager. Current protocols in molecular biology / edited by Frederick M Ausubel [et al] *Chapter 14*, Unit14.20.
Efeyan, A., Comb, W.C., and Sabatini, D.M. (2015). Nutrient-sensing mechanisms and pathways. Nature *517*, 302-310.

Egan, S.E., Giddings, B.W., Brooks, M.W., Buday, L., Sizeland, A.M., and Weinberg, R.A. (1993). ASSOCIATION OF SOS RAS EXCHANGE PROTEIN WITH GRB2 IS IMPLICATED IN TYROSINE KINASE SIGNAL TRANSDUCTION AND TRANSFORMATION. Nature *363*, 45-51.
Elmore, S. (2007). Apoptosis: A review of programmed cell death. Toxicologic Pathology *35*, 495-516.
Elstrom, R.L., Bauer, D.E., Buzzai, M., Karnauskas, R., Harris, M.H., Plas, D.R., Zhuang, H.M., Cinalli, R.M., Alavi, A., Rudin, C.M.*, et al.* (2004). Akt stimulates aerobic glycolysis in cancer cells. Cancer Research *64*, 3892-3899.
Fan, Z., Wirth, A.K., Chen, D., Wruck, C.J., Rauh, M., Buchfelder, M., and Savaskan, N. (2017). Nrf2-Keap1 pathway promotes cell proliferation and diminishes ferroptosis. Oncogenesis *6*, e371.
Farmer, H., McCabe, N., Lord, C.J., Tutt, A.N.J., Johnson, D.A., Richardson, T.B., Santarosa, M., Dillon, K.J., Hickson, I., Knights, C.*, et al.* (2005). Targeting the DNA repair defect in BRCA mutant cells as a therapeutic strategy. Nature *434*, 917-921.
Fearnhead, H.O., Vandenabeele, P., and Vanden Berghe, T. (2017). How do we fit ferroptosis in the family of regulated cell death? Cell Death And Differentiation *24*, 1991.
Feig, C., Gopinathan, A., Neesse, A., Chan, D.S., Cook, N., and Tuveson, D.A. (2012). The Pancreas Cancer Microenvironment. Clinical Cancer Research *18*, 4266-4276.
Fernandes, H.S., Teixeira, C.S.S., Fernandes, P.A., Ramos, M.J., and Cerqueira, N.M.F.S.A. (2017). Amino acid deprivation using enzymes as a targeted therapy for cancer and viral infections. Expert Opin Ther Pat *27*, 283-297.
Feun, L.G., Marini, A., Walker, G., Elgart, G., Moffat, F., Rodgers, S.E., Wu, C.J., You, M., Wangpaichitr, M., Kuo, M.T.*, et al.* (2012). Negative argininosuccinate synthetase expression in melanoma tumours may predict clinical benefit from arginine-depleting therapy with pegylated arginine deiminase. British Journal of Cancer *106*, 1481-1485.
Foley, G.E., Barell, E.F., Adams, R.A., and Lazarus, H. (1969). NUTRITIONAL REQUIREMENTS OF HUMAN LEUKEMIC CELLS - CYSTINE REQUIREMENTS OF DIPLOID CELL LINES AND THEIR HETEROPLOID VARIANTS. Exp Cell Res *57*, 129-&.
Forcina, G.C., Conlon, M., Wells, A., Cao, J.Y.N., and Dixon, S.J. (2017). Systematic Quantification of Population Cell Death Kinetics in Mammalian Cells. Cell Syst *4*, 600-+.
Friedmann Angeli, J.P., Schneider, M., Proneth, B., Tyurina, Y.Y., Tyurin, V.A., Hammond, V.J., Herbach, N., Aichler, M., Walch, A., Eggenhofer, E.*, et al.* (2014). Inactivation of the ferroptosis regulator Gpx4 triggers acute renal failure in mice. Nature Cell Biology *16*, 1180-1191.
Fuchs, B.C., and Bode, B.P. (2005). Amino acid transporters ASCT2 and LAT1 in cancer: Partners in crime? Semin Cancer Biol *15*, 254-266.
Fukumura, D., Gohongi, T., Kadambi, A., Izumi, Y., Ang, J., Yun, C.O., Buerk, D.G., Huang, P.L., and Jain, R.K. (2001). Predominant role of endothelial nitric oxide synthase in vascular endothelial growth factor-induced angiogenesis and vascular permeability. Proceedings of the National Academy of Sciences of the United States of America *98*, 2604-2609.
Fukumura, D., Kashiwagi, S., and Jain, R.K. (2006). The role of nitric oxide in tumour progression. Nat Rev Cancer *6*, 521-534.
Gao, M.H., Monian, P., Quadri, N., Ramasamy, R., and Jiang, X.J. (2015). Glutaminolysis and Transferrin Regulate Ferroptosis. Molecular Cell *59*, 298-308.
Gao, P., Tchernyshyov, I., Chang, T.C., Lee, Y.S., Kita, K., Ochi, T., Zeller, K.I., De Marzo, A.M., Van Eyk, J.E., Mendell, J.T.*, et al.* (2009). c-Myc suppression of miR-23a/b enhances mitochondrial glutaminase expression and glutamine metabolism. Nature *458*, 762-U100.
Gaschler, M.M., and Stockwell, B.R. (2017). Lipid peroxidation in cell death. Biochemical and Biophysical Research Communications *482*, 419-425.
Gingras, A.C., Raught, B., and Sonenberg, N. (1999). eIF4 initiation factors: Effectors of mRNA recruitment to ribosomes and regulators of translation. Annual Review of Biochemistry *68*, 913-963.

Gong, T.X., Zhang, N., Kong, K.V., Goh, D., Ying, C., Auguste, J.L., Shum, P.P., Wei, L., Humbert, G., Yong, K.T.*, et al.* (2016). Rapid SERS monitoring of lipid-peroxidation-derived protein modifications in cells using photonic crystal fiber sensor. J Biophotonics *9*, 32-37.
Gonzalez, A., and Hall, M.N. (2017). Nutrient sensing and TOR signaling in yeast and mammals. Embo J *36*, 397-408.
Green, D.R., and Reed, J.C. (1998). Mitochondria and apoptosis. Science *281*, 1309-1312.
Green, D.R., and Victor, B. (2012). The pantheon of the fallen: why are there so many forms of cell death? Trends in Cell Biology *22*, 555-556.
Greulich, H., Chen, T.H., Feng, W., Janne, P.A., Alvarez, J.V., Zappaterra, M., Bulmer, S.E., Frank, D.A., Hahn, W.C., Sellers, W.R.*, et al.* (2005). Oncogenic transformation by inhibitor-sensitive and -resistant EGFR mutants. Plos Medicine *2*, 1167-1176.
Griffith, O.W. (1980). DETERMINATION OF GLUTATHIONE AND GLUTATHIONE DISULFIDE USING GLUTATHIONE-REDUCTASE AND 2-VINYLPYRIDINE. Analytical Biochemistry *106*, 207-212.
Griffith, O.W. (1999). Biologic and pharmacologic regulation of mammalian glutathione synthesis. Free Radic Biol Med *27*, 922-935.
Griffith, O.W., and Meister, A. (1979). POTENT AND SPECIFIC-INHIBITION OF GLUTATHIONE SYNTHESIS BY BUTHIONINE SULFOXIMINE (S-NORMAL-BUTYL HOMOCYSTEINE SULFOXIMINE). Journal of Biological Chemistry *254*, 7558-7560.
Gromer, S., Arscott, L.D., Williams Jr, C.H., Schirmeri, R.H., and Becker, K. (1998). Human placenta thioredoxin reductase. Isolation of the selenoenzyme, steady state kinetics, and inhibition by therapeutic gold compounds. Journal of Biological Chemistry *273*, 20096-20101.
Gromer, S., Johansson, L., Bauer, H., Arscott, L.D., Rauch, S., Ballou, D.P., Williams, C.H., Schirmer, R.H., and Arner, E.S.J. (2003). Active sites of thioredoxin reductases: Why selenoproteins? Proceedings of the National Academy of Sciences of the United States of America *100*, 12618-12623.
Gueyen, N., Woolley, K., and Smith, J. (2015). Border between natural product and drug: Comparison of the related benzoquinones idebenone and coenzyme Q(10). Redox Biol *4*, 289-295.
Guiney, S.J., Adlard, P.A., Bush, A.I., Finkelstein, D.I., and Ayton, S. (2017). Ferroptosis and cell death mechanisms in Parkinson's disease. Neurochem Int *104*, 34-48.
Haber, P.S., Keogh, G.W., Apte, M.V., Moran, C.S., Stewart, N.L., Crawford, D.H.G., Pirola, R.C., McCaughan, G.W., Ramm, G.A., and Wilson, J.S. (1999). Activation of pancreatic stellate cells in human and experimental pancreatic fibrosis. Am J Pathol *155*, 1087-1095.
Habrook, C.J., and Lyssiotis, C.A. (2017). Employing Metabolism to Improve the Diagnosis and Treatment of Pancreatic Cancer. Cancer Cell *31*, 5-19.
Halpern, B.C., Clark, B.R., Hardy, D.N., Halpern, R.M., and Smith, R.A. (1974). EFFECT OF REPLACEMENT OF METHIONINE BY HOMOCYSTINE ON SURVIVAL OF MALIGNANT AND NORMAL ADULT MAMMALIAN-CELLS IN CULTURE. Proceedings of the National Academy of Sciences of the United States of America *71*, 1133-1136.
Hambright, W.S., Fonseca, R.S., Chen, L.J., Na, R., and Ran, Q.T. (2017). Ablation of ferroptosis regulator glutathione peroxidase 4 in forebrain neurons promotes cognitive impairment and neurodegeneration. Redox Biol *12*, 8-17.
Hanahan, D., and Weinberg, R.A. (2000). The hallmarks of cancer. Cell *100*, 57-70.
Hanahan, D., and Weinberg, R.A. (2011). Hallmarks of Cancer: The Next Generation. Cell *144*, 646-674.
Hanover, J.A. (2001). Glycan-dependent signaling: O-linked N-acetylglucosamine. Faseb Journal *15*, 1865-1876.
Hara, K., Yonezawa, K., Weng, Q.P., Kozlowski, M.T., Belham, C., and Avruch, J. (1998). Amino acid sufficiency and mTOR regulate p70 S6 kinase and eIF-4E BP1 through a common effector mechanism. Journal of Biological Chemistry *273*, 14484-14494.

Harding, H.P., Zhang, Y.H., Zeng, H.Q., Novoa, I., Lu, P.D., Calfon, M., Sadri, N., Yun, C., Popko, B., Paules, R.*, et al.* (2003). An integrated stress response regulates amino acid metabolism and resistance to oxidative stress. Molecular Cell *11*, 619-633.
Hartwell, L.H., Szankasi, P., Roberts, C.J., Murray, A.W., and Friend, S.H. (1997). Integrating genetic approaches into the discovery of anticancer drugs. Science *278*, 1064-1068.
Hassanein, M., Hoeksema, M.D., Shiota, M., Qian, J., Harris, B.K., Chen, H.D., Clark, J.E., Alborn, W.E., Eisenberg, R., and Massion, P.P. (2013). SLC1A5 Mediates Glutamine Transport Required for Lung Cancer Cell Growth and Survival. Clinical Cancer Research *19*, 560-570.
Hayano, M., Yang, W.S., Corn, C.K., Pagano, N.C., and Stockwell, B.R. (2016). Loss of cysteinyl-tRNA synthetase (CARS) induces the transsulfuration pathway and inhibits ferroptosis induced by cystine deprivation. Cell Death and Differentiation *23*, 270-278.
Heiden, M.G.V., Cantley, L.C., and Thompson, C.B. (2009). Understanding the Warburg Effect: The Metabolic Requirements of Cell Proliferation. Science *324*, 1029-1033.
Heitman, J., Movva, N.R., and Hall, M.N. (1991). TARGETS FOR CELL-CYCLE ARREST BY THE IMMUNOSUPPRESSANT RAPAMYCIN IN YEAST. Science *253*, 905-909.
Hensley, C.T., Wasti, A.T., and DeBerardinis, R.J. (2013). Glutamine and cancer: cell biology, physiology, and clinical opportunities. J Clin Invest *123*, 3678-3684.
Hinnebusch, A.G. (2005). Translational regulation of GCN4 and the general amino acid control of yeast. In Annual Review of Microbiology, pp. 407-450.
Hirayama, A., Kami, K., Sugimoto, M., Sugawara, M., Toki, N., Onozuka, H., Kinoshita, T., Saito, N., Ochiai, A., Tomita, M.*, et al.* (2009). Quantitative metabolome profiling of colon and stomach cancer microenvironment by capillary electrophoresis time-of-flight mass spectrometry. Cancer Research *69*, 4918-4925.
Holleman, A., den Boer, M.L., Kazemier, K.M., Janka-Schaub, G.E., and Pieters, R. (2003). Resistance to different classes of drugs is associated with impaired apoptosis in childhood acute lymphoblastic leukemia. Blood *102*, 4541-4546.
Holler, N., Zaru, R., Micheau, O., Thome, M., Attinger, A., Valitutti, S., Bodmer, J.L., Schneider, P., Seed, B., and Tschopp, J. (2000). Fas triggers an alternative, caspase-8-independent cell death pathway using the kinase RIP as effector molecule. Nature Immunology *1*, 489-495.
Horvath, K., Jami, M., Hill, I.D., Papadimitriou, J.C., Magder, L.S., and Chanasongcram, S. (1996). Isocaloric glutamine-free diet and the morphology and function of rat small intestine. J Parenter Enter Nutr *20*, 128-134.
Hosokawa, N., Hara, T., Kaizuka, T., Kishi, C., Takamura, A., Miura, Y., Iemura, S., Natsume, T., Takehana, K., Yamada, N.*, et al.* (2009). Nutrient-dependent mTORC1 Association with the ULK1-Atg13-FIP200 Complex Required for Autophagy. Mol Biol Cell *20*, 1981-1991.
Hsu, P.P., and Sabatini, D.M. (2008). Cancer cell metabolism: Warburg and beyond. Cell *134*, 703-707.
Huhn, D., Bolck, H.A., and Sartori, A.A. (2013). Targeting DNA double-strand break signalling and repair: recent advances in cancer therapy. Swiss Medical Weekly *143*, 14.
Iglehart, J.D., York, R.M., Modest, A.P., Lazarus, H., and Livingston, D.M. (1977). CYSTINE REQUIREMENT OF CONTINUOUS HUMAN LYMPHOID-CELL LINES OF NORMAL AND LEUKEMIC ORIGIN. Journal of Biological Chemistry *252*, 7184-7191.
Inoki, K., Li, Y., Xu, T., and Guan, K.L. (2003). Rheb GTPase is a direct target of TSC2 GAP activity and regulates mTOR signaling. Genes & Development *17*, 1829-1834.
Inoki, K., Li, Y., Zhu, T.Q., Wu, J., and Guan, K.L. (2002). TSC2 is phosphorylated and inhibited by Akt and suppresses mTOR signalling. Nature Cell Biology *4*, 648-657.
Jacinto, E., Facchinetti, V., Liu, D., Soto, N., Wei, S.N., Jung, S.Y., Huang, Q.J., Qin, J., and Su, B. (2006). SIN1/MIP1 maintains rictor-mTOR complex integrity and regulates Akt phosphorylation and substrate specificity. Cell *127*, 125-137.

Jacobetz, M.A., Chan, D.S., Neesse, A., Bapiro, T.E., Cook, N., Frese, K.K., Feig, C., Nakagawa, T., Caldwell, M.E., Zecchini, H.I., *et al.* (2013). Hyaluronan impairs vascular function and drug delivery in a mouse model of pancreatic cancer. Gut *62*, 112-U153.
Jain, M., Nilsson, R., Sharma, S., Madhusudhan, N., Kitami, T., Souza, A.L., Kafri, R., Kirschner, M.W., Clish, C.B., and Mootha, V.K. (2012). Metabolite Profiling Identifies a Key Role for Glycine in Rapid Cancer Cell Proliferation. Science *336*, 1040-1044.
Jiang, L., Kon, N., Li, T.Y., Wang, S.J., Su, T., Hibshoosh, H., Baer, R., and Gu, W. (2015). Ferroptosis as a p53-mediated activity during tumour suppression. Nature *520*, 57-+.
Joseph, E.W., Pratilas, C.A., Poulikakos, P.I., Tadi, M., Wang, W.Q., Taylor, B.S., Halilovic, E., Persaud, Y., Xing, F., Viale, A., *et al.* (2010). The RAF inhibitor PLX4032 inhibits ERK signaling and tumor cell proliferation in a V600E BRAF-selective manner. Proceedings of the National Academy of Sciences of the United States of America *107*, 14903-14908.
Kagan, V.E., Mao, G.W., Qu, F., Angeli, J.P.F., Doll, S., St Croix, C., Dar, H.H., Liu, B., Tyurin, V.A., Ritov, V.B., *et al.* (2017). Oxidized arachidonic and adrenic PEs navigate cells to ferroptosis. Nature Chemical Biology *13*, 81-90.
Kalhan, S.C., and Marczewski, S.E. (2012). Methionine, homocysteine, one carbon metabolism and fetal growth. Rev Endocr Metab Disord *13*, 109-119.
Kamata, T. (2009). Roles of Nox1 and other Nox isoforms in cancer development. Cancer Sci *100*, 1382-1388.
Kami, K., Fujimori, T., Sato, H., Sato, M., Yamamoto, H., Ohashi, Y., Sugiyama, N., Ishihama, Y., Onozuka, H., Ochiai, A., *et al.* (2013). Metabolomic profiling of lung and prostate tumor tissues by capillary electrophoresis time-of-flight mass spectrometry. Metabolomics *9*, 444-453.
Kamphorst, J.J., Nofal, M., Commisso, C., Hackett, S.R., Lu, W.Y., Grabocka, E., Vander Heiden, M.G., Miller, G., Drebin, J.A., Bar-Sagi, D., *et al.* (2015). Human Pancreatic Cancer Tumors Are Nutrient Poor and Tumor Cells Actively Scavenge Extracellular Protein. Cancer Research *75*, 544-553.
Kanemitsu, M.Y., and Lau, A.F. (1993). EPIDERMAL GROWTH-FACTOR STIMULATES THE DISRUPTION OF GAP JUNCTIONAL COMMUNICATION AND CONNEXIN43 PHOSPHORYLATION-INDEPENDENT OF 12-0-TETRADECANOYLPHORBOL 13-ACETATE-SENSITIVE PROTEIN-KINASE-C - THE POSSIBLE INVOLVEMENT OF MITOGEN-ACTIVATED PROTEIN-KINASE. Mol Biol Cell *4*, 837-848.
Kehrer, J.P., and Lund, L.G. (1994). CELLULAR REDUCING EQUIVALENTS AND OXIDATIVE STRESS. Free Radic Biol Med *17*, 65-75.
Keniry, M., and Parsons, R. (2008). The role of PTEN signaling perturbations in cancer and in targeted therapy. Oncogene *27*, 5477-5485.
Kim, D.H., Sarbassov, D.D., Ali, S.M., King, J.E., Latek, R.R., Erdjument-Bromage, H., Tempst, P., and Sabatini, D.M. (2002). MTOR interacts with Raptor to form a nutrient-sensitive complex that signals to the cell growth machinery. Cell *110*, 163-175.
Kim, D.H., Sarbassov, D.D., Ali, S.M., Latek, R.R., Guntur, K.V.P., Erdjument-Bromage, H., Tempst, P., and Sabatini, D.M. (2003). G beta L, a positive regulator of the rapamycin-sensitive pathway required for the nutrient-sensitive interaction between raptor and mTOR. Molecular Cell *11*, 895-904.
Kim, E., Goraksha-Hicks, P., Li, L., Neufeld, T.P., and Guan, K.L. (2008). Regulation of TORC1 by Rag GTPases in nutrient response. Nature Cell Biology *10*, 935-945.
Kirchhoff, F., Dringen, R., and Giaume, C. (2001). Pathways of neuron-astrocyte interactions and their possible role in neuroprotection. Eur Arch Psych Clin Neurosci *251*, 159-169.
Kirk, S.J., Regan, M.C., Wasserkrug, H.L., Sodeyama, M., and Barbul, A. (1992). ARGININE ENHANCES T-CELL RESPONSES IN ATHYMIC NUDE-MICE. J Parenter Enter Nutr *16*, 429-432.
Kischkel, F.C., Hellbardt, S., Behrmann, I., Germer, M., Pawlita, M., Krammer, P.H., and Peter, M.E. (1995). CYTOTOXICITY-DEPENDENT APO-1 (FAS/CD95)-ASSOCIATED PROTEINS FORM A DEATH-INDUCING SIGNALING COMPLEX (DISC) WITH THE RECEPTOR. Embo Journal *14*, 5579-5588.
Klionsky, D.J. (2007). Autophagy: from phenomenology to molecular understanding in less than a decade. Nature Reviews Molecular Cell Biology *8*, 931-937.

Kodama, R., Kato, M., Furuta, S., Ueno, S., Zhang, Y.G., Matsuno, K., Yabe-Nishimura, C., Tanaka, E., and Kamata, T. (2013). ROS-generating oxidases Nox1 and Nox4 contribute to oncogenic Ras-induced premature senescence. Genes to Cells *18*, 32-41.
Kornfeld, R., and Kornfeld, S. (1985). ASSEMBLY OF ASPARAGINE-LINKED OLIGOSACCHARIDES. Annual Review of Biochemistry *54*, 631-664.
Kottakis, F., Nicolay, B.N., Roumane, A., Karnik, R., Gu, H.C., Nagle, J.M., Boukhali, M., Hayward, M.C., Li, Y.Y., Chen, T.*, et al.* (2016). LKB1 loss links serine metabolism to DNA methylation and tumorigenesis. Nature *539*, 390-395.
Kreis, W., Baker, A., Ryan, V., and Bertasso, A. (1980). EFFECT OF NUTRITIONAL AND ENZYMATIC METHIONINE DEPRIVATION UPON HUMAN NORMAL AND MALIGNANT-CELLS IN TISSUE-CULTURE. Cancer Research *40*, 634-641.
Kreis, W., and Goodenow, M. (1978). METHIONINE REQUIREMENT AND REPLACEMENT BY HOMOCYSTEINE IN TISSUE-CULTURES OF SELECTED RODENT AND HUMAN MALIGNANT AND NORMAL CELLS. Cancer Research *38*, 2259-2262.
Krishna, M., and Narang, H. (2008). The complexity of mitogen-activated protein kinases (MAPKs) made simple. Cell Mol Life Sci *65*, 3525-3544.
Kyriakis, J.M., and Avruch, J. (2001). Mammalian mitogen-activated protein kinase signal transduction pathways activated by stress and inflammation. Physiol Rev *81*, 807-869.
Labuschagne, C.F., van den Broek, N.J.F., Mackay, G.M., Vousden, K.H., and Maddocks, O.D.K. (2014). Serine, but Not Glycine, Supports One-Carbon Metabolism and Proliferation of Cancer Cells. Cell Reports *7*, 1248-1258.
Lacey, J.M., and Wilmore, D.W. (1990). IS GLUTAMINE A CONDITIONALLY ESSENTIAL AMINO-ACID. Nutrition Reviews *48*, 297-309.
Laleu, B., Gaggini, F., Orchard, M., Fioraso-Cartier, L., Cagnon, L., Houngninou-Molango, S., Gradia, A., Duboux, G., Merlot, C., Heitz, F.*, et al.* (2010). First in class, potent, and orally bioavailable NADPH oxidase isoform 4 (Nox4) inhibitors for the treatment of idiopathic pulmonary fibrosis. Journal of Medicinal Chemistry *53*, 7715-7730.
Lamb, R.F. (2012). Amino acid sensing mechanisms: an Achilles heel in cancer? Febs Journal *279*, 2624-2631.
Lawlor, M.A., and Alessi, D.R. (2001). PKB/Akt: a key mediator of cell proliferation, survival and insulin responses? Journal of Cell Science *114*, 2903-2910.
Li, X.X., Lewis, M.T., Huang, J., Gutierrez, C., Osborne, C.K., Wu, M.F., Hilsenbeck, S.G., Pavlick, A., Zhang, X.M., Chamness, G.C.*, et al.* (2008). Intrinsic resistance of tumorigenic breast cancer cells to chemotherapy. J Natl Cancer Inst *100*, 672-679.
Linke, S.P., Clarkin, K.C., Di Leonardo, A., Tsou, A., and Wahl, G.M. (1996). A reversible, p53-dependent G(0)/G(1) cell cycle arrest induced by ribonucleotide depletion in the absence of detectable DNA damage. Genes & Development *10*, 934-947.
Linkermann, A., Skouta, R., Himmerkus, N., Mulay, S.R., Dewitz, C., De Zen, F., Prokai, A., Zuchtriegel, G., Krombach, F., Welz, P.S.*, et al.* (2014). Synchronized renal tubular cell death involves ferroptosis. Proceedings of the National Academy of Sciences of the United States of America *111*, 16836-16841.
Lis, M., Wizert, A., Przybylo, M., Langner, M., Swiatek, J., Jungwirth, P., and Cwiklik, L. (2011). The effect of lipid oxidation on the water permeability of phospholipids bilayers. Physical Chemistry Chemical Physics *13*, 17555-17563.
Locasale, J.W., Grassian, A.R., Melman, T., Lyssiotis, C.A., Mattaini, K.R., Bass, A.J., Heffron, G., Metallo, C.M., Muranen, T., Sharfi, H.*, et al.* (2011). Phosphoglycerate dehydrogenase diverts glycolytic flux and contributes to oncogenesis. Nature Genetics *43*, 869-U879.
Loewith, R., Jacinto, E., Wullschleger, S., Lorberg, A., Crespo, J.L., Bonenfant, D., Oppliger, W., Jenoe, P., and Hall, M.N. (2002). Two TOR complexes, only one of which is rapamycin sensitive, have distinct roles in cell growth control. Molecular Cell *10*, 457-468.

Long, G.V., Stroyakovskiy, D., Gogas, H., Levchenko, E., de Braud, F., Larkin, J., Garbe, C., Jouary, T., Hauschild, A., Grob, J.J*., et al.* (2014). Combined BRAF and MEK Inhibition versus BRAF Inhibition Alone in Melanoma. New England Journal of Medicine *371*, 1877-1888.
LoPachin, R.M., Gavin, T., Petersen, D.R., and Barber, D.S. (2009). Molecular Mechanisms of 4-Hydroxy-2-nonenal and Acrolein Toxicity: Nucleophilic Targets and Adduct Formation. Chemical Research in Toxicology *22*, 1499-1508.
Lord, C.J., and Ashworth, A. (2016). BRCAness revisited. Nat Rev Cancer *16*, 110-120.
Lorincz, T., Jemnitz, K., Kardon, T., Mandl, J., and Szarka, A. (2015). Ferroptosis is Involved in Acetaminophen Induced Cell Death. Pathology & Oncology Research *21*, 1115-1121.
Lowenstein, E.J., Daly, R.J., Batzer, A.G., Li, W., Margolis, B., Lammers, R., Ullrich, A., Skolnik, E.Y., Barsagi, D., and Schlessinger, J. (1992). THE SH2 AND SH3 DOMAIN CONTAINING PROTEIN GRB2 LINKS RECEPTOR TYROSINE KINASES TO RAS SIGNALING. Cell *70*, 431-442.
Lowy, D.R., and Willumsen, B.M. (1993). FUNCTION AND REGULATION OF RAS. Annual Review of Biochemistry *62*, 851-891.
Lu, J., and Holmgren, A. (2009). Selenoproteins. Journal of Biological Chemistry *284*, 723-727.
Lu, S.C. (1999). Regulation of hepatic glutathione synthesis: current concepts and controversies. Faseb Journal *13*, 1169-1183.
Lu, S.C. (2013). Glutathione synthesis. Biochim Biophys Acta-Gen Subj *1830*, 3143-3153.
Lucchesi, J.C. (1968). SYNTHETIC LETHALITY AND SEMI-LETHALITY AMONG FUNCTIONALLY RELATED MUTANTS OF DROSOPHILA MELANOGASTER. Genetics *59*, 37-&.
Luo, J., Manning, B.D., and Cantley, L.C. (2003). Targeting the PI3K-Akt pathway in human cancer: Rationale and promise. Cancer Cell *4*, 257-262.
Maddocks, O.D.K., Athineos, D., Cheung, E.C., Lee, P., Zhang, T., van den Broek, N.J.F., Mackay, G.M., Labuschagne, C.F., Gay, D., Kruiswijk, F*., et al.* (2017). Modulating the therapeutic response of tumours to dietary serine and glycine starvation. Nature *544*, 372-+.
Maddocks, O.D.K., Berkers, C.R., Mason, S.M., Zheng, L., Blyth, K., Gottlieb, E., and Vousden, K.H. (2013). Serine starvation induces stress and p53-dependent metabolic remodelling in cancer cells. Nature *493*, 542-+.
Maddocks, O.D.K., Labuschagne, C.F., Adams, P.D., and Vousden, K.H. (2016). Serine Metabolism Supports the Methionine Cycle and DNA/RNA Methylation through De Novo ATP Synthesis in Cancer Cells. Molecular Cell *61*, 210-221.
Mandal, P.K., Seiler, A., Perisic, T., Kolle, P., Canak, A.B., Forster, H., Weiss, N., Kremmer, E., Lieberman, M.W., Bannai, S*., et al.* (2010a). System x(c)(-) and Thioredoxin Reductase 1 Cooperatively Rescue Glutathione Deficiency. Journal of Biological Chemistry *285*, 22244-22253.
Mandal, P.K., Seiler, A., Perisic, T., Kölle, P., Canak, A.B., Förster, H., Weiss, N., Kremmer, E., Lieberman, M.W., Bannai, S*., et al.* (2010b). System xc- and thioredoxin reductase 1 cooperatively rescue glutathione deficiency. Journal of Biological Chemistry *285*, 22244-22253.
Mannes, A.M., Seiler, A., Bosello, V., Maiorino, M., and Conrad, M. (2011). Cysteine mutant of mammalian GPx4 rescues cell death induced by disruption of the wild-type selenoenzyme. FASEB Journal *25*, 2135-2144.
Manning, B.D., Tee, A.R., Logsdon, M.N., Blenis, J., and Cantley, L.C. (2002). Identification of the tuberous sclerosis complex-2 tumor suppressor gene product tuberin as a target of the phosphoinositide 3-Kinase/Akt pathway. Molecular Cell *10*, 151-162.
Mates, J.M., Segura, J.A., Martin-Rufian, M., Campos-Sandoval, J.A., Alonso, F.J., and Marquez, J. (2013). Glutaminase Isoenzymes as Key Regulators in Metabolic and Oxidative Stress Against Cancer. Curr Mol Med *13*, 514-534.
Mato, J.M., Corrales, F.J., Lu, S.C., and Avila, M.A. (2002). S-adenosylmethionine: a control switch that regulates liver function. Faseb Journal *16*, 15-26.

Matsushita, T., Oyamada, M., Fujimoto, K., Yasuda, Y., Masuda, S., Wada, Y., Oka, T., and Takamatsu, T. (1999). Remodeling of cell-cell and cell-extracellular matrix interactions at the border zone of rat myocardial infarcts. Circulation Research *85*, 1046-1055.
Mazurek, S. (2011). Pyruvate kinase type M2: A key regulator of the metabolic budget system in tumor cells. Int J Biochem Cell Biol *43*, 969-980.
McCabe, N., Turner, N.C., Lord, C.J., Kluzek, K., Bialkowska, A., Swift, S., Giavara, S., O'Connor, M.J., Tutt, A.N., Zdzienicka, M.Z*., et al.* (2006). Deficiency in the repair of DNA damage by homologous recombination and sensitivity to poly(ADP-ribose) polymerase inhibition. Cancer Research *66*, 8109-8115.
McCormick, F. (2015). KRAS as a Therapeutic Target. Clinical Cancer Research *21*, 1797-1801.
McGill, M.R., and Jaeschke, H. (2015). A direct comparison of methods used to measure oxidized glutathione in biological samples: 2-vinylpyridine and N-ethylmaleimide. Toxicology Mechanisms and Methods *25*, 589-595.
Meister, A., and Anderson, M.E. (1983). GLUTATHIONE. Annual Review of Biochemistry *52*, 711-760.
Menon, S., and Manning, B.D. (2008). Common corruption of the mTOR signaling network in human tumors. Oncogene *27 Suppl 2*, S43-51.
Mizushima, N., and Komatsu, M. (2011). Autophagy: renovation of cells and tissues. Cell *147*, 728-741.
Moran, M.F., Koch, C.A., Anderson, D., Ellis, C., England, L., Martin, G.S., and Pawson, T. (1990). SRC HOMOLOGY REGION-2 DOMAINS DIRECT PROTEIN-PROTEIN INTERACTIONS IN SIGNAL TRANSDUCTION. Proceedings of the National Academy of Sciences of the United States of America *87*, 8622-8626.
Mordente, A., Martorana, G.E., Minotti, G., and Giardina, B. (1998). Antioxidant Properties of 2,3-Dimethoxy-5-methyl- 6-(10-hydroxydecyl)-1,4-benzoquinone (Idebenone). Chemical Research in Toxicology *11*, 54-63.
Murphy, J.M., Czabotar, P.E., Hildebrand, J.M., Lucet, I.S., Zhang, J.G., Alvarez-Diaz, S., Lewis, R., Lalaoui, N., Metcalf, D., Webb, A.I*., et al.* (2013). The Pseudokinase MLKL Mediates Necroptosis via a Molecular Switch Mechanism. Immunity *39*, 443-453.
Myers, M.P., Pass, I., Batty, I.H., Van der Kaay, J., Stolarov, J.P., Hemmings, B.A., Wigler, M.H., Downes, C.P., and Tonks, N.K. (1998). The lipid phosphatase activity of PTEN is critical for its tumor suppressor function. Proceedings of the National Academy of Sciences of the United States of America *95*, 13513-13518.
Nagasawa, H., and Little, J.B. (1992). INDUCTION OF SISTER CHROMATID EXCHANGES BY EXTREMELY LOW-DOSES OF ALPHA-PARTICLES. Cancer Research *52*, 6394-6396.
Nagata, S. (1997). Apoptosis by death factor. Cell *88*, 355-365.
Nakase, T., Fushiki, S., Sohl, G., Theis, M., Willecke, K., and Naus, C.C.G. (2003). Neuroprotective role of astrocytic gap junctions in ischemic stroke. Cell Commun Adhes *10*, 413-417.
Naus, C.C.G., Ozog, M.A., Bechberger, J.F., and Nakase, T. (2001). A neuroprotective role for gap junctions. Cell Commun Adhes *8*, 325-+.
Nazarian, R., Shi, H.B., Wang, Q., Kong, X.J., Koya, R.C., Lee, H., Chen, Z.G., Lee, M.K., Attar, N., Sazegar, H*., et al.* (2010). Melanomas acquire resistance toB-RAF(V600E) inhibition by RTK or N-RAS upregulation. Nature *468*, 973-U377.
Nielsen, M.S., Axelsen, L.N., Sorgen, P.L., Verma, V., Delmar, M., and Holstein-Rathlou, N.H. (2012). Gap Junctions. Compr Physiol *2*, 1981-2035.
Noda, M., Ko, M., Ogura, A., Liu, D.G., Amano, T., Takano, T., and Ikawa, Y. (1985). SARCOMA-VIRUSES CARRYING RAS ONCOGENES INDUCE DIFFERENTIATION-ASSOCIATED PROPERTIES IN A NEURONAL CELL-LINE. Nature *318*, 73-75.
Ogrunc, M., Di Micco, R., Liontos, M., Bombardelli, L., Mione, M., Fumagalli, M., Gorgoulis, V.G., and d'Adda di Fagagna, F. (2014). Oncogene-induced reactive oxygen species fuel hyperproliferation and DNA damage response activation. Cell Death Differ *21*, 998-1012.

Ohnuma, T., Waligunda, J., and Holland, J.F. (1971). AMINO ACID REQUIREMENTS IN-VITRO OF HUMAN LEUKEMIC CELLS. Cancer Research *31*, 1640-+.
Ohtsubo, K., and Marth, J.D. (2006). Glycosylation in cellular mechanisms of health and disease. Cell *126*, 855-867.
Olivares, O., Mayers, J.R., Gouirand, V., Torrence, M.E., Gicquel, T., Borge, L., Lac, S., Roques, J., Lavaut, M.N., Berthezene, P.*, et al.* (2017). Collagen-derived proline promotes pancreatic ductal adenocarcinoma cell survival under nutrient limited conditions. Nat Commun *8*, 14.
Ono, M., Hirata, A., Kometani, T., Miyagawa, M., Ueda, S., Kinoshita, H., Fujii, T., and Kuwano, M. (2004). Sensitivity to gefitinib (Iressa, ZD1839) in non-small cell lung cancer cell lines correlates with dependence on the epidermal growth factor (EGF) receptor/extracellular signal-regulated kinase 1/2 and EGF receptor/Akt pathway for proliferation. Mol Cancer Ther *3*, 465-472.
Oppenheimer, L., Wellner, V.P., Griffith, O.W., and Meister, A. (1979). GLUTATHIONE SYNTHETASE - PURIFICATION FROM RAT-KIDNEY AND MAPPING OF THE SUBSTRATE BINDING-SITES. Journal of Biological Chemistry *254*, 5184-5190.
Ozes, O.N., Mayo, L.D., Gustin, J.A., Pfeffer, S.R., Pfeffer, L.M., and Donner, D.B. (1999). NF-kappa B activation by tumour necrosis factor requires the Akt serine-threonine kinase. Nature *401*, 82-85.
Pacold, M.E., Brimacombe, K.R., Chan, S.H., Rohde, J.M., Lewis, C.A., Swier, L., Possemato, R., Chen, W.W., Sullivan, L.B., Fiske, B.P.*, et al.* (2016). A PHGDH inhibitor reveals coordination of serine synthesis and one-carbon unit fate. Nature Chemical Biology *12*, 452-U118.
Paez, J.G., Janne, P.A., Lee, J.C., Tracy, S., Greulich, H., Gabriel, S., Herman, P., Kaye, F.J., Lindeman, N., Boggon, T.J.*, et al.* (2004). EGFR mutations in lung cancer: Correlation with clinical response to gefitinib therapy. Science *304*, 1497-1500.
Pain, V.M. (1994). TRANSLATIONAL CONTROL DURING AMINO-ACID STARVATION. Biochimie *76*, 718-728.
Paraiso, K.H.T., Fedorenko, I.V., Cantini, L.P., Munko, A.C., Hall, M., Sondak, V.K., Messina, J.L., Flaherty, K.T., and Smalley, K.S.M. (2010). Recovery of phospho-ERK activity allows melanoma cells to escape from BRAF inhibitor therapy. British Journal of Cancer *102*, 1724-1730.
Parmenter, T.J., Kleinschmidt, M., Kinross, K.M., Bond, S.T., Li, J., Kaadige, M.R., Rao, A., Sheppard, K.E., Hugo, W., Pupo, G.M.*, et al.* (2014). Response of BRAF-mutant melanoma to BRAF inhibition is mediated by a network of transcriptional regulators of glycolysis. Cancer Discovery *4*, 423-433.
Patel, S.A., Warren, B.A., Rhoderick, J.F., and Bridges, R.J. (2004). Differentiation of substrate and non-substrate inhibitors of transport system x(c)(-): an obligate exchanger of L-glutamate and L-cystine. Neuropharmacology *46*, 273-284.
Patil, M.D., Bhaumik, J., Babykutty, S., Banerjee, U.C., and Fukumura, D. (2016). Arginine dependence of tumor cells: targeting a chink in cancer's armor. Oncogene *35*, 4957-4972.
Pawson, T., and Schlessinger, J. (1993). SH2 AND SH3 DOMAINS. Current Biology *3*, 434-442.
Pearce, A., Haas, M., Viney, R., Pearson, S.A., Haywood, P., Brown, C., and Ward, R. (2017). Incidence and severity of self-reported chemotherapy side effects in routine care: A prospective cohort study. Plos One *12*, 12.
Pegg, A.E. (2009). Mammalian Polyamine Metabolism and Function. IUBMB Life *61*, 880-894.
Petit, C.S., Roczniak-Ferguson, A., and Ferguson, S.M. (2013). Recruitment of folliculin to lysosomes supports the amino acid-dependent activation of Rag GTPases. Journal of Cell Biology *202*, 1107-1122.
Phillips, M.M., Sheaff, M.T., and Szlosarek, P.W. (2013). Targeting Arginine-Dependent Cancers with Arginine-Degrading Enzymes: Opportunities and Challenges. Cancer Res Treat *45*, 251-262.
Pines, G., Köstler, W.J., and Yarden, Y. (2010). Oncogenic mutant forms of EGFR: Lessons in signal transduction and targets for cancer therapy. FEBS Letters *584*, 2699-2706.
Possemato, R., Marks, K.M., Shaul, Y.D., Pacold, M.E., Kim, D., Birsoy, K., Sethumadhavan, S., Woo, H.K., Jang, H.G., Jha, A.K.*, et al.* (2011). Functional genomics reveal that the serine synthesis pathway is essential in breast cancer. Nature *476*, 346-U119.

Possik, P.A., Müller, J., Gerlach, C., Kenski, J.C.N., Huang, X., Shahrabi, A., Krijgsman, O., Song, J.Y., Smit, M.A., Gerritsen, B.*, et al.* (2014). Parallel InVivo and InVitro Melanoma RNAi Dropout Screens Reveal Synthetic Lethality between Hypoxia and DNA Damage Response Inhibition. Cell Reports *9*, 1375-1386.
Poursaitidis, I., and Lamb, R.F. (2017). Metabolism in Pancreatic Cancer. In Pancreatic Cancer, J.P. Neoptolemos, R. Urrutia, J. Abbruzzese, and M.W. Büchler, eds. (New York, NY: Springer New York), pp. 1-22.
Pouyssegur, J., Volmat, V., and Lenormand, P. (2002). Fidelity and spatio-temporal control in MAP kinase (ERKs) signalling. Biochem Pharmacol *64*, 755-763.
Provenzano, P.P., Cuevas, C., Chang, A.E., Goel, V.K., Von Hoff, D.D., and Hingorani, S.R. (2012). Enzymatic Targeting of the Stroma Ablates Physical Barriers to Treatment of Pancreatic Ductal Adenocarcinoma. Cancer Cell *21*, 418-429.
Rabinowitz, J.D., and White, E. (2010). Autophagy and Metabolism. Science *330*, 1344-1348.
Radu, A., and Moldovan, N. (1991). 4-HYDROXYNONENAL REDUCES JUNCTIONAL COMMUNICATION BETWEEN ENDOTHELIAL-CELLS IN CULTURE. Exp Cell Res *196*, 121-126.
Rahman, I., Kode, A., and Biswas, S.K. (2006). Assay for quantitative determination of glutathione and glutathione disulfide levels using enzymatic recycling method. Nature Protocols *1*, 3159-3165.
Ravikumar, B., Vacher, C., Berger, Z., Davies, J.E., Luo, S.Q., Oroz, L.G., Scaravilli, F., Easton, D.F., Duden, R., O'Kane, C.J.*, et al.* (2004). Inhibition of mTOR induces autophagy and reduces toxicity of polyglutamine expansions in fly and mouse models of Huntington disease. Nature Genetics *36*, 585-595.
Ray, C.A., Black, R.A., Kronheim, S.R., Greenstreet, T.A., Sleath, P.R., Salvesen, G.S., and Pickup, D.J. (1992). VIRAL INHIBITION OF INFLAMMATION - COWPOX VIRUS ENCODES AN INHIBITOR OF THE INTERLEUKIN-1-BETA CONVERTING ENZYME. Cell *69*, 597-604.
Raymond, E., Faivre, S., and Armand, J.P. (2000). Epidermal growth factor receptor tyrosine kinase as a target for anticancer therapy. Drugs *60*, 15-23.
Reed, J.C. (1994). BCL-2 AND THE REGULATION OF PROGRAMMED CELL-DEATH. Journal of Cell Biology *124*, 1-6.
Rehman, F.L., Lord, C.J., and Ashworth, A. (2010). Synthetic lethal approaches to breast cancer therapy. Nature Reviews Clinical Oncology *7*, 718-724.
Reimer, K.A., Lowe, J.E., Rasmussen, M.M., and Jennings, R.B. (1977). WAVEFRONT PHENOMENON OF ISCHEMIC CELL-DEATH .1. MYOCARDIAL INFARCT SIZE VS DURATION OF CORONARY-OCCLUSION IN DOGS. Circulation *56*, 786-794.
Reitzer, L.J., Wice, B.M., and Kennell, D. (1979). EVIDENCE THAT GLUTAMINE, NOT SUGAR, IS THE MAJOR ENERGY-SOURCE FOR CULTURED HELA-CELLS. Journal of Biological Chemistry *254*, 2669-2676.
Riely, G.J., Pao, W., Pham, D.K., Li, A.R., Rizvi, N., Venkatraman, E.S., Zakowski, M.F., Kris, M.G., Ladanyi, M., and Miller, V.A. (2006). Clinical course of patients with non-small cell lung cancer and epidermal growth factor receptor exon 19 and exon 21 mutations treated with gefitinib or erlotinib. Clinical Cancer Research *12*, 839-844.
Roberts, P.J., and Der, C.J. (2007). Targeting the Raf-MEK-ERK mitogen-activated protein kinase cascade for the treatment of cancer. Oncogene *26*, 3291-3310.
Robinson, M.M., McBryant, S.J., Tsukamoto, T., Rojas, C., Ferraris, D.V., Hamilton, S.K., Hansen, J.C., and Curthoys, N.P. (2007). Novel mechanism of inhibition of rat kidney-type glutaminase by bis-2-(5-phenylacetamido-1,2,4-thiadiazol-2-yl)ethyl sulfide (BPTES). Biochemical Journal *406*, 407-414.
Rodriguezviciana, P., Warne, P.H., Dhand, R., Vanhaesebroeck, B., Gout, I., Fry, M.J., Waterfield, M.D., and Downward, J. (1994). PHOSPHATIDYLINOSITOL-3-OH KINASE AS A DIRECT TARGET OF RAS. Nature *370*, 527-532.
Saal, L.H., Johansson, P., Holm, K., Gruvberger-Saal, S.K., She, Q.-B., Maurer, M., Koujak, S., Ferrando, A.A., Malmstrom, P., Memeo, L.*, et al.* (2007). Poor prognosis in carcinoma is associated with a gene

expression signature of aberrant PTEN tumor suppressor pathway activity. Proceedings of the National Academy of Sciences of the United States of America *104*, 7564-7569.
Sancak, Y., Bar-Peled, L., Zoncu, R., Markhard, A.L., Nada, S., and Sabatini, D.M. (2010). Ragulator-Rag Complex Targets mTORC1 to the Lysosomal Surface and Is Necessary for Its Activation by Amino Acids. Cell *141*, 290-303.
Sancak, Y., Peterson, T.R., Shaul, Y.D., Lindquist, R.A., Thoreen, C.C., Bar-Peled, L., and Sabatini, D.M. (2008). The Rag GTPases bind raptor and mediate amino acid signaling to mTORC1. Science *320*, 1496-1501.
Sarbassov, D.D., Ali, S.M., Kim, D.H., Guertin, D.A., Latek, R.R., Erdjument-Bromage, H., Tempst, P., and Sabatini, D.M. (2004). Rictor, a novel binding partner of mTOR, defines a rapamycin-insensitive and raptor-independent pathway that regulates the cytoskeleton. Current Biology *14*, 1296-1302.
Sarbassov, D.D., Guertin, D.A., Ali, S.M., and Sabatini, D.M. (2005). Phosphorylation and regulation of Akt/PKB by the rictor-mTOR complex. Science *307*, 1098-1101.
Saxton, R.A., and Sabatini, D.M. (2017). mTOR Signaling in Growth, Metabolism, and Disease. Cell *168*, 960-976.
Scaffidi, C., Fulda, S., Srinivasan, A., Friesen, C., Li, F., Tomaselli, K.J., Debatin, K.M., Krammer, P.H., and Peter, M.E. (1998). Two CD95 (APO-1/Fas) signaling pathways. Embo Journal *17*, 1675-1687.
Schildknecht, S., Weber, A., Gerding, H.R., Pape, R., Robotta, M., Drescher, M., Marquardt, A., Daiber, A., Ferger, B., and Leist, M. (2014). The NOX1/4 Inhibitor GKT136901 as Selective and Direct Scavenger of Peroxynitrite. Curr Med Chem *21*, 365-376.
Schlessinger, J. (2000). Cell signaling by receptor tyrosine kinases. Cell *103*, 211-225.
Schlessinger, J., and Ullrich, A. (1992). GROWTH-FACTOR SIGNALING BY RECEPTOR TYROSINE KINASES. Neuron *9*, 383-391.
Schneider, C.A., Rasband, W.S., and Eliceiri, K.W. (2012). NIH Image to ImageJ: 25 years of image analysis. Nature Methods *9*, 671-675.
Scholl, C., Fröhling, S., Dunn, I.F., Schinzel, A.C., Barbie, D.A., Kim, S.Y., Silver, S.J., Tamayo, P., Wadlow, R.C., Ramaswamy, S*., et al.* (2009). Synthetic Lethal Interaction between Oncogenic KRAS Dependency and STK33 Suppression in Human Cancer Cells. Cell *137*, 821-834.
Schwab, M., Alitalo, K., Klempnauer, K.H., Varmus, H.E., Bishop, J.M., Gilbert, F., Brodeur, G., Goldstein, M., and Trent, J. (1983). AMPLIFIED DNA WITH LIMITED HOMOLOGY TO MYC CELLULAR ONCOGENE IS SHARED BY HUMAN NEURO-BLASTOMA CELL-LINES AND A NEURO-BLASTOMA TUMOR. Nature *305*, 245-248.
Seabra, M.C. (1998). Membrane association and targeting of prenylated Ras-like GTPases. Cell Signal *10*, 167-172.
Seshacharyulu, P., Ponnusamy, M.P., Haridas, D., Jain, M., Ganti, A.K., and Batra, S.K. (2012). Targeting the EGFR signaling pathway in cancer therapy. Expert Opin Ther Targets *16*, 15-31.
Sharma, R., Yang, Y., Sharma, A., Awasthi, S., and Awasthi, Y.C. (2004). Antioxidant role of glutathione S-transferases: Protection against oxidant toxicity and regulation of stress-mediated apoptosis. Antioxidants & Redox Signaling *6*, 289-300.
Shashidharan, P., Michaelidis, T.M., Robakis, N.K., Kresovali, A., Papamatheakis, J., and Plaitakis, A. (1994). NOVEL HUMAN GLUTAMATE-DEHYDROGENASE EXPRESSED IN NEURAL AND TESTICULAR TISSUES AND ENCODED BY AN X-LINKED INTRONLESS GENE. Journal of Biological Chemistry *269*, 16971-16976.
Shaw, R.J., and Cantley, L.C. (2006). Ras, PI(3)K and mTOR signalling controls tumour cell growth. Nature *441*, 424-430.
Shaw, R.M., Fay, A.J., Puthenveedu, M.A., von Zastrow, M., Jan, Y.N., and Jan, L.Y. (2007). Microtubule plus-end-tracking proteins target gap junctions directly from the cell interior to adherens junctions. Cell *128*, 547-560.

Sheen, J.H., Zoncu, R., Kim, D., and Sabatini, D.M. (2011). Defective Regulation of Autophagy upon Leucine Deprivation Reveals a Targetable Liability of Human Melanoma Cells In Vitro and In Vivo. Cancer Cell *19*, 613-628.
Shepherd, P.R., Withers, D.J., and Siddle, K. (1998). Phosphoinositide 3-kinase: the key switch mechanism in insulin signalling. Biochemical Journal *333*, 471-490.
Shigematsu, H., and Gazdar, A.F. (2006). Somatic mutations of epidermal growth factor receptor signaling pathway in lung cancers. International Journal of Cancer *118*, 257-262.
Shigematsu, H., Lin, L., Takahashi, T., Nomura, M., Suzuki, M., Wistuba, II, Fong, K.M., Lee, H., Toyooka, S., Shimizu, N.*, et al.* (2005). Clinical and biological features associated with epidermal growth factor receptor gene mutations in lung cancers. J Natl Cancer Inst *97*, 339-346.
Shyh-Chang, N., Locasale, J.W., Lyssiotis, C.A., Zheng, Y.X., Teo, R.Y., Ratanasirintrawoot, S., Zhang, J., Onder, T., Unternaehrer, J.J., Zhu, H.*, et al.* (2013). Influence of Threonine Metabolism on S-Adenosylmethionine and Histone Methylation. Science *339*, 222-226.
Skouta, R., Dixon, S.J., Wang, J.L., Dunn, D.E., Orman, M., Shimada, K., Rosenberg, P.A., Lo, D.C., Weinberg, J.M., Linkermann, A.*, et al.* (2014). Ferrostatins Inhibit Oxidative Lipid Damage and Cell Death in Diverse Disease Models. Journal of the American Chemical Society *136*, 4551-4556.
Slawson, C., Copeland, R.J., and Hart, G.W. (2010). O-GlcNAc signaling: a metabolic link between diabetes and cancer? Trends Biochem Sci *35*, 547-555.
Smit, V.T., Boot, A.J., Smits, A.M., Fleuren, G.J., Cornelisse, C.J., and Bos, J.L. (1988). KRAS codon 12 mutations occur very frequently in pancreatic adenocarcinomas. Nucleic Acids Res *16*, 7773-7782.
Son, J., Lyssiotis, C.A., Ying, H., Wang, X., Hua, S., Ligorio, M., Perera, R.M., Ferrone, C.R., Mullarky, E., Ng, S.C.*, et al.* (2013). Glutamine supports pancreatic cancer growth through a KRAS-regulated metabolic pathway. Nature *496*, 101-+.
Sonenberg, N., and Hinnebusch, A.G. (2009). Regulation of Translation Initiation in Eukaryotes: Mechanisms and Biological Targets. Cell *136*, 731-745.
Sosman, J.A., Kim, K.B., Schuchter, L., Gonzalez, R., Pavlick, A.C., Weber, J.S., McArthur, G.A., Hutson, T.E., Moschos, S.J., Flaherty, K.T.*, et al.* (2012). Survival in BRAF V600-Mutant Advanced Melanoma Treated with Vemurafenib. New England Journal of Medicine *366*, 707-714.
Sousa, C.M., Biancur, D.E., Wang, X.X., Halbrook, C.J., Sherman, M.H., Zhang, L., Kremer, D., Hwang, R.F., Witkiewicz, A.K., Ying, H.Q.*, et al.* (2016). Pancreatic stellate cells support tumour metabolism through autophagic alanine secretion. Nature *536*, 479-+.
Stambolic, V., Suzuki, A., de la Pompa, J.L., Brothers, G.M., Mirtsos, C., Sasaki, T., Ruland, J., Penninger, J.M., Siderovski, D.P., and Mak, T.W. (1998). Negative regulation of PKB/Akt-dependent cell survival by the tumor suppressor PTEN. Cell *95*, 29-39.
Steck, P.A., Pershouse, M.A., Jasser, S.A., Yung, W.K.A., Lin, H., Ligon, A.H., Langford, L.A., Baumgard, M.L., Hattier, T., Davis, T.*, et al.* (1997). Identification of a candidate tumour suppressor gene, MMAC1, at chromosome 10q23.3 that is mutated in multiple advanced cancers. Nature Genetics *15*, 356-362.
Stipanuk, M.H. (2004). Sulfur amino acid metabolism: Pathways for production and removal of homocysteine and cysteine. Annu Rev Nutr *24*, 539-577.
Stone, E., Paley, O., Hu, J., Ekerdt, B., Cheung, N.K., and Georgiou, G. (2012). De Novo Engineering of a Human Cystathionine-gamma-Lyase for Systemic L-Methionine Depletion Cancer Therapy. ACS Chem Biol *7*, 1822-1829.
Sturman, J.A., Gaull, G., and Raiha, C.R. (1970). ABSENCE OF CYSTATHIONASE IN HUMAN FETAL LIVER - IS CYSTINE ESSENTIAL. Science *169*, 74-&.
Sun, L.M., Wang, H.Y., Wang, Z.G., He, S.D., Chen, S., Liao, D.H., Wang, L., Yan, J.C., Liu, W.L., Lei, X.G.*, et al.* (2012). Mixed Lineage Kinase Domain-like Protein Mediates Necrosis Signaling Downstream of RIP3 Kinase. Cell *148*, 213-227.
Swanton, C. (2012). Intratumor Heterogeneity: Evolution through Space and Time. Cancer Research *72*, 4875-4882.

Syed, N., Langer, J., Janczar, K., Singh, P., Lo Nigro, C., Lattanzio, L., Coley, H.M., Hatzimichael, E., Bomalaski, J., Szlosarek, P.*, et al.* (2013). Epigenetic status of argininosuccinate synthetase and argininosuccinate lyase modulates autophagy and cell death in glioblastoma. Cell Death & Disease *4*, 11.
Szlosarek, P.W., Klabatsa, A., Pallaska, A., Sheaff, M., Smith, P., Crook, T., Grimshaw, M.J., Steele, J.P., Rudd, R.M., Balkwill, F.R.*, et al.* (2006). In vivo loss of expression of argininosuccinate synthetase in malignant pleural mesothelioma is a biomarker for susceptibility to arginine depletion. Clinical Cancer Research *12*, 7126-7131.
Szlosarek, P.W., Luong, P., Phillips, M.M., Baccarini, M., Ellis, S., Szyszko, T., Sheaff, M.T., and Avril, N. (2013). Metabolic Response to Pegylated Arginine Deiminase in Mesothelioma With Promoter Methylation of Argininosuccinate Synthetase. Journal of Clinical Oncology *31*, E111-E113.
Takac, I., Schröder, K., Zhang, L., Lardy, B., Anilkumar, N., Lambeth, J.D., Shah, A.M., Morel, F., and Brandes, R.P. (2011). The E-loop is involved in hydrogen peroxide formation by the NADPH oxidase Nox4. Journal of Biological Chemistry *286*, 13304-13313.
Tallal, L., Tan, C., Oettgen, H., Wollner, N., McCarthy, M., Helson, L., Burchenal, J., Karnofsky, D., and Murphy, M.L. (1970). ESCHERICHIA-COLI L ASPARAGINASE IN THE TREATMENT OF LEUKEMIA AND SOLID TUMORS IN 131 CHILDREN. Cancer *25*, 306-477.
Tan, Y.Y., Sun, X.H., Xu, M.X., An, Z.L., Tan, X.Z., Tan, X.Y., Han, Q.H., Miljkovic, D.A., Yang, M., and Hoffman, R.M. (1998). Polyethylene glycol conjugation of recombinant methioninase for cancer therapy. Protein Expression and Purification *12*, 45-52.
Tan, Y.Y., Xu, M.X., Tan, X.Z., Tan, X.Y., Wang, X., Saikawa, Y., Nagahama, T., Sun, X.H., Lenz, M., and Hoffman, R.M. (1997). Overexpression and large-scale production of recombinant L-methionine-alpha-deamino-gamma-mercaptomethane-lyase for novel anticancer therapy. Protein Expression and Purification *9*, 233-245.
Tang, X.H., Wu, J.L., Ding, C.K., Lu, M., Keenan, M.M., Lin, C.C., Lin, C.A., Wang, C.C., George, D., Hsu, D.S.*, et al.* (2016). Cystine Deprivation Triggers Programmed Necrosis in VHL-Deficient Renal Cell Carcinomas. Cancer Research *76*, 1892-1903.
Tape, C.J., Ling, S., Dimitriadi, M., McMahon, K.M., Worboys, J.D., Leong, H.S., Norrie, I.C., Miller, C.J., Poulogiannis, G., Lauffenburger, D.A.*, et al.* (2016). Oncogenic KRAS Regulates Tumor Cell Signaling via Stromal Reciprocation. Cell *165*, 910-920.
Thomas, J.B., Holtsberg, F.W., Ensor, C.M., Bomalaski, J.S., and Clark, M.A. (2002). Enzymic degradation of plasma arginine using arginine deiminase inhibits nitric oxide production and protects mice from the lethal effects of tumour necrosis factor alpha and endotoxin. Biochemical Journal *363*, 581-587.
Tibbetts, A.S., and Appling, D.R. (2010). Compartmentalization of Mammalian Folate-Mediated One-Carbon Metabolism. In Annual Review of Nutrition, Vol 30, R.J. Cousins, ed. (Palo Alto: Annual Reviews), pp. 57-81.
Tietze, F. (1969). ENZYMIC METHOD FOR QUANTITATIVE DETERMINATION OF NANOGRAM AMOUNTS OF TOTAL AND OXIDIZED GLUTATHIONE - APPLICATIONS TO MAMMALIAN BLOOD AND OTHER TISSUES. Analytical Biochemistry *27*, 502-&.
Toohey, J.I. (2006). Vitamin B-12 and methionine synthesis: A critical review. Is nature's most beautiful cofactor(*) misunderstood? Biofactors *26*, 45-57.
Trotman, L.C., and Pandolfi, P.P. (2003). PTEN and p53: Who will get the upper hand? Cancer Cell *3*, 97-99.
Tsai, J., Lee, J.T., Wang, W., Zhang, J., Cho, H., Mamo, S., Bremer, R., Gillette, S., Kong, J., Haass, N.K.*, et al.* (2008). Discovery of a selective inhibitor of oncogenic B-Raf kinase with potent antimelanoma activity. Proceedings of the National Academy of Sciences of the United States of America *105*, 3041-3046.

Tsai, W.B., Aiba, I., Lee, S.Y., Feun, L., Savaraj, N., and Kuo, M.T. (2009). Resistance to arginine deiminase treatment in melanoma cells is associated with induced argininosuccinate synthetase expression involving c-Myc/HIF-1 alpha/Sp4. Mol Cancer Ther *8*, 3223-3233.
Tsun, Z.Y., Bar-Peled, L., Chantranupong, L., Zoncu, R., Wang, T., Kim, C., Spooner, E., and Sabatini, D.M. (2013). The Folliculin Tumor Suppressor Is a GAP for the RagC/D GTPases That Signal Amino Acid Levels to mTORC1. Molecular Cell *52*, 495-505.
Uren, J.R., and Lazarus, H. (1979). L-CYST(E)INE REQUIREMENTS OF MALIGNANT-CELLS AND PROGRESS TOWARD DEPLETION THERAPY. Cancer Treatment Reports *63*, 1073-1079.
Uren, J.R., Ragin, R., and Chaykovsky, M. (1978). MODULATION OF CYSTEINE METABOLISM IN MICE - EFFECTS OF PROPARGYLGLYCINE AND L-CYST(E)INE-DEGRADING ENZYMES. Biochem Pharmacol *27*, 2807-2814.
Usatyuk, P.V., Parinandi, N.L., and Natarajan, V. (2006). Redox regulation of 4-hydroxy-2-nonenal-mediated endothelial barrier dysfunction by focal adhesion, adherens, and tight junction proteins. Journal of Biological Chemistry *281*, 35554-35566.
Vakifahmetoglu, H., Olsson, M., and Zhivotovsky, B. (2008). Death through a tragedy: mitotic catastrophe. Cell Death and Differentiation *15*, 1153-1162.
Vandenabeele, P., Galluzzi, L., Vanden Berghe, T., and Kroemer, G. (2010). Molecular mechanisms of necroptosis: an ordered cellular explosion. Nature Reviews Molecular Cell Biology *11*, 700-714.
Vander Heiden, M.G. (2013). Exploiting tumor metabolism: challenges for clinical translation. J Clin Invest *123*, 3648-3651.
Vanderkraaij, A.M.M., Dejonge, H.R., Esterbauer, H., Devente, J., Steinbusch, H.W.M., and Koster, J.F. (1990). CUMENE HYDROPEROXIDE, AN AGENT INDUCING LIPID-PEROXIDATION, AND 4-HYDROXY-2,3-NONENAL, A PEROXIDATION PRODUCT, CAUSE CORONARY VASODILATATION IN PERFUSED RAT HEARTS BY A CYCLIC-NUCLEOTIDE INDEPENDENT MECHANISM. Cardiovascular Research *24*, 144-150.
Vercammen, D., Brouckaert, G., Denecker, G., Van de Craen, M., Declercq, W., Fiers, W., and Vandenabeele, P. (1998). Dual signaling of the Fas receptor: Initiation of both apoptotic and necrotic cell death pathways. Journal of Experimental Medicine *188*, 919-930.
Vojtek, A.B., Hollenberg, S.M., and Cooper, J.A. (1993). MAMMALIAN RAS INTERACTS DIRECTLY WITH THE SERINE THREONINE KINASE RAF. Cell *74*, 205-214.
Wallberg, F., Tenev, T., and Meier, P. (2016). Time-Lapse Imaging of Cell Death. Cold Spring Harbor Protocols *2016*, pdb.prot087395.
Wan, P.T.C., Garnett, M.J., Roe, S.M., Lee, S., Niculescu-Duvaz, D., Good, V.M., Jones, C.M., Marshall, C.J., Springer, C.J., Barford, D*., et al.* (2004). Mechanism of activation of the RAF-ERK signaling pathway by oncogenic mutations of B-RAF. Cell *116*, 855-867.
Wang, D.C., Meng, G., Zheng, M.H., Zhang, Y.H., Chen, A.P., Wu, J.H., and Wei, J.W. (2016). The Glutaminase-1 Inhibitor 968 Enhances Dihydroartemisinin-Mediated Antitumor Efficacy in Hepatocellular Carcinoma Cells. Plos One *11*, 15.
Wang, F., and Permert, J. (2002). Specific amino acid profile in culture media conditioned by human pancreatic cancer cell lines. Pancreatology *2*, 402-406.
Wang, J., Alexander, P., Wu, L.J., Hammer, R., Cleaver, O., and McKnight, S.L. (2009). Dependence of Mouse Embryonic Stem Cells on Threonine Catabolism. Science *325*, 435-439.
Wang, J.-B., Erickson, J.W., Fuji, R., Ramachandran, S., Gao, P., Dinavahi, R., Wilson, K.F., Ambrosio, A.L.B., Dias, S.M.G., Dang, C.V*., et al.* (2010). Targeting Mitochondrial Glutaminase Activity Inhibits Oncogenic Transformation. Cancer Cell *18*, 207-219.
Wang, Z.Y., Shi, X.L., Li, Y.B., Zeng, X., Fan, J.J., Sun, Y., Xian, Z.S., Zhang, G.P., Wang, S.F., Hu, H.F*., et al.* (2014). Involvement of autophagy in recombinant human arginase-induced cell apoptosis and growth inhibition of malignant melanoma cells. Appl Microbiol Biotechnol *98*, 2485-2494.
Warburg, O. (1930). Note on the metabolism of tumours. Biochemische Zeitschrift *228*, 257-258.
Warburg, O. (1956a). ORIGIN OF CANCER CELLS. Science *123*, 309-314.

Warburg, O. (1956b). RESPIRATORY IMPAIRMENT IN CANCER CELLS. Science *124*, 269-270.
Ward, P.S., and Thompson, C.B. (2012). Metabolic Reprogramming: A Cancer Hallmark Even Warburg Did Not Anticipate. Cancer Cell *21*, 297-308.
Wek, R.C., Jackson, B.M., and Hinnebusch, A.G. (1989). JUXTAPOSITION OF DOMAINS HOMOLOGOUS TO PROTEIN-KINASES AND HISTIDYL-TRANSFER RNA-SYNTHETASES IN GCN2 PROTEIN SUGGESTS A MECHANISM FOR COUPLING GCN4 EXPRESSION TO AMINO-ACID AVAILABILITY. Proceedings of the National Academy of Sciences of the United States of America *86*, 4579-4583.
Wellbrock, C., Karasarides, M., and Marais, R. (2004). The RAF proteins take centre stage. Nature Reviews Molecular Cell Biology *5*, 875-885.
Wellen, K.E., Lu, C., Mancuso, A., Lemons, J.M.S., Ryczko, M., Dennis, J.W., Rabinowitz, J.D., Coller, H.A., and Thompson, C.B. (2010). The hexosamine biosynthetic pathway couples growth factor-induced glutamine uptake to glucose metabolism. Genes & Development *24*, 2784-2799.
Wengrod, J., Wang, D., Weiss, S., Zhong, H., Osman, I., and Gardner, L.B. (2015). Phosphorylation of eIF2 alpha triggered by mTORC1 inhibition and PP6C activation is required for autophagy and is aberrant in PP6C-mutated melanoma. Sci Signal *8*, 11.
Winterbourn, C.C. (1995). Toxicity of iron and hydrogen peroxide: The Fenton reaction. Toxicology Letters *82-3*, 969-974.
Wise, D.R., DeBerardinis, R.J., Mancuso, A., Sayed, N., Zhang, X.Y., Pfeiffer, H.K., Nissim, I., Daikhin, E., Yudkoff, M., McMahon, S.B.*, et al.* (2008). Myc regulates a transcriptional program that stimulates mitochondrial glutaminolysis and leads to glutamine addiction. Proceedings of the National Academy of Sciences of the United States of America *105*, 18782-18787.
Wise, D.R., and Thompson, C.B. (2010). Glutamine addiction: a new therapeutic target in cancer. Trends in Biochemical Sciences *35*, 427-433.
Wong-Ekkabut, J., Xu, Z., Triampo, W., Tang, I.M., Tieleman, D.P., and Monticelli, L. (2007). Effect of lipid peroxidation on the properties of lipid bilayers: A molecular dynamics study. Biophysical Journal *93*, 4225-4236.
Wu, G.Y., Flynn, N.E., Flynn, S.P., Jolly, C.A., and Davis, P.K. (1999). Dietary protein or arginine deficiency impairs constitutive and inducible nitric oxide synthesis by young rats. Journal of Nutrition *129*, 1347-1354.
Wullschleger, S., Loewith, R., and Hall, M.N. (2006). TOR signaling in growth and metabolism. Cell *124*, 471-484.
Wymann, M.P., BulgarelliLeva, G., Zvelebil, M.J., Pirola, L., Vanhaesebroeck, B., Waterfield, M.D., and Panayotou, G. (1996). Wortmannin inactivates phosphoinositide 3-kinase by covalent modification of Lys-802, a residue involved in the phosphate transfer reaction. Mol Cell Biol *16*, 1722-1733.
Yagoda, N., Von Rechenberg, M., Zaganjor, E., Bauer, A.J., Yang, W.S., Fridman, D.J., Wolpaw, A.J., Smukste, I., Peltier, J.M., Boniface, J.J.*, et al.* (2007). RAS-RAF-MEK-dependent oxidative cell death involving voltage-dependent anion channels. Nature *447*, 864-868.
Yan, L.J., and Lamb, R.F. (2012). Amino acid sensing and regulation of mTORC1. Seminars in Cell & Developmental Biology *23*, 621-625.
Yan, N., and Meister, A. (1990). AMINO-ACID-SEQUENCE OF RAT-KIDNEY GAMMA-GLUTAMYLCYSTEINE SYNTHETASE. Journal of Biological Chemistry *265*, 1588-1593.
Yang, C.D., Sudderth, J., Dang, T.Y., Bachoo, R.G., McDonald, J.G., and DeBerardinis, R.J. (2009). Glioblastoma Cells Require Glutamate Dehydrogenase to Survive Impairments of Glucose Metabolism or Akt Signaling. Cancer Research *69*, 7986-7993.
Yang, M., and Vousden, K.H. (2016). Serine and one-carbon metabolism in cancer. Nat Rev Cancer *16*, 650-662.
Yang, W.S., Sriramaratnam, R., Welsch, M.E., Shimada, K., Skouta, R., Viswanathan, V.S., Cheah, J.H., Clemons, P.A., Shamji, A.F., Clish, C.B.*, et al.* (2014). Regulation of ferroptotic cancer cell death by GPX4. Cell *156*, 317-331.

Yang, W.S., and Stockwell, B.R. (2008). Synthetic Lethal Screening Identifies Compounds Activating Iron-Dependent, Nonapoptotic Cell Death in Oncogenic-RAS-Harboring Cancer Cells. Chemistry and Biology *15*, 234-245.
Yang, W.S., and Stockwell, B.R. (2016). Ferroptosis: Death by Lipid Peroxidation. Trends in Cell Biology *26*, 165-176.
Ye, J.B., Palm, W., Peng, M., King, B., Lindsten, T., Li, M.O., Koumenis, C., and Thompson, C.B. (2015). GCN2 sustains mTORC1 suppression upon amino acid deprivation by inducing Sestrin2. Genes & Development *29*, 2331-2336.
Yeh, T.C., Marsh, V., Bernat, B.A., Ballard, J., Colwell, H., Evans, R.J., Parry, J., Smith, D., Brandhuber, B.J., Gross, S.*, et al.* (2007). Biological characterization of ARRY-142886 (AZD6244), a potent, highly selective mitogen-activated protein kinase kinase 1/2 inhibitor. Clinical Cancer Research *13*, 1576-1583.
Yi, P., Melnyk, S., Pogribna, M., Pogribny, I.P., Hines, R.J., and James, S.J. (2000). Increase in plasma homocysteine associated with parallel increases in plasma S-adenosylhomocysteine and lymphocyte DNA hypomethylation. Journal of Biological Chemistry *275*, 29318-29323.
Yi, X.M., Tesmer, V.M., Savre-Train, I., Shay, J.W., and Wright, W.E. (1999). Both transcriptional and posttranscriptional mechanisms regulate human telomerase template RNA levels. Mol Cell Biol *19*, 3989-3997.
Yin, H.Y., Xu, L.B., and Porter, N.A. (2011). Free Radical Lipid Peroxidation: Mechanisms and Analysis. Chem Rev *111*, 5944-5972.
Ying, H.Q., Kimmelman, A.C., Lyssiotis, C.A., Hua, S.J., Chu, G.C., Fletcher-Sananikone, E., Locasale, J.W., Son, J., Zhang, H.L., Coloff, J.L.*, et al.* (2012). Oncogenic Kras Maintains Pancreatic Tumors through Regulation of Anabolic Glucose Metabolism. Cell *149*, 656-670.
Yoo, M.H., Gu, X.L., Xu, X.M., Kim, J.Y., Carlson, B.A., Patterson, A.D., Cai, H.B., Gladyshev, V.N., and Hatfield, D.L. (2010). Delineating the Role of Glutathione Peroxidase 4 in Protecting Cells Against Lipid Hydroperoxide Damage and in Alzheimer's Disease. Antioxidants & Redox Signaling *12*, 819-827.
Yoon, S., and Seger, R. (2006). The extracellular signal-regulated kinase: Multiple substrates regulate diverse cellular functions. Growth Factors *24*, 21-44.
Yu, L., McPhee, C.K., Zheng, L.X., Mardones, G.A., Rong, Y.G., Peng, J.Y., Mi, N., Zhao, Y., Liu, Z.H., Wan, F.Y.*, et al.* (2010). Termination of autophagy and reformation of lysosomes regulated by mTOR. Nature *465*, 942-U911.
Yuan, H., Li, X.M., Zhang, X.Y., Kang, R., and Tang, D.L. (2016). Identification of ACSL4 as a biomarker and contributor of ferroptosis. Biochemical and Biophysical Research Communications *478*, 1338-1343.
Yuan, T.L., and Cantley, L.C. (2008). PI3K pathway alterations in cancer: variations on a theme. Oncogene *27*, 5497-5510.
Yun, C.H., Boggon, T.J., Li, Y.Q., Woo, M.S., Greulich, H., Meyerson, M., and Eck, M.J. (2007). Structures of lung cancer-derived EGFR mutants and inhibitor complexes: Mechanism of activation and insights into differential inhibitor sensitivity. Cancer Cell *11*, 217-227.
Zhang, D.-W., Shao, J., Lin, J., Zhang, N., Lu, B.-J., Lin, S.-C., Dong, M.-Q., and Han, J. (2009). RIP3, an Energy Metabolism Regulator That Switches TNF-Induced Cell Death from Apoptosis to Necrosis. Science *325*, 332-336.
Zhang, Y., Gao, X.S., Saucedo, L.J., Ru, B.G., Edgar, B.A., and Pan, D.J. (2003). Rheb is a direct target of the tuberous sclerosis tumour suppressor proteins. Nature Cell Biology *5*, 578-581.
Zhao, J., Jitkaew, S., Cai, Z.Y., Choksi, S., Li, Q.N., Luo, J., and Liu, Z.G. (2012). Mixed lineage kinase domain-like is a key receptor interacting protein 3 downstream component of TNF-induced necrosis. Proceedings of the National Academy of Sciences of the United States of America *109*, 5322-5327.
Zhao, L., and Vogt, P.K. (2008a). Class IPI3K in oncogenic cellular transformation. Oncogene *27*, 5486-5496.

Zhao, L., and Vogt, P.K. (2008b). Helical domain and kinase domain mutations in p110 alpha of phosphatidylinositol 3-kinase induce gain of function by different mechanisms. Proceedings of the National Academy of Sciences of the United States of America *105*, 2652-2657.
Zhao, Y., Butler, E.B., and Tan, M. (2013). Targeting cellular metabolism to improve cancer therapeutics. Cell Death & Disease *4*, 10.
Zilka, O., Shah, R., Li, B., Angeli, J.P.F., Griesser, M., Conrad, M., and Pratt, D.A. (2017). On the Mechanism of Cytoprotection by Ferrostatin-1 and Liproxstatin-1 and the Role of Lipid Peroxidation in Ferroptotic Cell Death. ACS Central Sci *3*, 232-243.
Zoncu, R., Efeyan, A., and Sabatini, D.M. (2011). mTOR: from growth signal integration to cancer, diabetes and ageing. Nature Reviews Molecular Cell Biology *12*, 21-35.
Zou, H., Li, Y.C., Liu, H.S., and Wang, X.D. (1999). An APAF-1 center dot cytochrome c multimeric complex is a functional apoptosome that activates procaspase-9. Journal of Biological Chemistry *274*, 11549-11556.

Appendix I Publication

Cell Reports

Report

Oncogene-Selective Sensitivity to Synchronous Cell Death following Modulation of the Amino Acid Nutrient Cystine

Graphical Abstract

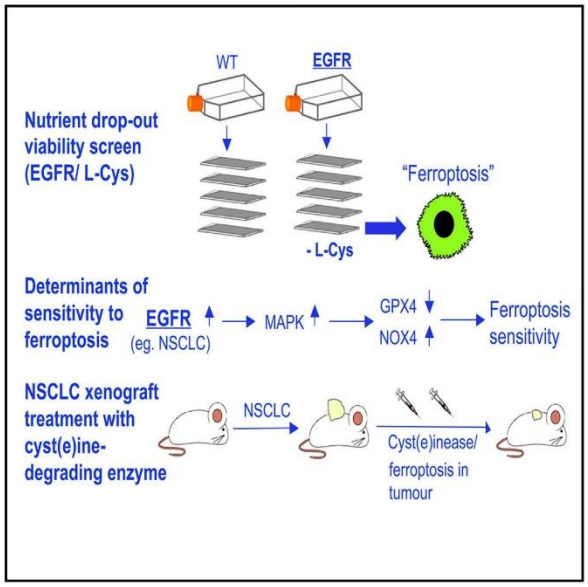

Authors

Ioannis Poursaitidis, Xiaomeng Wang, Thomas Crighton, ..., Scott W. Rowlinson, Everett Stone, Richard F. Lamb

Correspondence

lambr@hope.ac.uk

In Brief

Poursaitidis et al. show that EGFR and BRAF mutant cells are sensitive to ferroptosis. Sensitivity was related to activation of MAPK signaling and the generation and release of hydrogen peroxide. To show that this sensitivity can be exploited therapeutically, growth of an EGFR mutant NSCLC xenograft was inhibited by a cyst(e)ine-degrading enzyme.

Highlights

- A nutrient depletion screen revealed a selective role for cystine in promoting viability
- Cystine was shown to promote viability by preventing ferroptosis
- Sensitivity to depletion of cystine was related to activation of MAPK
- Depletion of cystine inhibited tumor growth in a NSCLC xenograft model

Poursaitidis et al., 2017, Cell Reports *18*, 2547–2556
March 14, 2017
http://dx.doi.org/10.1016/j.celrep.2017.02.054

CellPress

Cell Reports
Report

Oncogene-Selective Sensitivity to Synchronous Cell Death following Modulation of the Amino Acid Nutrient Cystine

Ioannis Poursaitidis,[2,9] Xiaomeng Wang,[2,9] Thomas Crighton,[2] Christiaan Labuschagne,[3] David Mason,[4] Shira L. Cramer,[5] Kendra Triplett,[5] Rajat Roy,[6] Olivier E. Pardo,[6] Michael J. Seckl,[6] Scott W. Rowlinson,[7] Everett Stone,[8] and Richard F. Lamb[1,10,*]

[1]School of Health Sciences, Liverpool Hope University, Hope Park Campus, Liverpool L16 9JD, UK
[2]Department of Molecular and Clinical Cancer Medicine, University of Liverpool North West Cancer Research Centre, University of Liverpool, 200 London Road, Liverpool L69 7ZB, UK
[3]Cancer Research UK Beatson Institute, Switchback Road, Bearsden, Glasgow G61 1BD, UK
[4]Centre for Cell Imaging, Institute of Integrative Biology, University of Liverpool, Biosciences Building, Crown Street, Liverpool L69 7ZB, UK
[5]Department of Chemical Engineering, The University of Texas at Austin, Austin, TX 78712, USA
[6]Division of Cancer CRUK Laboratories, 1st Floor ICTEM Building, Hammersmith Hospital Campus of Imperial College London, Du Cane Road, London W120NN, UK
[7]Aeglea BioTherapeutics, Austin, TX 78746, USA
[8]Department of Molecular Biosciences, The University of Texas at Austin, Austin, TX 78712, USA
[9]Co-first author
[10]Lead Contact
*Correspondence: lambr@hope.ac.uk
http://dx.doi.org/10.1016/j.celrep.2017.02.054

SUMMARY

Cancer cells reprogram their metabolism, altering both uptake and utilization of extracellular nutrients. We individually depleted amino acid nutrients from isogenic cells expressing commonly activated oncogenes to identify correspondences between nutrient supply and viability. In HME (human mammary epithelial) cells, deprivation of cystine led to increased cell death in cells expressing an activated epidermal growth factor receptor (EGFR) mutant. Cell death occurred via synchronous ferroptosis, with generation of reactive oxygen species (ROS). Hydrogen peroxide promoted cell death, as both catalase and inhibition of NADPH oxidase 4 (NOX4) blocked ferroptosis. Blockade of EGFR or mitogen-activated protein kinase (MAPK) signaling similarly protected cells from ferroptosis, whereas treatment of xenografts derived from EGFR mutant non-small-cell lung cancer (NSCLC) with a cystine-depleting enzyme inhibited tumor growth in mice. Collectively, our results identify a potentially exploitable sensitization of some EGFR/MAPK-driven tumors to ferroptosis following cystine depletion.

INTRODUCTION

Synthetic lethal screens have led to the identification of specific cancer cell vulnerabilities (Barbie et al., 2009; Possik et al., 2014; Scholl et al., 2009). One such vulnerability has previously been exploited therapeutically in acute lymphoblastic leukemia (ALL), where leukemic cells lacking asparagine synthase are known to require the amino acid asparagine and apoptose following administration of asparaginase (Holleman et al., 2003; Tallal et al., 1970). Overall amino acid abundance itself may be higher in cancerous tissue, suggesting an increased need for amino acids in some tumors (Hirayama et al., 2009; Kami et al., 2013). In pancreatic ductal adenocarcinoma (PDAC), KRAS is thought to induce a genetic program that favors metabolism of glutamine, rendering these cells particularly sensitive to glutamine withdrawal (Son et al., 2013). Some tumor cell lines (Scott et al., 2000) and primary tumors (Gonzalez and Byus, 1991) require exogenous arginine, indicating some selectivity in amino acid requirements. Here, we have explored the extracellular amino acid nutrient requirements of cells gene edited to introduce common oncogenic mutations. We identify a selective sensitivity to synchronous cell death by ferroptosis following deprivation of the amino acid nutrient cystine. Sensitization was found to be related to elevated mitogen-activated protein kinase (MAPK) signaling, with synchronous cell death involving hydrogen peroxide generation and release. Finally, we show that enzymatic cystine deprivation in vivo results in an inhibition of tumor growth in an EGFR mutant NSCLC xenograft model, suggesting that, by promoting ferroptosis, cystine depletion provides therapeutic benefit in some tumors.

RESULTS

EGFR Mutant HME Cells Undergo Cell Death when Deprived of the Amino Acid Nutrient Cystine

Human mammary epithelial (HME) cells were gene edited to introduce common oncogenic driver mutations (epidermal

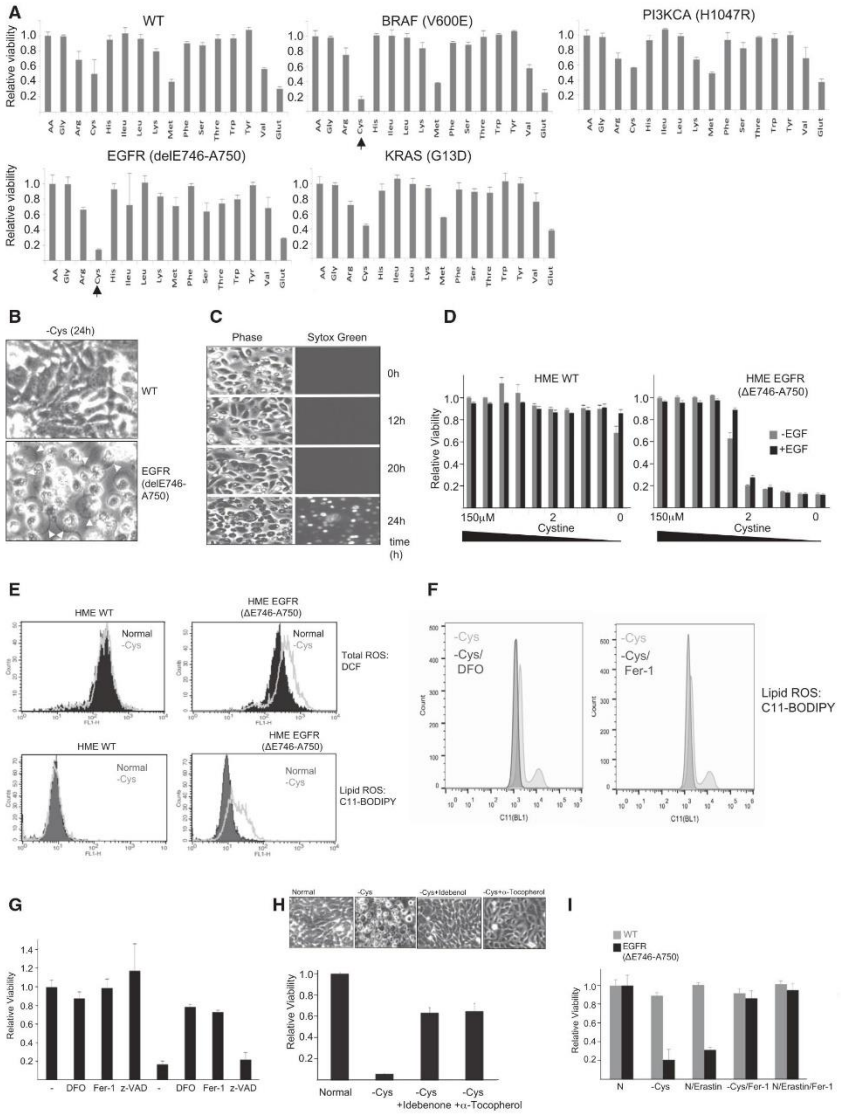

Figure 1. Deprivation of Cystine Induces Selective Cell Death by Ferroptosis in EGFR Mutant HME Cells

(A) Cell viability screen of HME cell lines deprived of individual amino acids for 72 hr. Histograms represent the average viability ± SD of three biological replicates relative to complete media assigned a value of 1 (+AA).

(B) Phase contrast micrographs of wild-type (WT) and EGFR (delE746-A750) HME cells deprived of cystine for 24 hr. Arrowheads indicate membrane extrusions.

(C) Time-lapse phase contrast (left) and Sytox Green (right) micrographs of live EGFR (delE746-A750) cells deprived of cystine for various times up to 24 hr.

(legend continued on next page)

growth factor receptor [EGFR] [delE746-A750], KRAS [G13D], BRAF [V600E], and PIK3CA [H1047R]) in an otherwise diploid genetic background (Di Nicolantonio et al., 2008). Following culture in media deficient in specific amino acids, we measured cell viability. All lines deprived of L-cystine (cystine) exhibited some loss of viability ranging from 40% to >80%. However, EGFR and BRAF mutant HME cells were especially sensitive, with viability inhibited by >80% (Figure 1A). Cystine deprivation induced a widespread loss of viability in EGFR mutant, but not wild-type HME, cells, with the majority of cells exhibiting a swollen or burst morphology (Figure 1B).

Next, we monitored EGFR mutant HME cells deprived of cystine by video time-lapse microscopy and observed rapid and synchronous cell swelling/bursting (Figure 1C; Movie S1). Sytox Green, a cell-impermeant nuclear stain, synchronously entered cells after cystine depletion (Figure 1C), indicating loss of plasma membrane integrity at <2 μM cystine (Figure 1D). Death was reversible upon re-supplementation of cystine for up to 10 hr but declined progressively thereafter and was not prevented by addition of D-cystine (Figure S1A).

Cell Death in Cystine-Deprived EGFR Mutant HME Cells Exhibits Hallmarks of Ferroptosis

This type of death resembled ferroptosis, an iron-dependent non-apoptotic cell death (Dixon et al., 2012). Because lipid reactive oxygen species (ROS) accumulation characterizes ferroptosis (Dixon et al., 2012), we measured ROS. Fluorescence-activated cell sorting (FACS) analysis indicated increased ROS accumulation in EGFR mutant HME cells following cystine deprivation (Figure 1E). EGFR mutant HME cells treated with known ferroptosis inhibitors inhibited lipid ROS generation (Figure 1F) and protected EGFR mutant (and BRAF mutant; Figure S1B) cells from cell death (Figure 1G), as did treatment with two other antioxidants (Figure 1H). Finally, erastin, an inhibitor of the system x_c^--cystine/glutamate antiporter (Dixon et al., 2012), also induced selective loss of viability in EGFR mutant cells (Figure 1H). Collectively, these data indicate that cell death in EGFR mutant cells occurs by ferroptosis.

MAPK Signaling Sensitizes EGFR Mutant Cells to Cell Death following Cystine Deprivation

EGFR activation results in activation of downstream signaling cascades (Pines et al., 2010). Ferroptosis had previously been shown to require MAPK signaling (Yagoda et al., 2007; Dixon et al., 2012). Treatment of EGFR mutant cells for >24 hr with EGFR or MAPK (MEK and ERK1/2) inhibitors inhibited EGFR and MAPK signaling (Figures 2A and S2A), restored normal adherens junction formation and gap junctional intercellular communication (GJIC) (Figures 2B and 2C), and rescued cell viability following cystine withdrawal (Figures 2D and S2B). Likewise, EGFR and MAPK inhibition in EGFR mutant cells inhibited ROS generation (Figures 2E, S2C, and S2D).

Cystine Promotes Viability in EGFR Mutant HME Cells via a Glutathione-Independent Mechanism

HME cells might resist ferroptosis by maintaining intracellular levels either of cystine or glutathione, the major cystine-derived antioxidant. To address the former possibility, we deprived cells of cystine and measured activation of GCN2, a sensor of amino acid depletion (Hinnebusch, 2005). However, in both wild-type and EGFR mutant HME cells, GCN2 was equivalently activated following cystine deprivation (Figure 3A). Basal cystine levels were also equivalent and declined similarly in wild-type and EGFR mutant cells following extracellular cystine depletion (Figure S3A). Recent data have suggested a role for glutaminolysis in promoting ferroptosis (Gao et al., 2015). However, both wild-type and EGFR mutant HME cells contained similar steady-state intracellular levels of glutamine that were largely unaltered by deprivation of cystine (Figure S3A). Similarly, total levels of glutathione declined equivalently in wild-type and EGFR mutant HME cells following cystine deprivation (Figure 3B). However, Iressa-treated EGFR mutant cells accumulated more oxidized glutathione (GSSG) in comparison to untreated EGFR mutant HME cells following deprivation of cystine, suggesting that EGFR inhibition increased ROS detoxification (Figure 3C). Surprisingly, an inhibitor of glutathione synthesis (buthionine sulfoximine [BSO]), although also depleting glutathione levels, did not induce cell death (Figure 3D) nor increase ROS in EGFR mutant HME cells, unlike deprivation of cystine (Figure S3B). We therefore asked whether short-term deprivation of cystine, or inhibition of cystine import, acted synergistically with glutathione depletion to induce cell death. Indeed, short-term deprivation of cystine or treatment with inhibitors of the system x_c^--antiporter induced significantly increased cell death when combined with glutathione depletion (Figure 3E). Treatment with auranofin, an inhibitor of the thioredoxin reductase/thioredoxin (TRX) system (Gromer et al., 1998) implicated in reduction of cystine to cysteine (Mandal et al., 2010; Pader et al., 2014), also synergized with glutathione depletion to promote loss of viability and lipid ROS induction (Figures S3B and S3C). Thus, EGFR mutant cells

(D) Cell viability following titration of cystine in WT and EGFR (delE746-A750) HME cells. Histogram represents the average viability ± SD of cells cultured in various concentrations of cystine ± EGF, relative to complete media (150 μM cystine; assigned an arbitrary value of 1).
(E) ROS in WT HME and EGFR (delE746-A750). (Upper panels) Total ROS measured using CMDCFDA (DCF) is shown; (lower panels) lipid ROS measured using C11 BODIPY 581/591 (C11-BODIPY) is shown. Dark traces, cells cultured in normal media for 12 hr; light traces, cells cultured in media lacking cystine for 12 hr.
(F) Lipid ROS in WT and EGFR (delE746-A750) HME cells. Dark traces, cells cultured in media lacking cystine in the presence of deferoxamine (DFO; 100 μM) or ferrostatin (Fer-1; 2 μM) for 12 hr; light traces, cells cultured in media lacking cystine for 12 hr.
(G) Cell viability of EGFR (delE746-A750) HME cells. Histogram is average viability ± SD cells cultured in normal media (left four bars, untreated [−] assigned an arbitrary value of 1) or media lacking cystine for 24 hr (right four bars) in the presence or absence of DFO, Fer-1, and z-VAD-fMK.
(H) Cell viability (bottom histogram) and phase-contrast microscopy (upper panels) of EGFR (delE746-A750) HME cells. Histogram is average viability ± SD of three biological replicates cultured in normal media (assigned an arbitrary value of 1) or media lacking cystine for 24 hr in the presence or absence of ROS scavengers idebenone and α-tocopherol.
(I) Cell viability of WT (gray bars) and EGFR (delE746-A750; black bars) HME cells. Histogram represents the average viability ± SD cells cultured in normal media or media lacking cystine for 24 hr in the presence or absence of erastin and Fer-1.

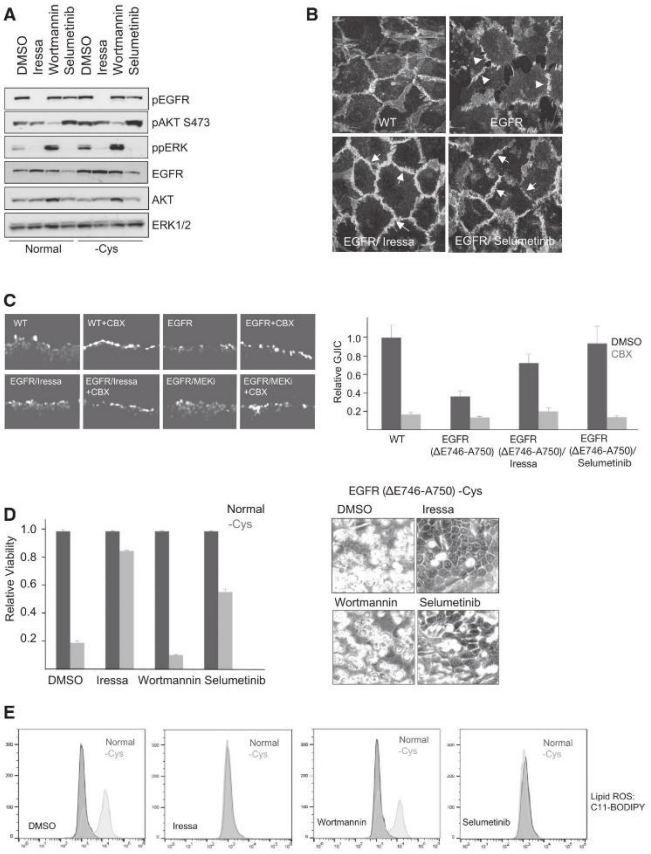

Figure 2. Active MAPK Signaling Promotes Sensitivity to Cystine Deprivation

(A) Immunoblots of EGFR (delE746-A750) HME cell lysates probed to detect phosphorylated EGFR, ERK, and AKT from cells cultured in normal media (normal) or media lacking cystine for 12 hr (−Cys) in the presence or absence of inhibitors added for a total of 30 hr.

(B) Confocal micrographs of adherens junctions stained with β-catenin antibody of WT or EGFR (delE746-A750) HME cells treated with vehicle (EGFR) or following treatment with inhibitors for 30 hr. Arrows indicate linear staining for β-catenin at intercellular junctions; arrowheads indicate presence of discontinuous adherens junctions.

(C) (Left panels) Fluorescence micrographs of GJIC measured by lucifer yellow infiltration in WT, EGFR (delE746-A750), Iressa-treated EGFR (delE746-A750; EGFR/Iressa), and selumetinib-treated EGFR (delE746-A750; EGFR/MEKi) in the presence or absence of carbenoxolone (CBX). (Right histogram) Quantification of GJIC is shown. Each condition was analyzed in six random 20× fields in three biological replicates with the values shown representing the mean and SEM and expressed relative to GJIC in WT HME cells assigned an arbitrary value of 1. Light bars represent GJIC in the presence of CBX.

(D) Cell viability (left histogram) and phase-contrast micrographs (right panels) of EGFR (delE746-A750) HME cells treated with inhibitors. Histogram is viability ± SD of cells cultured in normal media (dark bars) or media lacking cystine for 16 hr (light bars) in the presence or absence of inhibitors. Results were expressed for each condition separately, with viability in normal media assigned the arbitrary value of 1.

(E) FACS analyses of lipid ROS in EGFR (delE746-A750) cells following treatment with inhibitors. Dark traces, cells cultured in normal media; light traces, cells cultured in media lacking cystine for 12 hr.

oxidize less glutathione during cystine deprivation, contributing to ROS accumulation, whereas intracellular cysteine appears to play an additional role, aside from glutathione synthesis, in counteracting ROS and ferroptosis.

GPX4 Is Downregulated in EGFR Mutant HME Cells via MAPK Signaling and Modulates Sensitivity to Cell Death upon Cystine Deprivation

Glutathione peroxidases (GPXs) are good candidates for mediating sensitivity to ferroptosis. GPX4 has previously been implicated in ferroptosis (Friedmann Angeli et al., 2014; Yang et al., 2014), whereas GPX4 is induced following treatment with a BRAF inhibitor (Parmenter et al., 2014). By immunoblotting, GPX4, but not GPX1, expression was upregulated following either EGFR or MAPK (MEK and ERK; Figure S3D) inhibition, whereas GPX2 was not expressed in these cells (Figure 3E) and GPX3 is a secreted GPX expressed in the kidney (Maser et al., 1994). Suppression of GPX4 strongly promoted cell death in both wild-type (Figure 3G) and Iressa-treated EGFR mutant cells (Figure 3H). Lipid ROS similarly increased after suppression of GPX4 (Figure 3I). Thus, downregulation of GPX4 in EGFR mutant HME cells conferred increased sensitivity to ferroptosis following cystine deprivation. To determine whether loss of viability was related to low levels of GPX4, we expressed Flag-GPX4 in EGFR mutant cells. Indeed, ectopic expression of GPX4 significantly increased viability following deprivation of cystine (Figure 3J). Thus, downregulation of GPX4 plays a key role in sensitizing EGFR mutant HME cells to ferroptosis.

Synchronous Cell Death in EGFR Mutant HME Cells Involves Generation and Release of Hydrogen Peroxide

Hydrogen peroxide is implicated in synchronous ferroptosis in kidney tubule epithelia (Linkermann et al., 2014). Media

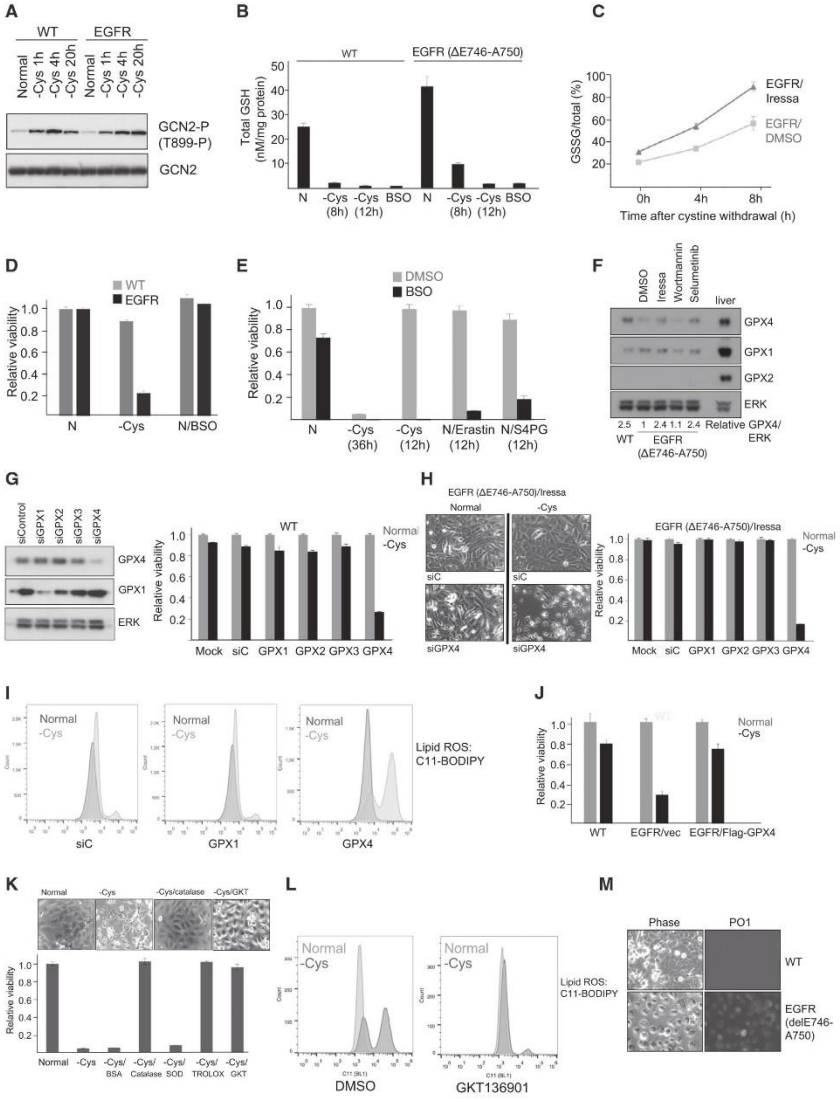

Figure 3. Involvement of Intracellular Cysteine, GPX4, and Hydrogen Peroxide in Sensitivity to Ferroptosis

(A) Immunoblots of cell lysates probed with an antibody to active GCN2 (T899-P). Cells were cultured in normal media for 24 hr (normal) or media lacking cystine for various times.

(B) Histogram of total glutathione levels in WT and EGFR (delE746-A750) cells cultured in normal media for 12 hr (N) or media lacking cystine for 8 or 12 hr. As a positive control, BSO was added to cells for 12 hr to deplete the glutathione pool by inhibiting glutathione synthesis.

(C) Time course of glutathione oxidation (GSSG/total) in EGFR (delE746-A750) treated with vehicle (EGFR/DMSO) or Iressa for 30 hr (EGFR/Iressa). Cells were cultured in media lacking cystine for 4 or 8 hr. Chart displays the average ratio of oxidized glutathione (GSSG) to total glutathione (GSH+GSSG) of three biological replicates.

(legend continued on next page)

containing soluble catalase similarly rescued viability of EGFR mutant HME cells (Figure 3K). Hydrogen peroxide is produced by NADPH oxidase 4 (NOX4) (Takac et al., 2011). A NOX4 inhibitor (GKT136901; Laleu et al., 2010) also rescued viability, to the same degree as addition of catalase (Figure 3K), and inhibited lipid ROS generation (Figure 3L). NOX4 expression was also increased in EGFR mutant HME cells and downregulated by both EGFR and MAPK inhibition (Figure S3E). Finally, increased accumulation of hydrogen peroxide was detected following deprivation of cystine in EGFR mutant cells (Dickinson et al., 2010; Figure 3M). Thus, hydrogen peroxide contributes to loss of viability of EGFR mutant HME cells deprived of cystine.

NSCLC Tumor Cell Lines Exhibit a Targetable Sensitivity to Ferroptosis

Mutations in the EGF receptor are found in non-small-cell lung cancers (NSCLCs) (Pao et al., 2004) that are sensitive to tyrosine kinase inhibitors (TKIs) (Paez et al., 2004). We removed cystine from NSCLC cell lines and measured viability and MAPK activation. Of nine NSCLC cell lines tested, three with the highest MAPK signaling (Figure S4A) demonstrated significant loss of viability following withdrawal of cystine (Figures 4A and S4B). In H3255 cells (EGFR L858R mutant), sensitivity was reversed by either EGFR or MAPK inhibition, whereas in Calu-6 cells (KRAS Q61K mutant), sensitivity was reversed by MAPK, but not EGFR, inhibition (Figure S4C). Thus, in NSCLC cell lines, the magnitude of MAPK activation is an important determinant in sensitization to ferroptosis, rather than the nature of the specific oncogenic driver that promotes MAPK signaling. In NCI-NH1650 cells (EGFR delE746-A750), viability was restored by addition of either α-tocopherol, the ferroptosis inhibitor Fer-1 (Figure 4B), or Iressa (data not shown) following cystine depletion, indicating that ferroptosis and EGFR signaling were responsible for loss of viability. Surprisingly, however, MEK inhibition in these cells did not rescue viability following cystine depletion (data not shown). Thus, MAPK activation may not invariably promote sensitivity to ferroptosis, and other unknown EGFR-dependent signaling pathway(s) can substitute.

Survival after treatment with TKIs in NSCLC is typically less than 1 year, with patients developing secondary EGFR mutations (Stewart et al., 2015). We therefore sought to determine whether EGFR mutant NSCLC cells might be responsive to low levels of cystine, potentially offering additional therapeutic options utilizing a novel cystine/cysteine-degrading enzyme (cyst(e)inase; AECase) engineered from cystathionine-γ-lyase (Cramer et al., 2017). Addition of AECase reduced viability in both HME delE746-A750 EGFR or NCI-NH1650 cells (Figures 4C and 4D) and induced widespread uptake of Sytox Green (Figure 4D; Movie S2). Finally, we injected mice bearing established NCI-NH1650 xenografts with AECase. Mirroring the in vitro results, tumor growth was significantly retarded in AECase-treated groups ($p = 0.0001$; Figure 4E). AECase-treated mice were also found to upregulate expression of COX2 (Figure 4F), indicating that they had experienced cystine depletion and initiated ferroptosis within the tumor (Yang et al., 2014). Thus, inhibition of tumor growth can be achieved in tumors sensitive to ferroptosis by enzymatic degradation of cystine/cysteine in vivo.

DISCUSSION

Cell death by ferroptosis has been implicated in diverse processes (Yang and Stockwell, 2016). Previous data indicated that ferroptosis could be induced preferentially in cells overexpressing mutant RAS oncoproteins (Dixon et al., 2012; Dolma et al., 2003; Yang and Stockwell, 2008) and in some sensitive cell lines could be blocked by MAPK inhibition (Yagoda et al., 2007).

(D) Cell viability of WT (light bars) or EGFR (delE746-A750; dark bars) HME cells. Histogram represents the average viability ± SD of cells cultured for 24 hr in normal media (N), normal media containing 200 μM BSO (N/BSO), or media lacking cystine (−Cys).
(E) Cell viability of EGFR (delE746-A750) pre-treated for 18 hr with DMSO vehicle (light bars) or 200 μM BSO (dark bars) in normal media (N), in normal media containing erastin (N/Erastin), or S4PG (N/S4PG) for 12 hr or following removal of cystine for 36 or 12 hr. Histogram represents the average viability ± SD of cells cultured in normal media (assigned a value of 1).
(F) Immunoblots of WT and EGFR (delE746-A750) cell lysates probed for GPX4, GPX1, GPX2, and ERK in the presence or absence of inhibitors. Relative GPX4/ERK was calculated using ImageJ from scanned autoradiographs of three biological replicates, with the ratio in EGFR (delE746-A750) cells assigned a value of 1.
(G) (Left panels) Immunoblots of WT HME lysates probed for GPX4, GPX1, and ERK1/2. (Right) Histogram of cell viability of HME cells cultured in normal media (light bars) or media lacking cystine (dark bars) for 24 hr. Histogram represents the average viability ± SD following knockdown GPX1–4. Results were expressed for each condition separately, with viability in normal media assigned a value of 1.
(H) (Left panels) Phase-contrast micrographs of EGFR (delE746-A750) HME cells following transfection with control (siC) or GPX4 small interfering RNAs (siRNAs) (siGPX4) and treated with Iressa for 30 hr followed by culture in normal media or media lacking cystine for 24 hr. (Right) Histogram is viability ± SD after knockdown of GPX1–4 in Iressa-treated EGFR (delE746-A750) cells. Viability of cells cultured in normal media (light bars) or media lacking cystine (dark bars) were determined. Results were expressed for each condition separately, with viability in normal media assigned the arbitrary value of 1.
(I) FACS analyses of lipid ROS in WT HME cells following knockdown of GPX1 and GPX4. Dark traces, cells cultured in normal media; light traces, cells cultured in media lacking cystine for 12 hr.
(J) Histogram is shown representing the average viability ± SD following overexpression of Flag-GPX4 (Mannes et al., 2011) in EGFR (delE746-A750) cells. Viability of WT HME cells or vector- or GPX4-transfected EGFR (delE746-A750) cells cultured in normal media (light bars) or media lacking cystine (dark bars) for 16 hr is shown. Results were expressed for each condition separately, with viability in normal media assigned a value of 1.
(K) (Top panels) Phase-contrast micrographs of EGFR (delE746-A750) HME cells in normal media or media deprived of cystine alone or containing catalase or GKT136901. (Bottom) Histogram representing the average viability ± SD of EGFR (delE746-A750) HME cells cultured for 24 hr in normal media (normal; assigned a value of 1) or media lacking cystine alone (−Cys) or with BSA, catalase, superoxide dismutase (SOD), Trolox, or GKT136901 added is shown.
(L) FACS analyses of lipid ROS in EGFR (delE746-A750) HME cells following treatment with the NOX4 inhibitor GKT136901. Dark traces, cells cultured in media lacking cystine; light traces, cells cultured in normal media.
(M) Live images of hydrogen peroxide detected with PO1. (Left) Phase-contrast images of WT and EGFR (delE746-A750) cells deprived of cystine for 24 hr and incubated with PO1 (right panels) are shown.

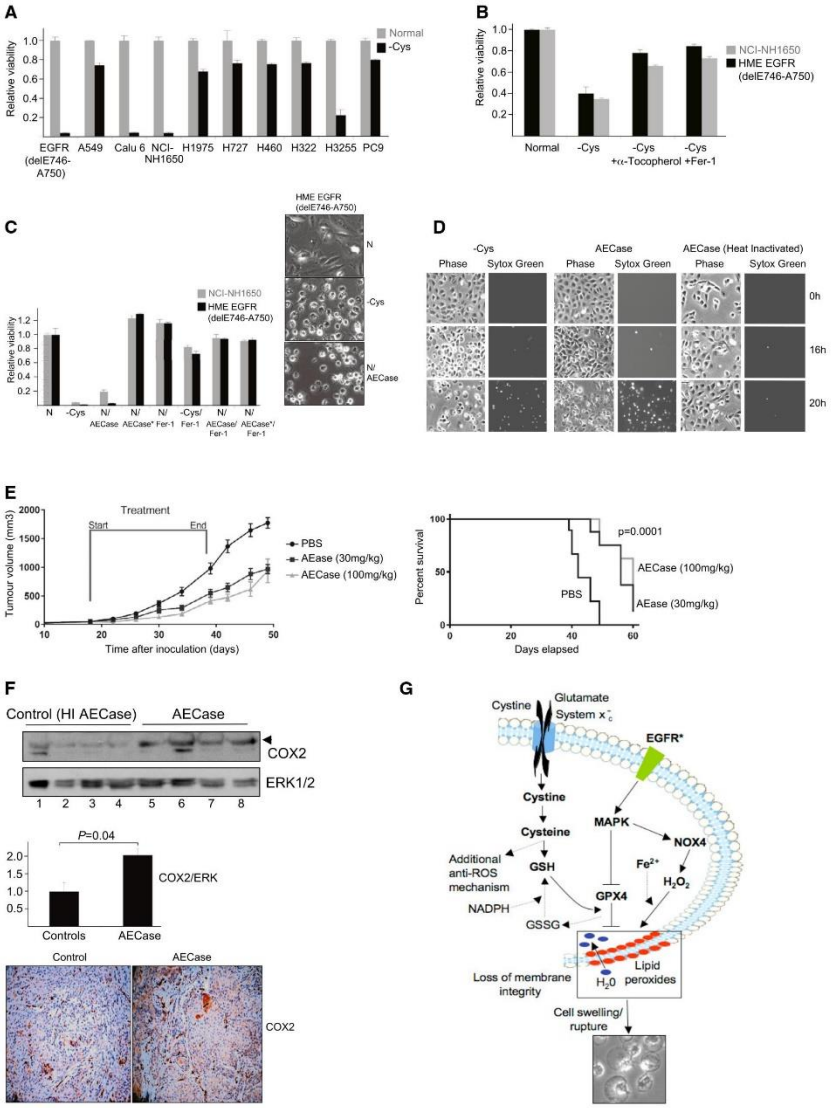

Figure 4. Ferroptosis Is Induced in Some NSCLC Cell Lines and Inhibits Tumor Growth

(A) Histogram of viability ± SD of EGFR (delE746-A750) HME and NSCLC cell lines cultured for 72 hr in normal media (light bars) or media lacking cystine (dark bars). Results were expressed for each cell line separately, with viability in normal media assigned a value of 1.

(B) Histogram representing the average viability ± SD of EGFR (delE746-A750) HME (dark bars) or NCI-NH1650 (light bars) cultured for 72 hr in normal media (N), normal media containing ferrostatin (N/Fer-1), media lacking cystine (−Cys), or media lacking cystine in the presence of α-tocopherol or Fer-1. Results were expressed for each cell line separately, with viability in normal media assigned a value of 1.

(legend continued on next page)

We identify here a selective cell death of EGFR mutant cells deprived of the amino acid cystine. Death was associated with synchronous loss of plasma membrane integrity. By a variety of criteria, this mode of cell death is ferroptosis. In our model (Figure 4G), active MAPK signaling downstream of active EGFR can sensitize cells to ferroptosis upon cystine depletion. Sensitization involves both impaired detoxification of lipid peroxides, due to reduced expression of GPX4, and generation of hydrogen peroxide, via NOX4. A major consequence of lipid peroxidation is loss of impermeability to water (Lis et al., 2011; Wong-Ekkabut et al., 2007), providing an explanation for the characteristic cell swelling and rupture we observe.

Sensitivity to induction of ferroptosis or cystine deprivation is likely to be modulated by additional, and possibly MAPK-independent, mechanisms, such as the utilization of the sulfur-containing amino acid methionine via the transsulfuration pathway (Hayano et al., 2016). Our results suggest, however, the possibility of exploiting ferroptosis sensitivity in a translational manner. Tumors with sustained MAPK activation, as found in NSCLC, are likely to respond to cystine depletion in vivo by inducing ferroptosis. Our results indicate that an enzymatic approach (Cramer et al., 2017) may be effective in reducing cystine levels in vivo, inducing ferroptosis. Collectively, our work indicates that it might therefore be possible both to identify tumors exhibiting increased sensitivity to ferroptosis and to treat them via cycles of cystine depletion.

EXPERIMENTAL PROCEDURES

Cell Culture and Treatments

The hTERT-HME cell lines were a kind gift from Prof. Alberto Bardelli (Institute for Cancer Research and Treatment, IRCC). Cells were grown in DMEM media as described (Di Nicolantonio et al., 2008). To deprive individual amino acids, cells were washed once in DMEM media lacking all amino acids (−AA) and switched to specific amino-acid-free media. DMEM media used for deprivation were made from powdered AA-free DMEM (US Biological), with 10% dialyzed fetal bovine serum (FBS) and additives (Di Nicolantonio et al., 2008). Amino acids (Sigma) at 50× concentrations in water were added at 1× concentration. All amino acids were added for complete media (+AA), with individual DMEM amino acids omitted to generate single amino-acid-deficient media. For the initial screen, 30,000 cells were plated per well in a 96-well plate and switched after 24 hr to depleted amino acid media for 72 hr. Viability was assessed in the initial screen using Calcein AM (Molecular Probes; ThermoFisher) at 1 μM for 2 hr and cells fixed for 15 min with 4% paraformaldehyde prior to analysis on a Genios plate reader and in all other experiments using the CellTiter-Glo luminescence assay (Promega).

FACS Analysis

To detect ROS, 200,000 cells were plated in 6-well plates and switched to cystine-deprived media for 12 hr prior to FACS analysis. CMDCFDA and C11-BODIPY581/591 (Molecular Probes; Thermo Fisher) were used to detect total and lipid ROS, respectively. Following deprivation of cystine for 12 hr, cells were washed with PBS, loaded with either CMDCFDA (10 μM) or C11 BODIPY (2 μM) in DPBS for 30 min, trypsinized with 0.25% Trypsin-EDTA, resuspended in PBS with 1% FBS, and analyzed using an Attune NxT flow cytometer (Thermo Fisher). Dyes were excited using a blue 488-nm laser, and emission was recorded on BL1 (530/30) for a minimum of 5,000 cells per sample.

Xenograft Tumor Model

2.5× 105 NCI-H1650 cells were inoculated 1:1 in Matrigel: PBS (100 mL) by subcutaneous injection into eight non-obese diabetic (NOD) severe combined immunodeficiency (SCID) gamma male mice. Tumors were allowed to engraft and grow for 30 days (tumor volume averaged ~200 mm3) and mice treated by intraperitoneal (i.p.) injection with 100 mg/kg cyst(e)inase or 100 mg/kg heat-inactivated cyst(e)inase (n = 4 ea.) on day 30, with a second dose given on day 33. Mice were necropsied 24 hr after the second dose. For analyses of COX2, control and treated tumors were excised and one-half preserved in 10% neutral buffered formalin for immunohistochemistry (IHC) and the remaining half frozen in liquid nitrogen for protein extraction. For IHC, anti-COX2 from Abcam (ab15191) was used with DAB detection.

Statistical Analyses

Data were analyzed using Microsoft Excel or GraphPad Prism software (GraphPad) and are presented as mean values ± SEM. All viability data represent the mean of three biological replicates/condition. Statistical analyses were performed using two-sided Student's t test. For Kaplan-Meier plots, statistical significance was analyzed by the log rank (Mantel-Cox) test. Sample variance was not significant between control and treatment groups prior to study onset. Significance was set at $p < 0.05$. All data are representative of at least two independent experiments.

SUPPLEMENTAL INFORMATION

Supplemental Information includes Supplemental Experimental Procedures, four figures, and two movies and can be found with this article online at http://dx.doi.org/10.1016/j.celrep.2017.02.054.

(C) (Left) Histogram of viability ± SD of EGFR (delE746-A750) HME (dark bars) or NCI-NH1650 (light bars) cells cultured for 48 hr in normal media (N) (assigned a value of 1), media lacking cystine (−Cys), normal media containing 125 nM cyst(e)inase (AECase) on its own (N/AECase) or with Fer-1 (N/AECase/Fer-1), or normal media containing 125 nM heat-inactivated AECase on its own (N/AECase*) or with Fer-1 (N/AECase*/Fer-1). (Right) Phase-contrast micrographs of EGFR (delE746-A750) HME cells in normal media, media deprived of cysteine, or normal media containing 125 nM AECase (N/AECase) for 48 hr are shown.

(D) Phase contrast (left), and Sytox Green (right) micrographs of H1650 cells deprived of cystine (left panels), treated with 125 nM AECase (middle panels), or treated with heat-inactivated AECase (right panels) for various times up to 20 hr.

(E) Cyst(e)inase (AECase) administration inhibits tumor growth in a NCI-NH1650 xenograft mouse model. (Left panel) Increase in tumor volume following i.p. administration of PBS control (dark circles) or 30 mg/kg (dark squares) or 100 mg/kg (light triangles) AECase is shown. Start and end of treatment times are also shown. (Right panel) Kaplan-Meier plots of median survival of PBS- or AECase-treated tumor-bearing mice are shown.

(F) (Top panels) Immunoblots of lysates from control (lanes 1–4) or AECase-treated (lanes 5–8) NCI-NH1650 xenograft lysates probed to detect COX2 (arrowhead). (Middle histogram) Quantification of relative COX2/ERK in control or AECase-treated groups is shown. $p = 0.04$; $n = 4$. (Bottom micrographs) Images of COX2 staining in control and AECase-treated tumors are shown.

(G) Model depicting role of activated EGFR in determining sensitivity to ferroptosis. Activated EGFR (EGFR*) stimulates MAPK signaling, reducing expression of GPX4 and inducing expression of NOX4. GPX4 utilizes reduced glutathione (GSH) derived from cystine transported via the System x_c^- cystine-glutamate exchanger to detoxify membrane lipid peroxides (red), generating oxidized glutathione (GSSG). GSSG is recycled to GSH using reducing equivalents derived from NADPH (dashed line). Cystine can be reduced to generate cysteine that can independently detoxify ROS and may have additional functions (e.g., Briggs et al., 2016). Lipid peroxides are generated from hydrogen peroxide (H_2O_2, derived from NOX4) and iron (Fe^{2+}), producing hydroxyl radicals that initiate lipid peroxidation. Lipid peroxidation leads to loss of membrane integrity, allowing uptake of water, cell swelling, and rupture.

AUTHOR CONTRIBUTIONS

I.P. and X.W. performed cell viability assays, inhibitor and siRNA treatments, FACS analyses, and immunoblotting experiments; T.C. performed immunofluorescence and assays of GJIC; C.L. performed amino acid analyses; D.M. assisted with methods of quantification; S.L.C., K.T., and E.S. designed and performed the xenograft experiments; R.R., O.E.P., and M.J.S. provided NSCLC cell lines; and S.W.R. provided AECase. R.F.L. conceived the study and wrote the paper.

ACKNOWLEDGMENTS

The p442-PL1 Flag-Strep-HA-GPx4 (Flag-GPX4) was from Marcus Konrad. We are grateful for the support of John Neoptolemos and to Cancer Research UK and the Liverpool Pancreatic Biomedical Research Unit for funding (to I.P. and R.F.L.). R.R. was supported by the Cancer Treatment and Research Trust and M.J.S. by the Imperial National Institute for Health Research (NIHR) Biomedical Research Centre and Imperial CRUK/NIHR Experimental Cancer Medicine Centre. X.W. and R.F.L. acknowledge support from North West Cancer Research and D.M. from the Medical Research Council. E.S. is an inventor on intellectual property related to part of this work, and E.S. and S.W.R. have an equity interest in Aeglea Biotherapeutics.

Received: August 8, 2016
Revised: November 30, 2016
Accepted: February 16, 2017
Published: March 14, 2017

REFERENCES

Barbie, D.A., Tamayo, P., Boehm, J.S., Kim, S.Y., Moody, S.E., Dunn, I.F., Schinzel, A.C., Sandy, P., Meylan, E., Scholl, C., et al. (2009). Systematic RNA interference reveals that oncogenic KRAS-driven cancers require TBK1. Nature *462*, 108–112.

Briggs, K.J., Koivunen, P., Cao, S., Backus, K.M., Olenchock, B.A., Patel, H., Zhang, Q., Signoretti, S., Gerfen, G.J., Richardson, A.L., et al. (2016). Paracrine Induction of HIF by Glutamate in Breast Cancer: EglN1 Senses Cysteine. Cell *166*, 126–139.

Cramer, S.L., Saha, A., Liu, J., Tadi, S., Tiziani, S., Yan, W., Triplett, K., Lamb, C., Alters, S.E., Rowlinson, S., et al. (2017). Systemic depletion of L-cyst(e)ine with cyst(e)inase increases reactive oxygen species and suppresses tumor growth. Nat. Med. *23*, 120–127.

Di Nicolantonio, F., Arena, S., Gallicchio, M., Zecchin, D., Martini, M., Flonta, S.E., Stella, G.M., Lamba, S., Cancelliere, C., Russo, M., et al. (2008). Replacement of normal with mutant alleles in the genome of normal human cells unveils mutation-specific drug responses. Proc. Natl. Acad. Sci. USA *105*, 20864–20869.

Dickinson, B.C., Huynh, C., and Chang, C.J. (2010). A palette of fluorescent probes with varying emission colors for imaging hydrogen peroxide signaling in living cells. J. Am. Chem. Soc. *132*, 5906–5915.

Dixon, S.J., Lemberg, K.M., Lamprecht, M.R., Skouta, R., Zaitsev, E.M., Gleason, C.E., Patel, D.N., Bauer, A.J., Cantley, A.M., Yang, W.S., et al. (2012). Ferroptosis: an iron-dependent form of nonapoptotic cell death. Cell *149*, 1060–1072.

Dolma, S., Lessnick, S.L., Hahn, W.C., and Stockwell, B.R. (2003). Identification of genotype-selective antitumor agents using synthetic lethal chemical screening in engineered human tumor cells. Cancer Cell *3*, 285–296.

Friedmann Angeli, J.P., Schneider, M., Proneth, B., Tyurina, Y.Y., Tyurin, V.A., Hammond, V.J., Herbach, N., Aichler, M., Walch, A., Eggenhofer, E., et al. (2014). Inactivation of the ferroptosis regulator Gpx4 triggers acute renal failure in mice. Nat. Cell Biol. *16*, 1180–1191.

Gao, M., Monian, P., Quadri, N., Ramasamy, R., and Jiang, X. (2015). Glutaminolysis and transferrin regulate ferroptosis. Mol. Cell *59*, 298–308.

Gonzalez, G.G., and Byus, C.V. (1991). Effect of dietary arginine restriction upon ornithine and polyamine metabolism during two-stage epidermal carcinogenesis in the mouse. Cancer Res. *51*, 2932–2939.

Gromer, S., Arscott, L.D., Williams, C.H., Jr., Schirmer, R.H., and Becker, K. (1998). Human placenta thioredoxin reductase. Isolation of the selenoenzyme, steady state kinetics, and inhibition by therapeutic gold compounds. J. Biol. Chem. *273*, 20096–20101.

Hayano, M., Yang, W.S., Corn, C.K., Pagano, N.C., and Stockwell, B.R. (2016). Loss of cysteinyl-tRNA synthetase (CARS) induces the transsulfuration pathway and inhibits ferroptosis induced by cystine deprivation. Cell Death Differ. *23*, 270–278.

Hinnebusch, A.G. (2005). Translational regulation of GCN4 and the general amino acid control of yeast. Annu. Rev. Microbiol. *59*, 407–450.

Hirayama, A., Kami, K., Sugimoto, M., Sugawara, M., Toki, N., Onozuka, H., Kinoshita, T., Saito, N., Ochiai, A., Tomita, M., et al. (2009). Quantitative metabolome profiling of colon and stomach cancer microenvironment by capillary electrophoresis time-of-flight mass spectrometry. Cancer Res. *69*, 4918–4925.

Holleman, A., den Boer, M.L., Kazemier, K.M., Janka-Schaub, G.E., and Pieters, R. (2003). Resistance to different classes of drugs is associated with impaired apoptosis in childhood acute lymphoblastic leukemia. Blood *102*, 4541–4546.

Kami, K., Fujimori, T., Sato, H., Sato, M., Yamamoto, H., Ohashi, Y., Sugiyama, N., Ishihama, Y., Onozuka, H., Ochiai, A., et al. (2013). Metabolomic profiling of lung and prostate tumor tissues by capillary electrophoresis time-of-flight mass spectrometry. Metabolomics *9*, 444–453.

Laleu, B., Gaggini, F., Orchard, M., Fioraso-Cartier, L., Cagnon, L., Houngninou-Molango, S., Gradia, A., Duboux, G., Merlot, C., Heitz, F., et al. (2010). First in class, potent, and orally bioavailable NADPH oxidase isoform 4 (Nox4) inhibitors for the treatment of idiopathic pulmonary fibrosis. J. Med. Chem. *53*, 7715–7730.

Linkermann, A., Skouta, R., Himmerkus, N., Mulay, S.R., Dewitz, C., De Zen, F., Prokai, A., Zuchtriegel, G., Krombach, F., Welz, P.S., et al. (2014). Synchronized renal tubular cell death involves ferroptosis. Proc. Natl. Acad. Sci. USA *111*, 16836–16841.

Lis, M., Wizert, A., Przybylo, M., Langner, M., Swiatek, J., Jungwirth, P., and Cwiklik, L. (2011). The effect of lipid oxidation on the water permeability of phospholipids bilayers. Phys. Chem. Chem. Phys. *13*, 17555–17563.

Mandal, P.K., Seiler, A., Perisic, T., Kölle, P., Banjac Canak, A., Förster, H., Weiss, N., Kremmer, E., Lieberman, M.W., Bannai, S., et al. (2010). System x(c)- and thioredoxin reductase 1 cooperatively rescue glutathione deficiency. J. Biol. Chem. *285*, 22244–22253.

Mannes, A.M., Seiler, A., Bosello, V., Maiorino, M., and Conrad, M. (2011). Cysteine mutant of mammalian GPx4 rescues cell death induced by disruption of the wild-type selenoenzyme. FASEB J. *25*, 2135–2144.

Maser, R.L., Magenheimer, B.S., and Calvet, J.P. (1994). Mouse plasma glutathione peroxidase. cDNA sequence analysis and renal proximal tubular expression and secretion. J. Biol. Chem. *269*, 27066–27073.

Pader, I., Sengupta, R., Cebula, M., Xu, J., Lundberg, J.O., Holmgren, A., Johansson, K., and Arnér, E.S. (2014). Thioredoxin-related protein of 14 kDa is an efficient L-cystine reductase and S-denitrosylase. Proc. Natl. Acad. Sci. USA *111*, 6964–6969.

Paez, J.G., Jänne, P.A., Lee, J.C., Tracy, S., Greulich, H., Gabriel, S., Herman, P., Kaye, F.J., Lindeman, N., Boggon, T.J., et al. (2004). EGFR mutations in lung cancer: correlation with clinical response to gefitinib therapy. Science *304*, 1497–1500.

Pao, W., Miller, V., Zakowski, M., Doherty, J., Politi, K., Sarkaria, I., Singh, B., Heelan, R., Rusch, V., Fulton, L., et al. (2004). EGF receptor gene mutations are common in lung cancers from "never smokers" and are associated with sensitivity of tumors to gefitinib and erlotinib. Proc. Natl. Acad. Sci. USA *101*, 13306–13311.

Parmenter, T.J., Kleinschmidt, M., Kinross, K.M., Bond, S.T., Li, J., Kaadige, M.R., Rao, A., Sheppard, K.E., Hugo, W., Pupo, G.M., et al. (2014). Response

of BRAF-mutant melanoma to BRAF inhibition is mediated by a network of transcriptional regulators of glycolysis. Cancer Discov. *4*, 423–433.

Pines, G., Köstler, W.J., and Yarden, Y. (2010). Oncogenic mutant forms of EGFR: lessons in signal transduction and targets for cancer therapy. FEBS Lett. *584*, 2699–2706.

Possik, P.A., Müller, J., Gerlach, C., Kenski, J.C.N., Huang, X., Shahrabi, A., Krijgsman, O., Song, J.-Y., Smit, M.A., Gerritsen, B., et al. (2014). Parallel in vivo and in vitro melanoma RNAi dropout screens reveal synthetic lethality between hypoxia and DNA damage response inhibition. Cell Rep. *9*, 1375–1386.

Scholl, C., Fröhling, S., Dunn, I.F., Schinzel, A.C., Barbie, D.A., Kim, S.Y., Silver, S.J., Tamayo, P., Wadlow, R.C., Ramaswamy, S., et al. (2009). Synthetic lethal interaction between oncogenic KRAS dependency and STK33 suppression in human cancer cells. Cell *137*, 821–834.

Scott, L., Lamb, J., Smith, S., and Wheatley, D.N. (2000). Single amino acid (arginine) deprivation: rapid and selective death of cultured transformed and malignant cells. Br. J. Cancer *83*, 800–810.

Son, J., Lyssiotis, C.A., Ying, H., Wang, X., Hua, S., Ligorio, M., Perera, R.M., Ferrone, C.R., Mullarky, E., Shyh-Chang, N., et al. (2013). Glutamine supports pancreatic cancer growth through a KRAS-regulated metabolic pathway. Nature *496*, 101–105.

Stewart, E.L., Tan, S.Z., Liu, G., and Tsao, M.S. (2015). Known and putative mechanisms of resistance to EGFR targeted therapies in NSCLC patients with EGFR mutations-a review. Transl. Lung Cancer Res. *4*, 67–81.

Takac, I., Schröder, K., Zhang, L., Lardy, B., Anilkumar, N., Lambeth, J.D., Shah, A.M., Morel, F., and Brandes, R.P. (2011). The E-loop is involved in hydrogen peroxide formation by the NADPH oxidase Nox4. J. Biol. Chem. *286*, 13304–13313.

Tallal, L., Tan, C., Oettgen, H., Wollner, N., McCarthy, M., Helson, L., Burchenal, J., Karnofsky, D., and Murphy, M.L. (1970). E. coli L-asparaginase in the treatment of leukemia and solid tumors in 131 children. Cancer *25*, 306–320.

Wong-Ekkabut, J., Xu, Z., Triampo, W., Tang, I.M., Tieleman, D.P., and Monticelli, L. (2007). Effect of lipid peroxidation on the properties of lipid bilayers: a molecular dynamics study. Biophys. J. *93*, 4225–4236.

Yagoda, N., von Rechenberg, M., Zaganjor, E., Bauer, A.J., Yang, W.S., Fridman, D.J., Wolpaw, A.J., Smukste, I., Peltier, J.M., Boniface, J.J., et al. (2007). RAS-RAF-MEK-dependent oxidative cell death involving voltage-dependent anion channels. Nature *447*, 864–868.

Yang, W.S., and Stockwell, B.R. (2008). Synthetic lethal screening identifies compounds activating iron-dependent, nonapoptotic cell death in oncogenic-RAS-harboring cancer cells. Chem. Biol. *15*, 234–245.

Yang, W.S., and Stockwell, B.R. (2016). Ferroptosis: death by lipid peroxidation. Trends Cell Biol. *26*, 165–176.

Yang, W.S., SriRamaratnam, R., Welsch, M.E., Shimada, K., Skouta, R., Viswanathan, V.S., Cheah, J.H., Clemons, P.A., Shamji, A.F., Clish, C.B., et al. (2014). Regulation of ferroptotic cancer cell death by GPX4. Cell *156*, 317–331.

Cell Reports, Volume *18*

Supplemental Information

Oncogene-Selective Sensitivity to Synchronous Cell Death following Modulation of the Amino Acid Nutrient Cystine

Ioannis Poursaitidis, Xiaomeng Wang, Thomas Crighton, Christiaan Labuschagne, David Mason, Shira L. Cramer, Kendra Triplett, Rajat Roy, Olivier E. Pardo, Michael J. Seckl, Scott W. Rowlinson, Everett Stone, and Richard F. Lamb

Supplemental Figures and Legends, Tables, Experimental Procedures, and References

Figure S1 (related to Figure 1).

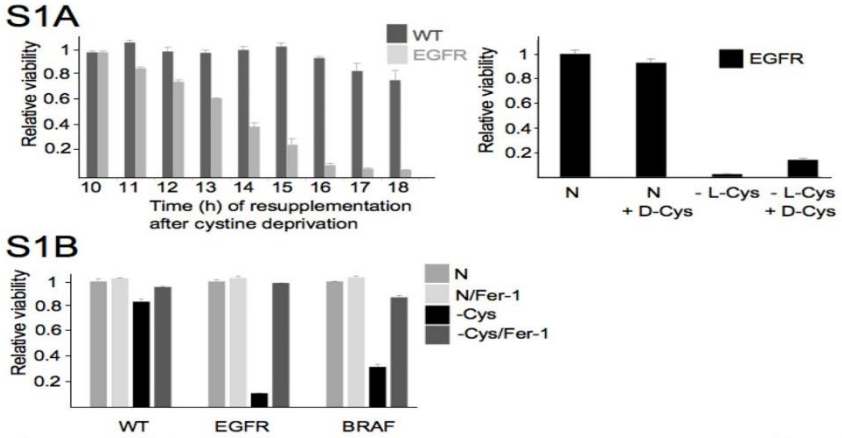

A, Left, cell viability following deprivation of cystine, followed by cystine resupplmentation, in wild type (WT) and EGFR (delE746-A750) HME cells. Histogram represents the average viability ± standard deviation (SD) of three biological replicates using CellTitre-Glo, relative to removal of cystine for 10 hours (assigned an arbitrary value of 1). Results are typical of experiments performed twice. Right, cell viability in normal media (N) or following deprivation of cystine (- L-Cys), followed by D-cystine addition (+ D-Cys, added at 150μM), in EGFR (delE746-A750) HME cells. Histogram represents the average viability ± standard deviation (SD) of three biological replicates using CellTitre-Glo with viability in normal media assigned an arbitrary value of 1. Results are typical of experiments performed twice.
B, Cell viability in normal media or following deprivation of cystine in the presence or absence of Fer-1 (2μM), in wild type (WT), EGFR (delE746-A750) and BRAF-mutant HME cells. Histogram represents the average viability ± standard deviation (SD) of three biological replicates using CellTitre-Glo, relative to normal media (N, assigned an arbitrary value of 1). Results are typical of experiments performed twice.

Figure S2 (related to Figure 2).

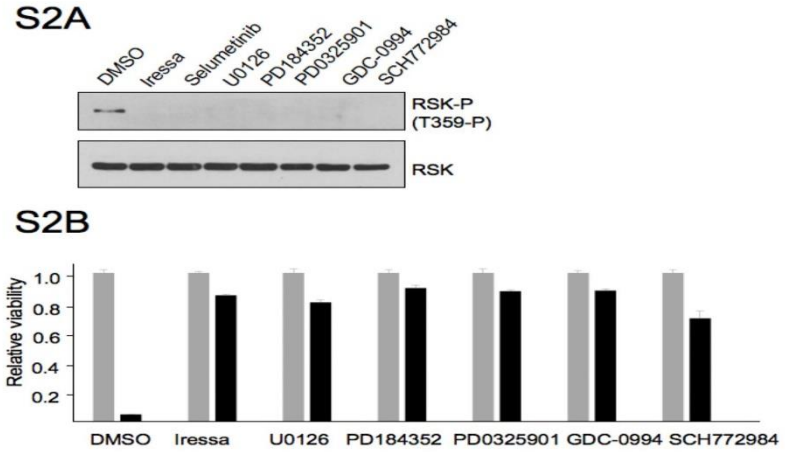

S2C

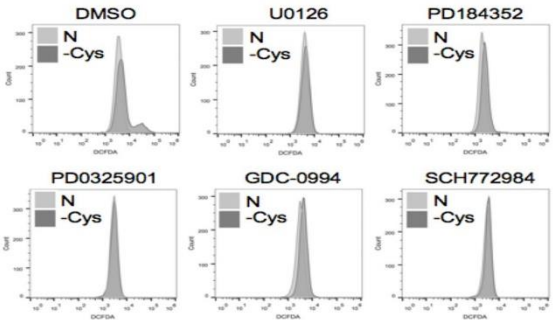

Total ROS:
DCF

S2D

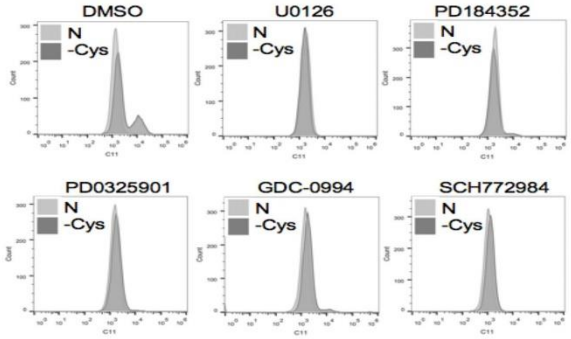

Lipid ROS:
C11-BODIPY

A, Immunoblots of EGFR (delE746-A750) HME cell lysates probed with antibodies detecting phosphorylated RSK (T359-P), and total RSK from cells cultured in normal media in the presence of vehicle (DMSO), Iressa, and the indicated MEK and ERK signalling inhibitors added for a total of 30 hours.
B, Cell viability of EGFR (delE746-A750) HME cells. Histogram represents the average viability ± standard deviation (SD) of three biological replicates cultured in normal media (assigned an arbitrary value of 1), or media lacking cystine for 24 hours measured using CellTitre-Glo, in the presence or absence of Iressa, and the indicated MEK and ERK signalling inhibitors added for a total of 30 hours prior to cystine deprivation. Results were expressed for each inhibitor condition separately, with viability in normal media assigned the arbitrary value of 1. Results are typical of experiments performed twice.
C, FACS analyses of total ROS in EGFR (delE746-A750) cells following treatment with MEK and ERK inhibitors. Dark traces, cells cultured in normal media; light traces, cells cultured in media lacking cystine for 12 hours. Results are typical of experiments performed twice.
D, FACS analyses of lipid ROS in EGFR (delE746-A750) cells following treatment with MEK and ERK inhibitors. Dark traces, cells cultured in normal media; light traces, cells cultured in media lacking cystine for 12 hours. Results are typical of experiments performed twice.

Figure S3 (related to Figure 3).

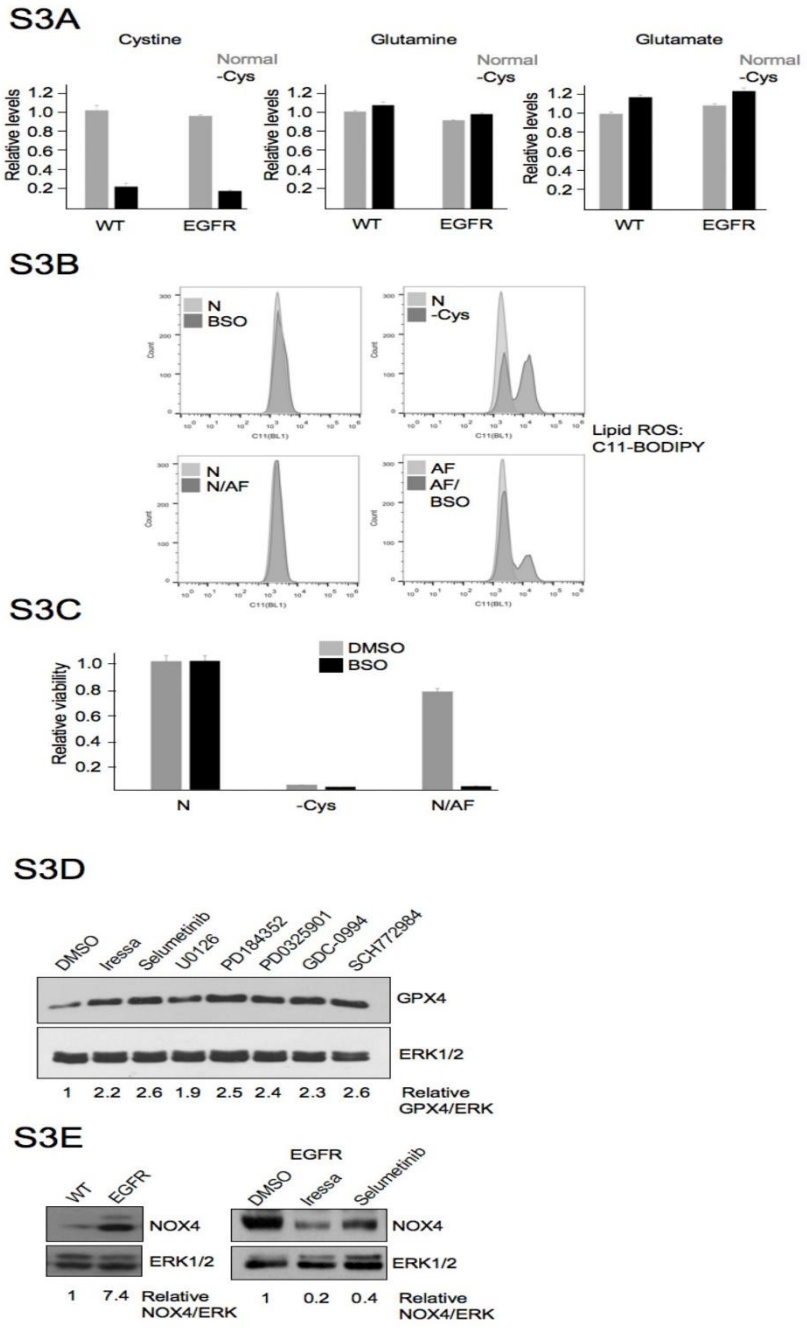

A, Amino acid analysis of steady-state levels of cystine, glutamine and glutamate measured by LC-MS in wild type and EGFR (delE746-A750) cells cultured in normal media (Normal, light bars) or media lacking cystine for for 8 hours. Histogram represents the average values ± standard deviation (SD) of three biological replicates with the level in normal media of wild type HME cells assigned the arbitrary value of 1. Results are typical of experiments performed twice.
B, FACS analyses of lipid ROS in EGFR (delE746-A750) cells following treatment for 14 hours with BSO alone or with auranofin. Light traces, cells cultured in normal media or normal media containing auranofin for 14 hours (N or N+AF); dark traces, cells treated for 14 hours with BSO alone (BSO), or cultured in media lacking cystine for 14 hours (-Cys) or treated with auranofin for 14h (N+AF) or treated auranofin for 6 hours following pretreatment with BSO for 14h. Results are typical of experiments performed twice.
C, Cell viability of EGFR (delE746-A750) HME cells. Viability of cells cultured for 18 hours in normal media containing DMSO vehicle (light bars), or containing 200μM BSO (BSO, dark bars), followed by deprivation of cystine, or treatment with auronofin for 24 hours, with viability measured using CellTitre-Glo. Histogram represents the average values ± standard deviation (SD) of three biological replicates with the level in normal media assigned the arbitrary value of 1. Results are typical of experiments performed twice.
D, Immunoblots of EGFR (delE746-A750) HME cell lysates probed with antibodies detecting GPX4, and ERK1/2 from cells cultured in normal media in the presence of vehicle (DMSO), Iressa, and the indicated MEK and ERK signalling inhibitors added for a total of 30 hours. Relative GPX4 was calculated using ImageJ from scanned autoradiographs with the ratio in DMSO-treated EGFR (delE746-A750) HME cells assigned the arbitrary value of 1.
E, Left, Immunoblots of wild type and EGFR (delE746-A750) HME cell lysates probed with antibodies detecting NOX4 and ERK1/2; right, from EGFR (delE746-A750) cells cultured in normal media in the presence of vehicle (DMSO), Iressa, or Selumetinib for a total of 30 hours. Relative NOX4 was calculated using ImageJ from scanned autoradiographs with the ratio in wild type or DMSO-treated EGFR (delE746-A750) HME cells assigned the arbitrary value of 1 in each case.

Figure S4 (related to Figure 4).

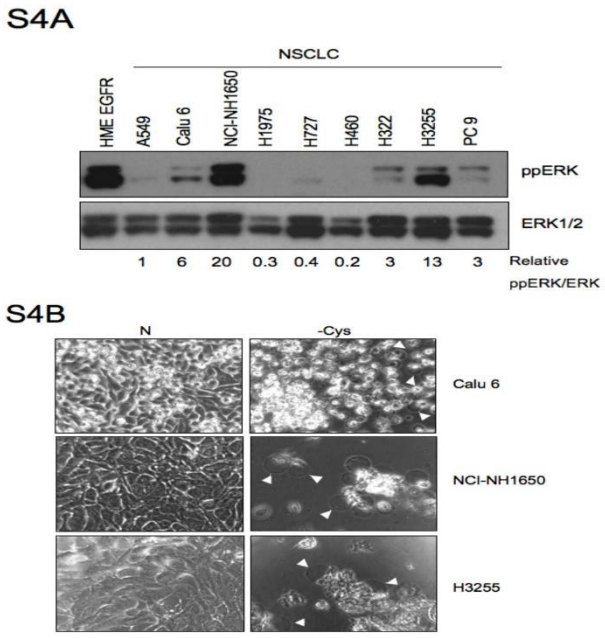

S4C

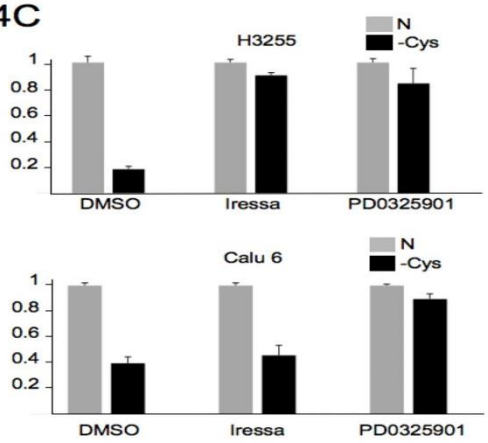

S4D

			Allred Score		
	Sample #	IHC	Intensity	Proportion	Global
controls	1	COX2	1	1	2
	2	COX2	1	1	2
	3	COX2	1	1	2
	4	COX2	1	1	2
AECase	5	COX2	1	2	3
	6	COX2	1	2	3
	7	COX2	1	5	6
	8	COX2	1	2	3

A, Immunoblots of EGFR (delE746-A750) HME and various NSCLC cell lysates probed with antibodies detecting ppERK and ERK1/2 Relative ppERK was calculated using ImageJ from scanned autoradiographs with the ratio in A549 assigned the arbitrary value of 1.
B, Left panels, phase contrast micrographs of Calu 6, NCI-NH1650 and H3255 cells followed by culture in normal media (left) or media lacking cystine for 72 hours (right). Arrowheads indicate balloon-like membrane extensions of cells that have undergone ferroptosis.
C, Histogram representing the average viability ± standard deviation (SD) of three biological replicates of Calu 6 and H3255 cells cultured for 30 hours in normal media containing DMSO, Iressa or PD0325901 (light bars) or media lacking cystine for 48 hours (dark bars). Results were expressed for each condition separately, with viability in normal media assigned the arbitrary value of 1. Results are typical of experiments performed twice.
D, Pathological evaluation of COX2 immunostaining in mice treated with heat-inactivated AECase (Controls 1-4) or AECase (5-8).

Supplemental Movies S1, S2
Movie S1 (related to Figure 1).
Withdrawal of cystine leads to synchronous cell death. EGFR (delE746-A750) HME cells grown to confluency in normal media were switched to media lacking cystine from which point images were collected by time-lapse phase contrast microscopy. Frames were taken every 5 mins for 24 hrs and saved for playback at 100ms intervals.
Movie S2 (related to Figure 4):
Withdrawal of cystine leads to synchronous cell death in NSCLC cells. NCI-NH1650 cells grown to confluency in normal media were switched to media lacking cystine and containing Sytox Green, from which point images were collected. Individual frames were obtained every 5 minutes in phase contrast and green fluorescence channels with Sytox Green used at 0.5μM concentration (Molecular Probes, Thermofisher) for 24 hrs and saved for dual-channel playback at 100ms interval.

Supplemental Experimental Procedures

siRNA knockdown and plasmid transfection

Lipofectamine 2000 (Invitrogen, ThermoFisher) was used for siRNA transfection of HME cells. 500,000 cells were plated in 6-well plates and either mock-transfected or transfected with either siCtrl or siGenome Smartpool siRNAs (Dharmacon, GE Lifesciences) to GPX1, GPX2, GPX3 and GPX4 at a final concentration of 50nM. A day after transfection cells were trypsinized and split between a 12-well plate well, with 250,000 cells, and 6 96-well plate wells, with 25,000 cells per well, for immunoblotting and viability assay respectively 3 days post transfection. For plasmid transfections, 5x105 EGFR-mutant cells were transfected in 3cm dishes with 5µg of Flag-GPX4 (p442-PL1 Flag-Strep-HA-GPX4, (Mannes et al., 2011)) or control vector using Lipofectamine 2000 (Invitrogen, ThermoFisher). 48h after transfection wild type or transfected cells were trypsinised and replated in a 96 well plate at 20,000 cells per well and the viability experiment performed following 16h of cystine deprivation.

Western Blotting

Cells were lysed in lysis buffer (50 mM Tris-HCl, pH 7.5, 1mM EGTA, 1 mM EDTA, 1% Triton X-100, 1mM Na3VO4, 50 mM NaF, 50 mM β-glycerolphosphate, 0.27M sucrose, 0.1% beta-mercaptoethanol, Complete protease inhibitors (Roche). Protein concentration was determined using Bradford assay reagent (Biorad) and 25 µg of total protein was loaded per sample.

Commercial antibodies used were: pEGFR Y1068 (Cell Signalling Technologies) #3777, EGFR (Cell Signalling Technologies) #2232, pAKT S473 (Cell Signalling Technologies) #9271, AKT (Upstate, EMD Millipore) 07-416, ppERK (Cell Signalling Technologies) #4370, ERK1/2 (Santa Cruz Biotech) sc-94, GCN2-P T899 (Epitomics, Abcam) 2425-1, GCN2 (Cell Signalling Technologies) #3302, GPX1 (R&D systems, Biotechne) AF3798, GPX2 (R&D systems, Biotechne) MAB5470, GPX4 (Abcam) ab125066, COX2 (Cayman Chemicals) #160112, NOX4 (Abcam) #, RSK-P Thr 359-P and RSK (Cell Signaling Technologies) 133303 and b-catenin (Transduction Labs) C19220.

GJIC scrape loading dye transfer assay

Confluent EGFR-mutant cells growing in 24-well plates were incubated with 1µM Iressa, 1µM Wortmannin, 5µM Selumetinib or 1µM DMSO (control) for 30h. Cells were then washed in Ca++-deficient PBS and transferred to PBS containing 0.5mg/mL Lucifer yellow (Sigma), 10mM glucose, 30mM HEPES buffer (Thermofisher), 0.1% BSA, 0.5 mg/mL rhodamine-dextran (Molecular Probes) and either vehicle (100mM DMSO) or 100mM carbenoxolone (Sigma). Wells were wounded via two perpendicular scratches to the monolayer and incubated for 15 minutes before being washed with PBS and fixed in 4% paraformaldehyde. Areas close to the wound margin were imaged for green fluorescence at 20X magnification using an AMG EVOS digital inverted microscope and the extent of Lucifer yellow infiltration into the monolayer was analysed using ImageJ software.

Confocal immunofluorescence microscopy

Confluent HME WT and EGFR-mutant cells growing on glass coverslips were incubated with 1µM Iressa, 1µM Wortmannin, 5µM Selumetinib or 1µM DMSO for 30h. Immunofluorescence labelling of β-catenin was undertaken as previously described (Menon et al.) and cells were imaged at 63X magnification with a confocal laser scanning microscope (Zeiss 31 LSM 800).

Additional cell treatments and microscopy

The timelapse microscope used was a Nikon TE-300 [motorised with Sutter filter wheels and a Conix block changer] equipped with a 10X phase contrast [PC] objective, encased in a Perspex 37°C incubation chamber with an insert for multi-well plates flushed with humidified, 5% CO2 air. Green fluorescence was acquired through a Nikon B-2A block split into Sutter filter wheels and a Conix block changer. Images were collected using a Hamamatsu Orca AG camera, with MicroManager software (Edelstein et al., 2010), converting time series to an ImageJ readable format using in-house software. Cells were plated in a 6-well plate at 500,000 cells per well and grown for 3 days prior to media switch to cystine-deprived media. The plates were then transferred in the microscope stage maintained at 37°C with 5% CO2. Individual frames were obtained every 5 minutes in phase contrast and green fluorescence channels for detection of nonviable cells by Sytox Green nuclear staining used at 0.5µM concentration (Molecular Probes, Thermofisher). Apoptosis inhibitor z-VAD-fMK (Selleck) was

used at 50μM. ROS scavengers Idebenone and α-Tocopherol (Sigma) were used at 1μM and 30μM respectively. Induction of ferroptotic death by erastin (Cayman Chemical) was achieved at a concentration of 2.5μg/ml. Other inhibitors used were catalase used at 1000U/ml (Sigma), superoxide dismutase used at 100U/ml (Sigma), NOX4 inhibitor GKT136901 (Aobious) at 20μM and the water-soluble vitamin E analogue Trolox at 5μM (Sigma). To determine ferroptotic cell death 10,000 EGFR HME cells were plated in a 96-well plate and allowed to grow for 3 days prior to a media shift in the presence of inhibitors of ferroptotic or apoptotic death or scavengers of reactive oxygen species. Ferroptosis inhibitor Ferrostatin1 (Fer-1, Sigma) was used at 2μM and iron chelator deferroxamine (DFO, Sigma) was used at 100μM.

To image H2O2 confluent cells were transferred to cystine-deficient media for 24 hours. Cells were then incubated with 10μM Peroxy Orange 1 (PO1, Tocris Bioscience) for 60 minutes before being washed three times in dPBS and imaged immediately at 20X magnification using an AMG EVOS digital inverted microscope. To inhibit signal transduction downstream of EGFR cells were treated for 24h prior to media switch with EGFR inhibitor Iressa (Tocris) at 1μM, MEK inhibitor Selumetinib (Selleckchem) at 5μM, PI3K inhibitor Wortmannin (Sigma) at 1μM. DMSO (Sigma) was used as a vehicle control. Additional MEK and ERK inhibitors used were U0126 (Calbiochem, 10μM), PD184352 (Sigma, 10μM), PD0325901 (Selleckchem, 1μM), GDC-0994 (ERK inhibitor, Selleckchem, 5μM) and SCH772984 (ERK inhibitor, Cayman Chemicals, 5μM). Following pre-treatment for 24h cells were switched to either complete or cysteine deficient media containing the same concentration of inhibitors for 12h prior to analysis. Wortmannin was re-added at the same concentration 1hour before collection. Auranofin and S4PG were from Santa Cruz and used at 1 and 100μM, respectively. NOX4 inhibitor GKT136901 (Aobious) was used at 20μM. PEGylated AECase was used at a final concentration of 125nM, heat inactivation was performed by incubation at 95 ^{0}C for 7 minutes, followed by brief centrifugation for 5 mins at 13,000 rpm.

For cystine titration cells were plated in triplicate cells at a final concentration of 30,000 per well in a 96-well plate (NUNC, Thermofisher) and the following day complete synthetic media containing or lacking EGF was serially diluted with DMEM lacking cystine to achieve a range of decreasing cystine concentrations. After 24h of treatment viability was determined using the CellTitre-Glo assay (Promega). An equal volume of CellTitre-Glo reagent was added and the plate was vortexed at 1000 rpm for 2 minutes to allow cell lysis. The plates were then analysed on a Tecan Genios plate reader.

GSH/GSSG quantification

For the quantification of cellular reduced (GSH) and oxidised (GSSG) glutathione the method described by Rahman et al (Rahman et al., 2006) was used, which utilises the reaction of GSH with 5,5′-Dithiobis (2-nitrobenzoic acid) (DTNB) that leads to the production of the 5′-thio-2-nitrobenzoic acid (TNB) chromophore measured at 412nm (Tietze, 1969). $1x10^{6}$ cells were plated in 6-well plates (Greiner) and the following day treated with 200μM of BSO or switched to cystine deficient media for 8h. Cells were then washed in cold PBS, trypsinised and resuspended in 0.2ml of ice-cold extraction buffer (0.1% Triton-X and 0.6% sulfosalicylic acid in 0.1 potassium phosphate buffer with 5 mM EDTA disodium salt, pH 7.5 (KPE)). Cells were then freeze-thawed four times (liquid nitrogen - 37°C water bath) and lysates subsequently centrifuged at 3000g for 5 min at 4 °C and supernatants collected. Protein concentrations were measured using a Bradford assay in order to express GSH and GSSG levels as nM/mg of total protein. Total glutathione (Total [GSH] = [GSH] + 2 × [GSSG]) was measured via a kinetic assay based on the reaction of DTNB with GSH and the recycling reaction by the enzyme glutathione reductase (GR) (Sigma) which in the presence of β-Nicotinamide adenine dinucleotide 2′-phosphate (β-NAPDH, Sigma) can reduce GSSG to GSH (Guntherb.H and Rost, 1966). The rate of TNB formation was calculated by measuring 415nm absorbance in a plate reader every 30sec. GSH standards of known concentration were made from stock GSH (Sigma) and their rate of formation used to create a standard curve. For measurement of GSSG, 2-vinylpyridine (Aldrich) is added to cell lysates at 18.5 mM for 1h creating a covalent bond with GSH therefore allowing measurement only of GSSG. Excess 2-vinylpyridine was then neutralised with 75mM triethanolamine (Sigma) for 30 min (Griffith, 1980). Levels of GSSG were determined by applying the recycling assay and measuring rate of formation of TNB as described above but using GSSG standard samples (Sigma) to create a standard curve. Reduced glutathione (GSH) could be then determined by subtraction of oxidised (GSSG) from Total glutathione (Total [GSH] = [GSH] + 2 × [GSSG]). All measurements were done in triplicate. Glutathione synthesis inhibitor buthionine sulfoximine (BSO, Santa Cruz Biotechnologies) was used at 200μM.

COX2 immunostaining

After immunostaining the slides were evaluated by a pathologist (Precision Pathology) for percentage of postive tumor cells in the sample and intensity of the staining after excluding all non-tumor cells and non-specific staining of any background stroma or other components. Each sample was assessed using the Allred scoring matrix that generates a global score ranging from 0 to 8. The global score was composed of stain intensity from 1 to 3+ and a proportion score of 0 to 5 (5 being the highest) that was apportioned based on the raw percentge of positive target cells in the sample. The percent of positive target cells is an average of at least 5 fields examined at 200X. The system was originally developed for scoring intensity and proportion of staining estimation of samples using a matrix of scores over a range of both intensity and proportion of positive cells in a given sample. Scores range from 0 to 3 for intensity and from 0 to 5 for proportion with the global score being intensity + proportion. Thus a sample where the staining is weak and is present in 15% of the target cells on the slide, the score would be 1 (intensity) + 1 (proportion) for a global score of 2. Conversely, a sample that showed strong diffuse staining of 98% of target cells would have a score of 8 (3 intensity + 5 proportion).

Amino acid anayses by Liquid Chromatography-Mass Spectrometry (LC-MS)

Wild type and EGFR-mutant HME cells were seeded in seven dishes at $5x10^{6}$/10cm dish for each cell line and the next day washed 3 times using DPBS. Three dishes of each cell line were then switched to –cys media, or normal media for 4h. The last dish was used to count cells from both cell lines to ensure similar cell number per volume of extraction buffer. Metabolites were extracted in a polar solvent (50% methanol, 30% acetonitrile, 20% water) and centrifuged to precipitate and remove any proteins present, in preparation for LC-MS analysis. The volume of extraction solution was calculated from the cell count with 1-2 x 10^{6} cells/ml. The cell metabolites were extracted from the samples by placing the cell culture plates on a rocking shaker at 0-4°C for 5 minutes. The extraction solution from each well was then pipetted into a microcentrifuge tube and shaken in the Thermomixer (Thermomixer comfort, Eppendorf AG, Hamburg, Germany) at high speed of 1400rpm at 0-4°C for 10 minutes. The microcentrifuge tubes were then centrifuged at 16,100 x g for 10 minutes at 0-4°C. The supernatants are transferred to glass HPLC vials and kept at -75°C prior to LC-MS analysis. Hydrophilic Interaction Liquid Chromatography with a Sequant ZIC-pHILIC column (2.1 × 150 mm, 5 µm) (Merck) was used to separate amino acids before detection with high-resolution, accurate-mass (HR/AM) Mass Spectrometry using an Orbitrap Exactive in line with an Accela autosampler and an Accela 600 pump (Thermo Scientific). The elution buffers used to elute the analytes were Acetonitrile (ACN) for A and 20 mM $(NH_4)_2CO_3$, 0.1% NH_4OH in H_2O for B. A linear gradient was programed starting from 80% A and ending at 20% A after 20 min at a flow rate of 200ul/min, followed by wash (20% A) and re-equilibration (80% A) steps at a flow rate of 400 µl/min. An Electrospray Ionization (ESI) probe was used to achieve ionization and the mass spectrometer operated in full-scan and polar-switching mode with the positive voltage at 4.5 kV and negative voltage at 3.5 kV. Metabolite identification and data analysis were done using TraceFinder ™ software (Thermo Scientific).

Supplemental References

Edelstein, A., Amodaj, N., Hoover, K., Vale, R., and Stuurman, N. (2010). Computer control of microscopes using Manager. Current protocols in molecular biology / edited by Frederick M Ausubel [et al] *Chapter 14*, Unit 14.20.

Griffith, O.W. (1980). Determination of glutathione and glutathione disulfide using glutathione-reductase and 2-vinylpyridine. Analytical Biochemistry *106*, 207-212.

Guntherb H., and Rost, J. (1966). True oxidized glutathione content of red blood cells obtained by new enzymic and paper chromatographic methods. Analytical biochemistry *15*, 205-&.

Rahman, I., Kode, A., and Biswas, S.K. (2006). Assay for quantitative determination of glutathione and glutathione disulfide levels using enzymatic recycling method. Nature Protocols *1*, 3159-3165.

Tietze, F. (1969). Enzymic method for quantitative determination of nanogram amounts of total and oxidized glutathione - applications to mammalian blood and other tissues. Analytical Biochemistry *27*, 502.

Appendix II Publication

Metabolism in Pancreatic Cancer

Ioannis Poursaitidis and Richard F. Lamb

Abstract

Despite knowledge of an increasing number of genetic changes present in pancreatic ductal adenocarcinoma (PDAC), the most common form of pancreatic cancer, it remains one of the cancers with the poorest prognosis, and the development of novel therapies that target its unusual biology and metabolic features is imminently required. Pancreatic tumor cells are thought to evolve under the conditions of limited oxygen and nutrient supply due to high levels of stromally produced extracellular matrix and associated poor blood supply. The prevalence of oncogenic KRAS mutations in PDAC, together with inactivation of TP53, CDKN2A, and SMAD4, predicates the engagement of distinct adaptive metabolic features that maximize the uptake and utilization of limiting oxygen and nutrients. Rewiring of the metabolism of glucose, amino acids, and lipids provides biosynthetic/metabolic intermediates required to maintain proliferation and survival, while the induction of autophagy and macropinocytosis permits repurposing of nutrients by PDAC tumor cells. Finally, PDAC tumor cells affect their neighboring cells, activating pancreatic stellate cells to produce a dense fibrotic stroma and provide nutrients in a paracrine manner, while inhibiting an effective antitumor immune response by restriction of nutrients from immune effector cells. It is hoped that by targeting such aberrant metabolism and nutrient utilization additional therapeutic options might soon be available in PDAC.

I. Poursaitidis
Department of Molecular and Clinical Cancer Medicine, Institute of Translational Medicine, University of Liverpool, Liverpool, UK
e-mail: Ioannis.Poursaitidis@liverpool.ac.uk

R.F. Lamb (✉)
School of Health Sciences, Liverpool Hope University, Hope Park Campus, Liverpool, UK
e-mail: rflamb83@gmail.com; lambr@hope.ac.uk

J.P. Neoptolemos et al. (eds.), *Pancreatic Cancer*,
DOI 10.1007/978-1-4939-6631-8_68-1

Keywords
PDAC • Metabolism • KRAS • p53 • Hypoxia • HIF • Desmoplasia

Contents

1 Introduction

PDAC is among the cancer types with the poorest prognosis, with around roughly 367,000 new cases diagnosed and 359,000 deaths in 2015. Overall PDAC has an extremely poor 5-year survival rate of around 6–8% that has not satisfactorily improved over the last four decades, and thus PDAC is expected to become the second most common cause of cancer-associated death before 2030 [1].

PDAC is thought to initiate and progress from a population of microscopic premalignant lesions termed PanINs (Pancreatic Intraepithelial Neoplasias) through multiple stages in a process that may take over two decades, while remaining asymptomatic to the patient [2]. Currently, there are neither diagnostic symptoms nor robust tumor biomarkers that might easily reveal the development of PDAC over this timeframe [3]. Thus, PDAC tumor cells can disseminate, resulting in metastasis to distant sites prior to overt diagnosis [4]. The main oncogenic event in PDAC, identified in the late 1980s, is mutations in the protooncogene KRAS [5], which occur in more than 90% of PanIN and PDAC [2, 6]. In later stages of PDAC progression, mutations and deletions of tumor-suppressor genes such as TP53, CDKN2A, and SMAD4 also occur with variable frequency [7].

Despite mutations in the proto-oncogene KRAS being identified as the key PDAC tumor-driving oncogene and the most common genetic change, and evidence that it plays distinct roles in mouse models both in tumor initiation and tumor maintenance (reviewed in [8]), the development of direct inhibitors of mutant KRAS has been problematic. Other indirect approaches that act to prevent the translocation of KRAS to the plasma membrane, its activation by exchange factors, or act in a synthetic lethal manner, may be more promising [9]. Current treatments in PDAC however utilize instead relatively nonselective cytotoxic agents, often in combination, but unfortunately with limited efficacy [1]. Moreover, such treatments can be difficult to tolerate without robust responses in many cases [1]. Therefore, there is a clear clinical need

both to understand in more depth the mechanisms of PDAC tumor evolution and heterogeneity, and to understand mechanisms of tumor maintenance in the face of limiting nutrients in order to develop new therapeutic strategies.

Recent studies have unveiled many metabolic adaptations activated downstream of KRAS signaling, which play important roles in determining the unique biology characteristic of PDAC, and which may ultimately lead to novel therapeutic regimens that target metabolic addictions found in PDAC (reviewed in [10–12]). These adaptations are found associated with several unique features of the biology of PDAC. In particular, the pancreatic tumor microenvironment contains a dense fibrotic stroma termed desmoplasia and a relatively low cancer cell cellularity in which intratumor interstitial pressure is high relative to normal pancreas [13]. Aside from PDAC tumor cells themselves, PDAC tumors contain a large population of activated fibroblasts (termed pancreatic stellate cells, PaSCs, or PSCs), which normally reside in exocrine areas of the pancreas, and various immune cells within the tumor microenvironment [14]. The high interstitial pressure found in advanced PDAC is thought to result at least in part from extensive deposition of ECM proteins from PSCs, including the glycosaminoglycan hyaluronan which is a CD44 ligand involved in cell-ECM adhesion [13]. As a result, the vascular capillaries collapse, limiting perfusion of oxygen and nutrients to the tumor and generating a hypoxic tumor microenvironment [14, 15] that acts to impair drug delivery to tumor cells [13]. Despite these harsh environmental conditions however, PDAC cells are capable of surviving, proliferating, and metastasizing due to various metabolic adaptations.

2 Nutrient Sensing

In normal cells, the utilization of extracellular nutrients depends both on the metabolic needs of the cell and their detection by a variety of nutrient-sensing mechanisms that prepare the cell to utilize nutrients for anabolic or maintenance functions. These mechanisms are normally tightly regulated to recognize changes in nutrient availability and elicit differential responses [16]. Critical responses that have been well studied include the activation of Adenosine MonoPhosphate–activated protein Kinase (AMPK) upon glucose restriction, and inhibition of the mechanistic Target of Rapamycin Complex 1 (mTORC1) upon amino acid restriction.

AMPK is generally activated physiologically upon detection of decreased cellular ATP levels, resulting in AMP accumulation, and phosphorylates an increasing variety of substrates [17]. Overall the result of AMPK activation in most cells is a cessation of energy-consuming anabolic processes such as protein and lipid synthesis, an enhancement of glucose and lipid catabolism to regenerate ATP, or induction of autophagy [17]. mTORC1, on the other hand, is activated by the presence of both growth factors and amino acid nutrients, promoting various aspects of cell growth including ribosome biogenesis and inhibiting autophagy, and in normal cells is inhibited by energy stress or by overall or specific amino acid restriction [16].

AMPK can itself repress mTORC1 activation, either by phosphorylation and activation of the mTORC1 pathway inhibitor, tumor sclerosis complex 2 (TSC2, [18]) or by phosphorylation of Raptor [19], a regulatory and structural component of the mTORC1 complex. The activation of mTORC1 inhibits autophagy [20] and therefore AMPK can induce autophagy either directly or indirectly through negative regulation of mTORC1. Additionally, AMPK can itself directly activate both bulk autophagy and mitophagy (breakdown of mitochondria) independently of its regulation of mTORC1 through phosphorylation and activation of ULK1 (Unc-51 Like Autophagy Activating Kinase 1) the mammalian ortholog of Atg1, a key initiator of the autophagic process in yeast [21]. AMPK can further promote mitophagy directly by facilitating mitochondrial fission through phosphorylation of a fission-promoting protein present on the outer mitochondrial membrane, MFF (Mitochondrial Fission Factor [22]).

During tumor progression, tumor cells are now appreciated to undergo metabolic reprogramming which enables them to utilize anabolic and catabolic pathways in a manner that promotes their survival and unrestricted proliferation. PDAC tumor cells exhibit many such adaptations and are capable of surviving in hypoxic microenvironments as well as in metastatic niches by activating both nutrient scavenging and nutrient acquisition pathways [10]. These strategies endow PDAC tumor cells with a selective advantage over normal pancreatic cells and are thought to be critical to promote their sustained viability and proliferation under harsh environmental conditions [11]. However, these aspects of deregulated PDAC cell function may themselves represent tumor-specific vulnerabilities and be sensitive to targeted therapies [10, 12].

3 Autophagy

The PDAC tumor microenvironment is characterized by local hypoxia [23] and limited accessibility to nutrients [15]. Therefore, PDAC tumor cells utilize a number of scavenging mechanisms to exploit the limited nutrients available through the vasculature. One of these mechanisms, leading to nutrient recycling, is autophagy (also termed macroautophagy), a process that normally results in the regulated degradation and recycling of cellular components for biosynthesis [24]. However autophagy also performs an important function in normal cells in cellular quality control by acting to eliminate potentially toxic protein aggregates and/or damaged organelles [25].

Through autophagy, macromolecules are first sequestered within double-membrane microtubule-associated protein 1A/1B-light chain 3 (LC3)-positive vesicles, the autophagosomes. Through a regulated series of events, autophagosomes ultimately fuse with lysosomes forming autolysosomes that mediate the digestion of the internalized cytoplasmic components. The autolysosome digestion products, namely amino acids, nucleotides, fatty acids, sugars, and ATP, are then transported back from the lysosome to the cytoplasm where they serve as biosynthetic precursors, cofactors or as an energy source for cells undergoing nutrient

starvation [26]. One of the key mechanisms used by nutrient-deprived cells for autophagy initiation is via the activation and suppression of the protein kinases AMPK and mTORC1, which regulate autophagic capacity through ULK1/2 and ATG13 proteins [24]. An alternative mechanism of autophagic stimulus (that is independent of ULK1 activation) occurs through the accumulation of ammonia produced by amino acid catabolism during glucose restriction [27].

Previous studies have indicated critical, but contrasting, roles for autophagy in cancer, and the same appears true in PDAC [28]. On the one hand, autophagy is thought to constitute a barrier to tumor formation through mitigation of oxidative stress/ROS and subsequent effects upon genomic integrity within premalignant PanINs [29]. In contrast, autophagy can also promote tumor formation in a number of cancer model systems (reviewed in [28]). In the progression of PDAC, autophagy appears also to play opposing tumor suppressive and tumor promoting roles [30]. Evidence for tumor suppressive function(s) of autophagy comes from pancreas-specific knockouts of autophagy regulators Atg5 or Atg7 that show an augmented emergence of KRASG12D-driven premalignant pancreatic lesions following autophagy inhibition [31]. Thus, it appears that in the early stages of PDAC progression autophagy acts in a tumor suppressive manner to prevent the initiation of premalignant lesions that act as a precursor to PDAC.

However, it is also clear that elevated basal autophagy (in the absence of starvation of nutrients) is a major feature of PDAC tumor cells, even when such cells are grown ex vivo under cell culture conditions in which nutrients are unlikely to be limiting, and is itself required for tumor progression in vivo [31]. Induction of autophagy however appears to be a relatively late event in PDAC development [31] and increased autophagy, as determined by LC3 immunocytochemistry, correlates with poorer clinical outcome in PDAC patients [32]. At least in part this is likely to be due to autophagy inhibition leading to a reduced degree of tumor cell proliferation rather than survival and is known to be dependent in some contexts upon intact TP53, but not in others [10]. Using an inducible mouse model of mutated KRAS in a p53Lox/WT background, thought to be analogous to that occurring in advanced PDAC, has shed further light on the role autophagy performs in advanced PDAC development. Ablation of KRAS in this model results in pancreatic tumor regression within 2–3 weeks followed by relapse after a few months. Transcriptome analysis of tumor cells surviving KRAS ablation revealed a significant enrichment of genes involved in lysosomal activity, mitochondrial electron transport chain, and autophagy, indicating that induction of increased autophagy and lysosomal activity was critical for tumor relapse [33].

Major questions that have arisen following these observations are what mechanisms lead to increased basal autophagy, and how they are related to the specific genetic changes found in PDAC? The increased number of autophagosomes and lysosomes frequently identified in PDAC tumor cells [34] suggests that some deregulation of the regulatory mechanisms controlling the abundance of these vesicular organelles occurs in PDAC. Indeed some human PDAC cells have been shown to exhibit both increased expression, and loss of cytoplasmic retention, of members of the microphthalmia/transcription factor E (MiT/TFE) family of

transcription factors [34] that are known to induce a transcriptional program that acts to increase lysosome biogenesis and therefore lysosomal catabolism [35].

In normal cells cultured under nutrient replete conditions, MiT/TFE factors are thought to be negatively regulated via phosphorylation by mTORC1 present on lysosomal membranes, leading to their interaction with cytosolic 14-3-3 proteins and nuclear exclusion [35, 36]. However, in PDAC cells, and despite elevated mTORC1 activity, MiT/TFE factors appear to be preferentially nuclear [34], indicating that additional regulatory events active in PDAC cells act to override mTORC1-mediated regulation, thereby promoting nuclear localization of MiT/TFE factors. Although the nature of these mechanisms, and how they operate preferentially in PDAC tumor cells, remain to be elucidated, they may impact on the function of importins such as IPO8/7 that direct nuclear import of specific cargo [37]. Thus, knockdown of these two importins in PDAC cells has been shown to prevent MiT/TFE nuclear localization [34].

Autophagy as a tumor promoting process might also represents a therapeutic target in PDAC. The antimalarial drug chloroquine (or its analog hydroxychloroquine, HCQ) is thought to block autophagic flux by increasing the normally low pH typical of lysosomes, thereby blocking the final stage of autophagy [38]. In preclinical studies, HCQ treatment has shown promise in inhibiting tumor growth in patient-derived xenograft (PDX) and human PDAC cell line xenograft mouse models [39]. Currently HCQ is in fact under evaluation in several clinical trials for PDAC treatment in the US, including as a single agent in metastatic cancer (trial designation: NCT01273805), in combination with gemcitabine (NCT01128296, [40]), in combination with gemcitabine/nab-paclitaxel (NCT01506973), or in combination with capecitabine with either radiation or proton therapy (NCT01494155). However, a key shortcoming of HCQ treatment is its poor drug pharmacodynamics whereby relatively long periods of drug administration are required to reach therapeutic levels [41]. However, when HCQ has been used under conditions where evidence of autophagy inhibition has been clearly established as a biomarker of drug efficacy [40], improved disease-free and overall survival in PDAC patients has been demonstrated. As an alternative to HCQ, Lys05, a novel dimeric derivative of chloroquine, has been shown to have significant in vivo activity, both as a single agent [42] and in combination with a BRAF inhibitor [43]. Interestingly, the inhibition of autophagy in PDAC is known to incur additional effects on metabolism that may have therapeutic implications. Thus, upon autophagy inhibition PDAC cells have been found to utilize less oxygen during oxidative phosphorylation in mitochondria, and instead switch to increased dependence upon glycolysis as a source of ATP [28, 31].

4 Macropinocytosis

In addition to autophagy and the recycling of intracellular material for biosynthesis, PDAC cells also have the ability to internalize extracellular macromolecules such as proteins and lipids through an endocytic process called macropinocytosis. After being internalized, the macromolecules are carried through large vesicles, the

macropinosomes, which ultimately fuse, as with autophagosomes during autophagy, with lysosomes [44], where the degradation of their components occurs. Degradation products are eventually transported from lysosomes and used to fuel other biosynthetic processes. Several studies have demonstrated that KRAS oncogenic mutations, including KRAS mutations found in human PDAC tumor cells, can strongly upregulate the process of macropinocytosis [45].

Macropinocytosis of serum proteins such as albumin has been shown to be a vital source of amino acid supplementation in PDAC cells undergoing glutamine starvation, and PDAC cell treatment with inhibitors that block macropinocytosis, as for example the endocytosis of albumin, can suppress tumor cell proliferation in vitro and tumor development in vivo [15, 45]. In addition, macropinocytosis can be used to internalize both extracellular material and membrane receptors. Thus, oncogenic KRAS-transformed primary pancreatic ductal cells have been shown to also internalize extracellular lipids to promote their proliferation [46, 47], while other cancer cells have also been shown to internalize extracellular ATP to support ATP-consuming biosynthetic processes [48]. In addition to accumulating soluble nutrients such as proteins and ATP, cancer cells are known to internalize a class of secreted vesicles, called exosomes or microvesicles, through macropinocytosis [49]. For PDAC tumor cells, internalizing exosomes requires KRAS and EGFR-dependent macropinocytosis [49], while other cell types, such as cancer-associated fibroblasts (CAFs), do not apparently require oncogenic KRAS signaling to internalize exosomes [50]. Interestingly, PDAC tumor cells can also release exosomes that may induce dysfunction in normal cells, although the consequences of this for disease progression are currently less clear. Thus, PDAC tumor cells have been shown to release exosomes that can be internalized by normal cells such as pancreatic β-cells, or subcutaneous adipose tissues, to negatively impact insulin secretion or stimulate lipid breakdown, respectively [51].

As cancer cells frequently employ macropinocytosis to aid in receptor regulation and internalize essential metabolites, extensive efforts have been underway in utilizing macropinocytosis therapeutically to deliver cytotoxic drugs specifically into PDAC and other cancers. Some anticancer agents innately undergo macropinocytosis, such as AS1411, which internalizes into various cancer cells through cell-surface nucleolin-dependent mechanisms that activate macropinocytosis only in malignant cells [52]. Other therapeutics specifically target cell surface receptors that may trigger macropinocytosis. For example, therapeutic drugs conjugated with peptides that target a combination of proteoglycans and keratinocyte growth factor receptors (KGFR) can selectively internalize into and kill KGFR-expressing lung cancer cells via macropinocytosis [53].

Another intriguing therapeutic front includes conjugating cytotoxic drugs onto albumin not only to enhance drug pharmacokinetics, but also because albumin has long been observed to accumulate within solid tumors through macropinocytosis [54]. An example includes the FDA-approved nanoparticle albumin-bound form of paclitaxel (nab-paclitaxel or Abraxane®) for treating multiple cancers, including PDAC [1]. However, cancers are still able to overcome these drugs through acquired resistance, likely via differential regulation of proteins that regulate

macropinocytosis, including cytoskeletal and lipid metabolism proteins [55], or through increased expression of drug exporters such as P-glycoprotein [56]. Other albumin-based conjugates targeting folate receptors have also demonstrated efficient delivery of cytotoxic compounds specifically into cancer cells [57]. Finally, as both the autophagic and macropinocytotic pathway converge into lysosomal uptake and digestion of macromolecules, the lysosome can be considered as a therapeutic target for both processes [11].

5 Redox Balance and Reactive Oxygen Species

Reactive Oxygen species (ROS) are damaging metabolic byproducts generated upon cellular metabolic processes, including oxidative phosphorylation in mitochondria and the action of cytosolic or membrane-associated nicotinamide adenine dinucleotide phosphate (NADPH) oxidases. They are responsible for damage via oxidation of proteins, DNA, and lipids, and when left unmanaged can lead to cell death. Furthermore, the oxidation of DNA is one of the leading causative factors of mutations through generation of 8-hydroxy-2′-deoxyguanosine [58]. However, ROS should no longer considered as simply a damaging byproduct of metabolism as they are now known to also play a significant role in regulating multiple cellular signaling processes, including immune responses, inflammation, adhesion, and cell migration [59].

The generation of ROS has been demonstrated to be crucial for both KRAS transformation and KRAS-driven PDAC tumor expansion [60, 61]. As mentioned earlier, PDAC is characterized by a predominant desmoplastic response, and the activation of PSCs appears to be mainly responsible for the desmoplasia typical of PDAC [14]. ROS may here be an important mediator in the activation of PSCs in this process. During hypoxia, ROS can activate PSCs by stabilization of the transcription factor hypoxia-inducible factor 1α (HIF-1α) and upregulation of the zinc finger transcription factor GLI1 (also known as glioma-associated oncogene) and promote release of other cytokines and growth factors such as IL-6, SDF-1, and VEGF-A to promote pancreatic cancer cell invasion [62]. ROS can also act as an adaptive strategy to inhibit autophagic cell death and its antiautophagic effect may be mediated by upregulating AKT/mTOR signaling in PDAC [63]. In PDAC, the presence of oncogenic KRAS might increase cytoplasmic ROS production through activating NADPH oxidase 4 (Nox4), which is regulated by mitogen-activated protein kinase (MAPK) signaling [64, 65]. As part of the desmoplastic reaction, extracellular components such as fibronectin and laminin may also positively promote Nox4 expression in a 5-lipoxygenase-dependent manner [66]. Oncogenic KRAS is also known to favor the generation of one type of ROS species, superoxide anion, by upregulating the levels of NADPH oxidase 2 (Nox2), an enzyme responsible for electron transfer from NADPH to oxygen molecules. Nox2 activity may critical for PDAC devolvement as Nox2 inhibition in PDAC cell lines can hamper clonal expansion [61]. Relatively similar results have been generated after Nox4 inhibition, indicating that Nox4 (which directly generates an alternative ROS

species, hydrogen peroxide) is also important for PDAC survival [67]. Reduced NADPH enables the preservation of the pool of reduced glutathione, which is essential for subsequent glutathione oxidation, a crucial event for the down-regulation of intracellular ROS levels. The redox capacity of the cells is maintained through the NADP+/NADPH balance that controls recycling of oxidized glutathione [68]. Elevated levels of intracellular ROS within PDAC tumor cells likely promote the progression of pancreatic cancer in the following ways: (1) supporting cell proliferation and survival [64, 66]; (2) promoting angiogenesis via increasing expression of IL-8 [69]; and (3) inducing invasion and metastasis through promoting EMT [70], and increasing the expression of matrix metalloproteases (MMPs) [71].

Cellular control of ROS levels occurs principally through the nuclear factor (erythroid-derived 2)-like 2 (Nrf2) transcription factor that promotes the transcription of various genes essential for ROS detoxification. Such genes include glutathione reductase, NADPH:quinone oxidoreductase 1 (NQO1), thioredoxin, as well as enzymes related to NADPH production such as malic enzyme ME1 [72]. Indeed, Nrf2 has been shown to be overexpressed and activated in PDAC and enables the tumor cells to elicit a sustained ROS detoxification response critical for KRAS-induced tumorigenesis in PDAC models [73]. Therefore, PDAC tumor cells utilize a number of different mechanisms in order to utilize, but carefully control, increased ROS levels to promote tumor survival and proliferation.

6 Glucose Metabolism

Glucose is the principal growth-supporting substrate in cancer cells and can act as a major provider of carbon for biosynthesis of various macromolecules. Cancer cells are now appreciated to exhibit an aberrant metabolic profile that differs from that of their differentiated counterparts [74]. A major manifestation of this profile is that the presence of oxygen does not restrict glycolysis. This phenomenon, termed aerobic glycolysis and described first by Otto Warburg, is the capacity of cancer cells to metabolize glucose even in the presence of sufficient oxygen, producing lactate [75, 76]. Many human tumors have now been shown to exhibit augmented glucose acquisition coupled to increased flux through downstream glycolytic metabolic pathways. Thus, it is not surprising that mutations in KRAS found in PDAC (as well as other oncogenes and tumor suppressors) reprogram cellular metabolism by acting upon both acquisition and metabolic flux of glucose [60]. Perhaps surprisingly however, in the vascular-poor PDAC microenvironment, overall levels of glucose, and glucose uptake, are thought to be modest compared with other tumor types, and steady-state glucose concentrations have been found not to be significantly elevated compared with normal pancreatic tissue [15]. However despite this, higher levels of glucose uptake (determined by 18F-fluoro-2-deoxyglucose positron emission tomography, FDG-PET) and expression of the glucose transporter GLUT1 have been shown to correlate with poor prognosis in PDAC [77]. Moreover, KRAS-driven alterations in glucose uptake and utilization have been shown to be required,

at least in part, for PDA tumorigenesis [78]. This increased glucose uptake might be facilitated further in PDAC lacking TP53 function, as expression of wild-type TP53 negatively regulates the expression of two different glucose transporters, GLUT1 and GLUT3 [79]. As might be anticipated, in an inducible transgenic GEM model, KRAS silencing strongly reduces glucose uptake and is associated with down-regulation of GLUT1 and multiple enzymes involved in subsequent stages of glycolysis [11, 78]. Indeed, although mutant KRAS can clearly activate the expression of several glycolytic enzymes and alter the glycolytic pathway flux [78], other mechanisms, including hypoxia, have similarly been shown to activate glycolytic enzyme gene expression in PDAC [80]. In contrast, mitochondrial metabolism/ATP generation is likely to be contributed to mainly by glutamine carbon in PDAC cell lines [78, 81].

With more glucose entering PDAC tumor cells, six-carbon units can be diverted into parallel biosynthetic routes, particularly via recruitment of glucose-6-phosphate and other glucose derivatives into both the nonoxidative pentose phosphate pathway (PPP) and hexosamine biosynthesis pathway (HBP) [78]. These twin alterations appear to be KRAS dependent in PDAC and occur via increased expression of two PPP enzymes (ribose-5-phosphate isomerase A and ribulose-5-phosphate-3-epimerase) that promote increased flux of ribulose-5-phosphate (R5P) through the nonoxidative PPP, as well as upregulation of the first enzyme in the HBP pathway, glutamine fructose-6-phosphate amidotransferase (GFPT1) [78]. Additionally however, hypoxia-driven HIF-1α stabilization can also enhance the nonoxidative arm of the PPP by increasing the expression of transketolase genes [82]. This unusual reliance upon the nonoxidative PPP may itself represent a therapeutic target in PDAC, as normal pancreatic cells are thought to generate R5P mainly via the oxidative phase of the PPP [83].

For HBP, the metabolic products are uridine diphosphate-*N*-acetylglucosamine and other nucleotide hexosamines which are major substrates for protein and lipid glycosylation [84]. Indeed, following suppression of KRAS in PDAC, the overall O-glycosylation and tumorigenicity has been found to be reduced dramatically [78]. Excessive O-glycosylation has been previously described in PDAC cells as eliciting an antiapoptotic effect by modulation of nuclear factor-kappa-B (NF-κB) [85]. It should also be noted that in hypoxic conditions, the levels of O-glycosylation in proteins are also thought to be elevated, possibly as an adaptive response to stabilize proteins important for the survival of cells under conditions of low nutrients and oxygen [86]. Thus both KRAS and a hypoxic microenvironment may synergize to elevate O-glycosylation, thereby contributing to PDAC tumor cell survival.

Although such metabolic diversions permit biosynthetic intermediates to be synthesized, the major fate of glucose in PDAC remains lactate [86], converted from pyruvate via lactate dehydrogenase (LDH). PDAC cells are known to alter the flux of this conversion of glucose to lactate in two ways: first, via a KRAS-driven increase in LDHA transcription [78]; and second, by deacetylation of lysine 5 in the LDHA protein, which acts to promote enzymatic activity [87]. To combat the increased accumulation of lactate, PDAC tumor cells also enhance the mechanisms of lactate efflux to the extracellular environment. This occurs in at least three ways.

Firstly, via a combined upregulation of the monocarboxylate transporters for lactate, MCT1 and MCT4, the latter particularly in hypoxic tumor regions [86]. Secondly, by upregulation of a specific G-protein-coupled receptor for lactate, GPR81, which can increase the expression of lactate transporters, and thirdly via increased expression of CD147 that acts as a chaperone for newly synthesized MCT transporters [10, 80].

Given the large production and efflux of lactate, other consequences might be anticipated. Indeed, the use of lactate as an alternative fuel for biosynthesis in some PDAC has been suggested, with lactate produced by PDAC tumor cells in hypoxic areas of the tumor feeding PDAC tumor cells in normoxic areas [86]. Lactate secretion also has been shown to have unexpected effects upon epithelial-stromal interactions. Thus lactate secreted from PDAC cells has been shown to contribute to polarization of a population of immunosuppressive macrophages [88]. Although the full consequences of excess lactate in the PDAC microenvironment remain to be established, in other cancers increased levels of lactate efflux have various other tumor-promoting effects. These include promoting the emergence of an immune-permissive microenvironment by attenuating monocyte migration [89] and dendritic [90] and T cell activation [91]. Furthermore, lactate accumulation is important to promote angiogenesis. Thus, lactate can induce secretion of the proangiogenic factor VEGF from tumor-associated stromal cells [92], while increased levels of lactate can stimulate hyaluronic acid production by fibroblasts, which may contribute to subsequent tumor invasiveness [93]. The final step of glycolysis, the conversion of pyruvate to lactate by LDH, is required to regenerate NAD+ and thus to facilitate continued cycles of glycolysis in PDAC. Thus, LDH represents a potentially attractive drug target in PDAC, as blocking lactate production would be expected to inhibit glycolysis. Indeed, FX11, an inhibitor of LDH [94] has been shown to reduce growth and induce apoptosis in PDAC PDXs in a preclinical study [95].

7 Glutamine Metabolism

The unexpected finding that the generation of pentoses is uncoupled from NADPH generation in PDAC, with a reliance instead upon the nonoxidative arm of the PPP [81], led to the issue of understanding how PDAC tumor cells can then generate enough NADPH to maintain redox homeostasis. An apparently PDAC-specific glutamine-consuming pathway generating NADPH identified in PDAC [78] has provided a potential explanation for this issue of NADPH deficit. Perhaps unsurprisingly, given its relative abundance in blood plasma [96], the amino acid glutamine plays critical metabolic roles in PDAC, particularly in maintenance of redox homeostasis [11].

In addition to its role in protein biosynthesis, glutamine acts as a major source of carbon and nitrogen for biosynthesis in proliferating cells [96]. PDAC cells grown in culture are known to require glutamine for both proliferation and redox balance [81]. Redox balance is thought to be achieved by two means: by increased generation of the antioxidant glutathione from glutamine-derived glutamate; by utilization of an unusual method of production of NADPH [81], which is itself involved in recycling

of oxidized glutathione and in other reducing reactions. In regard to glutamine-derived glutathione, glutathione abundance has been found to be increased in PDAC in comparison to normal pancreatic tissue, with inhibition of glutathione synthesis in vitro inducing growth inhibition and promoting apoptosis [97]. This latter pathway appears to be driven by oncogenic KRAS and converts glutamine-derived carbon into aspartate. This occurs within mitochondria via a series of reactions that firstly utilize the mitochondrial Asp aminotransferase (GOT2) [81]. Glutamine-derived aspartate is then transported into the cytosol and acted upon by a second enzyme, aspartate aminotransferase (GOT1), generating oxaloacetic acid (OAA). OAA is then converted to pyruvate by the cytoplasmic form of malic enzyme 1 (ME1), yielding NADPH [81]. This pathway of glutamine metabolism may also represent a specific metabolic vulnerability in PDAC as is has not been found to be used in normal pancreatic cells [81].

In addition to activation of the above mitochondrial/cytosolic pathway, as discussed previously mutant KRAS also initiates a nuclear Nrf2 transcription factor-dependent ROS detoxification program [72, 98]. The Nrf2 transcriptional response is normally activated in most cells by redox stress [99]; however, mutant KRAS constitutively activates this transcriptional program to suppress ROS and promote PDAC tumorigenesis and proliferation [100]. The Nrf2-directed transcriptional response has also been shown to redirect glucose and glutamine into anabolic and antioxidant pathways [72, 98]. Nrf2 also increases ME1 expression, thereby linking mutant KRAS with increased flux through ME1, generating increased NADPH to assist redox homeostasis [81]. Interestingly, the expression of malic enzymes ME1 and ME2 are transcriptionally repressed by wild-type TP53 [79], indicating again that the loss of TP53 function in advanced PDAC might synergize with KRAS to further increase metabolic flux to generate increased NADPH levels. Underscoring the importance of this antioxidant pathway, inhibition of these enzymes involved in NADPH generation in PDAC impairs viability both in vitro and in vivo [81]. Since Nrf2 also activates glutathione biosynthesis [98], mutant KRAS appears to enhance antioxidant defense in PDAC both via enhanced NADPH-dependent recycling of oxidized glutathione, and by an Nrf-2-dependent increase in glutathione synthesis.

In addition to contributing to redox homeostasis, glutamine plays a key role in providing substrates for biosynthesis via glutaminolysis by generating α-ketoglutarate (α-KG). α-KG is produced via the action of glutamate dehydrogenase (GLUD1) upon glutamate, with glutamate produced via breakdown of glutamine by glutaminases (GLSs) in mitochondria. Ultimately, this leads to the generation of α-KG–derived intermediates from the TCA cycle that are subsequently utilized in fatty acid (FA) synthesis [96], or in generating nonessential amino acids with glutamine acting as the nitrogen donor [96]. In PDAC tumor cells, KRAS acts to increase GOT1 while suppressing GLUD1 expression [81], suggesting that PDAC tumor cells preferentially utilize glutamine to counteract redox homeostasis and promote ROS detoxification, rather than to promote biosynthesis. Since ROS, generated by the action of NADPH oxidases Nox2 and Nox4, is increased by KRAS and is itself required for clonogenic growth [61, 67] and EMT [101] in

PDAC, it appears that the benefits of ROS for PDAC tumor cells are counteracted by glutamine-derived NADPH, thereby preventing excessive ROS inducing deleterious effects upon viability.

8 Alterations in Lipid Metabolism in PDAC

Metabolomic studies in the lipid metabolism mechanisms of PDAC cancers have surprisingly shown that they bear a lower fatty acid (FA) content when compared to normal surrounding tissue [43, 102]. However, when a study assessed the effects of dietary fat on a GEMM model of PDAC development, it was demonstrated that the high levels of lipids obtained from the diet led to a KRAS-COX2-dependent increase in the formation of PanINs and PDACs [103]. Indeed, high-fat diets and obesity are strongly linked with PDAC incidence [104], suggestive of a role of lipids in PDAC initiation or progression. Interestingly, PDAC tumor lines cultured with oleic (a monounsaturated omega-9 fatty acid) or linoleic acid (a polyunsaturated omega-6 fatty acid) have increased the rates of proliferation [105], suggesting that some FAs may be limiting for tumor growth, and rapidly metabolized. Consistent with this notion, KRAS transformation of normal immortalized pancreatic ductal epithelial cells (HPNE) is also known to increase scavenging of extracellular lysophospholipids as an alternative source of FAs [46], while PDAC cells exhibit increased acquisition of cholesterol [47]. Fatty acid synthase has also been reported to be upregulated in PDAC, likely downstream of KRAS via MAPK signaling, with increased expression correlating with poor prognosis [106].

9 Metabolic Crosstalk in the PDAC Tumor Microenvironment

One of the most prominent characteristics of PDA is an intense desmoplastic reaction around the tumor. Surrounding stroma occupies the largest volume of the tumor and it is developed from noncancerous cells including pancreatic stellate cells, immune cells, and endothelial cells surrounded by a dense extracellular matrix rich in collagen and hyaluronic acid [107]. As previously discussed, the formation of this unusual stroma induces a poorly vascularised microenvironment that limits the diffusion of oxygen and nutrients alike in PDAC [15, 108]. As a result of the limited vasculature, carcinomas are hypoxic and require adaptation to sustain their growth [11]. PSCs are the most abundant resident fibroblast-like cells present in lesions of the pancreas and a variety of evidence indicates are responsible for the desmoplastic reaction [14]. In healthy exocrine pancreas, PSCs are thought to maintain normal tissue architecture via regulation of the synthesis and degradation of extracellular matrix (ECM) proteins [109]. Following injury or inflammation, PSCs transform from their quiescent phase into an activated, myofibroblast-like phenotype, secreting excessive amounts of ECM proteins leading to the fibrosis typical of chronic pancreatitis and PDAC [109]. Furthermore, PSCs can also regulate the turnover of the tumor stroma through the expression of matrix metalloproteinases

such as MMP1 and MMP2 [110]. Targeting the stroma through enzymatic modulation of hyaluronic acid enhances the delivery of chemotherapeutic agents and therefore increases the cytotoxic potential of those drugs [13].

PDAC cells can initiate a reciprocal signaling network between the tumor cells and the neighboring PSCs [111]. In the face of poor nutrient supply from the vasculature, metabolites are accessed by PDAC tumor cells from surrounding stromal cells [112]. PSCs have for example been found to release nonessential amino acids (NEAAs) in response to culture with PDAC tumor cells [112]. PDAC cells in particular consume PSC-derived alanine and use it to fuel additional metabolic processes including mitochondrial metabolism, fatty acid synthesis, and synthesis of other amino acids [112]. The mechanism involved in such nutrient accessing by PDAC tumor cells appears to be via autophagy that is induced within PSCs. Indeed, the blockage of autophagy prevents alanine release from PSCs, although the specific mechanism of alanine release remains to be established [112].

Another component of the tumor microenvironment is infiltrating leucocytes. The T-lymphocytes account for the most abundant cell type in adaptive immunity and are responsible for the identification of foreign antigens which have been previously processed and presented by antigen-presenting cells (APCs), such as dendritic cells and macrophages. Antigen recognition mediated through T-cell-APC interaction leads to T-cell activation, clonal expansion, and migration toward the antigens where the T-cells exert various effects according to their subtype.

The T-cells are divided into CD4+ T-helper cells which are further subdivided into Th1, Th2, and Th17 populations; CD8+ cytotoxic cells; and regulatory T-cells (Tregs). Each of the T-cell subtypes has distinct functions; the polarization of the CD4+ cell populations is triggered by different cytokine combinations, and therefore Th1, Th2, and Th17 cells display differential cytokine production patterns with opposing effects. The CD8+ cells are responsible for cell-mediated cytotoxicity whereas the Tregs exhibit immunosuppressive properties [115].

CD8+ cells are capable of infiltrating tumor sites and killing cancer cells and have therefore been associated with better prognosis in numerous cancer types, among them melanoma, head and neck cancer, lung, breast, and colon cancer. However, human PDAC is characterized by poor CD8+ T-cell infiltration to the tumor site. This could be attributed to the low mutation rate observed in PDAC in contrast to other KRAS-induced cancers (e.g., lung cancer), which leads to the limited formation of neoantigens that could be recognized by the T-cells [113]. Furthermore, the formation of a tumor microenvironment with a predominant presence of Th2 cells, Tregs, MDSCs, and immunosuppressive cytokines further impedes the CD8+ T-cell activation, favoring tumor sustainability and progression.

CD4+ T-cells play a pivotal role in the regulation of CD8+ T-cell function and therefore the predominance of the Th2 cells in the PDAC tumor milieu are thought to significantly hamper the activation of the CD8+ T-cells through the production of immunosuppressive cytokines such as IL-4, IL-5, and IL-10 [114]. On the other hand, the Th1 cells can suppress tumor proliferation by producing IL-2 and IFN-g which have a proinflammatory effects and are essential for CD8+ T-cell activation and proliferation [115]. Therefore, the Th1/Th2 ratio is crucial in order to determine

whether the elicited immune response at the tumor site will either suppress or promote tumour growth [115].

Aside from the large amounts of Th2 cells, the PDAC tumor microenvironment is also preoccupied with another Tregs, which have a prominent immunosuppressive role [116]. The Tregs can inhibit the function of several immune cell types such as natural killer cells (NK), B-cells, and dendritic cells through granzyme B production but can also secrete several cytokines such as TGF-β1, IL-6, TNFa, and the receptor activator of NF-κB, which strongly enhance further tumor development [117].

The metabolic landscape of pancreatic cancer microenvironment further enhances tumor progression by dampening the immune response. Infiltration of immune cells can be observed early in the development of pancreatic cancer. PanINs initiate the accumulation of leukocytes that consist mostly of macrophages, $CD4^+$ T regulatory cells (Tregs), and myeloid-derived suppressor cells (MDSC) that all act in an immunosuppressive manner [118]. Effector $CD8^+$ T cells that could suppress tumor growth have only been found in low numbers and with no indication of activity [118].

One of the underlying causes for the lack of significant effector immunity could be the nutrient competition between immune cells and cancer cells. T cells are also known to utilize aerobic glycolysis to support their high needs of energy upon clonal expansion and secretion of various cytokines [119]. Glucose deprivation of T cells leads to "exhaustion," a phenomenon that blocks effector function of T cells and leads to low levels of IFN-γ production [120]. Such an effect has been observed in the studies of sarcoma and melanoma models where the existing pool of glucose in the tumor microenvironment is diminished due to excessive glycolytic metabolism of cancer cells, leading to glucose restriction of nonregulatory CD4+ T helper cells (TH1) [120]. TH1 cells subsequently fail to mount a prominent presentation of the antigen or recruit effector cells.

10 Conclusion

Altered metabolism is now recognized as an important hallmark of cancer [121], and efforts are ongoing to therapeutically exploit some of these metabolic differences between normal and cancer cells [12]. In the case of pancreatic cancer, metabolism is known now to be significantly impacted upon by mutation of the KRAS proto-oncogene, presenting exciting potential opportunities for selective targeting of metabolism in PDAC. Together with KRAS mutations, the hypoxic microenvironment generated by stromal deposition similarly forces PDAC tumor cells to rely on alternative sources of nutrients, and to utilize unique methods to obtain them. Unfortunately however, there are currently no clinical useful mutant KRAS inhibitors, and only a few clinically viable Ras-effector treatments that might be the most direct way to combat altered metabolism in PDAC deriving from mutant KRAS.

Of other mechanisms that might be therapeutically viable in PDAC, recent work indicates that constitutive autophagy – a major feature of PDAC tumor cells – and glutamine utilization, fuelling NADPH reserve to maintain redox homeostasis,

would appear to be two of the most promising avenues for therapeutic intervention. Inhibitors of autophagy, such as HCQ, are currently being assessed in PDAC clinical trials, although HCQ pharmacostability is likely to be an issue, as is penetrance of any small molecule inhibitor through the dense stroma and hypoxic PDAC microenvironment. In the case of therapeutic targeting glutamine utilization, the use of an apparently PDAC-specific breakdown of glutamine is particularly attractive, although whether there are other normal tissues that might use such a strategy would need to be more completely explored.

Confounding such approaches however will likely be the presence within PDAC of distinct metabolic subtypes and significant intratumoral heterogeneity. These might allow significant tumor evolution during the course of any therapy aimed at targeting one specific metabolic feature [122]. In addition, unlike specific fixed genetic alterations such as mutant KRAS, metabolic networks are now known to exhibit inherent plasticity and are therefore likely to be rewired in the face of targeted therapies unless cell death is rapidly obtained [123]. Finally, although there is great interest in dissecting immune responses in the PDAC microenvironment and evolving immunotherapies that attack PDAC cancer cells [124], glycolysis inhibitors targeting PDAC tumor cells may further interfere, in unknown ways, with antitumor immune responses by blocking metabolic alterations also critical for immune cell activation.

11 Cross-References

- ▶ Approaching Pancreatic Cancer Phenotypes via Metabolomics
- ▶ Emerging Therapeutic Targets in Pancreatic Adenocarcinoma
- ▶ Stromal Inflammation in Pancreatic Cancer: Mechanisms and Translational Applications
- ▶ Tumor-Stromal Interactions in Invasion and Metastases 2nd ed
- ▶ Vaccine Therapy and Immunotherapy for Pancreatic Cancer

References

1. Kleeff J, Korc M, Apte M, La Vecchia C, Johnson CD, Biankin AV, et al. Pancreatic cancer. Nat Rev Dis Primers. 2016;2:22.
2. Kanda M, Matthaei H, Wu J, Hong SM, Yu J, Borges M, et al. Presence of somatic mutations in most early-stage pancreatic intraepithelial neoplasia. Gastroenterology. 2012;142(4):730–3.e9.
3. Chan A, Diamandis EP, Blasutig IM. Strategies for discovering novel pancreatic cancer biomarkers. J Proteomics. 2013;81:126–34.
4. Yachida S, Jones S, Bozic I, Antal T, Leary R, Fu B, et al. Distant metastasis occurs late during the genetic evolution of pancreatic cancer. Nature. 2010;467(7319):1114–7.
5. Almoguera C, Shibata D, Forrester K, Martin J, Arnheim N, Perucho M. Most human carcinomas of the exocrine pancreas contain mutant c-K-ras genes. Cell. 1988;53(4):549–54.

6. Jones S, Zhang XS, Parsons DW, Lin JCH, Leary RJ, Angenendt P, et al. Core signaling pathways in human pancreatic cancers revealed by global genomic analyses. Science. 2008;321(5897):1801–6.
7. Yachida S, Iacobuzio-Donahue CA. Evolution and dynamics of pancreatic cancer progression. Oncogene. 2013;32(45):5253–60.
8. Collins MA, Pasca di Magliano M. Kras as a key oncogene and therapeutic target in pancreatic cancer. Front Physiol. 2014;4:407.
9. Cox AD, Fesik SW, Kimmelman AC, Luo J, Der CJ. Drugging the undruggable RAS: mission possible? Nat Rev Drug Discov. 2014;13(11):828–51.
10. Perera RM, Bardeesy N. Pancreatic cancer metabolism: breaking it down to build it back up. Cancer Discov. 2015;5(12):1247–61.
11. Sousa CM, Kimmelman AC. The complex landscape of pancreatic cancer metabolism. Carcinogenesis. 2014;35(7):1441–50.
12. Habrook CJ, Lyssiotis CA. Employing metabolism to improve the diagnosis and treatment of pancreatic cancer. Cancer Cell. 2017;31(1):5–19.
13. Provenzano PP, Cuevas C, Chang AE, Goel VK, Von Hoff DD, Hingorani SR. Enzymatic targeting of the stroma ablates physical barriers to treatment of pancreatic ductal adenocarcinoma. Cancer Cell. 2012;21(3):418–29.
14. Feig C, Gopinathan A, Neesse A, Chan DS, Cook N, Tuveson DA. The pancreas cancer microenvironment. Clin Cancer Res. 2012;18(16):4266–76.
15. Kamphorst JJ, Nofal M, Commisso C, Hackett SR, Lu WY, Grabocka E, et al. Human pancreatic cancer tumors are nutrient poor and tumor cells actively scavenge extracellular protein. Cancer Res. 2015;75(3):544–53.
16. Yan LJ, Lamb RF. Amino acid sensing and regulation of mTORC1. Semin Cell Dev Biol. 2012;23(6):621–5.
17. Hardie DG, Schaffer BE, Brunet A. AMPK: an energy-sensing pathway with multiple inputs and outputs. Trends Cell Biol. 2016;26(3):190–201.
18. Inoki K, Zhu T, Guan KL. TSC2 mediates cellular energy response to control cell growth and survival. Cell. 2003;115(5):577–90.
19. Gwinn DM, Shackelford DB, Egan DF, Mihaylova MM, Mery A, Vasquez DS, et al. AMPK phosphorylation of raptor mediates a metabolic checkpoint. Mol Cell. 2008;30(2):214–26.
20. Kamada Y, Funakoshi T, Shintani T, Nagano K, Ohsumi M, Ohsumi Y. Tor-mediated induction of autophagy via an Apg1 protein kinase complex. J Cell Biol. 2000;150(6):1507–13.
21. Egan DF, Shackelford DB, Mihaylova MM, Gelino S, Kohnz RA, Mair W, et al. Phosphorylation of ULK1 (hATG1) by AMP-activated protein kinase connects energy sensing to mitophagy. Science. 2011;331(6016):456–61.
22. Toyama EQ, Herzig S, Courchet J, Lewis TL Jr, Loson OC, Hellberg K, et al. Metabolism. AMP-activated protein kinase mediates mitochondrial fission in response to energy stress. Science. 2016;351(6270):275–81.
23. Koong AC, Mehta VK, Le QT, Fisher GA, Terris DJ, Brown JM, et al. Pancreatic tumors show high levels of hypoxia. Int J Radiat Oncol Biol Phys. 2000;48(4):919–22.
24. Rabinowitz JD, White E. Autophagy and metabolism. Science. 2010;330(6009):1344–8.
25. Mizushima N, Komatsu M. Autophagy: renovation of cells and tissues. Cell. 2011; 147(4):728–41.
26. Bento CF, Renna M, Ghislat G, Puri C, Ashkenazi A, Vicinanza M, et al. Mammalian autophagy: how does it work? Annu Rev Biochem. 2016;85:685–713.
27. Cheong H, Lindsten T, Wu J, Lu C, Thompson CB. Ammonia-induced autophagy is independent of ULK1/ULK2 kinases. Proc Natl Acad Sci U S A. 2011;108(27):11121–6.
28. Guo JY, Xia B, White E. Autophagy-mediated tumor promotion. Cell. 2013;155(6):1216–9.
29. Mathew R, Karp CM, Beaudoin B, Vuong N, Chen G, Chen HY, et al. Autophagy suppresses tumorigenesis through elimination of p62. Cell. 2009;137(6):1062–75.
30. Kimmelman AC. The dynamic nature of autophagy in cancer. Genes Dev. 2011; 25(19):1999–2010.

31. Yang SH, Wang XX, Contino G, Liesa M, Sahin E, Ying HQ, et al. Pancreatic cancers require autophagy for tumor growth. Genes Dev. 2011;25(7):717–29.
32. Fujii S, Mitsunaga S, Yamazaki M, Hasebe T, Ishii G, Kojima M, et al. Autophagy is activated in pancreatic cancer cells and correlates with poor patient outcome. Cancer Sci. 2008; 99(9):1813–9.
33. Viale A, Pettazzoni P, Lyssiotis CA, Ying HQ, Sanchez N, Marchesini M, et al. Oncogene ablation-resistant pancreatic cancer cells depend on mitochondrial function. Nature. 2014; 514(7524):628–32.
34. Perera R, Stoykova S, Nicolay BN, Ross KN, Fitamant J, Boukhali M, et al. Transcriptional control of autophagy-lysosome function drives pancreatic cancer metabolism. Nature. 2015;524(7565):361–5. U251.
35. Sardiello M, Palmieri M, di Ronza A, Medina DL, Valenza M, Gennarino VA, et al. A gene network regulating lysosomal biogenesis and function. Science. 2009;325(5939):473–7.
36. Roczniak-Ferguson A, Petit CS, Froehlich F, Qian S, Ky J, Angarola B, et al. The transcription factor TFEB links mTORC1 signaling to transcriptional control of lysosome homeostasis. Sci Signal. 2012;5(228):ra42.
37. Chook YM, Suel KE. Nuclear import by karyopherin-betas: recognition and inhibition. Biochim Biophys Acta. 2011;1813(9):1593–606.
38. Poole B, Ohkuma S. Effect of weak bases on the intralysosomal pH in mouse peritoneal macrophages. J Cell Biol. 1981;90(3):665–9.
39. Yang A, Rajeshkumar NV, Wang XX, Yabuuchi S, Alexander BM, Chu GC, et al. Autophagy is critical for pancreatic tumor growth and progression in tumors with p53 alterations. Cancer Discov. 2014;4(8):905–13.
40. Boone BA, Bahary N, Zureikat AH, Moser AJ, Normolle DP, Wu WC, et al. Safety and biologic response of pre-operative autophagy inhibition in combination with gemcitabine in patients with pancreatic adenocarcinoma. Ann Surg Oncol. 2015;22(13):4402–10.
41. Tett SE, Cutler DJ, Day RO, Brown KF. A dose-ranging study of the pharmacokinetics of hydroxy-chloroquine following intravenous administration to healthy volunteers. Br J Clin Pharmacol. 1988;26(3):303–13.
42. McAfee Q, Zhang Z, Samanta A, Levi SM, Ma XH, Piao S, et al. Autophagy inhibitor Lys05 has single-agent antitumor activity and reproduces the phenotype of a genetic autophagy deficiency. Proc Natl Acad Sci U S A. 2012;109(21):8253–8.
43. Ma XH, Piao SF, Dey S, McAfee Q, Karakousis G, Villanueva J, et al. Targeting ER stress-induced autophagy overcomes BRAF inhibitor resistance in melanoma. J Clin Invest. 2014;124(3):1406–17.
44. Racoosin EL, Swanson JA. Macropinosome maturation and fusion with tubular lysosomes in macrophages. J Cell Biol. 1993;121(5):1011–20.
45. Commisso C, Davidson SM, Soydaner-Azeloglu RG, Parker SJ, Kamphorst JJ, Hackett S, et al. Macropinocytosis of protein is an amino acid supply route in Ras-transformed cells. Nature. 2013;497(7451):633–7.
46. Kamphorst JJ, Cross JR, Fan J, de Stanchina E, Mathew R, White EP, et al. Hypoxic and Ras-transformed cells support growth by scavenging unsaturated fatty acids from lysophospholipids. Proc Natl Acad Sci U S A. 2013;110(22):8882–7.
47. Guillaumond F, Bidaut G, Ouaissi M, Servais S, Gouirand V, Olivares O, et al. Cholesterol uptake disruption, in association with chemotherapy, is a promising combined metabolic therapy for pancreatic adenocarcinoma. Proc Natl Acad Sci U S A. 2015;112(8):2473–8.
48. Qian Y, Wang X, Liu Y, Li Y, Colvin RA, Tong L, et al. Extracellular ATP is internalized by macropinocytosis and induces intracellular ATP increase and drug resistance in cancer cells. Cancer Lett. 2014;351(2):242–51.
49. Nakase I, Kobayashi NB, Takatani-Nakase T, Yoshida T. Active macropinocytosis induction by stimulation of epidermal growth factor receptor and oncogenic Ras expression potentiates cellular uptake efficacy of exosomes. Sci Rep. 2015;5:10300.

50. Zhao HY, Yang LF, Baddour J, Achreja A, Bernard V, Moss T, et al. Tumor microenvironment derived exosomes pleiotropically modulate cancer cell metabolism. Elife. 2016;5:e10250.
51. Sagar G, Sah RP, Javeed N, Dutta SK, Smyrk TC, Lau JS, et al. Pathogenesis of pancreatic cancer exosome-induced lipolysis in adipose tissue. Gut. 2016;65(7):1165–74.
52. Reyes-Reyes EM, Teng Y, Bates PJ. A new paradigm for aptamer therapeutic AS1411 action: uptake by macropinocytosis and its stimulation by a nucleolin-dependent mechanism. Cancer Res. 2010;70(21):8617–29.
53. Iglesias R, Koria P. Leveraging growth factor induced macropinocytosis for targeted treatment of lung cancer. Med Oncol. 2015;32(12):259.
54. Kratz F. Albumin as a drug carrier: design of prodrugs, drug conjugates and nanoparticles. J Control Release. 2008;132(3):171–83.
55. Zhao M, Li H, Bu X, Lei C, Fang Q, Hu Z. Quantitative proteomic analysis of cellular resistance to the nanoparticle Abraxane. ACS Nano. 2015;9(10):10099–112.
56. Zhao M, Lei C, Yang Y, Bu X, Ma H, Gong H, et al. Abraxane, the nanoparticle formulation of paclitaxel can induce drug resistance by up-regulation of P-gp. PLoS One. 2015; 10(7):e0131429.
57. Shi M, Cui J, Du J, Wei D, Jia Z, Zhang J, et al. A novel KLF4/LDHA signaling pathway regulates aerobic glycolysis in and progression of pancreatic cancer. Clin Cancer Res. 2014; 20(16):4370–80.
58. Matsui A, Ikeda T, Enomoto K, Hosoda K, Nakashima H, Omae K, et al. Increased formation of oxidative DNA damage, 8-hydroxy-2′-deoxyguanosine, in human breast cancer tissue and its relationship to GSTP1 and COMT genotypes. Cancer Lett. 2000;151(1):87–95.
59. Sena LA, Chandel NS. Physiological roles of mitochondrial reactive oxygen species. Mol Cell. 2012;48(2):158–67.
60. Weinberg F, Hamanaka R, Wheaton WW, Weinberg S, Joseph J, Lopez M, et al. Mitochondrial metabolism and ROS generation are essential for Kras-mediated tumorigenicity. Proc Natl Acad Sci U S A. 2010;107(19):8788–93.
61. Du J, Nelson ES, Simons AL, Olney KE, Moser JC, Schrock HE, et al. Regulation of pancreatic cancer growth by superoxide. Mol Carcinog. 2013;52(7):555–67.
62. Lei J, Huo X, Duan W, Xu Q, Li R, Ma J, et al. alpha-Mangostin inhibits hypoxia-driven ROS-induced PSC activation and pancreatic cancer cell invasion. Cancer Lett. 2014; 347(1):129–38.
63. Fiorini C, Cordani M, Gotte G, Picone D, Donadelli M. Onconase induces autophagy sensitizing pancreatic cancer cells to gemcitabine and activates Akt/mTOR pathway in a ROS-dependent manner. Biochim Biophys Acta. 2015;1853(3):549–60.
64. Ogrunc M, Di Micco R, Liontos M, Bombardelli L, Mione M, Fumagalli M, et al. Oncogene-induced reactive oxygen species fuel hyperproliferation and DNA damage response activation. Cell Death Differ. 2014;21(6):998–1012.
65. Poursaitidis I, Wang X, Crighton T, Labuschagne C, Mason D, Cramer SL, et al. Oncogene-selective sensitivity to synchronous cell death following modulation of the amino acid nutrient cystine. Cell Rep. 2017;18(11):2547–56.
66. Edderkaoui M, Hong P, Vaquero EC, Lee JK, Fischer L, Friess H, et al. Extracellular matrix stimulates reactive oxygen species production and increases pancreatic cancer cell survival through 5-lipoxygenase and NADPH oxidase. Am J Physiol Gastrointest Liver Physiol. 2005;289(6):G1137–47.
67. Vaquero EC, Edderkaoui M, Pandol SJ, Gukovsky I, Gukovskaya AS. Reactive oxygen species produced by NAD(P)H oxidase inhibit apoptosis in pancreatic cancer cells. J Biol Chem. 2004;279(33):34643–54.
68. Trachootham D, Lu WQ, Ogasawara MA, Valle NRD, Huang P. Redox regulation of cell survival. Antioxid Redox Signal. 2008;10(8):1343–74.
69. Sawai H, Funahashi H, Okada Y, Matsuo Y, Sakamoto M, Yamamoto M, et al. Interleukin-1alpha enhances IL-8 secretion through p38 mitogen-activated protein kinase and reactive

oxygen species signaling in human pancreatic cancer cells. Med Sci Monit. 2005; 11(10):BR343–50.
70. Hiraga R, Kato M, Miyagawa S, Kamata T. Nox4-derived ROS signaling contributes to TGF-beta-induced epithelial-mesenchymal transition in pancreatic cancer cells. Anticancer Res. 2013;33(10):4431–8.
71. Binker MG, Binker-Cosen AA, Richards D, Oliver B, Cosen-Binker LI. EGF promotes invasion by PANC-1 cells through Rac1/ROS-dependent secretion and activation of MMP-2. Biochem Biophys Res Commun. 2009;379(2):445–50.
72. De Nicola GM, Karreth FA, Humpton TJ, Gopinathan A, Wei C, Frese K, et al. Oncogene-induced Nrf2 transcription promotes ROS detoxification and tumorigenesis. Nature. 2011; 475(7354):106–9. U28.
73. Lister A, Nedjadi T, Kitteringham NR, Campbell F, Costello E, Lloyd B, et al. Nrf2 is overexpressed in pancreatic cancer: implications for cell proliferation and therapy. Mol Cancer. 2011;10:37.
74. Pavlova NN, Thompson CB. The emerging hallmarks of cancer metabolism. Cell Metab. 2016;23(1):27–47.
75. Warburg O. Note on the metabolism of tumours. Biochem Z. 1930;228:257–8.
76. Warburg O. Origin of cancer cells. Science. 1956;123(3191):309–14.
77. Kitasato Y, Yasunaga M, Okuda K, Kinoshita H, Tanaka H, Okabe Y, et al. Maximum standardized uptake value on 18F-fluoro-2-deoxy-glucose positron emission tomography/computed tomography and glucose transporter-1 expression correlates with survival in invasive ductal carcinoma of the pancreas. Pancreas. 2014;43(7):1060–5.
78. Ying HQ, Kimmelman AC, Lyssiotis CA, Hua SJ, Chu GC, Fletcher-Sananikone E, et al. Oncogenic Kras maintains pancreatic tumors through regulation of anabolic glucose metabolism. Cell. 2012;149(3):656–70.
79. Berkers CR, Maddocks ODK, Cheung EC, Mor I, Vousden KH. Metabolic regulation by p53 family members. Cell Metab. 2013;18(5):617–33.
80. Baek G, Tse YF, Hu ZP, Cox D, Buboltz N, McCue P, et al. MCT4 defines a glycolytic subtype of pancreatic cancer with poor prognosis and unique metabolic dependencies. Cell Rep. 2014;9(6):2233–49.
81. Son J, Lyssiotis CA, Ying H, Wang X, Hua S, Ligorio M, et al. Glutamine supports pancreatic cancer growth through a KRAS-regulated metabolic pathway. Nature. 2013;496(7443):101–5.
82. Semenza GL. HIF-1 mediates metabolic responses to intratumoral hypoxia and oncogenic mutations. J Clin Invest. 2013;123(9):3664–71.
83. Boros LG, Puigjaner J, Cascante M, Lee WNP, Brandes JL, Bassilian S, et al. Oxythiamine and dehydroepiandrosterone inhibit the nonoxidative synthesis of ribose and tumor cell proliferation. Cancer Res. 1997;57(19):4242–8.
84. Slawson C, Copeland RJ, Hart GW. O-GlcNAc signaling: a metabolic link between diabetes and cancer? Trends Biochem Sci. 2010;35(10):547–55.
85. Ma ZY, Vocadlo DJ, Vosseller K. Hyper-O-GlcNAcylation is anti-apoptotic and maintains constitutive NF-kappa B activity in pancreatic cancer cells. J Biol Chem. 2013; 288(21):15121–30.
86. Guillaumond F, Leca J, Olivares O, Lavaut MN, Vidal N, Berthezene P, et al. Strengthened glycolysis under hypoxia supports tumor symbiosis and hexosamine biosynthesis in pancreatic adenocarcinoma. Proc Natl Acad Sci U S A. 2013;110(10):3919–24.
87. Zhao D, Zou SW, Liu Y, Zhou X, Mo Y, Wang P, et al. Lysine-5 acetylation negatively regulates lactate dehydrogenase A and is decreased in pancreatic cancer. Cancer Cell. 2013; 23(4):464–76.
88. Hutcheson J, Balaji U, Porembka MR, Wachsmann MB, McCue PA, Knudsen ES, et al. Immunologic and metabolic features of pancreatic ductal adenocarcinoma define prognostic subtypes of disease. Clin Cancer Res. 2016;22(14):3606–17.

89. Goetze K, Walenta S, Ksiazkiewicz M, Kunz-Schughart LA, Mueller-Klieser W. Lactate enhances motility of tumor cells and inhibits monocyte migration and cytokine release. Int J Oncol. 2011;39(2):453–63.
90. Gottfried E, Kunz-Schughart LA, Ebner S, Mueller-Klieser W, Hoves S, Andreesen R, et al. Tumor-derived lactic acid modulates dendritic cell activation and antigen expression. Blood. 2006;107(5):2013–21.
91. Fischer K, Hoffmann P, Voelkl S, Meidenbauer N, Ammer J, Edinger M, et al. Inhibitory effect of tumor cell-derived lactic acid on human T cells. Blood. 2007;109(9):3812–9.
92. Constant JS, Feng JJ, Zabel DD, Yuan H, Suh DY, Scheuenstuhl H, et al. Lactate elicits vascular endothelial growth factor from macrophages: a possible alternative to hypoxia. Wound Repair Regen. 2000;8(5):353–60.
93. Stern R, Shuster S, Neudecker BA, Formby B. Lactate stimulates fibroblast expression of hyaluronan and CD44: the Warburg effect revisited. Exp Cell Res. 2002;276(1):24–31.
94. Le A, Cooper CR, Gouw AM, Dinavahi R, Maitra A, Deck LM, et al. Inhibition of lactate dehydrogenase A induces oxidative stress and inhibits tumor progression. Proc Natl Acad Sci U S A. 2010;107(5):2037–42.
95. Rajeshkumar NV, Dutta P, Yabuuchi S, de Wilde RF, Martinez GV, Le A, et al. Therapeutic targeting of the Warburg effect in pancreatic cancer relies on an absence of p53 function. Cancer Res. 2015;75(16):3355–64.
96. Hensley CT, Wasti AT, DeBerardinis RJ. Glutamine and cancer: cell biology, physiology, and clinical opportunities. J Clin Invest. 2013;123(9):3678–84.
97. Schnelldorfer T, Gansauge S, Gansauge F, Schlosser S, Beger HG, Nussler AK. Glutathione depletion causes cell growth inhibition and enhanced apoptosis in pancreatic cancer cells. Cancer. 2000;89(7):1440–7.
98. Mitsuishi Y, Taguchi K, Kawatani Y, Shibata T, Nukiwa T, Aburatani H, et al. Nrf2 redirects glucose and glutamine into anabolic pathways in metabolic reprogramming. Cancer Cell. 2012;22(1):66–79.
99. Nguyen T, Nioi P, Pickett CB. The Nrf2-antioxidant response element signaling pathway and its activation by oxidative stress. J Biol Chem. 2009;284(20):13291–5.
100. Chio II, Jafarnejad SM, Ponz-Sarvise M, Park Y, Rivera K, Palm W, et al. NRF2 promotes tumor maintenance by modulating mRNA translation in pancreatic cancer. Cell. 2016; 166(4):963–76.
101. Li W, Cao L, Han L, Xu Q, Ma Q. Superoxide dismutase promotes the epithelial-mesenchymal transition of pancreatic cancer cells via activation of the H2O2/ERK/NF-kappaB axis. Int J Oncol. 2015;46(6):2613–20.
102. Yao X, Zeng M, Wang H, Fei S, Rao S, Ji Y. Metabolite detection of pancreatic carcinoma by in vivo proton MR spectroscopy at 3T: initial results. Radiol Med. 2012;117(5):780–8.
103. Philip B, Roland CL, Daniluk J, Liu Y, Chatterjee D, Gomez SB, et al. A high-fat diet activates oncogenic Kras and COX2 to induce development of pancreatic ductal adenocarcinoma in mice. Gastroenterology. 2013;145(6):1449–58.
104. Bracci PM. Obesity and pancreatic cancer: overview of epidemiologic evidence and biologic mechanisms. Mol Carcinog. 2012;51(1):53–63.
105. Wang F, Kumagai-Braesch M, Herrington MK, Larsson J, Permert J. Increased lipid metabolism and cell turnover of MiaPaCa2 cells induced by high-fat diet in an orthotopic system. Metabolism. 2009;58(8):1131–6.
106. Bian Y, Yu Y, Wang S, Li L. Up-regulation of fatty acid synthase induced by EGFR/ERK activation promotes tumor growth in pancreatic cancer. Biochem Biophys Res Commun. 2015;463(4):612–7.
107. Chu GC, Kimmelman AC, Hezel AF, DePinho RA. Stromal biology of pancreatic cancer. J Cell Biochem. 2007;101(4):887–907.
108. Ying HQ, Dey P, Yao WT, Kimmelman AC, Draetta GF, Maitra A, et al. Genetics and biology of pancreatic ductal adenocarcinoma. Genes Dev. 2016;30(4):355–85.

109. Apte MV, Wilson JS. Dangerous liaisons: pancreatic stellate cells and pancreatic cancer cells. J Gastroenterol Hepatol. 2012;27:69–74.
110. Zhang WW, Erkan M, Abiatari I, Giese NA, Felix K, Kayed H, et al. Expression of extracellular matrix metalloproteinase inducer (EMMPRIN/CD147) in pancreatic neoplasm and pancreatic stellate cells. Cancer Biol Ther. 2007;6(2):218–27.
111. Tape CJ, Ling S, Dimitriadi M, McMahon KM, Worboys JD, Leong HS, et al. Oncogenic KRAS regulates tumor cell signaling via stromal reciprocation. Cell. 2016;165(4):910–20.
112. Sousa CM, Biancur DE, Wang XX, Halbrook CJ, Sherman MH, Zhang L, et al. Pancreatic stellate cells support tumour metabolism through autophagic alanine secretion. Nature. 2016;536(7617):479–83.
113. Schumacher TN, Schreiber RD. Neoantigens in cancer immunotherapy. Science. 2015; 348(6230):69–74.
114. Tassi E, Gavazzi F, Albarello L, Senyukov V, Longhi R, Dellabona P, et al. Carcinoembryonic antigen-specific but not antiviral CD4(+) T cell immunity is impaired in pancreatic carcinoma patients. J Immunol. 2008;181(9):6595–603.
115. Ostrand-Rosenberg S. Immune surveillance: a balance between protumor and antitumor immunity. Curr Opin Genet Dev. 2008;18(1):11–8.
116. Nummer D, Suri-Payer E, Schmitz-Winnenthal H, Bonertz A, Galindo L, Antolovich D, et al. Role of tumor endothelium in CD4(+)CD25(+) regulatory T cell infiltration of human pancreatic carcinoma. J Natl Cancer Inst. 2007;99(15):1188–99.
117. Byrne WL, Mills KHG, Lederer JA, O'Sullivan GC. Targeting regulatory T cells in cancer. Cancer Res. 2011;71(22):6915–20.
118. Clark CE, Hingorani SR, Mick R, Combs C, Tuveson DA, Vonderheide RH. Dynamics of the immune reaction to pancreatic cancer from inception to invasion. Cancer Res. 2007; 67(19):9518–27.
119. Frauwirth KA, Thompson CB. Regulation of T lymphocyte metabolism. J Immunol. 2004; 172(8):4661–5.
120. Chang CH, Qiu J, O'Sullivan D, Buck MD, Noguchi T, Curtis JD, et al. Metabolic competition in the tumor microenvironment is a driver of cancer progression. Cell. 2015;162(6):1229–41.
121. Hanahan D, Weinberg RA. Hallmarks of cancer: the next generation. Cell. 2011; 144(5):646–74.
122. Daemen A, Peterson D, Sahu N, McCord R, Du XN, Liu BN, et al. Metabolite profiling stratifies pancreatic ductal adenocarcinomas into subtypes with distinct sensitivities to metabolic inhibitors. Proc Natl Acad Sci U S A. 2015;112(32):E4410–7.
123. Davidson SM, Papagiannakopoulos T, Olenchock BA, Heyman JE, Keibler MA, Luengo A, et al. Environment impacts the metabolic dependencies of Ras-driven non-small cell lung cancer. Cell Metab. 2016;23(3):517–28.
124. Beatty GL, Chiorean EG, Fishman MP, Saboury B, Teitelbaum UR, Sun WJ, et al. CD40 agonists alter tumor stroma and show efficacy against pancreatic carcinoma in mice and humans. Science. 2011;331(6024):1612–6.